An Investigation of Beryllium Coordination Chemistry Using Electrospray Ionisation Mass Spectrometry

A thesis

submitted in fulfilment

of the requirements for the degree

of

Doctor of Philosophy in Chemistry

at

The University of Waikato

by

ONYEKACHI RAYMOND

THE UNIVERSITY OF
WAIKATO
Te Whare Wānanga o Waikato

2018

Abstract

The electrospray ionisation mass spectrometric behaviour of various complexes of beryllium have been investigated in this thesis. These beryllium complexes were prepared *in situ* on a small scale by preparing appropriate molar mixtures of the Be^{2+} ion with ligands in a range of solvent systems. In view of the toxicity of beryllium compounds, this combinatorial type screening, involving miniscule amounts of material in solution, proved to be a safe strategy to pursue the coordination chemistry of beryllium.

Starting from simple beryllium compounds which includes the metal salts (Chapter 2), the speciation and hydrolysis of beryllium ions in aqueous solution has been studied over a pH range of 2.5-6.0 using electrospray ionisation mass spectrometry (ESI-MS). Ions observed by ESI-MS revealed that the speciation of beryllium with hydroxide ligands in solution was preserved into the gas phase *via* charge reduction by ion pairing with the salt anion. The pH-dependent hydrolytic tendencies of the Be^{2+} cation presented as an ESI-MS speciation diagram for beryllium hydrolysis is in good agreement with previous speciation data which vindicates the ability of ESI-MS as a quick, sensitive and safe screening technique for observing beryllium speciation with ligands of interest at low concentrations. Collision induced dissociation patterns further confirmed that the trimer $[Be_3(OH)_3]^{3+}$ is the most stable beryllium hydroxido-aggregate arrangement while the pronounced ion pairing of the beryllium cation with the sulfato ligand yielded additional beryllium ion cluster arrangements such as $Be_3(\mu_3\text{-}O)$ aggregate and mixed sulfato-/hydroxido- species. These ions were further investigated using computational techniques simulated in the gas and aqueous environment which allowed for the first time, the molecular dynamics simulations of the ligand exchange processes of the Be^{2+} cation (Chapter 3). A major finding from the *ab initio* molecular simulations was that hydrogen bonding was relevant in stabilising the tetraaquaberyllium complex in beryllium solutions. Therefore, in the gas phase where the solvation shell of such beryllium species is very much compromised, the formation of inner sphere complexes is commonplace as observed from the ion signal assignment in the ESI mass spectra. While these extraneous species may not be an exact representation of the solution state, these ions provided insight into plausible modes of beryllium aggregation that are not otherwise easily investigated.

Building on these results, a variety of beryllium complexes was generated with various ligands in solutions and subjected to detailed characterisation by ESI-MS. These ligands containing functional groups or architecture of interest, varied from simple monodentate ligands such as the acetate ion to more common beryllium chelators including 1,3-diketone, hydroxy keto, malonic acid, chromotropic acid and crown ethers (Chapter 4). Generally, there was excellent correlation between the species observed in the mass spectrum and those confirmed to exist in solution by other techniques. This lent strong credence to the ESI-MS methodology used as an efficient analytical technique for the easy screening of a diverse range of potential ligands for the divalent beryllium ion.

A fundamental issue in beryllium research is the search for suitable chelating ligands for environmental and biomedical application. Therefore, the ESI-MS methodology was further employed to investigate several multidentate aminopolycarboxylic acids which are well-known commercial and biomedical chelating agents (Chapter 5). Notable among these are the nitrilotripropionic acid (NTP) and related tetradentate ligands designed towards the full encapsulation of the Be^{2+} cation. Stoichiometric information which was readily obtained from the ESI mass spectra was found to be effective for the preliminary screening of potential encapsulation by tetradentate coordination from a single ligand. Lastly, to corroborate ESI-MS speciation results, beryllium complexes with these class of ligands were synthesised on a larger scale and characterised by ^{9}Be NMR and single-crystal X-ray crystallography.

Acknowledgements

Getting straight to the point: I would like to appreciate all the academics who contributed to the development of the ideas and concepts in this thesis. Firstly, I acknowledge my chief supervisor Prof. Bill Henderson who for his immeasurable support, excellent communication and for offering me a Postgraduate study award. At this point, I will also mention Assoc. Prof. Paul Plieger (Massey University) who was the principal investigator on Marsden Fund Grant (contract MAU1204, administered by the Royal Society of New Zealand) which sponsored this research and associate investigator Prof. Penny Brothers as well as my fellow PhD students on the project Lakshika Perera and David Nixon. Furthermore, many thanks to Assoc. Prof. Michael Mucalo and Dr Jo Lane - my co-supervisors at the University of Waikato.

My immense gratitude also goes to Prof. Michael Bühl (University of St Andrews, Scotland) for introducing and training me on the technique of *ab initio* molecular dynamics as well as a generous computer allocation. Special thanks to Prof. Florian Kraus and Dr Magnus Buchner who were my hosts during a research visit to Philipps Universität Marburg, Germany. Lastly, a big thank you to my numerous officemates especially here at the University of Waikato and other laboratories I visited.

I would also like to thank the support of Cheryl Ward (Science Librarian) and the library team (especially the Interloan services). Other teams whose support and services helped progress this research include the postgraduate team, the university research office, the scholarship office and the school of science administration (especially Vicki and Gloria). Many thanks as well to the technical staff of Chemistry, School of Science, University of Waikato and other universities I visited including Dr Herbert Früchtl (University of St Andrews, Scotland), who kept me connected to the University of St Andrews High performance computing (HPC) facilities.

Outside the laboratories, the first person whom I want to thank is my fiancée whose contributions to this thesis are so convoluted to be delved into. The support of my parent and siblings was the bed rock which my survival rested. "Family is everything" and though I had put it second at one point or the other, I want to say a big thank for their understanding and love. Thank you as well to my church family at Freedom Christian Church, Hamilton as well as to my music team.

Finally, I would like to say thank you to all my flatmates, friends and countrymen whom I have mingled with here in New Zealand and overseas.

Table of Contents

List of Figures

List of Tables

List of Abbreviations

BLPT	Beryllium lymphocyte proliferation test
CBD	Chronic beryllium disease
AIMD	*Ab initio* molecular dynamics
BLYP	Becke 88 exchange and Lee-Yang-Parr correlation functional
B3LYP	Becke's three parameter hybrid functional
CPMD	Car Parrinello molecular dynamics
GGA	Generalised gradient approximation
ΔA	Helmholtz free energy difference
ESI-MS	Electrospray ionisation mass spectrometry
CID	Collision induced dissociation
CEV	Capillary exit voltage
m/z	Mass-to-charge ratio
TOF	Time of Flight
12C4	12-Crown-4
15C5	15-Crown-5
18C6	18-Crown-6
Hacac	Acetylacetone
HBQ	10-hydroxybenzoquinolone
Hdbm	Dibenzoylmethane
H5DTPA	Diethylenetriaminepenta acetic acid
Hmal	Maltol
H3NTA	Nitrilotriacetic acid
H3NTP	Nitrilotripropionic acid
HOAc	Acetic acid
Htfac	Trifluoroacetylacetone
Htrop	Tropolone
Htta	Thenoyl Trifluoroacetylacetone
Pc	Phthalocyanine
z/r	Charge-to-size

Chapter One

The chemistry and metallurgy of beryllium

1.1 Introduction

Beryllium (Be), the first of the group 2 (alkali-earth) elements, is a silver-grey metal possessing an unmatched combination of physical and mechanical properties vital for a variety of applications that offer tremendous benefits to our society.[1, 2] It is the lightest workable metal with a density of 1.84 g cm^{-3} and only two-thirds the weight of aluminium, yet it has six times the stiffness of steel and a very high melting point (1287 ºC) making it a speciality metal ideal for stiffness-dependent and weight-limited applications. The chart in Figure 1-1 illustrates how much beryllium outclasses related engineering materials with respect to thermal conductivity and dimensional stability (ability of a material to retain its uniformity under stress measured as the Young's modulus to density ratio). These unique properties of beryllium translate into outstanding performance enhancement in end-user products when compared to substitute materials. For instance, the James Webb Space Telescope, which will exclusively utilise a 6.5 m wide beryllium mirror, will reveal images of distant galaxies 200 times beyond what has ever been sighted.

Unfortunately, beryllium is also problematic mainly due to its extreme toxicity for which it is allegedly regarded as the most toxic non-radioactive element in the Periodic Table.[3-5] In addition, beryllium metal is also brittle, hard to machine and expensive. Surprisingly, these deterrents have not slowed the production and usage of beryllium components but have persistently dwarfed the exploration of the fundamental coordination chemistry of this element. For this reason, intense beryllium coordination chemistry research, which is the main plot of this thesis, is highly imperative both for intellectual progress as well as industrial and environmental purposes.

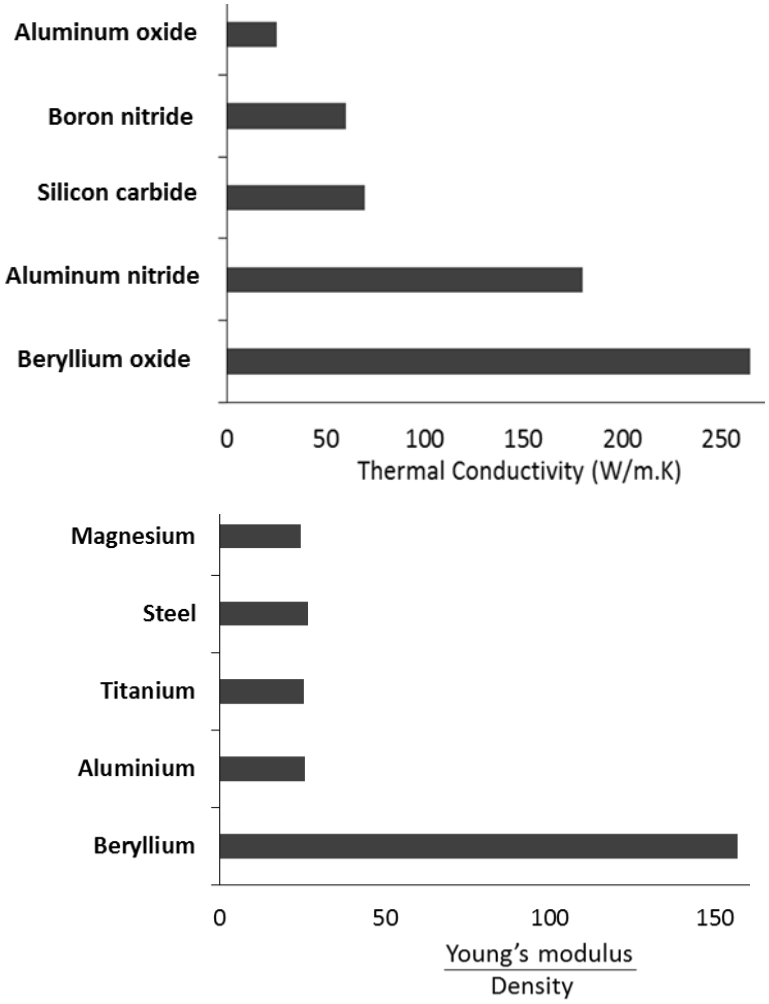

Figure 1-1 Some properties of beryllium and beryllium oxide as compared with alternatives (Thermal conductivities used with permission from American Beryllia Inc.)

Beryllium is an s block element with a relative atomic mass of u = 9.01218307(8) and an atomic number of z = 4. The coordination chemistry of beryllium is largely governed by its small size and high charge density. Its ground state electron configuration is $1s^2\ 2s^2$ and the loss of the $2s^2$ electrons leads to its dominant ion- Be^{2+}. The small beryllium dication (ionic radius 31 pm) has a charge to size ratio (z/r) of 6.45 which is comparable to the Al^{3+} cation (6.0) hence these two elements notoriously illustrate a typical diagonal relationship among the main group elements. Indeed, the chemistry of beryllium shows more similarities to aluminium rather than its heavier alkali earth metal congeners such as magnesium and calcium. This striking similarity between the two metals resulted in beryllium being overlooked as a constituent of beryl until 1724. In fact even after beryllium's discovery, scientists presumed beryllium to have an oxidation state of +3 and placed it above aluminium in group 13 of the periodic table. However, aluminium still

exhibits some differences from beryllium. For instance aluminium being a larger sized cation prefers an octahedral coordination geometry and is therefore complexed more effectively by EDTA while beryllium which maintains a four-coordinate tetrahedral geometry shows poor binding with EDTA. Interestingly, the human body also effectively distinguishes Al^{3+} from Be^{2+} such that the former triggers no related immune response as compared to inhalation of beryllium particles.

This chapter introduces the properties of beryllium along with recent advances in the coordination chemistry of this element, especially focusing on coordination by ligands possessing oxygen and/or nitrogen donor atoms. Worthy of mention is the existence of earlier reviews and relevant text, which have covered various aspects of beryllium coordination such as aqueous chemistry of beryllium, coordination with sequestering ligands, beryllium halides, amides and coordination to *O*-donor ligands etc.[6-14] However, the ongoing renaissance of research interest in the chemistry of beryllium has furnished a vast number of new beryllium complexes which reveal especially the rich albeit untapped coordination chemistry of the beryllium ion.[12, 15, 16] Lastly, in this chapter, a brief introduction to the major techniques employed in the thesis, namely mass spectrometry and *ab initio* molecular dynamics, is outlined.

1.2 Sources and production of beryllium

Beryllium is the 44th most abundant element in the earth crust and occurs naturally in fossil fuels, air and water. In addition, beryllium is found in food and drinking water but there is no known biological role of this metal either in plants or the human body.[17] Discovered in 1724 by Vauquelin, but isolated independently by Bussy and Wöhler in 1828, beryllium was originally named glucinium (Gl) (after its sweet tasting oxide) while its present name was adopted in 1957 by the International Union of Pure and Applied Chemistry (IUPAC). Commercial outlets for beryllium began in the 1920s and its usage has increased over the years to an estimated annual demand for the element of 500 tonnes by 2018.[1] Nevertheless, mining of beryllium is only viable from a few of its minerals including beryl ($Be_3Al_2Si_6O_{18}$, 4% by weight beryllium) and bertrandite ($Be_4(OH)_2Si_2O_7$, 1% by weight beryllium) which are mined in the United States, China, Kazakhstan,

Mozambique, Brazil, Australia and Madagascar. Beryl also occurs naturally in New Zealand in pegmatite on the West Coast and Hawk's Crag Breccia in the Buller Gorge.[2] However, over two-thirds of the world's beryllium is produced by the US while the rest comes from China, Kazakhstan and Russia. To extract beryllium, its minerals are first crushed and leached with acids to produce a beryllium salt solution from which the metal hydroxide is precipitated.[10] The resultant hydroxide is further processed into beryllium's three most useful forms namely the pure metal, beryllium oxide, and its alloys (with metals such as copper, nickel and aluminium). The low beryllium content and stability of most beryllium ore minerals, require costly extraction processes, making beryllium an expensive metal.

1.3 Properties and uses

Beryllium is vital and indispensable in many of its applications which is best illustrated in its status as a critical and strategic metal in Europe and the USA*.[1] Interestingly, while the usage of beryllium in certain applications has been discontinued for safety reasons, new and crucial applications have emerged leading to its continuous demand and production.[2]

The application of beryllium in aerospace and military equipment has been the most extensive.[1] It is found in missiles, sensors, jet fighters, helicopters, landing gears, heat shields and brakes for military and commercial aircrafts. Components made from beryllium are essential in spacecraft and military equipment because of its high strength which can sustain various structures without adding weight or losing strength from vibrations, thereby ensuring safety, precision and reliability in the end product. The high infra-red reflectivity of beryllium also makes it an idea optical material for military, navigation and communication satellites, for instance, in the James Webb Telescope and Galileo Navigation Satellite System.

Besides aerospace and military applications, beryllium components have gained prominence in telecommunications, consumer and automobile electronics which now account for 45% of beryllium usage. The exceptional thermal conductivity and electrical insulation of beryllium ceramics makes it an excellent heat sink for electronic devices to support miniaturisation and the design of compact

* Metals whose shortage or substitution could significantly impact on the economy, national security and defence. (see reference 1)

components. Furthermore, alloys containing beryllium in various proportions exhibit highly enhanced properties utilised for air bag sensors, electrical relays in automobiles, non-spark tools for oil and gas exploration, fatigue resistant springs and housing for undersea cables. In comparison with other metals, beryllium is very transparent to X-rays due to its low atomic number and is applied in X-ray windows for medical and scientific equipment.

Beryllium also possesses interesting nuclear properties. It has a high neutron scattering cross section and is applied as a neutron moderator, reflector, and shield. In construction of nuclear fusion reactors, beryllium is a superior material for the lining of interior walls as it erodes more slowly and retains less of the plasma while the inclusion of beryllium oxide in fuels for nuclear fission can speed up cooling, thereby offering significant improvements to the safety and efficiency of nuclear power plants.[18]

1.4 Toxicity

Although beryllium possesses highly attractive properties, it is extremely toxic, both as a carcinogen and as an initiator of acute and chronic beryllium disease (CBD).[5, 19, 20] However, its carcinogenicity has only been established in animals while carcinogenicity in humans is still a subject of debate.[5] Nevertheless, exposure to beryllium fumes or dust particles by inhalation (and possibly dermal contact) can lead to beryllium sensitisation and further progress into CBD in certain individuals (1-15%). Chronic beryllium disease (CBD) is a debilitating granulomatous lung disorder resulting from an uncontrolled cell-mediated immune response marked by the proliferation of the $CD4^+$ T cells.[19] The dissolution, speciation and exact mechanism by which beryllium particles trigger CBD is not clearly understood. Current molecular understanding of the disease proposes that inhaled beryllium is detected by antigen-presenting cells which trigger the body's immune system into producing blood cells that engulf the particles forming granulomas that eventually harden the lungs causing respiratory abnormalities.[19] The onset of CBD can be delayed for over 20 years after exposure and there is no strong correlation between levels of exposure and CBD development, suggesting that a change in the beryllium speciation could be culpable. More intriguing is the recent emergence of genetic correlation to the disease as research evidences suggest that the risk of CBD is

increased by the presence of a specific gene- HLA-DPB1.[20-22] Based on this, a beryllium lymphocyte proliferation test (BLPT) has been developed for routine use in diagnosis and workplace screening to predict the susceptibility of beryllium worker towards the disease.[23] Another interesting correlation with CBD is that it is associated only with the processed forms of beryllium, such as beryllium metal and its oxide. Beryl and other ores of beryllium do not trigger a similar immune response possibly due to the lack of bioavailability of beryllium from these ores as they are insoluble in aqueous solution. It has also been observed that there is no beryllium oxido cluster (Be-O-Be) in the beryl structure ($Be_3Al_2Si_6O_{18}$), but rather silicon oxide units bridge beryllium and aluminium.[19]

1.5 Beryllium in New Zealand

Beryllium is neither mined nor processed in New Zealand but its components and alloys are imported for various applications. Although beryllium components are found in electronic devices and other consumer products, they are well encased and offer no hazard to general users. However, appropriate disposal via the segregation of these components is recommended considering the imminent increase of beryllium in electronic waste. Exposure to beryllium can also result from the combustion of fossil fuels, especially coal which can contain significant amounts of beryllium. While it is possible for beryllium to accumulate in the lung as a result of inhalation of tobacco and cigarette smoke, the extent of this risk is still undetermined.[24] The main concern for beryllium exposure involves occupational related activities with beryllium components. The occupational exposure limit for beryllium in New Zealand is 2 $\mu g\ m^{-3}$ for an 8 hour time-weighted average but it remains unclear if this limit adequately protects beryllium workers from developing CBD. Pleasantly, no CBD case has been recorded in New Zealand although a single case of beryllium sensitisation was reported among aircraft maintenance staff in Air New Zealand.[25, 26] The company thereafter set up a copper beryllium project in 2006, sampling work areas to identify and manage potential health risks to its workers involved in beryllium work areas. Noteworthy in their findings was the uncharted occupational hazards associated with beryllium-related operations in New Zealand.

1.6 Aqueous chemistry of the Be^{2+} cation

Generally, only a few inorganic ligands can compete with aqua ligands for a binding site with beryllium because in aqueous solution the Be^{2+} ion is strongly solvated with evidence from a wide array of experimental and computational techniques strongly supporting a discrete primary coordination sphere comprised of four aqua ligands.[6, 27] The Be-OH_2 bonds typically range from 1.61-1.69 Å and the BeO_4 tetrahedron is relatively regular with O-Be-O angles between 105-117° although these values vary depending on the technique and the nature of ion-pairing in the species.[27] The tetraaquaberyllium cation $[Be(H_2O)_4]^{2+}$ exists only in acidic solutions (pH < 3) above which it is extensively hydrolysed furnishing a variety of oligomeric species which includes the $[Be_2OH]^{3+}$, $[Be_3(OH)_3]^{3+}$, $[Be_5(OH)_6]^{4+}$ and $[Be_6(OH)_8]^{4+}$ species (see Figure 1-2).

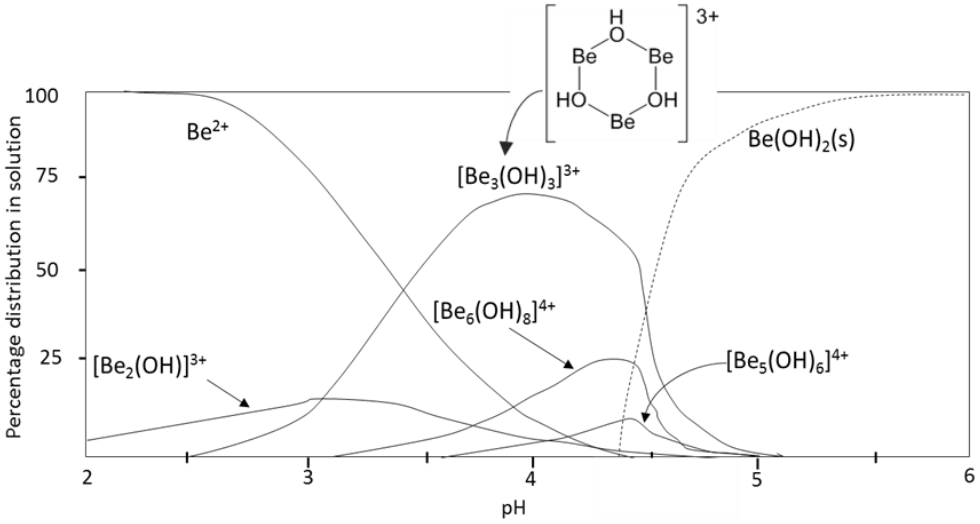

Figure 1-2 Beryllium hydroxido species distribution diagram in acidic solutions. The water molecules completing the tetracoordination beryllium have removed for clarity. (Adapted from ref. 6 with permission from the Royal Society of Chemistry).

These species have been well studied by various solution based techniques all of which have pointed out the beryllium hydroxido trimer as the most abundant species, while several X-ray crystal structures of the $[Be_3(\mu\text{-}OH)_3]$ trimeric motif have been reported confirming its stability and cyclic structure.* Between pH 5.5-12.0, insoluble beryllium hydroxide $Be(OH)_2$ precipitates which dissolves at higher

* A CCDC search for the $[Be_3(OH)_3]^{3+}$ structural motif revealed 17 hits comprising of 10 distinct beryllium complexes of the type $[Be_3(OH)_3(L)_3]$ while two complexes contained the $[Be_3O_3]$ unit (Also note that 4 or probably a few more $[Be_3(OH)_3(L)_3]$ species were not deposited in the data base).

pH to furnish yet another mix of beryllium hydroxido anions including the $[Be(OH)_3]^-$, $[Be(OH)_4]^{2-}$, $[Be_2(OH)_7]^{3-}$ and $[Be_4(OH)_{10}]^{2-}$ species.

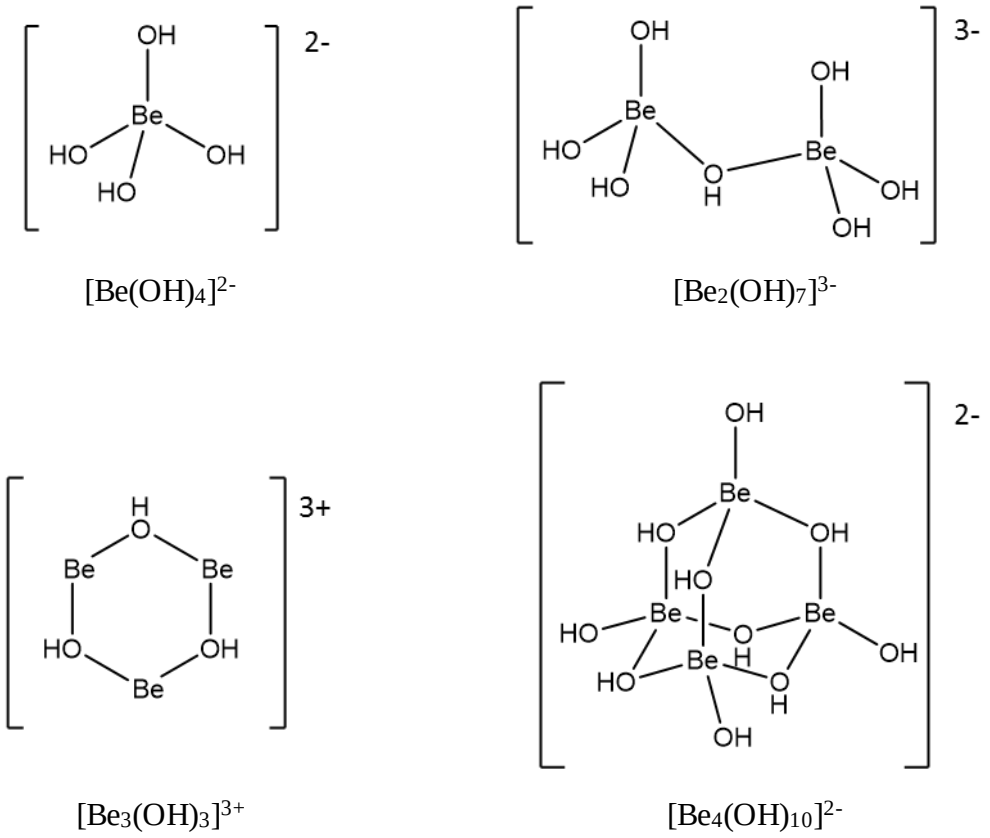

$[Be(OH)_4]^{2-}$ $[Be_2(OH)_7]^{3-}$

$[Be_3(OH)_3]^{3+}$ $[Be_4(OH)_{10}]^{2-}$

Figure 1-3 Structurally characterised beryllium hydroxido motifs (see ref. 6, 14, 29 and 30)

Although salts of the type $M[Be(OH)_4]$ where M = Ca, Sr or Ba have earlier been proposed, attempts to synthesise the $Ca[Be(OH)_4]$ complex (at pH 13.5-14) resulted in the isolation of a crystal that contained the hydroxidoberyllate trianion $[Be_2(OH)_7]^{3-}$.[28] The presence of yet another hydroxidoberyllate anion $[Be_4(OH)_{10}]^{2-}$ was further identified revealing an adamantane structure where four beryllium atoms occupy the vertices of a regular tetrahedron with a terminal hydroxyl group at each metal centre while the remaining six bridging hydroxyl groups completed the tetracoordination to beryllium ions.[29] (see Figure 1-3) Also, the elusive tetrahydroxidoberyllate anion has recently been synthesised *via* hydrothermal method and structurally characterised by X-ray diffraction.[30]

As a result of its tetrahedral geometry, the tetraaquaberyllium cation $[Be(H_2O)_4]^{2+}$ has been of particular interest as a model employed in trying out new experimental techniques to delineate mechanisms and rates of ligand substitution reactions on metal ions.[27] Consequently, a variety of methods have been employed

to offer detailed mechanistic data of the water exchange on the Be^{2+} cation.[27] In addition, because the water exchange rates from the first and second coordination sphere around the Be^{2+} ion is relatively slow (2-10 ms), the exchange process on the Be^{2+} has been also been explored by NMR techniques.[27] Merbach and co-workers[31] have reported a very negative activation volume $\Delta V^{\ddagger}$ of -13.6 cm^3 mol^{-1} (the most negative value observed for water exchange on an aqua metal ion) which implies a shrinkages of the ion space-wise. Although this value tends to suggest the aqua exchange process proceeds *via* a limiting associative mechanism the significant role of both the entering and leaving ligand on the Be^{2+} ion observed for several ligands indicates the process to be closer to an associative interchange mechanism.[32] However, in a case of considerable steric bulk of the entering ligands, it has been shown that the favourable mechanism could be altered such that a dissociative mechanism was proposed from the positive activation volume $\Delta V^{\ddagger}$ for bulky ligands such as tetramethylurea and dimethylpropyleneurea.[31] Recently, Puchata and co-workers[33] have extensively explored the ligand exchange process at the beryllium centre using computational techniques but a major challenge pointed out in all their investigations was the treatment of the solvation environment of the Be^{2+} cation. Following the lowering of the activation energy barrier of the ligands exchange reaction on the beryllium ion when employing a polarisable continuum and/or explicit microsolvated clusters in the gas phase, they summarily recommended further *ab initio* molecular dynamics simulations.

One of the anions, which extensively exchanges with aqua ligands at the beryllium centre, is the fluoride ion due to its hardness according to the Pearson HSAB principle.[6, 14] Based on various equilibrium measurements from various sources,[6, 14] the fluoride ion clearly exhibits high affinity for beryllium and effectively competes with aqua ligands to form all four substitution products $[Be(H_2O)_{4-n}F_n]^{(2-n)+}$ (n = 1-4) up to pH 8, at which point $Be(OH)_2$ precipitates. ^{19}F NMR investigations of these species often give rise to signals of 1:1:1:1 quartet splitting due to the coupling to the ^9Be nuclei while the presence of the $[BeF(H_2O)_3]^+$, $[BeF_2(H_2O)_2]$ and $[BeF_3(H_2O)]^-$ species are distinguishable as separate signals of a 1:1 doublet, 1:2:1 triplet and 1:3:3:1 quartet in the ^9Be NMR spectrum. Furthermore, the observation of the quartet in ^{19}F NMR suggests that the fluoride anions are attached to a single beryllium and do not form bridges between two beryllium atoms while the relative intensity of the signals pointed out the

extensive species redistribution in beryllium fluoride solutions. Similar inner sphere complexes with beryllium are also known to be dominant in the presence of chelating oxoanions such as the sulfate and phosphate ligands. Moreover, NMR investigations have revealed species such as $[Be_2(OH)(H_2PO_4)]^{2+}$, $Be_3(OH)_3(H_2PO_4)_3$ and $[Be_3O(H_2PO_4)_6]^{2-}$ while vibrational spectroscopy and X-ray diffraction have been used to identify distinct $(O_3SO)Be(H_2O)_3$ and $[Be(H_2O)_2(SO_4)_2]^{2-}$ species respectively.[34-37]

1.7 Coordination by *O*-donor ligands

The significance of the chelate effect in beryllium's interactions with ligands is highlighted by the fact that bidentate dicarboxylate ligands have increased binding to beryllium compared to the monocarboxylate ligands while dicarboxylate ligands possessing rigid structures that prevent chelation show poor binding with the beryllium ion.[14] Acetate, a typical monocarboxylate ligand, forms a polynuclear beryllium complex species $Be_4O(O_2CCH_3)_6$ where six acetates act as bridging ligands for four beryllium ions. In contrast to this, the dicarboxylate ligands reveal beryllium species of the types $[Be(H_2O)_2L]$, $[BeL_2]^{2-}$ and $[Be_3(OH)_3(L)_3]^{3-}$. The trimeric hydroxido/dicarboxylato species $[Be_3(OH)_3(L)_3]^{3-}$ was further crystallised for the malonate, highlighting the stability of the hydroxido trimer and the competing hydrolytic tendency in the presence of other ligands in aqueous solution.[6]

Further support for the enhanced interaction and stability of beryllium with ligands that form suitable chelate rings can be shown by the survey of formation constants (log *k* values) among analogous ligands of varying chelate ring size as shown in Figure 1-4. Ligands that form six-membered rings with beryllium are the most stable for the binding of beryllium since they offer the most compatibility for a tetrahedral geometry with the small sized Be^{2+} cation. Consequently, malonate which forms a six-membered ring binds beryllium more strongly than oxalate which forms a five-membered ring, while succinic and maleic acids which form seven-membered chelate rings reveal weaker binding. Also, chromotropic acid, the strongest bidentate ligand for beryllium, forms a six-membered chelate ring

5 membered chelate rings	6 membered chelate rings	7 membered chelate rings

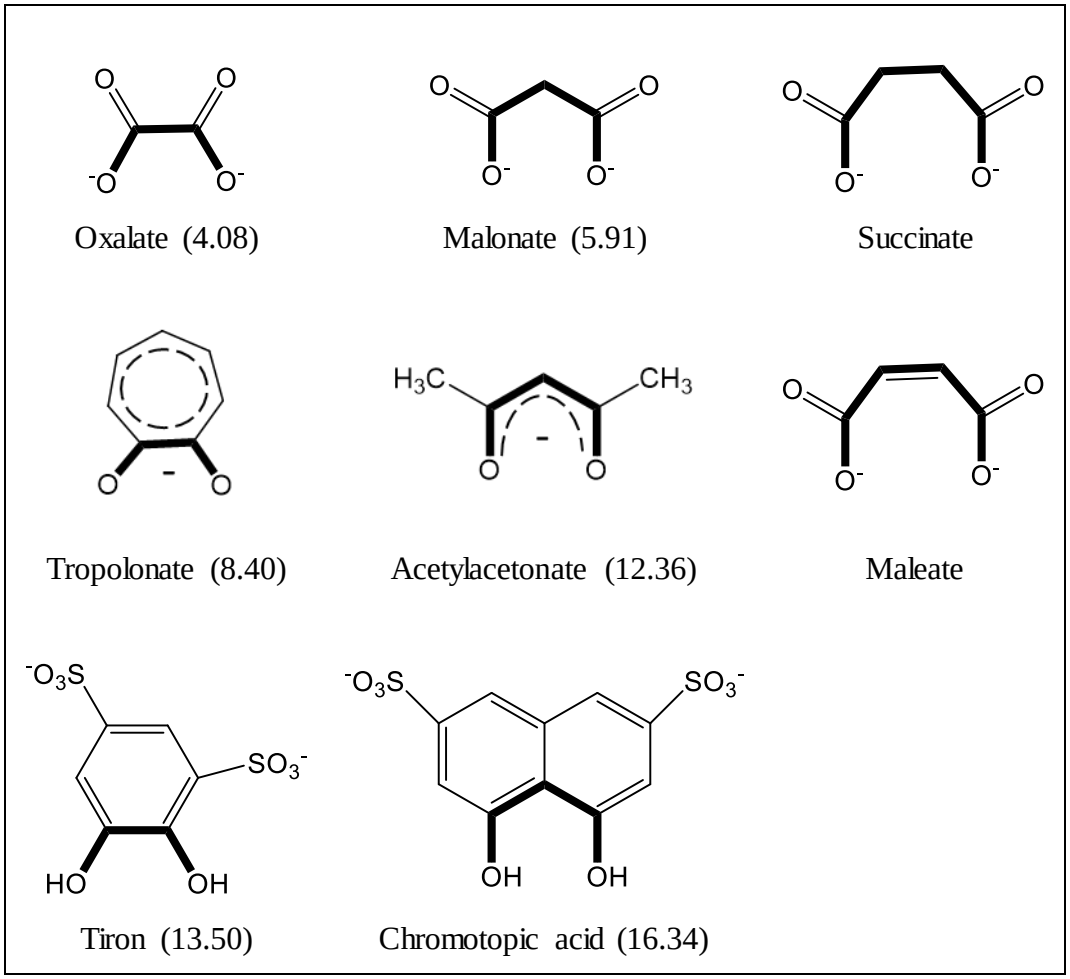

Figure 1-4 Formation constant (log *k*) of beryllium complexes formed with analogous ligands forming 5 and 6 membered chelate rings. Log *k* values from ref 8.

The interactions of the beryllium ion with hydroxycarboxylate ligands have been extensively investigated because they exhibit significant binding with beryllium and can serve as models for ligands of biological interest. In fact, the aromatic hydroxycarboxylate aurin tricarboxylate (aluminon) was earlier developed for chelation therapy in beryllium poisoning and for environmental detection.[8, 38] In a remarkable contrast, aliphatic hydroxycarboxylates generally show a weaker interaction with beryllium with the exception of citric acid. Citric acid is an excellent ligand for beryllium, capable of solubilising beryllium at molar concentrations across the entire pH range. It binds beryllium in a polynuclear fashion with a metal to ligand ratio of 2:1 (Figure 1-5a). To further understand the strong binding of citric acid with beryllium, six other aliphatic hydroxycarboxylic acids have been studied, each chosen to highlight the relevance of the hydroxyl or carboxylate functionality toward a strong beryllium chelation. Competition experiments have shown that the significant binding of beryllium to citric acid

could be attributed to the formation of a five- and six-membered ring Be-O-Be motif *via* a bridging hydroxyl group.[39] In agreement with this, two aromatic analogues, 2-hydroxyisophthalic acid and 2,3-dihydroxybenzoic acid (Figure 1-5b, c), which offer a similar polynuclear binding pocket for beryllium via a carboxylate and a bridging hydroxyl group, revealed an even stronger interaction with beryllium as well as excellent selectivity in the presence of other metal ions.[40] This development is of particular interest considering the abundance of similar functionalities in the MHC class II receptor gene implicated for the genetic susceptibility in CBD cases.

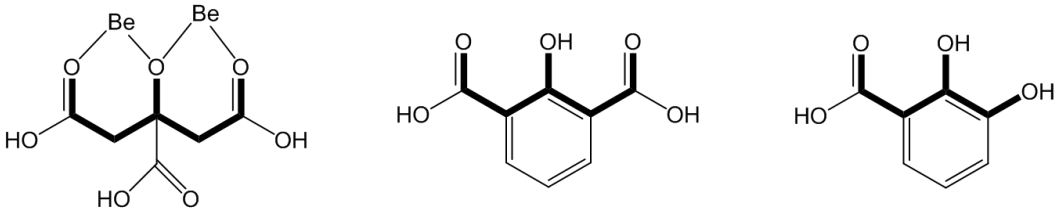

Figure 1-5 2:1 Be-citric acid complex (a) and similar ligands (2-hydroxyisophthalic acid (b) and 2,3-dihydroxybenzoic acid (c)), possessing a polynuclear binding pocket for beryllium *via* a carboxylate and a bridging hydroxyl group.

However, other ligands lacking the characteristic polynuclear binding pocket of citric acid have equally been observed to bind beryllium strongly. An example is the benzo-9-crown-3 derivative which binds beryllium extremely well and is part of commercial beryllium detection systems and extraction protocols as a result of the high selectivity of the ligand toward beryllium.[38] On the other hand, the desirable macrocyclic effect of other crown ethers and similar groups of ligands have not been reproduced towards the Be^{2+} cation due to their incompatible fit for the very small cation. X-ray structures of beryllium complexes with 12-crown-4 and 15-crown-5 reveal the beryllium ion just sitting on top of the macrocyclic ring in the former while the latter essentially chelates beryllium in a bidentate fashion. The larger 18-crown-6 ligand forms a binuclear beryllium complex (Figure 1-6).[41-43]

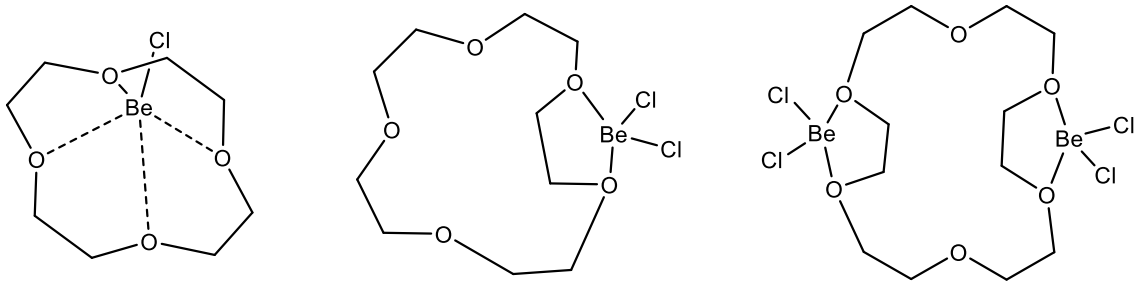

BeCl[12-C-4] $BeCl_2$[15-C-5] $(BeCl)_2$[18-C-6]

Figure 1-6 Partially encapsulated beryllium complexes formed by crown ethers of different cavity sizes.

Another functional group relevant for beryllium binding is the phosphonate group but fewer studies have investigated the solution chemistry of beryllium phosphonate complexes despite the fact that phosphonate ligands (PO moiety) form stronger complexes than carboxylate/hydroxyl ligands (CO moiety). For instance methylphosphonate, a monodentate ligand, forms a stronger complex than the malonate ligand while methylenediphosphonate, which offers a similar six membered chelate ring as malonate, reveals a much stronger interaction with beryllium.[44] Using potentiometric and multinuclear NMR methods, the interaction of beryllium with some phosphonate ligands have been ordered as malonate < methylphosphonate < phosphonopropionate < phosphonoacetate < methylenediphosphonate (see Figure 1-7). The superior interaction of the PO moiety with beryllium is again revealed in the stronger interaction of methylenediphosphonate over phosphonoacetate. Both ligands differ only in a second donor site. Methylenediphosphonate possesses two phosphonate groups while the phosphonoacetate coordinates via a phosphonate and carboxylate group. The stronger binding of methylenediphosphonate and phosphonoacetate over phosphonopropionate is presumably due to the latter forming a seven membered chelate ring.[45] Accordingly, all the bidentate ligands in Figure 1-7 containing phosphonate groups exhibit superior binding with beryllium compared to the monodentate methylphosphonate. This is relevant since metal complexes of nucleotides containing the phosphate groups such as adenosine 5-monophosphate, -diphosphate (ADP) and –triphosphate (ATP) play a fundamental role in biological processes. For instance higher stability constants for the $[Be(ATP)]^{2-}$ (log k 6.52) species have been observed in comparison to the corresponding $[Mg(ATP)]^{2-}$ (log

k 4.10) in addition to the known ability of beryllium to inhibit alkaline phosphatase and DNA replication.[7, 46] Using a competitive fluorimetric approach, it was further observed that the decrease in the number of phosphate groups from ATP to ADP resulted in a remarkable decrease in binding affinity confirming that the Be^{2+} cation is chelated by adjacent phosphate groups in ATP.[47] Ferritin is also another phosphate-binding biomolecule. It is an iron storage protein that reveals significant binding with beryllium and such is likely to provide binding sites that allow beryllium to pass through cellular systems.[19, 47]

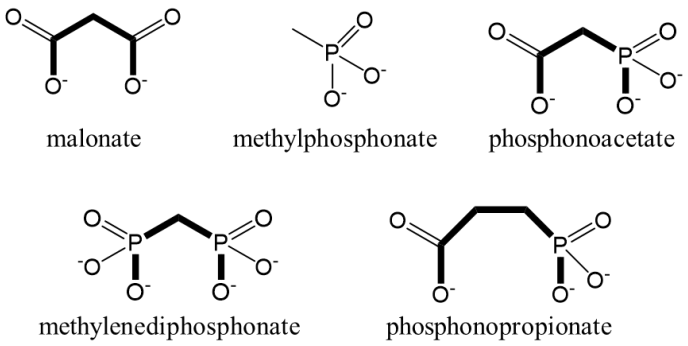

Figure 1-7 Malonate and ligands with the phosphonate functionality.

1.8 Coordination by *N*-donor ligands

1.9 Neutral monodentate *N*-donor ligands

Aqua and ammonia ligands are the simplest oxygen and nitrogen donor ligand respectively but unlike the extensively studied tetraaquaberyllium complex $[Be(H_2O)_4]^{2+}$,[6, 27] not much is known about the analogous tetraammineberyllium cation $[Be(NH_3)_4]^{2+}$. Earlier investigations to determine the predominant beryllium complex in ammonia solution have been discrepant particularly in the assignment of ^{9}Be NMR chemical shift.[48-50] Kraus *et al* have reported the first solid state structural confirmation of the tetraammineberyllium species $[Be(NH_3)_4]^{2+}$ and a convincing report of its ^{9}Be NMR chemical shift at 3.3 ppm.[51, 52] In the solid state, four ammonia ligands were found to tetracoordinate the beryllium ion forming BeN_4 linkages with Be-N bond distances in the range of 1.725Å to 1.733 Å and N-Be-N angles between $108^o - 110^o$ similar to the BeO_4 tetrahedron. Evident from the crystal structure of the beryllium chloride-ammonia system in the solid state is the primary coordination of the ammonia ligand ahead of the chlorido ligand in an

ammonia solution. The chloride ion was found to reside in the outer coordination sphere amidst an extensive network of $N-H\cdots N$ and $N-H\cdots Cl$ hydrogen bonding involving the bulk ammonia molecules. However, thermogravimetric analysis of the complex pointed out an inner sphere beryllium dichlorido complex $[Be(NH_3)_2Cl_2]$ after the loss of two ammonia molecules at 175 °C beyond which the complex tends to sublime.[53] In contrast to the chloride ion, the more electronegative fluoride ion exhibits higher affinity for the beryllium ion in ammonia solution such that the $[Be(NH_3)_2F_2]$ complex is the dominant species in ammonia solution of beryllium fluoride.[51, 54] This complex, which has been characterised in the solid state and in ammonia solution by ^{9}Be and ^{19}F NMR spectroscopic studies, reveals a ^{9}Be NMR lone 1:2:1 triplet at a chemical shift of 1.5 ppm, ruling out the presence of any fluoride/ammonia substitution series as well as the previously proposed ionic adduct $[Be(NH_3)_4]^{2-}[BeF_4]^{2+}$.[51, 54] More so, the ^{19}F NMR signal found at -164.5 ppm appeared as a 1:1:1:1 quartet due to splitting from a quadrupolar ^{9}Be nucleus.[51] In comparison to beryllium chloride, the absence of the tetraammineberyllium cation $[Be(NH_3)_4]^{2+}$ in ammonia solution of beryllium fluoride is attributable to the stronger affinity of beryllium ion for the fluoride ion.[51, 52, 54]

Due to the high oxophilicity of the Be^{2+} cation and the inherent basicity of an aqueous ammonia solution, aqua ligands readily displaced ammonia ligands from the tetraammineberyllium cation $[Be(NH_3)_4]^{2+}$ leading to the formation of the following ammonia-coordinated hydroxido complexes in solution $[Be_2(\mu\text{-}OH)(NH_3)_6]^{3+}$, $[Be_2(\mu\text{-}OH)_2(NH_3)_4]^{2+}$, $[Be_3(\mu\text{-}OH)_3(NH_3)_6]^{3+}$ (see Figure 1-8). These species have been identified by their ^{9}Be NMR chemical shifts at 3.1, 2.9 and 2.4 ppm respectively (Table 1-1). The ammonia-solvated beryllium trimer $[Be_3(\mu\text{-}OH)_3(NH_3)_6]^{3+}$ has further been isolated and structurally characterized revealing a near planar trimeric core with reasonable similarity to the analogous aqua solvated beryllium trimer $[Be_3(\mu\text{-}OH)_3(H_2O)_6]^{3+}$.[55, 56]

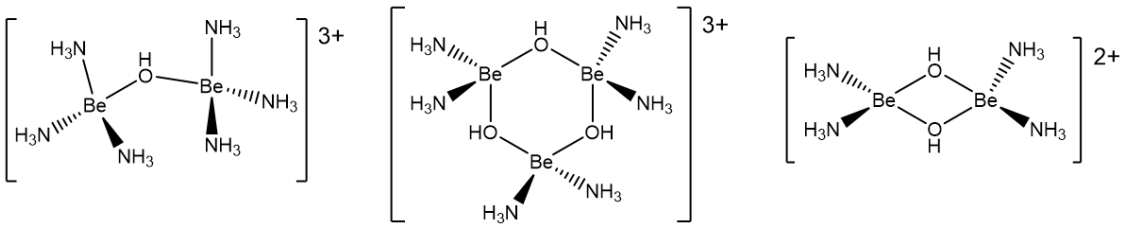

Figure 1-8 Cationic beryllium ammine hydroxido complexes in liquid ammonia.

The Lewis acidity of the metal centre in beryllium halides transverses much of the chemistry of beryllium complexes with simple *N*-donor ligands, furnishing a variety of donor-acceptor complexes with aliphatic and aromatic amines. Employing beryllium chloride salt dissolved in diethyl ether, secondary and aromatic amine ligands L such as pyridine, pyrazole, pyrrolidine, piperidine and diethylamine have been shown to displace diethyl ether- a weakly coordinating oxygen donor ligand affording the corresponding *N*-coordinated Lewis acid donor acceptor complex L_2BeCl_2.[57] While the more basic amines like pyrrolidine successfully displaced a chlorido ligand to yield the monocation $[L_3BeCl]^+$, the less basic nitrogen donor in a pyrazole ligand resulted in the ligand displacing only one molecule of diethylether to yield $[LBe(OEt)_2Cl]^+$. Additional species observed include a complex $[L(OEt)BeCl]_2$ where L = pyrimidine, pyrazole. Furthermore, no reaction was observed in stronger oxygen donor solvents such as tetrahydrofuran. ^{9}Be NMR chemical shifts for these species revealed broad signals shown in Table 1-1. Noteworthy is the fact that the $[BeL_4]^{2+}$ species have been rarely achieved from these simple nitrogen donor molecules in the presence of the chloride or fluoride ion. However, in a series of studies, nitrogen tetra-coordinated complexes of beryllium of the type $[BeL_4]^{2+}$ where L = pyridine, methyl imidazole and carbodiimide have been synthesized *in situ* from beryllium metal and iodine. Using the same technique, the $[BeBr_2(CH_3CN)_2]$ complex has been isolated while the analogous $[BeCl_2(CH_3CN)_2]$ complex was characterised in solution elsewhere.[56-60]. *N*-coordination to beryllium by other ligands such as cyanide, dimethylcyanamide, 4,4-bipyridine and morpholine have also been illustrated *via* reaction of the ligand with the more versatile bis-tetraphenylphosphonium hexachlorodiberyllate, $(Ph_4P)_2[Be_2Cl_6]$.[12, 61, 62].

Table 1-1 Selected ^{9}Be NMR chemical shifts of beryllium complexes with simple *N*-donors ligands.

Complexes	L	^{9}Be-NMR shift (ppm)	Ref
$[BeL_4]^{2+}$	NH_3	3.3	8
$Be_2(OH)L$	NH_3	3.1	8
$Be_2(OH)_2L$	NH_3	2.9	8
$Be_3(OH)_3L$	NH_3	2.4	8
$[BeF_4]L_n$	NH_3	1.5	8
L_2BeCl_2	benzonitrile	2.01	14
L_2BeCl_2	3,5-dimethylpyridine	1.73	14
$LBe(OEt)Cl_2$	pyrazole	1.04	14
$[L_2Be(\mu\text{-}OEt)Cl_2]_2$		5.57, 5.97	14
L_2BeCl_2	pyrrolidine	1.70	14
L_3BeCl		1.64	14
L_2BeCl_2	piperidine	-0.95	14

1.10 Anionic monodentate *N*-donor ligands

Simple inorganic derivatives of beryllium *N*-coordinated pseudohalides BeX_2 [X = CN^-, NCS^-, N_3^-] are well known and have been covered by several early reviews.[11] Recent studies however, have paid considerable attention to the Lewis acidic behaviours of the metal centres in these compounds toward the isolation and structural characterisation of simple adducts of the type BeX_nL_{4-n} [n = 0-2] where L can also be *N*-coordinated neutral Lewis base donors such as acetonitrile and pyridine.[11, 63-67] Further interest in these complexes has been geared towards obtaining metal framework structures in the solid state from the Lewis acid-base adduct of binary cyanide, thiocyanate and azide.[66-68] Although belated, the structural confirmation of the beryllium azide derivatives in comparison to related main group metals have equally revealed interesting oligomeric cages involving terminal and bridging azides.[69, 70] The azidohalidoberyllate anionic complexes $[Be_4X_4(\mu\text{-}N_3)_6]^{2-}$ X=Cl, Br **1** featuring an adamantane cage structure were prepared from trimethylsilylazide and the corresponding halidoberyllate $[Be_2X_6]^{2-}$.[71] Similar

metathesis alongside a hydrolytic reaction with Me_3SiOH afforded the dimeric beryllium complex $(Ph_4P)_2[Be(\mu\text{-}OSiMe_3)(N_3)_2]_2$ **2** with bridging siloxido and terminal azides.[72] Other terminally bound azide Lewis acid –base complexes of beryllium described includes $Be(N_3)_2L$ where L = pyridine and THF.[69, 73]

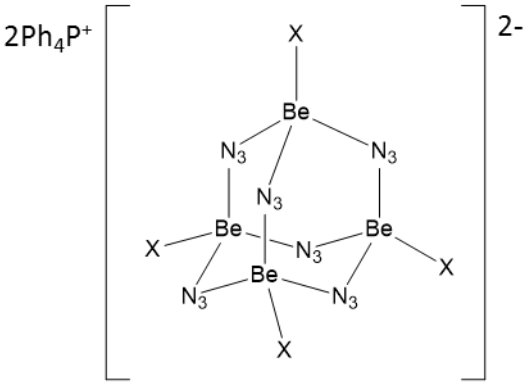

1 [X = Cl, Br]

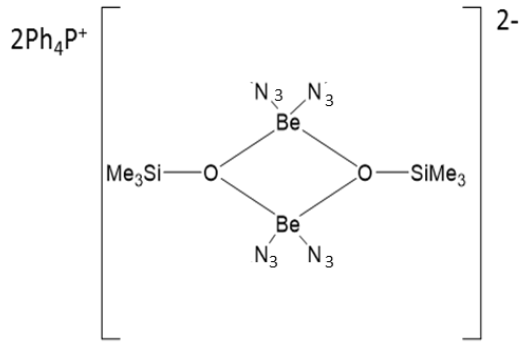

2

The chemistry of beryllium amides and related derivatives has been investigated quite extensively and in particular, ^9Be NMR spectroscopy was employed in describing the coordination at the beryllium centre. Based on the collection of NMR data the structures of many of the synthesised beryllium amide compounds were convincingly described, most of which have been considered elsewhere in a review of metal amides.[13] Recently, greater light has been shed on the linear monomeric NBeN framework in the previously proposed two-coordinated beryllium trimethylsilylamide $Be[N(SiMe_3)_2]_2$.[74] In comparison to the Be-N found in a similar but heteroleptic two-coordinate beryllium amide $BeL[N(SiMe_3)_2]$ (Be-N = 1.562 Å) where L=2,6-Mes_2-C_6H_3, the $Be[N(SiMe_3)_2]_2$ species reveals rather short Be-N bond distances of 1.525 and 1.519 Å suggesting the possibility of Be-N π-bonding.[75] While employing other more bulky imine ligands, Neumüller and Dehnicke have vastly explored the chemistry of beryllium phosphoraneiminato complexes reporting interesting Be-N ring clusters.[71, 76] The tetra-coordinate requirement for the Be^{2+} cation as well the ability of the $[R_3PN]^-$ ligands to coordinate metal centres *via* a variety of terminal, μ_2-*N*- or μ_3-*N*-bridging bonding modes readily have afforded monomeric and oligomeric structures including the heterocubane structural motif $[MX(NPR_3)]_4$.[77] The tetrameric beryllium phosphoraneiminato complexes $[Be_4Cl_4(\mu_3\text{-}Cl)(\mu_3\text{-}NPEt_3)_3]$ **3** and $[BeCl(\mu_3\text{-}NPEt_3)]_4$ **4** with a heterocubane structure were readily obtained from the

thermolysis of the donor-acceptor complex $BeCl_2(Me_3SiNPEt_3)$ at 160 °C. In addition, a tetrameric adduct of two dimers $[BeCl_2(\mu\text{-}HNPEt_3)]_2$ **5** was formed alongside as a by-product due to the abstraction of Cl^- ion from CH_3Cl and protonation of the imide nitrogen. While the X-ray crystal structure of **3** revealed a near perfect Be_4N_4 cubanoid core with correspondingly similar N-Be-N angles, the exchange of a μ_3-$NPEt_3$ with μ_3-Cl in **3** drastically distorts the heterocubane (Figure 1-9).

Similarly, a trimeric phosphoraneiminato beryllium complex $[Be_3Cl_2(NPPh_3)_4]$ was prepared by the reaction of $(Ph_4P)_2[Be_2Cl_6]$ with $[LiNPPh_3]_6$ while an additional monomeric complex $[BeCl_2(HNPPh_3)_2]$ was isolated as a by-product.[76] Generally, beryllium phosphoraneiminato complexes predominantly revealed the bent Be-N-P moiety with Be-N-P angles ranging from 125-134° while Be-N bond distances in the μ_3-*N*-PR_3 complex ranges between 1.737-1.759 Å were slightly shorter than in the μ_2-*N* phosphoraneiminato complexes $[Be_3Cl_2(NPPh_3)_4]$ (1.779-1.790 Å).[12]

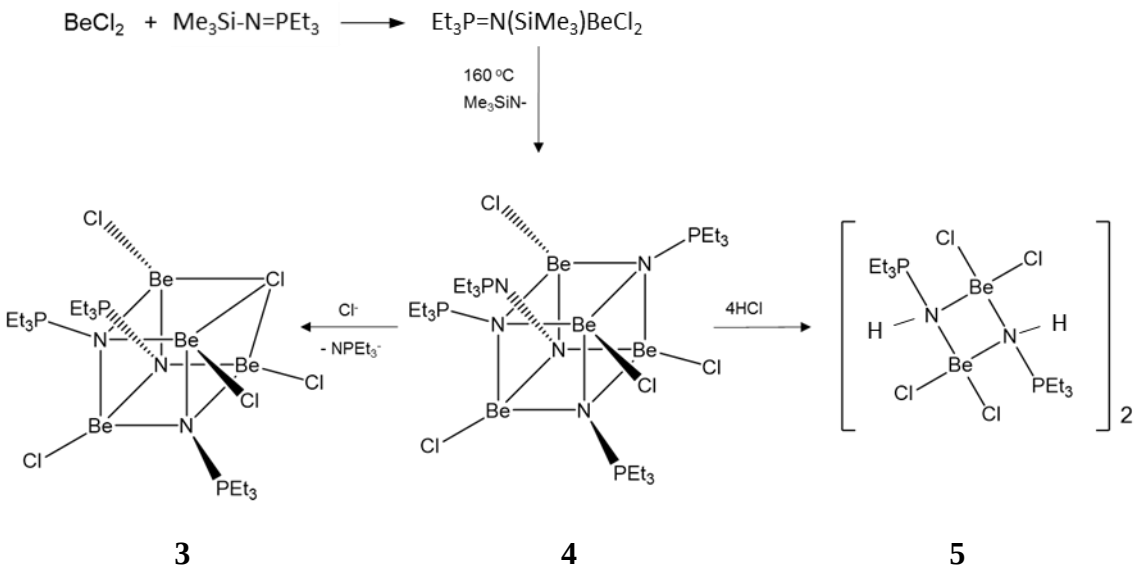

Figure 1-9 Selected beryllium phosphoraneiminato complexes (see ref. [76]).

1.11 Bidentate and tridentate *N*-donor ligands

1.11.1 Four-membered ring chelates

Although the chelate effect is expected to confer additional stability, beryllium complexes containing bidentate *N*, *N*-donor ligands are equally rare and

require considerable steric bulk for their stability. Among the family of typical *N, N* four-membered ring chelating ligands, only the beryllium complexes of amidinate and diiminophosphinate ligands have been reported.[75, 78, 79] Transmetallation reactions of beryllium chloride with the lithium amidinate $Li(NSiMe_3)_2C$-Ph resulted in a monomeric bis(amidinate) $Be(NSiMe_3)_2C$-Ph **6** and the dimeric complex $(Me_3Si)_2N$-$Be_2\mu$-$(NSiMe_3)_2C$-Ph **7** with a bridging amidinate unit.[75] The anionic beryllium dichloro amidinate $[BeCl_2(NSiMe_3)_2C\text{-Ph}]^-$ **8** have been prepared from the reaction of bis(tetraphenylphosphonium) hexachlorodiberyllate $(Ph_4P)_2[Be_2Cl_6]$ with *N,N,N'*-tris(trimethylsilyl)amidine Ph-C[$N(SiMe_3)_2(NSiMe_3)$].[79] Similarly, the $[Be((NSiMe_3)_2PPh_2)_2]$ complex **9** featuring a 1:2 monomeric beryllium complex was obtained from metal exchange with the lithium derivative.[78] X-ray structures have revealed a small bite angles of 79.6° in **6** and 86.1° in **9** resulting in a distorted tetrahedral metal centre. This chelate ring strain in **6** perhaps explains the formation of an additional dimeric co-product **7** in which the amidinate occupies a more comfortable position bridging two beryllium metal centres. Furthermore, the different coordination environments of beryllium in the monomeric and dimeric beryllium amidinates is consistent with their ^{9}Be NMR chemical shifts in which the more symmetrical bis(amidinate) was observed at 5.5 ppm alongside a significantly narrower peak width in comparison to the dimeric amidinato beryllium complex observed at 11.4 ppm.

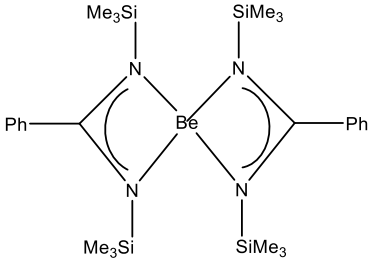

6

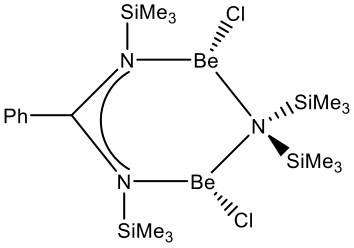

7

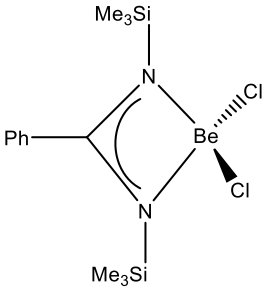

8

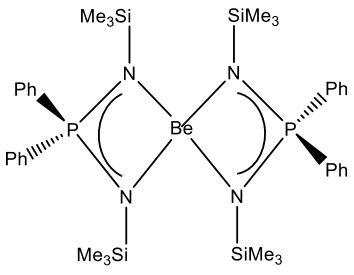

9

1.11.2 Five-membered ring chelates

Beryllium complexes with anionic nitrogen-donor ligands such as 2-(2-pyridyl)indole, substituted 1,4-diazabutadiene and cyclohexyl-1,2-diamine which coordinate to form five-membered chelate rings are known (Figure 1-10).[73, 80, 81] Single crystal X-ray structure determinations showed monomeric 1:2 beryllium complexes of the type BeL_2 although a dimeric adduct with THF was also observed for the 1,4-diazabutadiene ligand. Also, the beryllium complex of 2-(2-pyridyl)indole gave the first illustration of the electroluminescence from an all *N*-donor beryllium complex.

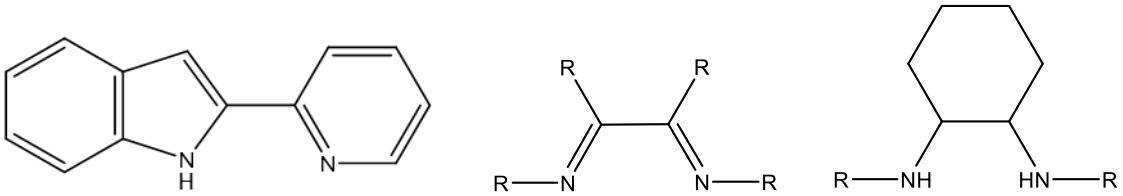

2-(2-pyridyl)indole 1,4-diazabutadiene cyclohexyl-1,2-diamine

Figure 1-10 Five-membered ring *N*,*N*-chelating ligands

So far, the only complex illustrating tridentate coordination to beryllium *via* *N*-donor atoms has been synthesised using the pincer type pentamethyldiethylentriamine ligand (PMDETA). In this complex **10** the beryllium centre is partially encapsulated by two five-membered chelate rings and a terminal chloride.[82] On the other hand, the bidentate tetramethylethylenediamine (TMEDA) ligand forms both 2:2 and 2:1 dinuclear beryllium complexes $[HBe\text{-}\mu\text{-}NMe_2C_2H_4NMe_2]_2$ **11** and $[(BeCl_3)_2NMe_2C_2H_4NMe_2]^{2-}$ **12**. The former involves the two TMEDA ligands each chelating a beryllium centre while the second nitrogen donor bridges both beryllium centres to form a Be_2N_2 core.[79, 82]

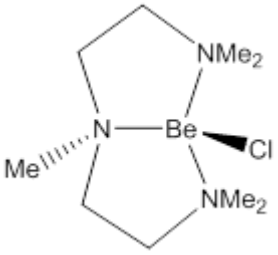

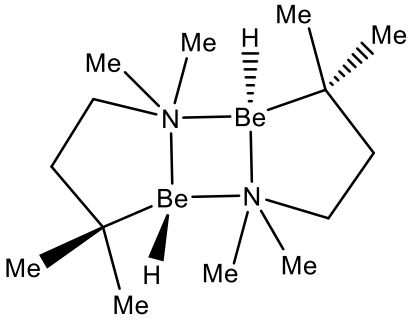

10 **11**

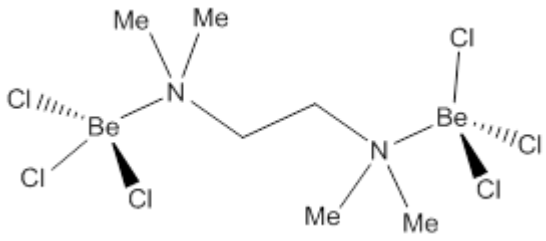

12

1.11.3 Six-membered ring chelates

Heteroleptic beryllium complexes of the type [LBeX] have been synthesised and structurally characterised where L includes *N*-chelating bidentate *β*-diketiminate $HC(CMeNDipp)_2$ (Dipp = 2,6-diisopropylphenyl), diphenylphosphininomethane $[CH(PPh_2N\text{-}2,6\text{-}i\text{-}Pr_2C_6H_3)_2]$ and tridentate tris(1-pyrazolyl)borate.[83-86] In these investigations, a variety of beryllium complexes involving a range of X substituent (halides, amides, alkyl, hydroxyl) obtained by ligand substitution and metathesis reactions, were structurally characterized by X-ray crystallography and their ^{9}Be NMR chemical shifts. Having played a successful role in the isolation of main group metal complexes with the metal centres in a lower oxidation state,[83] beryllium complexation with the *β*-diketiminate group of ligands are of interest in the quest to demonstrate similar chemistry. Furthermore, the controllable change in the beryllium coordination environment by facile manipulation of the X substituent (in **13**-**14**) has been useful in investigation of ^{9}Be NMR spectroscopy as an alternative tool for the *in situ* characterisation of beryllium complexes (Table 1-2).

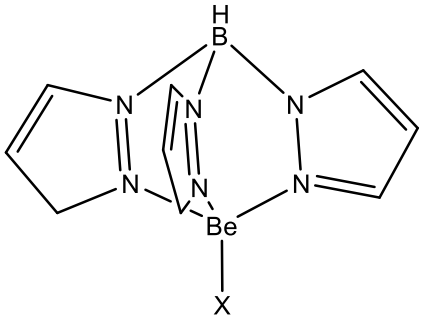

13

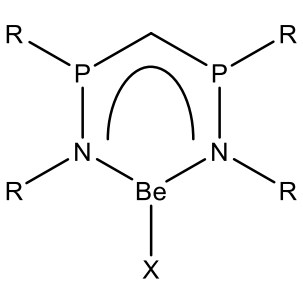

14

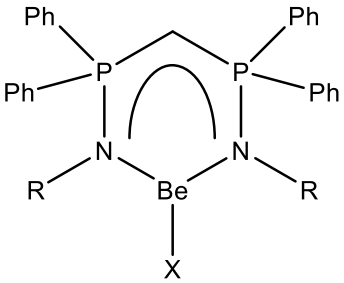

15

Table 1-2 Selected ^{9}Be NMR chemical shifts of beryllium complexes containing *N*-donor with six-membered chelate rings

Compound	X	^{9}Be NMR	ref
$HC(CMeNDipp)_2BeX$	Cl	12.2	41
	I	13.4	41
	Me	16.6	41
	^{n}Bu	14.9	41
	OH, OCH_3, OPh	8.0	41
	$OC(CH_3)_3$	6	41
$[CH(PPh_2N\text{-}2,6\text{-}i\text{-}Pr_2C_6H_3)_2]BeEt$	Et	15.62	42
$[C(PPh_2NSiMe_3)_2]\text{-}(BeEt)_2$	Et	0.93	42
$[C(PPh_2NPh)_2](BeEt)$	Et	19.23	42
TpBeX	Cl	5.23	44
	I	4.85	44
	Br	5.15	44
	F	4.54	44
	H	5.11	44
	N_3	3.30	44
$(Tp)_3Be_3(OH)_3$		4.38(20^{o}C)	12

In a series of other studies, the pyrazolylborate ligands were investigated in aqueous solution as complexing agents for the selective extraction of the Be^{2+} cation.[87-89] Interestingly, these are the only group of nitrogen ligands, which have shown significant complexation of beryllium over hydrolysis and oligomerisation. Although pyrazolylborate can be potentially tridentate as has been observed in non-aqueous media, the bidentate coordination *via* two of its pyrazolyl groups is the stable structural arrangement in aqueous solutions. However, the tetrakis(1-pyrazolyl)borate tends to form stable BeL_2 complexes up to a pH of 4.5 while the tris(1-pyrazolyl)borate which has one less pyrazolyl group yields a stable $Be_3(OH)_3L_3$ complex at pH 3.5. Therefore, based on liquid-liquid extraction studies on the homologous series of pyrazolylborates $[H_nB(pz)_{4-n}]$ (n = 0-2, pz=pyrazolyl), the order of stability of their monomeric beryllium complexes was proposed to be $[B(pz)_4]_2Be$ > $[HB(pz)_3]_2Be$ > $[H_2B(pz)_2]_2Be$ due to the decrease in strain energy

of the free ligand upon complexation with beryllium. Additionally, the stability of the $Be_3(OH)_3L_3$ complex (L= tris(1-pyrazolyl)borate) is attributed to the favourable hydrogen bonding between the beryllium hydroxido core and the remaining uncoordinated pyrazolyl group.[55]

1.12 *N*-donor macrocyclic ligands

Contrary to the customary belated structural exploration of beryllium complexes with regular ligands in coordination chemistry, the phthalocyaninato complex of beryllium was among the earliest metal phthalocyaninates described.[90] Its X-ray structure reveals a beryllium ion observed to be in a very unusual four-coordinate planar geometry enforced by the rigidity of the macrocyclic aromatic rings with elongated Be-N bonds of 1.856-1.864 Å. This coordination is quite unfavourable for the beryllium metal and as a result, the complex is very reactive and unstable. Also, in comparison to the other group 2 metal phthalocyaninato complexes, intermolecular interactions between beryllium and the aromatic rings of molecules in neighbouring stacks were absent.[91] Further exploration of this beryllium complex has provided many derivatives by straightforward recrystallisation with the desired secondary ligand. In the solid state, these beryllium complexes are interesting because they reveal a beryllium metal centre in a square pyramidal five-coordinate geometry consisting of axially coordinated secondary ligands L and other adducts. (L = H_2O, 4-picoline, 3-picoline, 3-cyanopyridine, 4-cyanopyridine).[91-95] Molecular structure of these beryllium complexes such as the $BePcH_2O$ (Pc= phthalocyanine) also show extensive π-π stacking into saucer-shaped dimers wherein the axially coordinated aqua ligand engages in hydrogen bonding to the azamethine nitrogen (Figure 1-11). Subsequent exchange reaction at the axial coordination site have revealed the substitution of *N*-ligating molecules by aqua ligand upon exposure to moisture.[94]

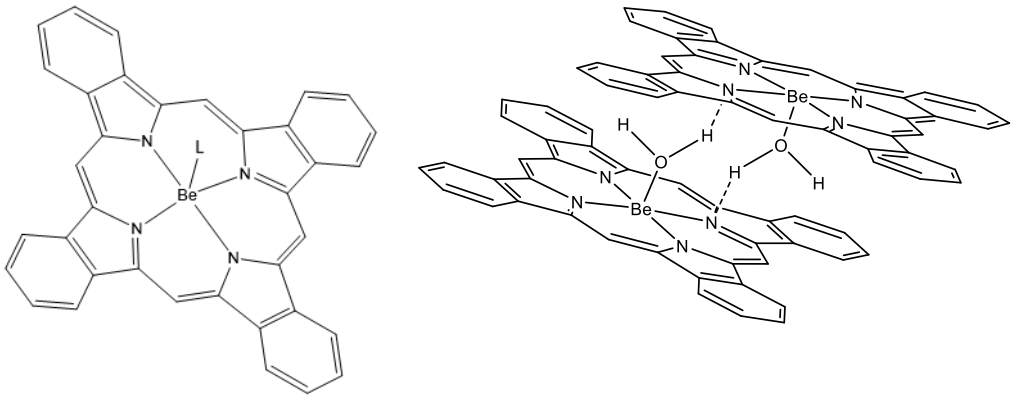

Figure 1-11 Phthalocyaninato beryllium complex

1.13 *N/O* mixed donor ligands

As expected, ligands containing a combination of N and O donor atoms coordinate to beryllium more strongly than nitrogen-only donor ligands since the more electronegative oxygen donor provides an extra driving force for beryllium complexation. More surprising is the excellent complexation of beryllium by these ligands, which in some cases is higher than *O/O* donor bidentate ligands. For instance, the *N/O* donor ligand 10-hydroxybenzoquinolone (HBQ) (log k = 17.0), binds beryllium more strongly than excellent beryllium binders such as chromotropic acid (log k = 16.2) and salicylic acid (log k = 12.4) suggesting that other stabilising contributions towards the beryllium complexation can outweigh its well-known oxophilicity.

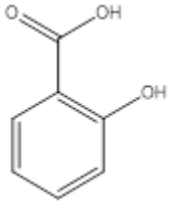

Salicylic acid

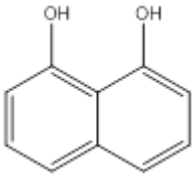

Chromotropic acid

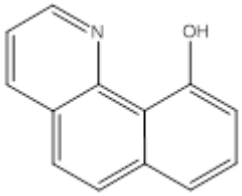

10-Hydroxybenzoquinolone (HBQ)

An explanation of this is related to the small size of the Be^{2+} cation which closely correlates it to a kind of "tetrahedral proton" capable of displacing uniquely hydrogen bonded protons ($N\cdots H\cdots O$ or $O\cdots H\cdots O$).[96, 97] These hydrogen bonds, distinguished by their shortened $N-O$ or $O-O$ distances compared to the Van der Waals radii, have been observed among good beryllium binders such as HBQ, citrate, chromotropic acid as well as proteins.

A key feature of mixed *N/O* donor set of ligands is their selectivity towards the Be^{2+} cation and notable fluorescence behaviour upon complexation with beryllium ions. Consequently, this property is continuously being explored in the design of electroluminescent materials,[98-104] and fluorescent indicators/reagents in environmental and physiological detection of beryllium (see Figure 1-12).[47, 105-109]

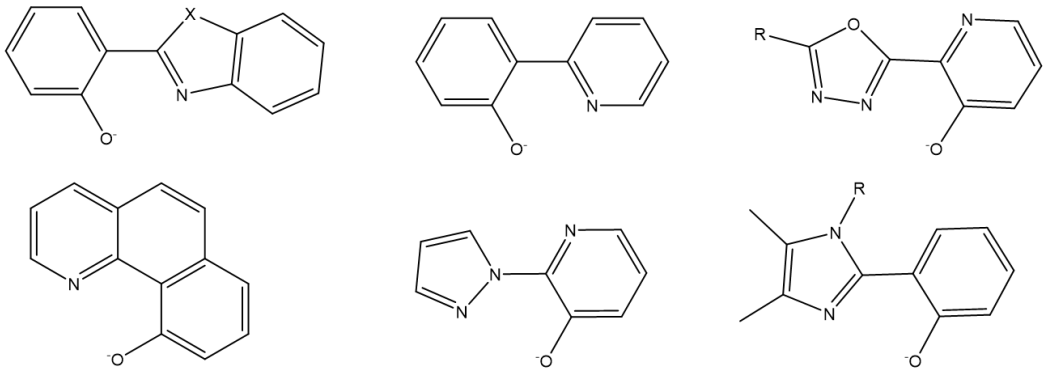

Figure 1-12 Beryllium bischelating N/O donor ligands based on phenol- imidazole/pyridine motifs

Furthermore, extensive solution-based investigations on interaction of Be^{2+} with *N/O* coordinating ligands capable of multidentate coordination to beryllium and their associated stability constants have been determined.[110-113] These ligands which mainly consist of the aminopolycarboxylic acids are of interest due to their successful application in chelation therapies.[114] A notable fact about these ligands is the poor interaction of EDTA with beryllium unlike the nitrilotriproprionate (NTP) ligand which complexes beryllium quite well (log k=9.23).[110, 113] Based on the strong and selective binding of beryllium by NTP, other more rigidly pre-organised tetradentate ligands have been designed and investigated with an interest in their being an exclusive encapsulating agent for beryllium (Figure 1-13).[115]

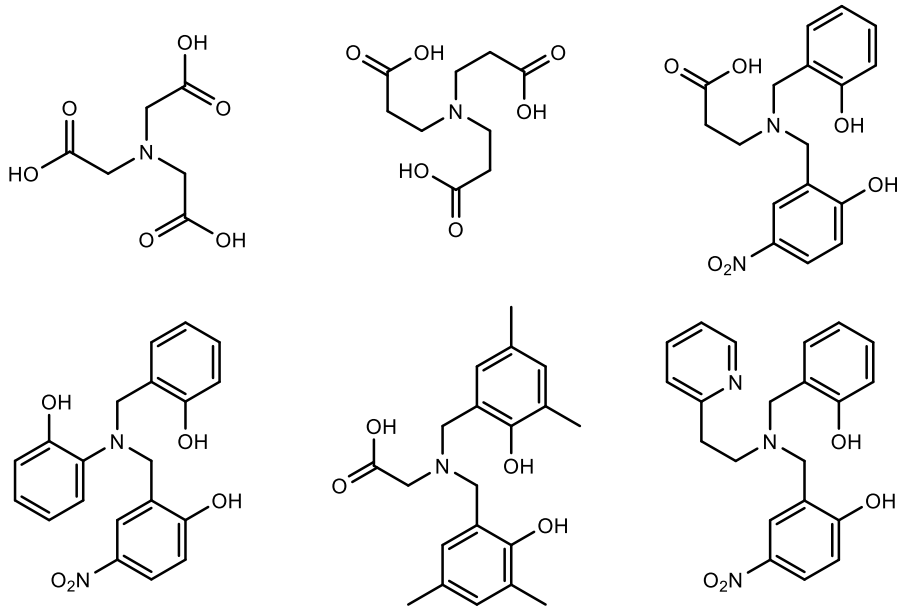

Figure 1-13 Multidentate *N*/*O*-ligands investigated for the potential encapsulation of beryllium

From a ligand design perspective, additional interest in the *N/O* donor group of ligands comes from the advantage of a nitrogen atom as being a more versatile donor atom, which allows for the design of tailor-made multidentate ligands potentially capable of selectively encapsulating the Be^{2+} cation. The complete encapsulation of Be^{2+} cation by tetradentate coordination from a single ligand has only been structurally illustrated by the aminopolycarboxylate and salen type ligands.[110, 116] For the salen type ligands, full encapsulation by a single ligand was achieved by linking two bidentate salicyladimine ligands by their nitrogen atom, to provide a tetrahedral binding pocket as shown in beryllium complexes **16-18** (Figure 1-14).

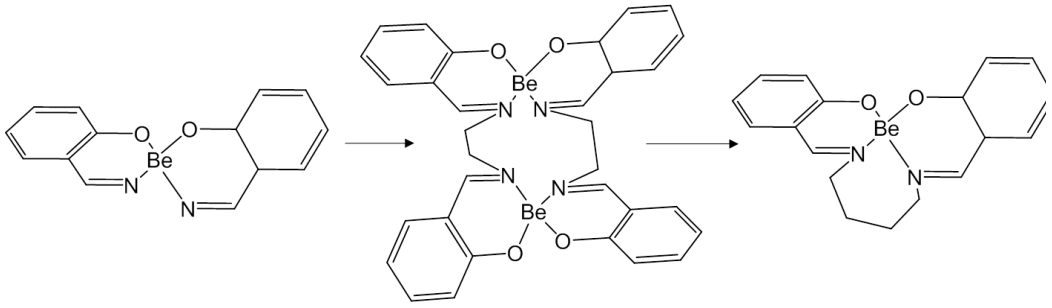

16 **17** **18**

Figure 1-14 Progression in beryllium encapsulating ligand design from a bischelating salicyladimine to the tetradentate salen ligands

1.14 Methodologies

1.14.1 Electrospray ionisation mass spectrometry - basics

An invaluable and unique piece of information required for the discernment of the constituent of any chemical species is the knowledge of its molecular weight which can be obtained from mass spectrometry (MS). Given that the mass of a substance (in addition to other information such as isotope and fragmentation patterns) is often a unique property, mass spectrometry is highly relevant in any chemical analysis as long as the following two conditions can be fulfilled. Firstly, the chemical species must be charged (either positive or negative) or at least be able to acquire a charge. Secondly, the charged chemical species (ions) must be transferred into the gas phase (for only in the gas phase can mass analysis be executed). Consequently, a mass spectrometry technique consists of an ion source/sample inlet, mass analyser and mass detector as shown in Figure 1-15.

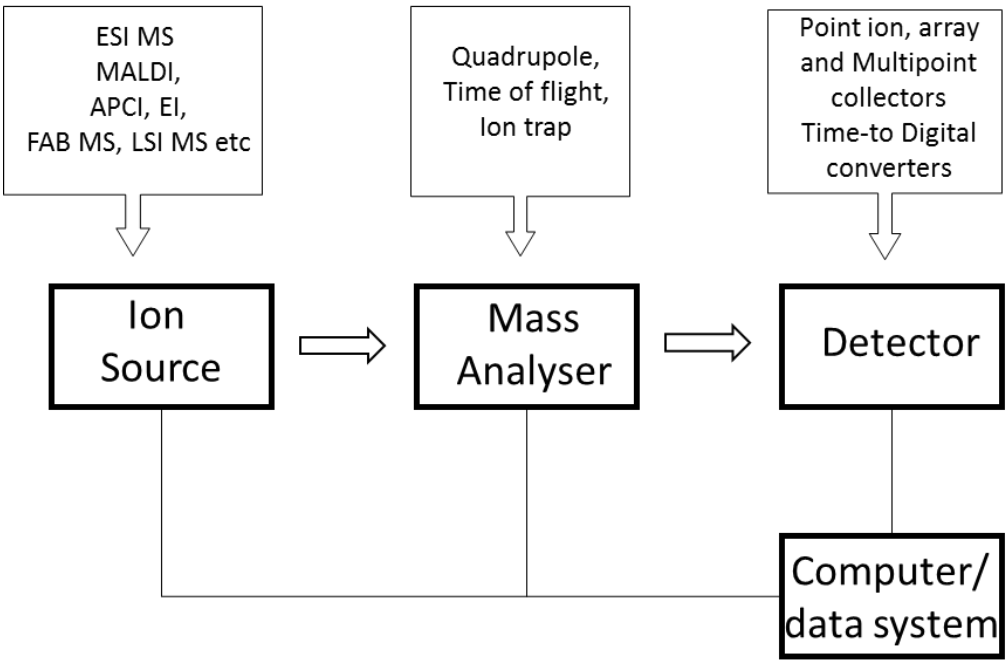

Figure 1-15 Schematics of a mass spectrometer.

In order to expand the application of mass spectrometry to all phases (solid, liquid and gas), various sample inlet/ion sources exist but the technique of interest to this research is electrospray ionisation mass spectrometry (ESI-MS). By

transferring pre-existing solution phase ions into the gas phase, ionisation by the electrospray has granted mass spectrometric access to a wide variety of compounds especially thermally fragile, non-volatile and high molecular weight biological molecules; an area in which it was first applied[117]. However, ESI-MS is equally well-suited for the analysis of inorganic and organometallic compounds.[118] The simplicity of this method has evolved the ESI-MS into a popular support tool for the characterization of organometallics and coordination complexes.

The idea of electrospray as an ionisation technique was initially conceived by Malcolm Dole[119] while John B. Fenn successfully coupled an electrospray ionisation source to a mass analyser in an achievement for which he shared the 2002 Nobel Prize in chemistry.[120] Electrospray ionisation involves pumping the mobile phase through a capillary nozzle held at a high voltage (see Figure 1-16).

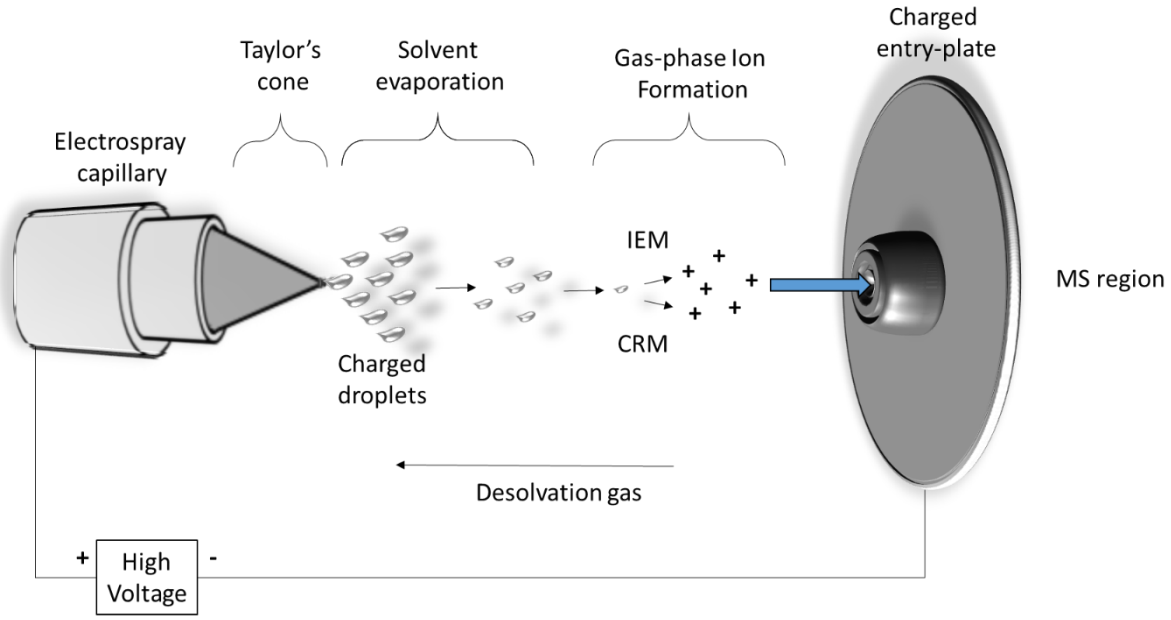

Figure 1-16 The electrospray process.

Under the influence of the electric field, the solution assumes a conical shape (Taylor's cone) at the tip of the needle and emerges as a spray of fine droplets with excess charges on the surface. The counter current flow of a curtain gas evaporates the solvent resulting in droplet shrinkage and a concomitant increase in repulsion of the surface charges. A limit is reached (Rayleigh limit) at which charge repulsion exceeds the surface tension of the solvent such that parent droplet subsequently,

ejects several other daughter droplets (Coulomb explosion). Two models have been proposed to explain experimental observations of the mechanism by which gas phase ions are produced. The Charge Residue Model[121] initially proposed by Dole suggests that solvent evaporation and Coulomb explosion continues repeatedly until gas phase analyte ions are left bare while Iribarne and Thomson's Ion Evaporation Model[122] explains that below a particular diameter (10 nm), it becomes more favourable for gas phase analyte ions to simply evaporate from the droplet's surface. While the two models may be indistinguishable because of the very small radii involved, they both agree that gas phase ions result from tiny solution droplets and this has led to modifications such as the nanospray. The resultant gas phase ions are then drawn into the mass analyser passing through skimmer orifices positioned to effectively discriminate the entrance of neutrals and solvent molecules. By reversing the electric field the instrument can be operated in a positive or negative ion mode for the transfer of cationic or anionic solution species into the mass spectrometer. Finally, the ions are detected and presented as a spectrum of intensity against mass-to-charge ratio.

1.14.2 High resolution MS with orthogonal time of flight analyser

The time of flight (TOF) mass analyser is a relatively old and simple means of mass analysis reinvigorated within the last decade. Its basic principle involves measuring the amount of time it takes discharged ions of equal kinetic energy to travel along a tube of fixed length. Accelerating the ions through an electric field provides a uniform kinetic energy and if they are of the same charge, the time of travel would be proportional to their masses (and charges). A key advantage of time of flight mass spectrometry is its high mass range (although not critical in these studies), high ion transmission and simultaneous detection of all species. A consequence of the latter is that all ions have to start off at the same time making the TOF analyser naturally adaptable to pulsed ionisation sources such as the MALDI and less adaptable to continuous ion sources such as ESI. However, this can be circumvented by enforcing orthogonal acceleration (oTOF) via a repeller or pulsing electrode positioned to generate an electric field gradient at right angles (orthogonal) to the continuous beam of ions that will push a pulse of ions in the flight tube. Another important component in a TOF mass analyser employed to improve resolution is the reflectron. A reflectron is an electrostatic mirror used to

induce a 'U-turn' on the ions such that they are reflected and travel along a second path. High resolution is achieved using a reflectron firstly because, it increases the flight distance travelled as well as the time taken, thereby allowing a better distribution of ions according to their *m/z* values. Secondly, in practice, ions of similar *m/z* value would not attain the same kinetic energy nor would they start at the same time resulting in different time of arrival. However, the reflectron introduces a levelling effect which refocuses all ions of the same *m/z* values such that they attain a uniform arrival time at the detector. This is possible mainly because ions with greater kinetic energy travel farther into the reflectron before returning while ions with lower kinetic energy barely penetrate the reflectron therefore they all arrive at approximately the same time. The ESI-TOF-MS was employed in this study mainly because of its high resolution, relevant in accurate peak assignment.

1.14.3 MS/MS with quadrupole ion trap analyser

Collision induced dissociation (CID) experiments, (often denoted as MS^n where n is the number of steps) can be carried out utilising ion trap mass spectrometry. CID is also possible with ESI-TOF-MS by adjusting the instrument parameters particularly the capillary exit voltage (CEV), to provide harsher ionisation conditions but the fragment ions produced can only be observed simultaneously with the mixture of all parent ions resulting in complex spectra. However, with ion trap mass spectrometry, individual ions (both parent or fragment ions) can be selectively examined from a mixture of ions. Mass analysis by the ion trap involves manipulating, differentiating and subsequently ejecting ions according to the frequencies at which they oscillate in an rf field which also corresponds to their *m/z* values. MS^n can also be achieved on the trapped ions creating a variety of applications for this mass analyser in gas phase studies. The architecture of the ion trap consists of two endcaps and one ring electrode, all of hyperbolic geometry assembled such that the application of a potential on the electrodes generates a quadrupole field that can destabilise or stabilise certain ions within its cavity. By tipping the field's potential towards a particular direction, ions can be confined or expunged in a controllable manner (according to their *m/z*).

1.14.4 *Ab initio* molecular dynamics (AIMD)

Molecular dynamics is a computational technique that involves the stimulation of the microscopic state of a system and its dynamic evolution with time. Starting from an initial set of positions and velocities, a molecular dynamics step is carried out by calculating the forces acting on the atoms or molecules and integrating the Newtonian's equation to yield a new set of positions and velocities. The iteration of this process with time yields a trajectory of the atoms in a system at a microscopic level, which is then correlated to experimental quantities of the real system by the subject of statistical mechanics. The fundamental issues involved in the molecular dynamics simulation and details of established methodologies are beyond the scope of this project however, it must be emphasised that the most important consideration in molecular dynamics (just as in computational chemistry in general) is to employ models which adequately describe the real system as much as possible.[123, 124] For instance to counter the exaggerated surface effect potentially present in the simulation of a finite system, periodic boundary conditions (PBC) are employed whereby the simulation box is virtually replicated to form an infinite lattice shown in Figure 1-17. Over the course of the simulation, when a particle moves out of the simulation region, its periodic image moves in exactly the same way so that at least in principle the system has no surface and resembles the macroscopic bulk (although PBC in itself introduces other artefacts to the simulation).

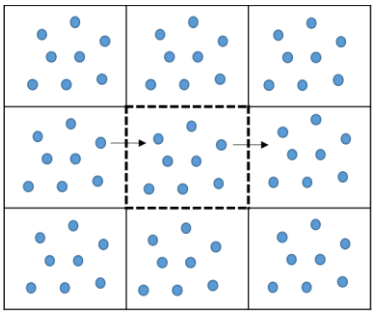

Figure 1-17 Illustration of periodic boundary condition to eliminate surface effect in MD simulations

The two variants of molecular dynamics, (which are classical molecular dynamics, and *ab initio* molecular dynamics) differ only in the mode of generating the forces acting on the atoms. In the former, atoms as treated as classical particles by considering only their nuclear degrees of freedom while the electronic degrees

of freedom are replaced by interaction potentials known as force fields that are predesigned empirically or from externally calculated electronic structure. This greatly simplifies the calculation such that larger systems can be stimulated but with the disadvantage of being unable to stimulate chemical reaction within the realm of electronic structure. On the other hand, *ab initio* molecular dynamics goes beyond the traditional approach and incorporates the electronic structure calculation "on the fly". This therefore enables the stimulation of actual chemical events such as bond breaking and forming and polarisation effects with a swarm of explicit solvent molecules alongside the concomitant increase in the computational cost.

1.14.5 Incorporating electronic structure calculation into molecular dynamics

In this research, the Car-Parrinello (CP) variant of *ab initio* molecular dynamics referred to as Car-Parrinello molecular dynamics (CPMD) was executed employing the Hohenberg-Kohn-Sham approach of density functional theory to calculate atomic forces.[125] According to the Kohn-Sham formulation,[126] the total ground state energy of an interacting system of electrons with classical nuclei is obtained as the minimum of the Kohn-Sham energy which is decomposed into the energy functional shown in eqn (2-1);

$$E_{DFT} = T_S[\rho] + E_{ne}[\rho] + J[\rho] + E_{xc}[\rho] \qquad (2\text{-}1)$$

$T_S[\rho]$ is the so called Kohn-Sham kinetic energy of a non-interacting reference system.

$E_{ne}[\rho]$ is the external potential on an interaction system which is the attraction between the nuclei and electrons (noting that the nuclear-nuclear repulsion is a constant within the Born-Oppenheimer approximation)

$J[\rho]$ is the Hartree potential due to the electron-electron interaction.

The fourth term $E_{xc}[\rho]$ is the relatively minor but critical exchange and correlation energy, which is an unknown term that can only be estimated from various functional expressions. Although new functional are constantly proposed in a continuum thought to culminate into a 'divine functional'(akin to Jacob's ladder

leading unto heaven) the generalised gradient approximation (GGA) methods have been shown to be the most compatible with AIMD.[127, 128] The Becke's exchange along with Lee, Yang and Parr correlation functional (BLYP) remains one of the better for the description of liquid water although potential shortcoming of the BLYP functional in comparison to other GGAs have equally been pointed out.[129-131] While attempts to incorporate other functional especially the hybrid and parameterized functional are being considered,[127] these more demanding functional puts *ab initio* molecular dynamics beyond the realm of present day computer capabilities.

The task of unifying electronic structure (quantum) with molecular dynamics (classical) stimulations was achieved by Roberto Car and Michele Parrinello in 1985 by formulating the Langrangian shown in eqn (2-2) where the orthonormality of the orbitals must be kept by the Lagrange multipliers Λ_{ij}.[132]

$$\mathcal{L}_{\mathrm{CP}} = \sum_I \frac{1}{2} M_I \dot{\mathbf{R}}_I^2 + \sum_i \frac{1}{2} \mu_i \langle \dot{\phi} | \dot{\phi} \rangle - \langle \Psi | H_e^{KS} | \Psi_0 \rangle + \sum_{i,j} \Lambda_{ij} \left(\langle \phi | \phi \rangle - \delta_{ij} \right) \qquad (2\text{-}2)$$

Where the electronic degrees of freedom are given an artificial inertia known as the fictitious mass parameter μ. The required equation of motion can be obtained from the Euler-Lagrange equation for the nuclear positions and orbitals in eqn (2-3) and (2-4)

$$\frac{d}{dt} \frac{\partial \mathcal{L}}{\partial \dot{\mathbf{R}}_I} = \frac{\partial \mathcal{L}}{\partial \mathbf{R}_I} \qquad (2\text{-}3)$$

$$\frac{d}{dt} \frac{\partial \mathcal{L}}{\partial \dot{\phi}_i^*} = \frac{\partial \mathcal{L}}{\partial \phi_i^*} \qquad (2\text{-}4)$$

which generates the corresponding Car-Parrinello equations of motion in eqn (2-5) and (2-6).

$$M_I \ddot{\mathbf{R}}_I(t) = -\nabla_I \langle \Psi | H_e^{KS} | \Psi_0 \rangle \qquad (2\text{-}5)$$

$$\mu \ddot{\emptyset}_i(t) = -H_e^{KS} \emptyset_i + \sum_{i,j} \Lambda_{ij} \emptyset_j \qquad (2\text{-}6)$$

A key ingredient that brought AIMD simulations into the realm of practical applications as reflected by its increasing popularity over the last decade is the pseudopotential and plane wave approach. This entails using a pseudopotential to replace both the atomic nucleus and the core electrons by a fixed potential which represents the nuclear potential and the orthogonality requirement while the valence electrons are expanded with the plane wave basis set. The inherent synergy in the practical implementation of the pseudopotential and plane wave approach alongside periodic boundary conditions makes this a very efficient and effective strategy in AIMD simulations.[127]

1.15 Research aims and objectives

The research reported in this thesis is part of a bigger project "The Good without the Bad: Selective Chelators for Beryllium" (Marsden contract 12-MAU-047) which is aimed at the design and synthesis of beryllium specific ligands, capable of strong and selective interaction with beryllium for industrial and environmental applications.

In line with the parent project, the goal of this present research, is to extensively investigate beryllium coordination chemistry and solution speciation using electrospray ionisation mass spectrometry (ESI-MS) as a screening technique to identify beryllium complexation. Without doubt, the search or design of a competitive and selective beryllium chelator will require an improved understanding of the fundamental requirements for the coordination of a variety of ligands to beryllium while at the same time meeting the challenges of working with this toxic element. Therefore, the specific objectives of this thesis are

- Establishing the proof of concept for the metal-ligand combinatory approach in utilising ESI-MS as an experimental technique to probe beryllium speciation in solution while generating information on the beryllium-ligand binding processes and reactivity.
- Analysing the aqueous speciation of simple beryllium compounds and thermodynamically stable beryllium complexes containing important classes of ligands and biomolecules using ESI-MS as a safe solution technique to identify predominant or new beryllium species.

- ESI-MS screening of designer ligands, competition and selectivity studies of the ligands towards beryllium and similar metal ions.
- Computational investigation to corroborate beryllium speciation from ESI-MS data and provide additional insight into beryllium reactivity in an aqueous environment.
- Attempting the macroscale syntheses of selected beryllium complexes and further characterisation using other techniques.

The role of this research in the bigger project is unique in that the high sensitivity of ESI-MS is being employed to analyse beryllium solution equilibrium species in their starting environment while competition and selectivity for a wide variety of ligands as well as analogous metal ions delineate features for selective and strong beryllium binding. This provides basic information regarding the suitability of the newly designed ligands with regards to satisfying the coordination preferences of a small cation. In parallel to ESI-MS screenings, computational chemistry technique is additionally being utilised to model a wide range of beryllium complexes to offer information on the geometric, energetic and chemical properties in correlation to ESI-MS and other experimental data. This provides invaluable information to complement ESI-MS experiments, because the mass spectra only provide information on the elemental composition of a complex, but not its structure. Furthermore, explicit treatment of the beryllium solvation environment using the rapidly growing Car-Parrinello variant of *ab initio* molecular dynamics provides detailed insights into the dynamical structure of the complexes as a function of the environment. This research is be the first to extensively use ESI-MS as a primary screening tool to explore the coordination chemistry of beryllium while the CPMD approach is unprecedented in beryllium studies.

1.16 Thesis Outline

The remainder of this thesis is divided into 6 chapters. Chapters 2-5 present result and discussions of all experiments and computational studies. Results in Chapter 2 are from the ESI-MS investigations of solutions of simple beryllium salts including beryllium sulfate and beryllium chloride. These results formed the basis for Chapter 3 in which *ab initio* molecular dynamics is used to simulate inner and outer sphere beryllium complexes with fluoride, chloride and sulfate ligands. Chapter 4 presents the ESI-MS investigation of beryllium with a variety of ligands

in solution representing important functional groups and ligand architectures in beryllium complexation. Lastly, the results and discussions in Chapter 5 involves the ESI-MS microscale screening of the selectivity and trends in binding affinity of potentially encapsulating ligands. These information are concluded in Chapter 6 and some future work are suggested. Chapter 7 which is the last chapter in this thesis reports the details of all experimental and computational work conducted this thesis. Due to the nature of this research, it was preferable to cumulate all the experimental and computational details in a latter chapter and throughout the thesis, references are made to this experimental chapter.

1.17 References

1. D. McGroarty and S. Wirtz, *Reviewing Risk:Critical Metals & National Security, American Resources Policy Network Report, 2012, http://americanresources.org/wp-content/uploads/2012/06/ARPN_Quarterly_Report_WEB.pdf. Accessed June 2017*.

2. M. A. Boland, *U.S. Geological Survey Fact Sheet, 2012, https://pubs.usgs.gov/fs/2012/3056/pdf/fs_2012_3056.pdf. Acessed June 2017.*, 2012, **3056**, 2.

3. L. S. Newman, *Chemical & Engineering News*, 2003, http://pubs.acs.org/cen/80th/beryllium.html. Accessed June 2017.

4. K. Kreiss, G. A. Day and C. R. Schuler, *Annual Review of Public Health*, 2007, **28**, 259-277.

5. C. Strupp, *Annals of Occupational Hygiene*, 2011, **55**, 43-56.

6. L. Alderighi, P. Gans, M. Stefeno and A. Vacca, in *Advances in Inorganic Chemistry*, eds. A. G. Sykes and A. Cowley, H, Academic Press, Califorornia, 2000, vol. 50, pp. 109-197.

7. A. Mederos, S. Domínguez, E. Chinea, F. Brito and F. Cecconi, *Journal of Coordination Chemistry*, 2001, **53**, 191-222.

8. C. Y. Wong and J. D. Woollins, *Coordination Chemistry Reviews*, 1994, **130**, 243-273.

9. D. A. Everest, *The Chemistry of Beryllium*, Elsevier, Amsterdam, 1964.

10. K. A. Walsh and E. E. Vidal, *Beryllium Chemistry and Processing*, ASM International, Ohio, 2009.

11. N. Bell, *Advances in Inorganic Chemistry and Radiochemistry*, 1972, **14**, 255-332.

12. K. Dehnicke and B. Neumüller, *Zeitschrift für Anorganische und Allgemeine Chemie*, 2008, **634**, 2703-2728.

13. M. F. Lappert, A. Protchenko, P. Power and A. Seeber, *Metal amide chemistry*, John Wiley & Sons, United Kingdom, 2008.

14. H. Schmidbaur, *Coordination Chemistry Reviews*, 2001, **215**, 223-242.

15. K. J. Iversen, S. A. Couchman, D. J. Wilson and J. L. Dutton, *Coordination Chemistry Reviews*, 2015, **297**, 40-48.

16. D. Naglav, M. R. Buchner, G. Bendt, F. Kraus and S. Schulz, *Angewandte Chemie International Edition*, 2016, **55**, 10562-10576.

17. H. A. Vaessen and B. Szteke, *Food Additives & Contaminants*, 2000, **17**, 149-159.

18. *IBC Advanced Alloys, Nuclear Fuels Initiative; Increasing Efficiency and Safety, 2011, http://www.ibcadvancedalloys.com/clientuploads/RelatedArticles/Nuclear-Fuels-Fact-Sheet-R5.pdf, Accessed June 2017.*

19. B. L. Scott, T. M. McCleskey, A. Chaudhary, E. Hong-Geller and S. Gnanakaran, *Chemical Communications*, 2008, **25**, 2837-2847.

20. L. Richeldi, R. Sorrentino and C. Saltini, *Science*, 1993, **262**, 242-244.

21. G. M. Clayton, Y. Wang, F. Crawford, A. Novikov, B. T. Wimberly, J. S. Kieft, M. T. Falta, N. A. Bowerman, P. Marrack and A. P. Fontenot, *Cell*, 2014, **158**, 132-142.

22. S. Dai, M. T. Falta, N. A. Bowerman, A. S. McKee and A. P. Fontenot, *Current Opinion in Immunology*, 2013, **25**, 775-780.

23. C. Muller, S. Audusseau, F. Salehi, G. Truchon, G. Chevalier, B. Mazer, G. Kennedy and J. Zayed, *Toxicology and Industrial Health*, 2010, **26**, 39-45.

24. R. S. Pappas, *Metallomics*, 2011, **3**, 1181-1198.

25. A. Gregory, *Safeguard Magazine*, 2009, **116**, 39.

26. J. Young and M. Ward, Copper Beryllium Alloys – The Value of Occupational Hygiene Principles When Investigating an Occupational Health Issue Within Aircraft Maintenance Operations, (accessed http://www.ohsig.org.nz/uploads/images/documents/library/OSIGH%20Copper%20Beryllium%20Alloys.pdf. Accessed April 2015.).

27. D. T. Richens, *The Chemistry of Aqua Ions: Synthesis, Structure, and Reactivity : A Tour Through the Periodic Table of the Elements*, Wiley, Chichester, 1997.

28. M. Schmidt, A. Schier, J. Riede and H. Schmidbaur, *Inorganic Chemistry*, 1998, **37**, 3452-3453.

29. H. Schmidbaur, M. Schmidt, A. Schier, J. Riede, T. Tamm and P. Pyykkö, *Journal of the American Chemical Society*, 1998, **120**, 2967-2968.

30. B. T. Littlefield, C. Hinde and M. T. Weller, *Dalton Transactions*, 2011, **40**, 782-784.

31. P.-A. Pittet, G. Elbaze, L. Helm and A. E. Merbach, *Inorganic chemistry*, 1990, **29**, 1936-1942.

32. R. Puchta, N. van Eikema Hommes and R. van Eldik, *Helvetica Chimica Acta*, 2005, **88**, 911-922.

33. R. Puchta, E. Pasgreta and R. van Eldik, *Advances in Inorganic Chemistry*, 2009, **61**, 523-571.

34. L. Ciavatta, M. Iuliano, R. Porto, P. Innocenti and A. Vacca, *Polyhedron*, 2000, **19**, 1043-1048.

35. W. W. Rudolph, *Journal of Solution Chemistry*, 2010, **39**, 1039-1059.

36. W. W. Rudolph, D. Fischer, G. Irmer and C. C. Pye, *Dalton Transactions*, 2009, 6513-6527.

37. M. Georgiev, M. Wildner, D. Stoilova and V. Karadjova, *Journal of Molecular Structure*, 2005, **753**, 104-112.

38. M. J. Brisson and A. A. Ekechukwu, *Beryllium: Environmental Analysis and Monitoring*, Royal Society of Chemistry, United Kingdom, 2009.

39. T. S. Keizer, N. N. Sauer and T. M. McCleskey, *Journal of Inorganic Biochemistry*, 2005, **99**, 1174-1181.

40. T. S. Keizer, N. N. Sauer and T. M. McCleskey, *Journal of the American Chemical Society*, 2004, **126**, 9484-9485.

41. B. Neumüller and K. Dehnicke, *Zeitschrift für Anorganische und Allgemeine Chemie*, 2006, **632**, 1681-1686.

42. B. Neumüller, K. Dehnicke and R. Puchta, *Zeitschrift für Anorganische und Allgemeine Chemie*, 2008, **634**, 1473-1476.

43. R. Putcha, R. Kolbig, F. Weller, B. Neumüller, W. Massa and K. Dehnicke, *Zeitschrift für Anorganische und Allgemeine Chemie*, 2010, **636**, 2364-2371.

44. L. Alderighi, A. Vacca, F. Cecconi, S. Midollini, E. Chinea, S. Dominguez, A. Valle, D. Dakternieks and A. Duthie, *Inorganica Chimica Acta*, 1999, **285**, 39-48.

45. A. Valle, E. Chinea, S. Domínguez, A. Mederos, S. Midollini and A. Vacca, *Polyhedron*, 1999, **18**, 3253-3256.

46. L. Alderighi, S. Dominguez, P. Gans, S. Midollini, A. Sabatini and A. Vacca, *Journal of Coordination Chemistry*, 2009, **62**, 14-22.

47. Y. Zheng, L. Lin, W. Hang, X. Yan and B. L. Marrone, *Talanta*, 2011, **85**, 638-643.

48. A. Grigor'ev, V. Sipachev and A. Novoselova, *Russian Journal of Inorganic Chemistry*, 1967, **12**, 319-321.

49. R. A. Kovar and G. L. Morgan, *Journal of the American Chemical Society*, 1970, **92**, 5067-5072.

50. K. Schmidt and A. Müller, *Coordination Chemistry Reviews*, 1976, **19**, 41-97.

51. F. Kraus, S. A. Baer, M. R. Buchner and A. J. Karttunen, *Chemistry: A European Journal* 2012, **18**, 2131-2142.

52. F. Kraus, *BioInorganc Reaction Mechanisms*, 2012, **8**, 29-39.

53. F. Kraus, S. A. Baer, M. Hoelzel and A. J. Karttunen, *European Journal of Inorganic Chemistry*, 2013, **2013**, 4184-4190.

54. F. Kraus, M. B. Fichtl and S. A. Baer, *Zeitschrift für Naturforschung B*, 2009, **64**, 257-262.

55. D. Naglav, B. Tobey, C. Wölper, D. Bläser, G. Jansen and S. Schulz, *European Journal of Inorganic Chemistry*, 2015.

56. B. Neumüller and K. Dehnicke, *Zeitschrift für Anorganische und Allgemeine Chemie*, 2010, **636**, 1516-1521.

57. M. P. Dressel, S. Nogai, R. J. Berger and H. Schmidbaur, *Zeitschrift für Naturforschung B*, 2003, **58**, 173-182.

58. B. Neumüller and K. Dehnicke, *Zeitschrift für Anorganische und Allgemeine Chemie*, 2010, **636**, 515-517.

59. B. Neumüller and K. Dehnicke, *Zeitschrift für Anorganische und Allgemeine Chemie*, 2010, **636**, 1767-1771.

60. F. W. Wehrli and S. L. Wehrli, *Journal of Magnetic Resonance (1969)*, 1982, **47**, 151-155.

61. B. Neumüller and K. Dehnicke, *Zeitschrift für Anorganische und Allgemeine Chemie*, 2006, **632**, 1206-1212.

62. B. Neumüller and K. Dehnicke, *Zeitschrift für Anorganische und Allgemeine Chemie*, 2007, **633**, 103-105.

63. H. Böhland and W. Hanay, *Zeitschrift für Chemie*, 1974, **14**, 286-287.

64. H. Böhland, W. Hanay, A. Meisel and R. Scheibe, *Zeitschrift für Chemie*, 1981, **21**, 372-373.

65. H. Böhland, W. Hanay, M. Noltemeyer, A. Meller and H. Schmidt, *Fresenius' Journal of Analytical Chemistry*, 1998, **361**, 725-728.

66. A. Chizmeshya, C. Ritter, T. Groy, J. Tice and J. Kouvetakis, *Chemistry of Materials*, 2007, **19**, 5890-5901.

67. B. Neumüller and K. Dehnicke, *Zeitschrift für Anorganische und Allgemeine Chemie*, 2010, **636**, 1206-1211.

68. D. Williams, B. Pleune, K. Leinenweber and J. Kouvetakis, *Journal of Solid State Chemistry*, 2001, **159**, 244-250.

69. T. M. Klapötke and T. Schütt, *Main Group Metal Chemistry*, 1999, **22**, 357-360.

70. N. Wiberg, W. C. Joo and K. Schmid, *Zeitschrift für Anorganische und Allgemeine Chemie*, 1972, **394**, 197-208.

71. B. Neumüller and K. Dehnicke, *Zeitschrift für Anorganische und Allgemeine Chemie*, 2004, **630**, 347-349.

72. B. Neumüller and K. Dehnicke, *Zeitschrift für Anorganische und Allgemeine Chemie*, 2006, **632**, 931-933.

73. B. Neumüller and K. Dehnicke, *Zeitschrift für Anorganische und Allgemeine Chemie*, 2007, **633**, 2262-2267.

74. D. Naglav, A. Neumann, D. Bläser, C. Wölper, R. Haack, G. Jansen and S. Schulz, *Chemical Communications*, 2015, **51**, 3889-3891.

75. M. Niemeyer and P. P. Power, *Inorganic Chemistry*, 1997, **36**, 4688-4696.

76. B. Neumüller and K. Dehnicke, *Zeitschrift für Anorganische und Allgemeine Chemie*, 2004, **630**, 369-376.

77. K. Dehnicke, M. Krieger and W. Massa, *Coordination Chemistry Reviews*, 1999, **182**, 19-65.

78. R. Fleischer and D. Stalke, *Inorganic Chemistry*, 1997, **36**, 2413-2419.

79. B. Neumüller and K. Dehnicke, *Zeitschrift für Anorganische und Allgemeine Chemie*, 2003, **629**, 2529-2534.

80. S.-F. Liu, Q. Wu, H. L. Schmider, H. Aziz, N.-X. Hu, Z. Popovic and S. Wang, *Journal of the American Chemical Society*, 2000, **122**, 3671-3678.

81. K. H. Thiele, V. Lorenz, G. Thiele, P. Zönnchen and J. Scholz, *Angewandte Chemie International Edition in English*, 1994, **33**, 1372-1373.

82. B. Neumüller and K. Dehnicke, *Zeitschrift für Anorganische und Allgemeine Chemie*, 2005, **631**, 1029-1031.

83. M. Arrowsmith, M. S. Hill, G. Kociok-Köhn, D. J. MacDougall, M. F. Mahon and I. Mallov, *Inorganic Chemistry*, 2012, **51**, 13408-13418.

84. M. Bayram, D. Naglav, C. Wölper and S. Schulz, *Organometallics*, 2016.

85. S. J. Bonyhady, C. Jones, S. Nembenna, A. Stasch, A. J. Edwards and G. J. McIntyre, *Chemistry–A European Journal*, 2010, **16**, 938-955.

86. D. Naglav, D. Bläser, C. Wölper and S. Schulz, *Inorganic Chemistry*, 2014, **53**, 1241-1249.

87. Y. Sohrin, H. Kokusen, S. Kihara, M. Matsui, Y. Kushi and M. Shiro, *Journal of the American Chemical Society*, 1993, **115**, 4128-4136.

88. Y. Sohrin, M. Matsui, Y. Hata, H. Hasegawa and H. Kokusen, *Inorganic Chemistry*, 1994, **33**, 4376-4383.

89. Y. Sohrin, H. Kokusen, S. Kihara, M. Matsui, Y. Kushi and M. Shiro, *Chemistry Letters*, 1992, 1461-1464.

90. R. Linstead and J. M. Robertson, *Journal of the Chemical Society*, 1936, 1736-1738.

91. R. Kubiak, A. Waśkowska, M. Śledź and A. Jezierski, *Inorganica Chimica Acta*, 2006, **359**, 1344-1350.

92. J. Janczak and R. Kubiak, *Journal of Molecular Structure*, 2012, **1030**, 149-156.

93. R. Kubiak and J. Janczak, *Journal of Molecular Structure*, 2009, **935**, 53-59.

94. R. Kubiak, J. Janczak, M. Śledź and E. Bukowska, *Polyhedron*, 2007, **26**, 4179-4186.

95. R. Kubiak, J. Janczak, M. Śledź and E. Bukowska, *Polyhedron*, 2008, **27**, 3044-3052.

96. T. M. McCleskey, D. S. Ehler, T. S. Keizer, D. N. Asthagiri, L. R. Pratt, R. Michalczyk and B. L. Scott, *Angewandte Chemie International Edition*, 2007, **119**, 2723-2725.

97. T. M. McCleskey and B. L. Scott, *Journal of Occupational and Environmental Hygiene*, 2009, **6**, 751-757.

98. N. X. Hu, M. Esteghamatian, S. Xie, Z. Popovic, A. M. Hor, B. Ong and S. Wang, *Advanced Materials*, 1999, **11**, 1460-1463.

99. Y. Li, Y. Liu, W. Bu, D. Lu, Y. Wu and Y. Wang, *Chemistry of Materials*, 2000, **12**, 2672-2675.

100. C. S. Oh, C. W. Lee and J. Y. Lee, *Chemical Communications*, 2013, **49**, 3875-3877.

101. C. S. Oh and J. Y. Lee, *Israel Journal of Chemistry*, 2014, **54**, 967-970.

102. C. S. Oh and J. Y. Lee, *Dyes and Pigments*, 2014, **101**, 25-29.

103. C. S. Oh and J. Y. Lee, *Organic Electronics*, 2015, **24**, 315-319.

104. Y.-P. Tong, S.-L. Zheng and X.-M. Chen, *Inorganic Chemistry*, 2005, **44**, 4270-4275.

105. H. V. Diyabalanage, K. Ganguly, D. S. Ehler, G. E. Collis, B. L. Scott, A. Chaudhary, A. K. Burrell and T. M. McCleskey, *Angewandte Chemie International Edition*, 2008, **120**, 7442-7444.

106. A. Agrawal, J. Cronin, J. Tonazzi, T. M. McCleskey, D. S. Ehler, E. M. Minogue, G. Whitney, C. Brink, A. K. Burrell and B. Warner, *Journal of Environmental Monitoring*, 2006, **8**, 619-624.

107. A. Agrawal, J. P. Cronin, A. Agrawal, J. C. Tonazzi, L. Adams, K. Ashley, M. J. Brisson, B. Duran, G. Whitney and A. K. Burrell, *Environmental Science & Technology*, 2008, **42**, 2066-2071.

108. H. Matsumiya and H. Hoshino, *Analytical Chemistry*, 2003, **75**, 413-419.

109. H. Matsumiya, H. Hoshino and T. Yotsuyanagi, *Analyst*, 2001, **126**, 2082-2086.

110. E. Chinea, S. Dominguez, A. Mederos, F. Brito, J. M. Arrieta, A. Sanchez and G. Germain, *Inorganic Chemistry*, 1995, **34**, 1579-1587.

111. A. Mederos, S. Dominguez, E. Chinea and F. Brito, *Quimica Analitica-Bellaterra*, 1996, **15**, S21-S29.

112. A. Mederos, S. Dominguez, E. Chinea, F. Brito, S. Midollini and A. Vacca, *Boletin de la Sociedad Chilena de Quimica*, 1997, **42**, 281-295.

113. A. Mederos, S. Domínguez, A. Medina, F. Brito, E. Chinea and K. Bazdikian, *Polyhedron*, 1987, **6**, 1365-1373.

114. A. E. Martell and R. D. Hancock, *Metal Complexes in Aqueous Solutions*, Springer Science & Business Media, New York, 1996.

115. K. J. Shaffer, R. J. Davidson, A. K. Burrell, T. M. McCleskey and P. G. Plieger, *Inorganic Chemistry*, 2013, **52**, 3969-3975.

116. J. Reglinski, A. R. Kennedy and G. Steel, *New Journal of Chemistry*, 2015, **39**, 2437-2439.

117. R. B. Cole, *Electrospray and Maldi Mass Spectrometry:Fundamentals, Instrumentation, Practicalities, and Biological Applications*, Wiley, New Jersey, 2nd edn., 2010.

118. W. Henderson and J. S. McIndoe, *Mass Spectrometry of Inorganic, Coordination and Organometallic Compounds:Tools, Techniques, Tips*, Wiley, Chichester, 2005.

119. J. B. Fenn, *Journal of Biomolecular Techniques*, 2002, **13**, 101-118.

120. J. B. Fenn, *Angewandte Chemie International Edition*, 2003, **42**, 3871-3894.

121. M. Dole, L. Mack, R. Hines, R. Mobley, L. Ferguson and M. d. Alice, *The Journal of Chemical Physics*, 1968, **49**, 2240.

122. J. Iribarne and B. Thomson, *The Journal of Chemical Physics*, 1976, **64**, 2287.

123. M. P. Allen and D. J. Tildesley, *Computer Simulation of Liquids*, Oxford University Press, New York, 1989.

124. D. Frenkel and B. Smit, *Understanding Molecular Simulation: From Algorithms to Applications*, Academic Press, San Diego, 2001.

125. P. Hohenberg and W. Kohn, *Physical Review*, 1964, **136**, B864.

126. W. Kohn and L. J. Sham, *Physical Review*, 1965, **140**, A1133.

127. D. Marx and J. Hutter, *Ab Initio Molecular Dynamics:Basic Theory and Advanced Methods*, Cambridge University Press, New York, 2009.

128. K. Laasonen, M. Sprik, M. Parrinello and R. Car, *The Journal of Chemical Physics*, 1993, **99**, 9080-9089.

129. J. VandeVondele, F. Mohamed, M. Krack, J. Hutter, M. Sprik and M. Parrinello, *The Journal of Chemical Physics*, 2005, **122**, 014515.

130. M. Sprik, J. Hutter and M. Parrinello, *The Journal of Chemical Physics*, 1996, **105**, 1142-1152.

131. J. C. Grossman, E. Schwegler, E. W. Draeger, F. Gygi and G. Galli, *The Journal of Chemical Physics*, 2004, **120**, 300-311.

132. R. Car and M. Parrinello, *Physical Review Letters*, 1985, **55**, 2471.

Chapter Two

Electrospray ionisation mass spectrometric (ESI-MS) investigation of solutions of simple beryllium salts

2.1 Introduction

From the review of the chemistry and metallurgy of beryllium presented in Chapter one, the element beryllium has been referred to as "$^{9}_{4}$Beauty and $^{9}_{4}$Beast".* On the one hand, beryllium metal, alloys and oxide are attractive engineering materials which possess a combination of physical and mechanical properties that often make them indispensable, particularly in high-tech devices.[1, 2] On the other hand, the inhalation of beryllium particles sensitises the human lungs by triggering a mediated immune response *via* a network of interactions yet to be fully understood.[3-5] Despite its toxicity, the production and usage of beryllium components have continued unabated, renewing research interest in the chemistry of beryllium and its interactions with ligands of biological interest over the last decade.[6-10] Of particular interest to coordination and materials chemists in this area is beryllium's coordination to uniquely designed ligands with the ability to selectively sequester beryllium for applications such as light emitting materials,[11] physiological and environmental detection,[8, 12] and therapies for beryllium-exposed individuals.[13, 14] In addition to this, significant research efforts have also been geared toward exploring and optimising various solution-based analytical techniques for the *in situ* investigation of beryllium compounds.[15-19] As of the time of writing this thesis, much of the known aqueous chemistry of beryllium has only been studied by employing potentiometric measurements although additional

* In reference to the winning presentation in the 2014 University of Waikato 3MT competition. (see https://www.youtube.com/watch?v=s64psOGTfvU, accessed 27th June, 2017). Also the analogy was used at the Asian Pacific 3MT competition, 2015 (Queensland, Australia) and AMP ignite 2015 (Auckland, New Zealand).

techniques including ^{9}Be NMR and vibrational spectroscopy have equally been explored in more recent reports.[18, 20, 21] Undoubtedly, safe methodologies and sensitive analytical techniques suitable for investigating the solution speciation of toxic beryllium would be of great significance towards the ongoing expansion of the underdeveloped coordination chemistry of beryllium.[22, 23]

Electrospray ionisation mass spectrometry (ESI-MS) appears to be a technique of choice for the investigation of beryllium speciation in solution, being able to transfer pre-existing solution species into the gas phase where they are analysed by the mass spectrometer. The importance of this technique lies in its sensitivity as it requires a minuscule amount of sample in solution, thereby minimising any exposure to beryllium dust and allowing rich information to be gained utilising only tiny quantities of beryllium compounds. Furthermore, ESI-MS is well-known as an invaluable technique to obtain stoichiometric information, and to some extent, the relative stability of the metal-ligand interactions making it appropriate for preliminary microscale screening prior to characterisation using other techniques such as X-ray crystallography and NMR spectroscopy.[24-26] In this study, we demonstrate for the first time the use of ESI-MS as an alternative technique for the solution study of beryllium chemistry utilising the well-characterized beryllium hydroxido speciation in aqueous solution. This has been done to assess the potential of the ESI-MS technique for subsequent microscale studies of other beryllium-ligand systems. In addition, this is especially relevant because the Be^{2+} cation exhibits a complex pH- and concentration-dependent aqueous chemistry ranging from the 4-coordinate aqua species $[Be(H_2O)_4]^{2+}$ to hydroxido-bridged polynuclear aggregates which include core species such as $[Be_2OH]^{3+}$, $[Be_3(OH)_3]^{3+}$, $[Be_5(OH)_6]^{4+}$, and $[Be_6(OH)_8]^{4+}$ proposed from potentiometric titrations.[20, 27-29] Moreover, understanding the aqueous speciation of the beryllium cation and its high propensity for hydrolysis is relevant in achieving a competitive binding site capable of solubilising beryllium at physiological pH.[30, 31] It is expected that soft ionisation, high sensitivity, and an ability to directly reflect solution species in a mass spectrum would make ESI-MS an important tool to support the existence of various beryllium hydroxido solution species and even identify other species of minor abundances.

2.2 Results and discussion

2.2.1 Ion assignments

Firstly, the electrospray mass spectrometric investigation of beryllium solutions was centred on a simple and commercially available beryllium sulfate which was also the starting material for most of the complexation reaction. However, during the course of this project, it was observed that the beryllium sulfate solution was a relatively poor starting material in the formation of beryllium complexes primarily due to the strong and versatile complexation of the sulfate anions to the beryllium ion. Hence, there was a need to obtain solutions of other beryllium salts. Unfortunately, beryllium compound are not readily available from commercial outlets perhaps due to its toxicity, cost, and low demand among researchers. Therefore, an aqueous solution of beryllium chloride was prepared by dissolving beryllium metal granule in 1 mol L^{-1} hydrochloric acid and diluting the solution (see Chapter 7).

(a) (b)

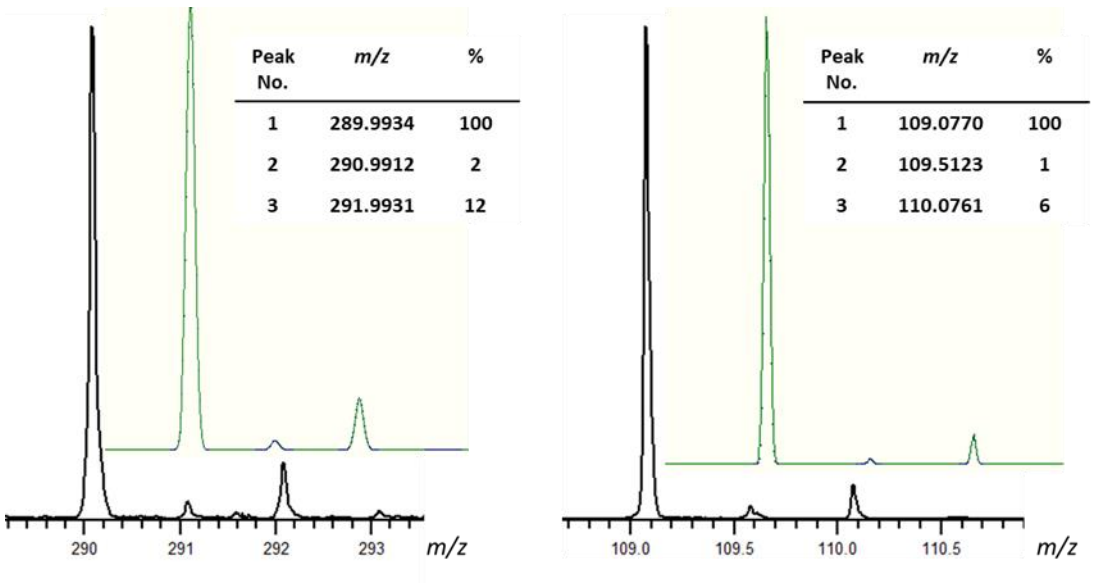

Figure 2-1 Experimental (black) and calculated (grey and offset for clarity) isotope pattern for the ESI-MS ions (a) $[Be_3(OH)_3(HSO_4)_2(H_2O)]^+$ (b) $[Be_3(OH)_3(HSO_4)(BeO)(H_2O)]^{2+}$

The common method of assignment of ions observed in ESI-MS by the comparison of the observed and predicted *m/z* value alongside their isotope distribution pattern is not sufficient since beryllium is monoisotopic. Therefore, signals observed in the mass spectra of beryllium sulfate solutions had less

informative isotope distributions (effectively one major peak in the isotope pattern, together with low intensity minor peaks due to heavier isotopes of sulfur, oxygen and hydrogen see Figure 2-1).

Illustrative isotopic pattern observed in the ESI mass spectra of aqueous beryllium sulfate solution are shown in Figure 2-1. In comparison to the mass spectra of beryllium sulfate, ESI-MS speciation of the aqueous solution of beryllium chloride cation is more complicated majorly as a consequence of the richer isotope composition of a chloride ion (^{35}Cl, 75.5%; ^{37}Cl, 24.5%). While this resulted in more complex mass spectra, the chloride isotope data were highly relevant in peak assignment. For instance, the number of chloride ions bound to beryllium complexes detected from their unique isotopic distributions was the only means of distinguishing closely related signals consisting of $[Cl]^-$ *m/z* 34.9683 or $[OH(H_2O)]^-$ *m/z* 35.0127 species. Also, worthy of mention is that due to the numerous signals that can arise in correspondence to an ion, only the *m/z* value of the most abundance isotope signal (which is not necessarily the first *m/z* value) is reported.

(a) (b)

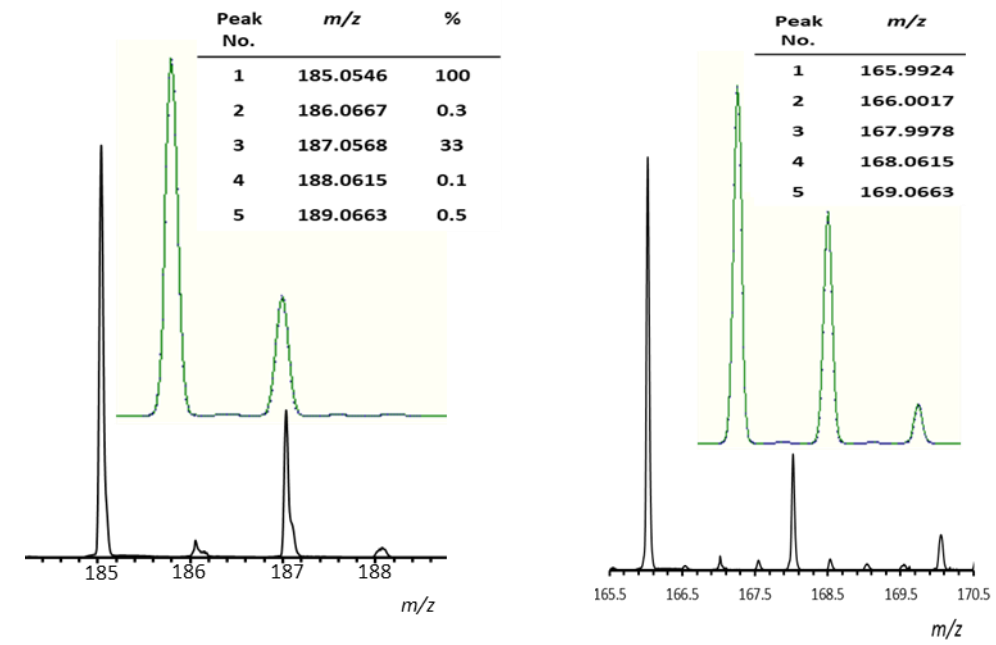

Figure 2-2 Experimental (black) and calculated (grey/green) isotope pattern for the ESI-MS ions a) $[Be_3(OH)_3Cl(H_2O)_4]^+$ b) $[Be_3(OH)_3Cl_2(H_2O)]^{2+}$

Importantly, the high resolution mass spectrometer was relevant in distinguishing ions of closely related *m/z* values (in the absence of sufficient isotope

patterns). For instance, the species $[Be_3(OH)_3(OH)_2(H_2O)]^+$ and $[Be_5(OH)_6SO_4(H_2O)]^{2+}$ are observed at *m/z* 130.0 and 130.5 respectively. It is also worth pointing out that the isotope pattern is very relevant in distinguishing the charge on an ion. For instance, in the ESI-MS of the beryllium sulfate solution, the isotope pattern of singly charged species are separated by 1 *m/z*, while the pattern corresponding to a double charged ion is separated by 0.5 mass unit (see Figure 2-1). Whereas with the beryllium chloride solution, the intensity of peaks in the isotope pattern are more distinct depending on the charge of the ion (see Figure 2-2). Further support toward the assignment of ambiguous signals was the concomitant peaks arising from water series, for example the ESI-MS ion $[Be_3(OH)_3(SO_4)(H_2O)_n]^+$ revealed a series of signals at *m/z* 174, 192, 210, 228 corresponding to n = 0-3 respectively and differing by 18 units. Furthermore, the trimeric beryllium ions such as $[Be_3(OH)_3(SO_4)(H_2O)_{0\text{-}3}]^+$ *m/z* 174, 192, 210, 228 were always observed at an even number *m/z* value while the dimeric ion series $[Be_2(OH)(SO_4)(H_2O)_{0\text{-}3}]^+$ *m/z* 131, 149, 167, 185 revealed odd number *m/z* values because the mass of the trimer $[Be_3(OH)_3]^{3+}$ and dimer $[Be_2(OH)]^{3+}$ (which are even and odd, respectively) were often charge-reduced by any of the doubly-charged counterions present in the sulfate solution (O^{2-}/$[OH]_2^{2-}$, $[HSO_4]_2^{2-}$, SO_4^{2-}). Since the mass spectra cannot confirm structural information, assignments for ions containing fragments such as $[O(H_2O)]^{2-}$ *vs* $[2OH]^{2-}$], $Be(OH)_2$ *vs* $BeO(H_2O)$, $[(HSO_4)(BeO)]^-$ *vs* $[(OH)(BeSO_4)]^-$ and $[(OH)(HSO_4)]^{2-}$ *vs* $[(SO_4)(H_2O)]^{2-}$ could not be distinguished. Therefore, the most reasonable arrangements were chosen based on the known solution chemistry of beryllium, CID investigations and the relative behaviour of signals with varying experimental conditions.

Table 2-1 Summary of ions observed in the positive ion ESI mass spectra of 2.2 x 10^{-3} mol L^{-1} aqueous beryllium sulfate solutions across pH 2.5 – 6.0 and capillary exit voltages of 60 – 180 V.

Experimental ***m/z***	**Theoretical** ***m/z***	**ESI-MS ions**	**Experimental** ***m/z***	**Theoretical** ***m/z***	**ESI-MS ions**	**Experimental** ***m/z***	**Theoretical** ***m/z***	**ESI-MS ions**
62.0707	*62.0355*	$[BeOH(H_2O)_2]^+$	*148.1316*	*148.0708*	$[Be_3(OH)_3(OH)_2(H_2O)_2]^+$	*228.0445*	*228.0276*	$[Be_3(OH)_3SO_4(H_2O)_3]^+$
160.0808	*160.0028*	$[BeHSO_4(H_2O)_3]^+$	*289.9954*	*289.9738*	$[Be_3(OH)_3(HSO_4)_2(H_2O)]^+$	*210.0970*	*210.0170*	$[Be_3(OH)_3SO_4(H_2O)_2]^+$
142.0025	*141.9923*	$[BeHSO_4(H_2O)_2]^+$	*272.0585*	*271.9638*	$[Be_3(OH)_3(HSO_4)_2]^+$	*192.0904*	*192.0065*	$[Be_3(OH)_3SO_4(H_2O)]^+$
123.9893	*123.9817*	$[BeHSO_4(H_2O)]^+$	*308.0891*	*307.9852*	$[Be_3(OH)_3(HSO_4)_2(H_2O)_2]^+$	*174.0067*	*173.9959*	$[Be_3(OH)_3SO_4]^+$
111.0351	*110.9742*	$[BeHSO_4(H_2SO_4)]^+$	*254.0424*	*253.9527*	$[Be_3OHO(HSO_4)_2]^+$	*112.1095*	*112.0496*	$[Be_3(OH)_3(OH)_2]^+$
102.0205	*101.9690*	$[BeHSO_4(H_2SO_4)]^+$	*333.9357*	*333.9095*	$[Be_3O(HSO_4)_3]^+$	*180.0870*	*180.9924*	$[Be_4O_3HSO_4]^+$
199.1013	*199.0030*	$[Be_4O_3HSO_4(H_2O)]^+$	*109.0770*	*109.0104*	$[Be_3(OH)_3(HSO_4)(BeO)(H_2O)]^{2+}$	*199.1013*	*199.0030*	$[Be_4O_3HSO_4(H_2O)]^+$
185.0221	*185.0099*	$[Be_2OH(SO_4)(H_2O)_3]^+$	*118.0834*	*118.0157*	$[Be_3(OH)_3(HSO_4)(BeO)(H_2O)_2]^{2+}$	*430.9911*	*430.9589*	$[Be_3(OH)_3(SO_4)_2BeSO_4(H_2O)_3]^+$
167.0115	*166.9994*	$[Be_2OH(SO_4)(H_2O)_2]^+$	*127.0828*	*127.0210*	$[Be_3(OH)_3(HSO_4)(BeO)(H_2O)_3]^{2+}$	*333.0136*	*332.9915*	$[Be_3(OH)_3(HSO_4)_2(BeO)(H_2O)_2]^+$
149.0982	*148.9888*	$[Be_2OH(SO_4)(H_2O)]^+$	*136.0855*	*136.0262*	$[Be_3(OH)_3(HSO_4)(BeO)(H_2O)_4]^{2+}$	*130.5961*	*130.5192*	$[Be_5(OH)_6SO_4(H_2O)]^{2+}$
69.0675	*69.0320*	$[Be_2OH(O)(H_2O)]^+$	*297.0828*	*296.9704*	$[Be_3(OH)_3(HSO_4)_2(BeO)]^+$	*121.4618*	*121.5139*	$[Be_5(OH)_6SO_4]^{2+}$
87.0813	*87.0425*	$[Be_2OH(O)(H_2O)_2]^+$	*322.0157*	*321.9775*	$[Be_3(OH)_3(HSO_4)_2(BeO)_2]^+$	*134.0910*	*134.0175*	$[Be_5(OH)_6SO_4(BeO)]^{2+}$
105.0980	*105.0531*	$[Be_2OH(O)(H_2O)_3]^+$	*304.0121*	*303.9669*	$[Be_3(OH)_2(HSO_4)SO_4(BeO)_2]^+$	*143.0986*	*143.0228*	$[Be_6(OH)_8SO_4]^{2+}$
265.0606	*264.9667*	$[Be_2OH(HSO_4)_2(H_2O)_2]^+$	*413.0543*	*412.9483*	$[Be_3(OH)_3(HSO_4)_2BeSO_4(H_2O)_2]^+$	*243.2049*	-	Unassigned
130.0098	*130.0602*	$[Be_3(OH)_3(OH)_2(H_2O)]^+$						

2.2.2 ESI-MS behaviour of beryllium sulfate solutions

Illustrative mass spectra of beryllium sulfate solutions across various capillary exit voltages and solution pH are shown in Figure 2-3 and Figure 2-4 while the assignments of the majority of ions have been compiled in Table 2-1. The spectra were complex, with peaks revealing a variety of ESI-MS ions which certainly required careful understanding of the gas phase modifications to identify the originating species in solution. In most cases, it was also relevant to investigate a variety of experimental and instrument conditions in order to obtain suitably representative spectra. As expected, positive ion mode was best suited for observing hydrolysis species in acidic beryllium sulfate solutions since the pre-existing species are positive ions.

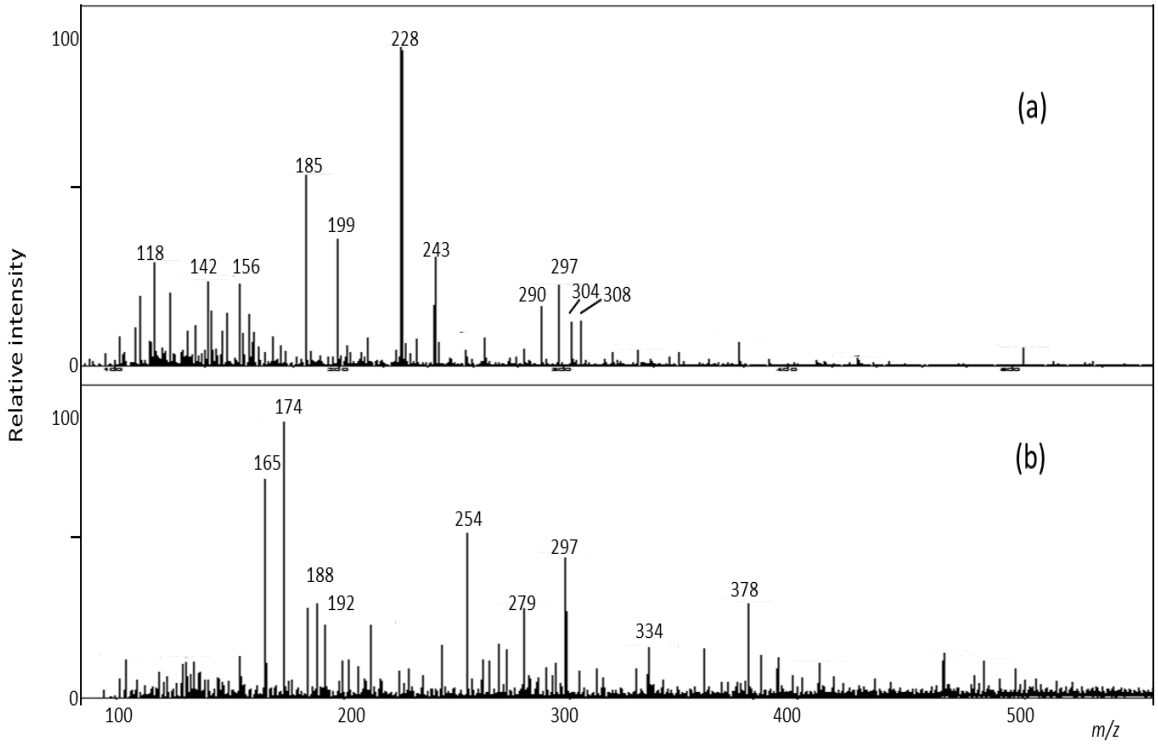

Figure 2-3 Positive ion ESI mass spectra of 2.2 x 10^{-3} mol L^{-1} aqueous beryllium sulfate solution at capillary exit voltages (CEV) of (a) 80 V and (b) 160 V.

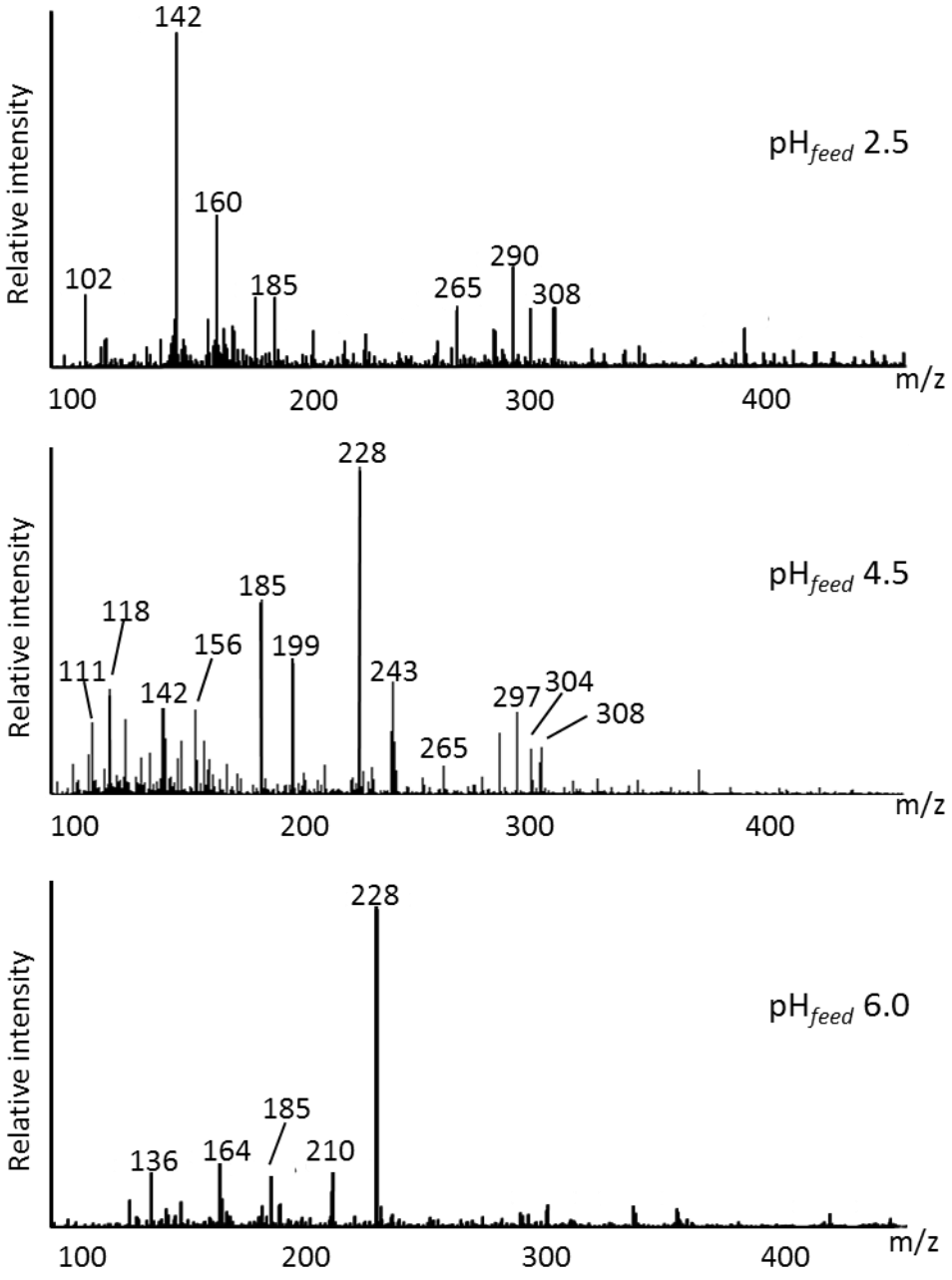

Figure 2-4 Positive ion ESI mass spectra of 2.2 x 10^{-3} mol L^{-1} aqueous beryllium sulfate solutions at pH (a) 2.5, (b) 4.5 and (c) 6.0 at a capillary exit voltage (CEV) of 60 V

Although the ESI-MS technique has been shown to be capable of introducing multiply-charged solvated metal ion species into the gas phase,[32] the majority of the species identified in Table 1 were singly-charged. This is not unexpected considering the high charge density of the beryllium solution species. Unlike the solution phase, wherein the tetraaquaberyllium cation $[Be(H_2O)_4]^{2+}$ is

stabilised by extensive solvation,[31] the transfer mechanism of a solution species into the mass spectrometer would inherently involve the shrinking of the sprayed solution droplets until gas phase ions are obtained having various degrees of microsolvation (see Figure 2-5). Under such ESI-MS conditions, highly charged solution species will typically undergo a charge reduction process, often by ion pairing or deprotonation of a coordinated solvent molecule (such as water, methanol, etc.) that contains a labile, acidic proton. This is a well-known feature of multiply-charged metal ions in the gas phase,[32-35] but was observed to be pronounced in the ESI-MS of beryllium in comparison with other dications.[32, 36] Prevalent in this study is charge reduction by ion pairing perhaps due to the fairly strong interaction of the negatively-charged sulfato ligand with beryllium in the gas phase as compared to a neutral aqua ligand. In addition, the sulfato ligand, which is capable of terminal, bridging or bidentate coordination depending on the amount of hydration, revealed several complexes such as a series in which sulfato ligands progressively replace the hydroxido ligands to yield the ions $[Be_3O_2(HSO_4)]^+$, $[Be_3(OH)O(HSO_4)_2]^+$ and $[Be_3O(HSO_4)_3]^+$ in the gas phase. Therefore where possible, the ion assignments in Table 2-1 have been depicted as the most probable charge-reduced ESI-MS ion originating from the beryllium species in solution. Furthermore, a higher charge density and partial desolvation would result in the polarisation of the remaining coordinated water molecules such that proton(s) are easily lost by collision or thermal agitation in the gas phase. Therefore, at higher capillary exit voltages, which effect more fragmentation, there is further deprotonation to formally yield the neutral oxide $(BeO)_n$. The resultant beryllium oxide forms further adducts with pre-existing solution species to reveal other polynuclear beryllium species peculiar to the gas phase. Similar gas phase species have also been observed previously and are thought to be enhanced by the shorter measuring time in a time-of-flight mass analyser as compared to a quadrupole mass analyser.[37, 38] However, it is also worth pointing out that although the ion pairing of beryllium with the sulfate anion appears to be exaggerated by ESI-MS, the low activation energy barrier (11 kcal mol^{-1}, approx. 45.3 kJ mol^{-1}) involved in the substitution of aqua ligands by the sulfate ion in solution suggest the existence of pre-existing beryllium sulfato/hydroxido mixed complexes in reasonable abundance.[39] This has also been corroborated employing

Raman spectroscopic data on beryllium speciation in the presence of SO_4^{2-}, Cl^-, NO_3^-, or ClO_4^- in which the sulfate anion showed the highest involvement in primary coordination sphere of the Be^{2+} cation in solution.[21, 40]

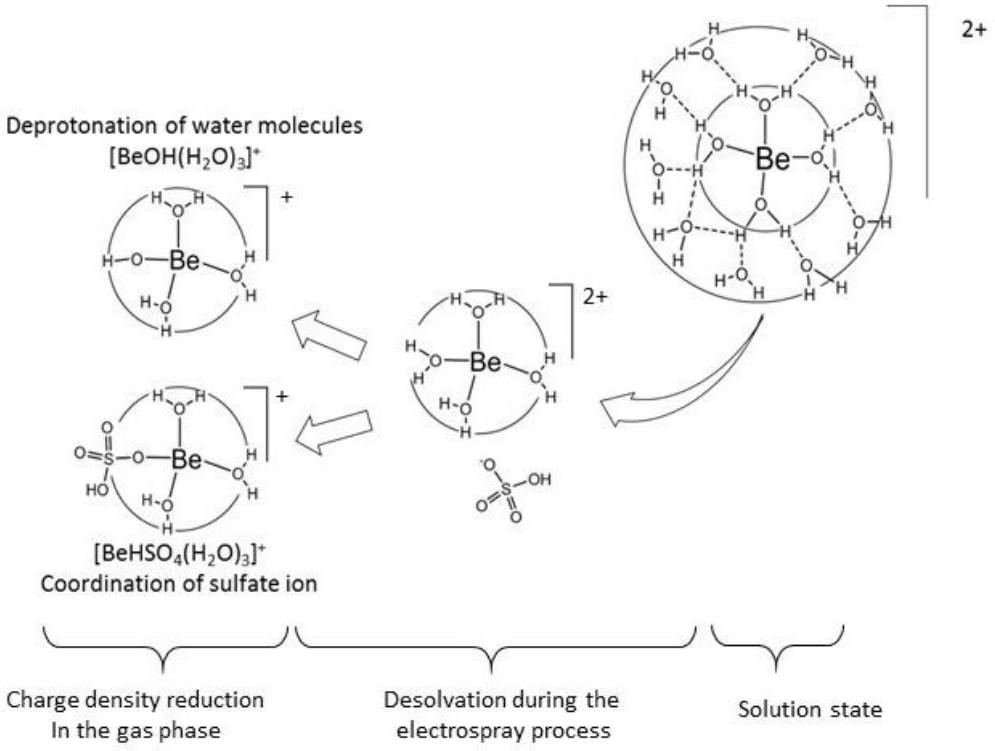

Figure 2-5 Modification of the beryllium species from the solution into the gas phase

2.2.3 ESI-MS ions in time of flight (TOF) vs ion trap mass spectrometers

After the transfer of the pre-existing solution species into the gas phase, a significant level of extraneous chemistry can start off in the gas environment depending on the nature of the species and the ionisation condition.[32] In addition, the different environment and time of analysis associated with the various mass analyser concerned can exacerbate these gas phase reactions as has been reported in a comparison of the ESI-MS speciation of aluminium salt solution using a time of flight and quadrupole mass analyser.[37, 38] A higher number of polynuclear and

sulfato species was observed with the time of flight (ESI-TOF-MS) as compared to the quadrupole (ESI-Q-MS) instrument and this was attributed to the slightly longer time the ions spent in the time of flight region. With this caveat in mind, the ESI-MS species observed from a TOF and ion-trap mass analyser was investigated noting that the ions will spend longer time in the latter as they are trapped and individually ejected. A similar ESI-MS experiment was conducted with the same beryllium sulfate solution using an ESI-TOF-MS and ESI-ion trap-MS. Selected ion assignments are shown in Figure 2-6. Unfortunately, the ion-trap mass spectrometer used in this study was a low resolution instrument and most of the signals (especially those completely absent in the high resolution TOF instrument) could not be assigned.

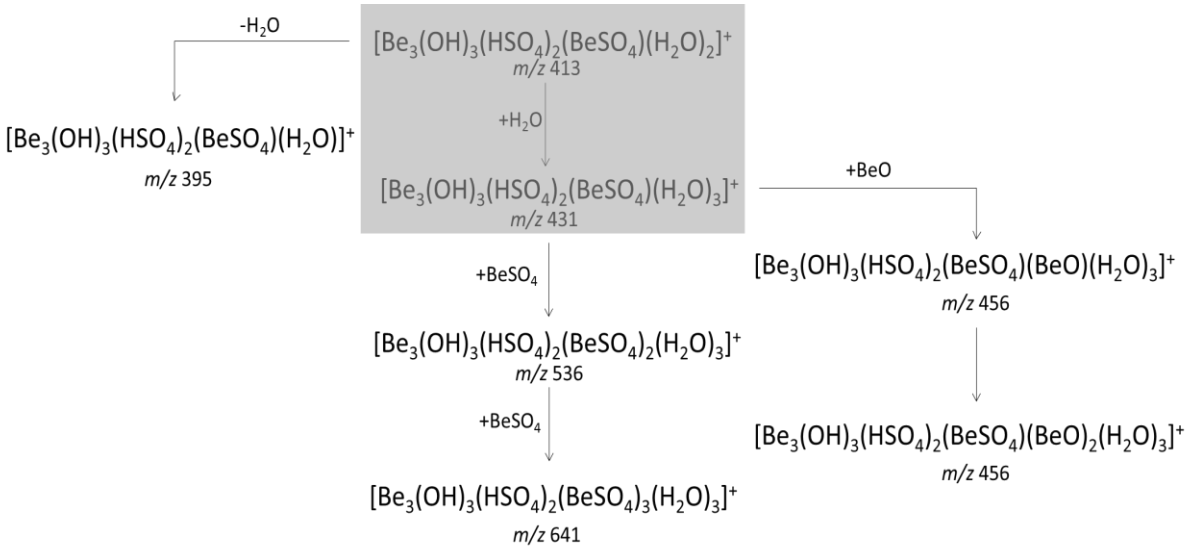

Figure 2-6 Proposed aggregation path of ESI-MS ions in the time of flight (TOF) and ion trap mass spectrometers. (ESI-MS ions in grey signify ions observed in an ESI-MS experiments using a ESI-TOF-MS and ESI-ion trap-MS while the remaining ions were observed only from the ion trap mass spectrometer)

Firstly, the well-known lower sensitivity of the TOF mass analyser in the low mass region was observed such that signal corresponding to *m/z* values less than 80 were observed with poor intensity (below 5%). In contrast, these species are well represented by the spectra from the ion-trap mass analyser. However, this could also be as a result of such species in solution not reaching the detector but rather aggregating to form other species more stable in the gas phase.

Secondly, in agreement with the argument that aggregation in the gas phase is related to the travelling time an ion spent before reaching the detector, many more ions were observed in the high mass region from the ion-trap mass analyser. For instance, by the addition of neutral species such as H_2O, BeO and $BeSO_4$ to an ion observed by both the TOF and ion-trap mass analysers, several aggregates peculiar to the ion-trap mass analyser were assigned creating an understanding of the possible gas phase aggregation as shown in Figure 2-6. Since similar extraneous species have also been observed in aluminium spectra in the presence of the sulfate ions,[37, 38, 41, 42] this is well related to the high charge density of these ion as well as the versatile coordinating ability of the sulfate ion.

Lastly in the comparison of mass spectra data from the TOF and ion trap mass spectrometer, more sulfate rich ESI-MS ions were observed with the ion trap mass analyser. Since the sulfato ligands can exist as two species, namely SO_4^{2-} or the hydrogen sulfate ion HSO_4^- charge reduction with the latter tends to be more prevalent in the ion trap spectra. This is perhaps due to the fact that the monoanionic charged HSO_4^- species will permit the trapped ions to aggregate and further stabilized the beryllium hydroxido trimer as shown in eqn (2-1). Nevertheless, this could also be related to the available metal centres present in the particular ESI-MS ions as this trend is not replicated with the corresponding dimeric ESI-MS ions. The sulfato species $[Be_2(OH)(SO_4)(H_2O)_3]^+$ at *m/z* 185 showed a more significant abundance than the hydrogen sulfato species $[Be_2(OH)(HSO_4)_2(H_2O)_2]^+$ *m/z* 265 both in the TOF and ion trap instrument). Most important in all these observations, was the fact that the cores of the suggested complexes were very similar and representative of the solution state irrespective of the mass analyser employed.

$$\underset{m/z\ 174}{[Be_3(OH)_3SO_4]^+} + H^+ \longrightarrow [Be_3(OH)_3HSO_4]^{2+} \xrightarrow{+\ HSO_4^-} \underset{m/z\ 272}{[Be_3(OH)_3(HSO_4)_2]^+} \qquad (2\text{-}7)$$

It is clear that the core species from a time of flight and ion trap mass analyser are similar although there existed subtle distinctions attributable to the uniqueness and strength of the instrument as a method of mass analysis. Therefore,

the unique strengths of each of the mass analysers were employed for different purposes throughout this study. While the correlation of ESI-MS ions to previously known beryllium species was conducted on spectra from the TOF mass analyser, the invaluable ion trapping and storage capability of the ion trap mass analyser was employed in the fragmentation studies.

Table 2-2 Correlation of observed ESI-MS ions with pre-existing core species in solution

Beryllium core species in solution	**Ions observed by ESI-MS**	n_{av}	*m/z*	**Relative signal intensity with pH_{feed}**		
				2.5	4.5	6.0
Be^{2+}	$[BeHSO_4(H_2O)_2]^+$	2.4	142	100	27	6
	$[BeHSO_4(H_2O)_3]^+$		160	46	16	3
	$[BeHSO_4(H_2O)]^+$		124	3	-	-
	$[Be(H_2SO_4)_2]^{2+}$		102	23	-	-
$[Be_2OH]^{3+}$	$[Be_2OH(SO_4)(H_2O)_3]^+$	2.9	185	23	60	16
	$[Be_2OH(SO_4)(H_2O)_2]^+$		167	12	5	5
	$[Be_2OH(SO_4)(H_2O)]^+$		149	2	0	1
	$[Be_2OH(HSO_4)_2(H_2O)_2]^+$	2.0	265	20	9	2
$[Be_3(OH)_3]^{3+}$	$[Be_3(OH)_3SO_4(H_2O)_3]^+$	2.8	228	-	100	100
	$[Be_3(OH)_3SO_4(H_2O)_2]^+$		210	2	5	18
	$[Be_3(OH)_3SO_4(H_2O)]^+$		192	-	3	3
	$[Be_3(OH)_3SO_4]^+$		174	3	7	-
	$[Be_3(OH)_3(HSO_4)_2(H_2O)]^+$	1.5	290	2	19	4
	$[Be_3(OH)_3(HSO_4)_2(H_2O)_2]^+$		308	-	16	-
$[Be_5(OH)_6]^{4+}$	$[Be_5(OH)_6SO_4]^{2+}$	-	121.5	3	10	4
$[Be_6(OH)_8]^{4+}$	$[Be_6(OH)_8SO_4]^{2+}$	-	143.0	12	21	6

n_{av} is the average hydration number calculated at capillary exit voltage (CEV) 60 V as $n_{av} = \sum(n \,.\, rI^n) / \sum(rI^n)$ where n = hydration number and rI^n is the relative intensity of individual ESI-MS ions in a water series

2.2.4 Correlation of ESI-MS ions with pre-existing species in solution

With a proper understanding of the modification in the gas phase, excellent qualitative speciation data as illustrated in Table 2-2 were obtained using the ESI-MS technique. For the majority of the ESI-MS ions, the beryllium hydroxide core was preserved and the processes involved in their modifications into ESI-MS ions were distinct. However, a few other ions remained ambiguous in their comparison

with the solution state species. For instance, the Be_4 cores observed in ions such as $[Be_4(OH)_3(HSO_4)_{1-2}(H_2O)_{1-4}]^{n+}$ and $[Be_4(OH)_2(SO_4)_3(H_2O)_{2-4}]^{n+}$ had no obvious correlation to any solution species but originated from aggregation in the gas phase particularly by the adduction of beryllium oxide (BeO) to the trimer $[Be_3(OH)_3]^{3+}$. This is further supported by the observation of a $(BeO)_n$ series with 25 *m/z* units separation in ions such as $[Be_3(OH)_3(HSO_4)_2(BeO)_n]^+$ observed at *m/z* 272, 297 and 322 where n = 0-2. Furthermore, the stripping of water molecules and replacement by beryllium oxide revealed a series of peaks separated by 7 *m/z* units (the mass difference between H_2O and BeO). Other neutral species such as $BeSO_4$ and $Be(OH)_2$ were similarly observed to adduct with pre-existing solution species yielding a variety of ESI-MS ions. There is also the possibility ESI-MS ions with Be_4 cores originating from the fragmentation of a pentamer or other high nuclearity species that actually exist in solution but this is inconsistent with the observed fragmentation patterns and is very unlikely due to the low concentration of the $[Be_5(OH)_6]^{4+}$ and $[Be_6(OH)_8]^{4+}$ species.

The tetraaquaberyllium cation $[Be(H_2O)_4]^{2+}$ correlates to the ESI-MS ion $[BeOH(H_2O)_n]^+$ n = 1, 2, 3 at *m/z* 44, 62, 80 in agreement with previous gas-phase and theoretical investigations of doubly-charged metal ions.[32, 36] Although the $[BeOH]^+$ species could also exist in solution, it is thought to be transient and aggregates to form the more stable trimeric species $[Be_3(OH)_3]^{3+}$.[29] However, the most abundant monomeric ESI-MS ions in the mass spectra of beryllium sulfate solution were the sulfato species $[BeHSO_4(H_2O)_n]^+$ (n = 1, 2, 3) observed at *m/z* 124, 142 and 160 in agreement with the preference for charge reduction by interaction with the sulfato ligand rather than the deprotonation of coordinated water molecules (see Figure 2-5). Similarly, ESI-MS ions originating from the dimeric $[Be_2OH]^{3+}$ and trimeric $[Be_3(OH)_3]^{3+}$ beryllium species in solution were the $[Be_2OH(SO_4)(H_2O)_n]^+$ and $[Be_3(OH)_3SO_4(H_2O)_n]^+$ species where n = 0-3. Noteworthy is the observation that the solution pH equally influenced the counterion involvement with the ESI-MS ions in the gas phase. For instance at a higher capillary exit voltage (>100 V) or pH value 2.5, the ESI-MS ions involving the hydrogen sulfato species $[Be_2OH(HSO_4)_2(H_2O)_n]^+$ and $[Be_3(OH)_3(HSO_4)_2(H_2O)_n]^+$ became dominant due to increased protonation and

charge reduction. On the other hand, higher polynuclear species in solution were solely observed with the SO_4^{2-} anions as $[Be_5(OH)_6SO_4]^{2+}$ and $[Be_6(OH)_8SO_4]^{2+}$ at *m/z* 121 and 143 respectively, perhaps because the beryllium ions can cluster around SO_4^{2-} better than they can around HSO_4^-.

Other previously reported species[20] such as $[Be_2(OH)_2]^{2+}$, $[Be_3(OH)_4]^{2+}$, $[Be_5(OH)_7]^{3+}$ and $[Be_6(OH)_9]^{3+}$ could not be correlated to ESI-MS data, although the interpretation remains unclear about the existence of a sulfate-bound $[Be_2(OH)_2]^{2+}$ species in solution as a result of the ambiguity in differentiating $[(HSO_4)(OH)]^{2-}$ and $[(SO_4)(H_2O)]^{2-}$ as found in the signal at *m/z* 149. However, solvation and fragmentation trends suggest $[Be_2(OH)]^{3+}$ as the dimeric species in solution. On the other hand, ions at *m/z* 156 and 181 which were assigned to the species $[Be_3O_2(HSO_4)]^+$ and $[Be_4O_3(HSO_4)]^+$ respectively, agreed with the existence of a $[Be(OBe)_x]^{2+}$ species observed in a beryllium oxide and beryllium sulfate solution mixture.[43] Its occurrence in the ESI-MS spectra can be rationalised as $(BeO)_n$ adducts of the monomeric species $[Be(HSO_4)(BeO)_n]^+$ (where n = 1, 2, 3) corresponding to ions at *m/z* 131, 156 and 181 respectively.

2.2.5 Correlation of the negative ion mass spectra

In contrast to the ESI-MS spectra in the positive ion mode, fewer ions were observed in the negative mode with relatively low abundance except for the dominant hydrogen sulfate anion $[HSO_4]^-$ at *m/z* 97 as displayed in Figure 2-7. Other beryllium-containing ions such as $[HSO_4(BeO)_n]^-$ n=1,2 at *m/z* 122, 147, $[Be_2OH(SO_4)_2]^-$ *m/z* 227, $[Be_3O(OH)(SO_4)_2]^-$ *m/z* 252 and $[Be_3(OH)(SO_4)_3]^-$ *m/z* 332 could also be identified. While the suppression of the other species is due to the fact that the ion efficiency of the negative hydrogen sulfate ion is so dominant, it is also attributable to the poor electrospray properties of the aqueous solvent employed. Apparently, neat water is a poor electrospray solvent especially in the negative ion mode due to corona discharge at the capillary tip therefore prompting the need for further ESI-MS analysis in mixed solvent systems.[44]

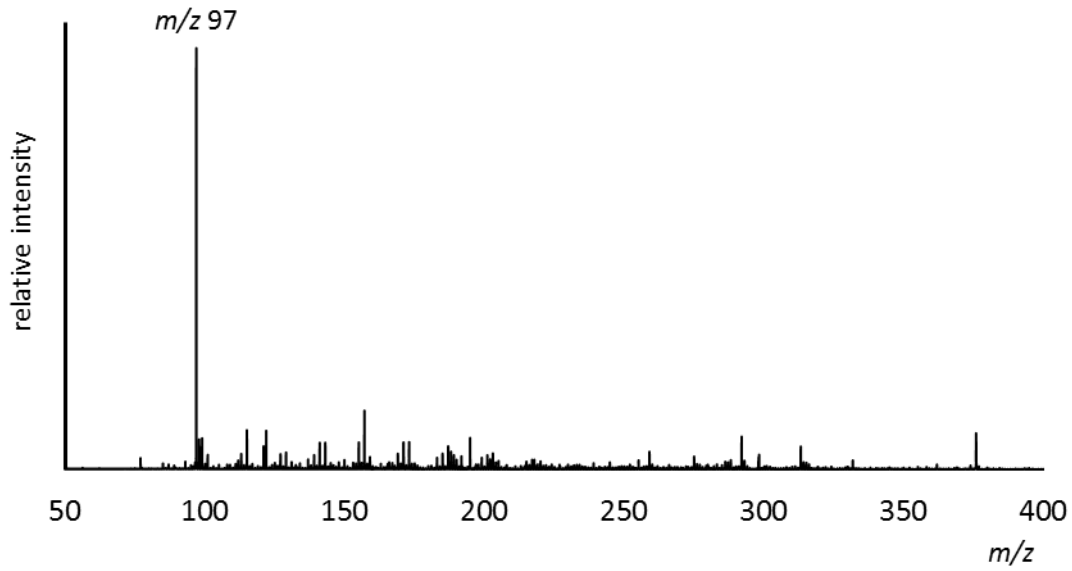

Figure 2-7 Negative ion ESI mass spectrum of 2.2 x 10^{-3} mol L^{-1} aqueous beryllium sulfate solution at a capillary exit voltage (CEV) of 80 V

2.2.6 ESI-MS investigation of beryllium sulfate in a mixed solvent system

Inherent to the ESI-MS technique is the electrostatic spraying of the liquid phase into an aerosol from which gas phase ion could be generated (see Chapter 1). This makes the choice of solvent for ESI-MS analysis not only an important consideration in order to obtain a good ion transmission but the solvent system is also a useful experimental variable for the confirmation of peak assignment.[26] In principle, any moderately polar solvent can be used for ESI-MS experiment although methanol and acetonitrile are the most commonly used solvents. However, with the continuous improvement in modern electrospray design and technology other solvents have been successfully employed especially with proper adjustment and fine-tuning of the instrument parameters such as the drying gas.[45] Nevertheless, pure water is a poor solvent for ESI-MS experiment since it has a high surface tension that degrades droplets fission and would require a higher source temperature to effectively desolvate the species into the gas phase. Nevertheless, the total ion chromatogram (TIC) for several ESI-MS experiments employing the beryllium sulfate solution in water only and in 1:1 methanol-water solution displayed in Figure 2-8 clearly illustrate the advantages of a more appropriate solvent system.

The improvement of the total ion transferred from the solution into the gas phase when employing a more suitable solvents is evident as indicated from the intensity count in Figure 2-8. Comparing ESI-MS experiments of beryllium sulfate of the similar concentration in water only (labelled B) and in 1:1 methanol-water (labelled A) solution (see Figure 2-8), the latter reveal a much higher signal intensity and fewer fluctuations in the transmission of the ions pointing out the improvement in the electrospray process (see Figure 2-8). Therefore, ESI-MS spectra of beryllium sulfate in H_2O/MeOH were considered in more detail.

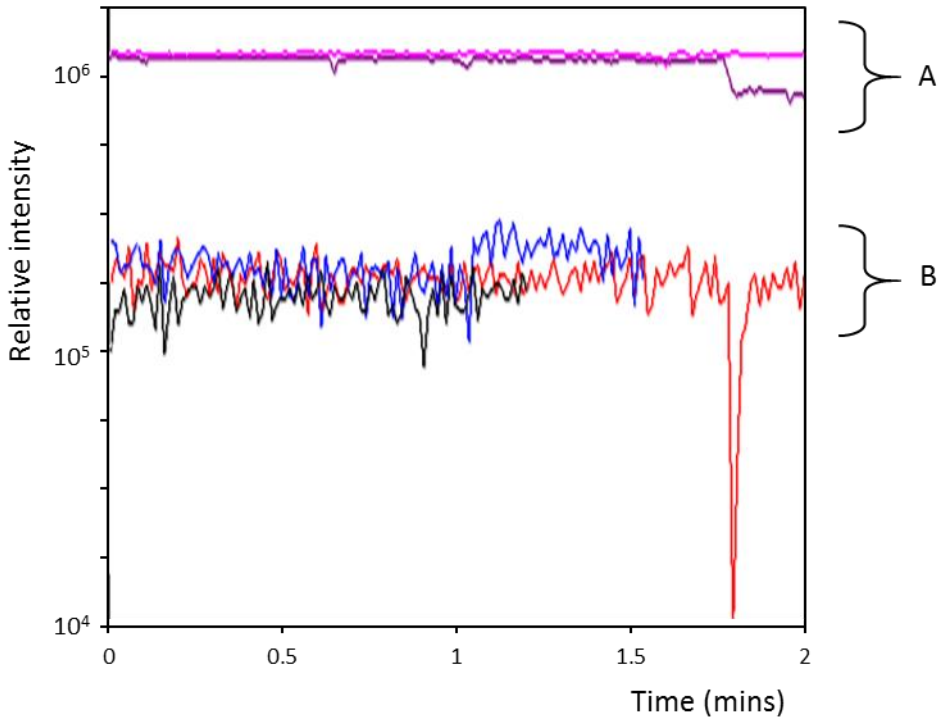

Figure 2-8 Total ion chromatrogram (TIC) for ESI-MS experiments of beryllium sulfate of similar concentration in (A) 1:1 methanol-water solutions (higher signal intensity and stable spray) (B) water only (lower signal intensity and less stable spray). Each line (colour) represents a different experiment conducted on different days.

The assignment of the majority of the ions observed in the ESI-MS experiment of beryllium sulfate in the 1:1 methanol-water solvent system are summarised in Table 2-3. The most pertinent observation is the preferential solvation of the Be^{2+} cation by the methanol over the aqua ligands in the gas phase. Almost all the species observed were solvated by methanol while previously dominant aqua solvated ions (see Table 2-1) were absent or diminished in intensity

compared to the spectra from pure water solutions. Secondly, because the methanol molecule has a labile proton which can be deprotonated, methoxido-bridged beryllium species were well observed although these species cannot be confidently distinguished by the mass spectrometer as a result of the possibilities of other assignment e.g. OH/CH_3OH, OCH_3/H_2O. Also, the observation of most peaks corresponding to the beryllium hydroxide species suggest that the hydroxide brigdes are still preferred over the corresponding methoxido-bridges. Lastly, the ESI-MS of beryllium sulfate in methanol-water solution revealed that the superior coordination of methanol solvent slightly reduced the observation of oligomeric species including the trimer.

Table 2-3 Summary of ions observed in the positive ion ESI mass spectra of 2.2 x 10^{-3} mol L^{-1} beryllium sulfate in 1:1 methanol-water solutions across capillary exit voltages of 60 – 180 V.

Expt ***m/z***	**Theoretical** ***m/z***	**ESI-MS ions**	**Expt** ***m/z***	**Theoretical** ***m/z***	**ESI-MS ions**
97.0579	97.0633	$[BeOCH_3(BeO)(CH_3OH)]^+$	140.0777	140.0809	$[Be_3(OH)_3(OCH_3)_2]^+$
129.0852	129.0895	$[BeOCH_3(BeO)(CH_3OH)_2]^+$	137.9938	137.9974	$[BeHSO_4(CH_3OH)]^+$
83.0418	83.0476	$[BeOH(BeO)(CH_3OH)]^+$	170.0694	170.0236	$[BeHSO_4(CH_3OH)_2]^+$
101.0425	101.0593	$[BeOH(BeO)(CH_3OH)(H_2O)]^+$	173.9917	173.9959	$[Be_3(OH)_3SO_4]^+$
115.0689	115.0738	$[BeOH(BeO)(CH_3OH)_2]^+$	188.0067	188.0115	$[(BeO)_2BeHSO_4(CH_3OH)]^+$
90.0940	90.0668	$[Be(OH)(CH_3OH)_2]^+$	213.0153	213.0186	$[(BeO)_3BeHSO_4(CH_3OH)]^+$
94.0923	94.0617	$[BeOH(H_2O)_2(CH_3OH)]^+$	238.0404	238.0257	$[(BeO)_4BeHSO_4(CH_3OH)]^+$
104.0815	104.0824	$[Be(OCH_3)(CH_3OH)_2]^+$	206.0179	206.0221	$[Be_3(OH)_3SO_4(CH_3OH)]^+$
108.0513	108.0773	$[BeOH(H_2O)(CH_3OH)_2]^+$	195.0818	195.0307	$[Be_2(OH)(SO_4)(CH_3OH)_2]^+$
122.1295	122.0930	$[Be(OH)(CH_3OH)_3]^+$	137.9938	137.9974	$[BeHSO_4(CH_3OH)]^+$
126.0628	126.0653	$[Be_3(OH)_3(OH)(OCH_3)]^+$	170.0694	170.0236	$[BeHSO_4(CH_3OH)_2]^+$
136.0576	136.1086	$[Be(OCH_3)(CH_3OH)_3]^+$			

2.2.7 Hydrolysis of beryllium ions in a H_2O/DMSO mixed solvent system

ESI-MS data of beryllium sulfate hydrolysis in a H_2O/DMSO solvent mixture indicated a diminished trend for beryllium hydrolysis to give polymeric species in the presence of a more strongly coordinating and less volatile solvent

(DMSO), consistent with trends observed from potentiometric measurements.[27] In contrast to hydrolysis in aqueous solution, the dominant ions in the ESI mass spectra of beryllium sulfate in a H_2O/DMSO solution are the dimeric and the monomeric species $[Be(DMSO)_4]^{2+}$ *m/z* 160, $[BeOH(DMSO)_2]^{+}$ *m/z* 182, and $[Be_2OH(SO_4)(DMSO)_2]^{2+}$ *m/z* 287 (see Figure 2-9). In the H_2O/DMSO mixed solvent system, the observed tetra-solvated beryllium dication $[Be(DMSO)_4]^{2+}$ at *m/z* 160 pointed to the superior stabilising ability of DMSO toward highly charged species in the gas phase and such DMSO-solvated metal dications $[M(DMSO)_4]^{2+}$, as well as other highly charged solvated metal ions species have been previously observed.[46] However, the stabilisation and preservation of multiply-charged hydroxido solution species into the gas phase (through possible ions such as $[Be_3(OH)_3(DMSO)_n]^{3+}$) was unsuccessful, as revealed in an illustrative mass spectrum of beryllium sulfate in H_2O/DMSO in Figure 2-9. As in the aqueous solution, ESI-MS of beryllium sulfate in H_2O/DMSO solvent mixtures also exhibited charge reduction by coordination of the sulfato ligand suggesting this interaction to be of significance even in solution. However, in the H_2O/DMSO mixed solvent systems, the sulfato ligands played a lesser role, hence a prominent signal assigned to the monomeric hydroxide $[BeOH(DMSO)_2]^{+}$ species was observed at *m/z* 182 while the trimeric ESI-MS ions $[Be_3(OH)_3SO_4(DMSO)_n]^{+}$ at *m/z* 330, 408 and other higher polymeric species were diminished in intensity. Also notable is the absence of BeO aggregates since a more strongly coordinating solvent

ligand would stabilise the charge density of the solvated Be^{2+} cation and reduce its propensity to be further deprotonated in the gas phase.

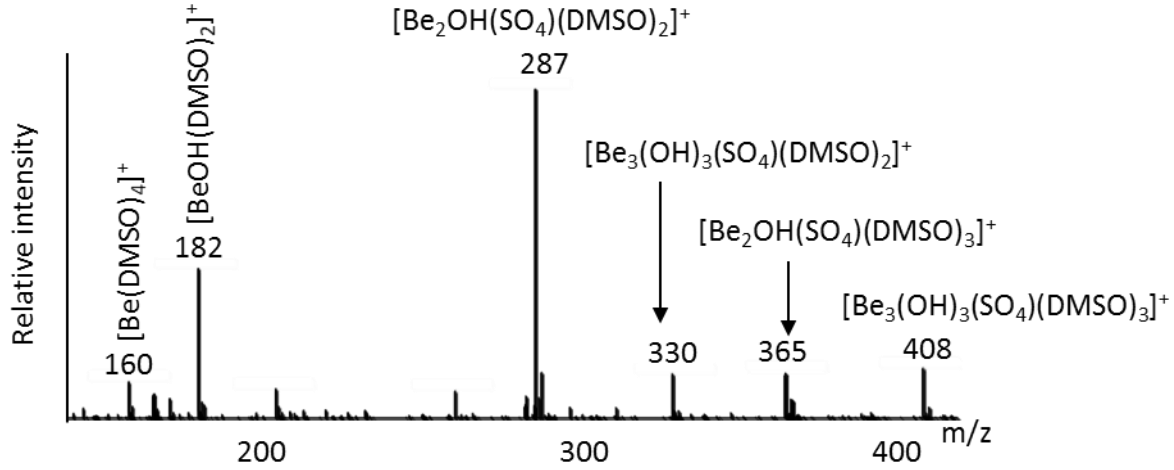

Figure 2-9 Positive ion ESI mass spectrum of 2.2 x 10^{-3} mol L^{-1} beryllium sulfate in a 1:1 H_2O/DMSO solvent mixture at a capillary exit voltage (CEV) of 120 V

2.2.8 Correlation of ESI-MS ions with concentration and pH of solution

Using a semi-quantitative approach (see Table 2-2), the relative peak intensities of ESI-MS ions were examined in correlation with the pH of beryllium solutions injected into the ESI-MS. The ESI-MS representation of the hydrolytic tendencies of beryllium ions with change in solution pH is shown in Figure 2-10.

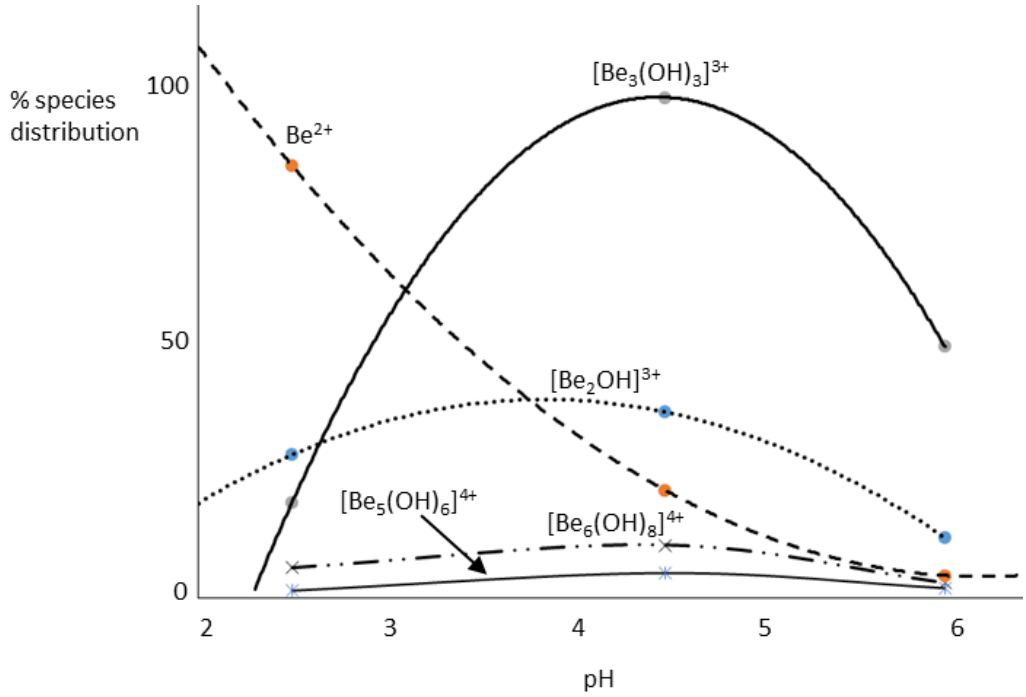

Figure 2-10 ESI-MS speciation diagram showing the pH-dependent hydrolytic trend of beryllium ions in a 2.2 x 10^{-3} mol L^{-1} solution. (Deduced from the peak intensities of representative ESI-MS ions correlated to the beryllium hydroxido cores of the species in solution ignoring H_2O, SO_4^{2-} ions and other adducts)

Signal intensities from the illustrative ESI mass spectra at pH_{feed} 2.5, 4.5 and 6.0 shown in Figure 2-4 have further been summarised in Table 2-2. Data from the relative abundance of species in the mass spectra clearly confirms that the predominant species in beryllium hydrolysis is the beryllium trimer $[Be_3(OH)_3]^{3+}$. In acidic solutions of pH less than 3, beryllium exists as the monomeric tetraaqua coordinated dicationic species $[Be(H_2O)_4]^{2+}$ and this is consistent with the observation of its representative monomeric ESI-MS ion $[Be(HSO_4)(H_2O)_2]^+$ *m/z* 142 as the base peak at pH_{feed} 2.5 (see Figure 2-4). The higher concentration of protons at this pH also resulted in the abundance of ESI-MS ions containing the hydrogen sulfate species $[HSO_4]^-$ such as $[Be_2OH(HSO_4)_2(H_2O)_2]^+$ at *m/z* 265 and $[Be_3(OH)_3(HSO_4)_2(H_2O)]^+$ at *m/z* 290.

Upon increasing the pH of the beryllium solution, the onset of polymerisation in solution can be seen in the distribution of the ESI-MS ions at pH_{feed} 4.5 and 6.0. At pH_{feed} 4.5, the beryllium trimer is already the most dominant species in solution but is now observed in the ESI mass spectra with the sulfate

anion as the species $[Be_3(OH)_3SO_4(H_2O)_3]^+$ at *m/z* 228. Figure 2-4 also reveals that the ESI spectra of beryllium sulfate solution at pH_{feed} 4.5 were the most complicated of all the pHs examined. This is because the trimer $[Be_3(OH)_3]^{3+}$ (which is predominant at pH_{feed} 4.5) yielded a variety of aggregates in the gas phase. Potentiometric measurements of aqueous beryllium solution at pH 6.0 have pointed out the predominance of a $Be(OH)_2$ species alongside a decline in the trimer $[Be_3(OH)_3]^{3+}$ abundance in solution.[20, 29] However, ESI mass spectra of the beryllium solution at pH_{feed} 4.5 and 6.0 showed the trimeric ion $[Be_3(OH)_3SO_4(H_2O)_3]^+$ *m/z* 228 as the base peak. This may be related to the pH decreasing during droplet evaporation such that the actual pH in the droplet (which of course cannot be controlled) will be lower than the starting pH.[47] Nevertheless, since $Be(OH)_2$ is neutral and cannot be adequately represented in the mass spectra (except as adducts with pre-existing charged species), the trimer $[Be_3(OH)_3]^{3+}$ remained the most abundant solution species suitably charged to yield corresponding ESI-MS ions at both pH_{feed} 4.5 and 6.0. Adducts which likely contained the $Be(OH)_2$ species included $[Be_3(OH)_3(HSO_4)Be(OH)_2(H_2O)_3]^{2+}$ *m/z* 136 and $[Be_3(OH)_3(HSO_4)_2Be(OH)_2(H_2O)]^+$ *m/z* 333. The emergence of these species and increase in their relative abundance from pH_{feed} 4.5 to pH_{feed} 6.0 supports the existence of $Be(OH)_2$ in solution prior to precipitation, most likely as colloidal dispersed species due to the low concentration in this study. Furthermore, at pH_{feed} 6.0 the relative intensity of the dimeric species declined to 16% from an intensity of 60% at pH_{feed} 4.5 while the monomeric species reduced to 6% from 100% at pH_{feed} 2.5 (Table 2). This is consistent with the formation of polynuclear hydroxido species with increasing pH in solution up to 6.0.

The potential of ESI-MS as a sensitive technique for the detection of Be speciation is evident not only by its ability to illustrate the existence of the beryllium hydroxido species $[Be_5(OH)_6]^{4+}$ and $[Be_6(OH)_8]^{4+}$ but also to further provide insightful quantitative data over their relative abundance in solution. These species are known to exist at low abundance in beryllium solutions and are often undetectable at lower concentrations.[20] In a beryllium solution of concentration 10^{-3} mol L^{-1}, ESI-MS data suggest that the $[Be_6(OH)_8]^{4+}$ derived species exist in about 20% abundance while the $[Be_5(OH)_6]^{4+}$ exist in 10% abundance relative to the

trimer species $[Be_3(OH)_3]^{3+}$. The formation of polymeric hydroxido species in beryllium hydrolysis is equally dependent on the solution concentration. At a concentration of 10^{-4} mol L^{-1}, the ratio of the signal intensity for the monomeric, dimeric and trimeric ESI-MS ions is 1:14:4 showing the diminished significance of the trimeric species in solution as the beryllium concentration reduces. At concentrations of 10^{-6} mol L^{-1} the only species expected in solution are species derived from the mononuclear complexes $[Be(H_2O)_4]^{2+}$ and $Be(OH)_2$ (the latter is by mass spectrometry). However, the poor electrospray properties of pure water[47] coupled with the low ionisation efficiency of species in this study limited their observation due to an increased signal to noise ratio that was noted at lower concentrations ($<10^{-5}$ mol L^{-1}).

While correlating the relative peak intensities of ESI-MS ions with the abundance of beryllium hydroxido species in solution, the inclusion of the beryllium oxide adducts such as $[Be_3(OH)_3(BeO)_n(H_2O)_n]^+$ revealed a better correlation with the abundance of the trimer in solution. However, it resulted in an underestimation of monomeric species in solution which were the likely origin of the beryllium oxide adducts $(BeO)_n$. Likewise, the shrinking of the droplets during the electrospray process can segregate among species transferred into the gas phase depending on their solvation energies and this further distorts speciation data from ESI-MS. Unfortunately, standardisation of peak intensity is difficult to achieve because of the complex equilibria between the hydroxido species in solution and the complicated ESI-MS spectra obtained. Nevertheless, ESI results revealed an impressive representation of the trend in beryllium hydrolysis probably due to the interaction of the solution species with the sulfato ligands to yield species of similar charge density in the gas phase.

2.2.9 Fragmentation of hydrolysed beryllium species

To confirm assignments of ESI-MS ions and their correlation to beryllium hydroxido species in solution, gas phase collision-induced dissociation (CID) experiments have further been carried out on selected dimeric and trimeric ESI-MS ions. Using ESI ion-trap mass spectrometry, ions were isolated, activated by collision and allowed to dissociate providing information on the degradation

pathway and stability of these beryllium hydroxido species. Depending on the level of collision energy supplied, the fragmentation pathway consisted of consecutive stripping of water molecules to degradation into the mononuclear metal hydroxide alongside and oftentimes further re-aggregation into a trimer. The stripping of water molecules which was earlier noted as intrinsic to the ionisation process was already initiated during the electrospray process even under very mild ionisation conditions and ESI-MS experiments across capillary exit voltages from 60 to 180 V afforded a change of relative intensity trends among the fragmentation series as shown in Figure 2-11. The average hydration number (n_{av}) of the monomer, dimer and trimeric clusters shown in Table 2-2 was calculated under mild ionisation conditions (60 V) according to the equation $n_{av} = \sum(n.rI^n)/\sum(rI^n)$ where rI^n is the relative intensity of a given beryllium cluster with hydration number n. Clearly, the level of hydration is consistent with the degree of polymerisation but it is further reduced by the coordination of the sulfate ion.

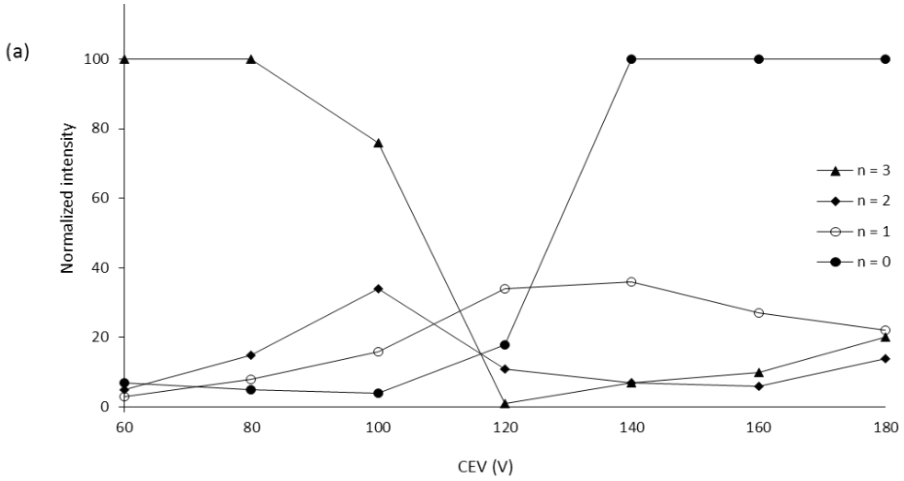

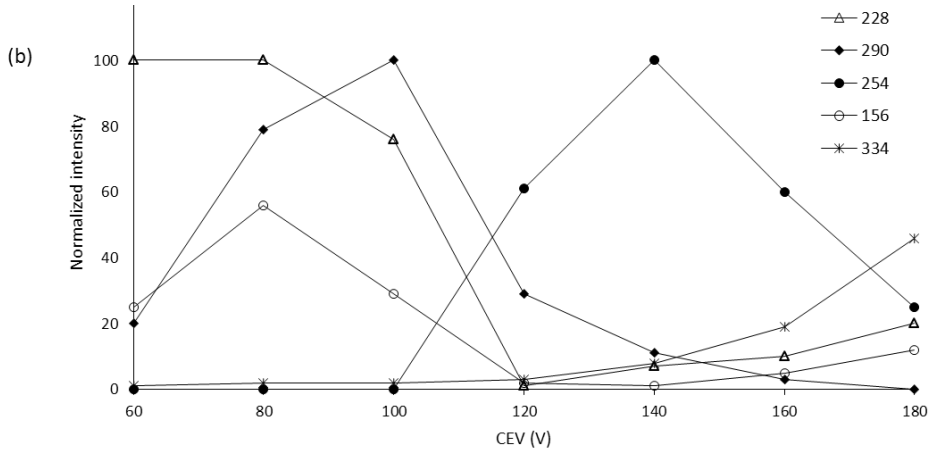

Figure 2-11 (a) ESI-MS trends of signals *m/z* 174, 192, 210 and 228 corresponding to $[Be_3(OH)_3SO_4(H_2O)_n]^+$ where n = 0-3. (b) ESI-MS trends of signals *m/z* 228 $[[Be_3(OH)_3SO_4(H_2O)_3]^+]$, *m/z* 290 $[Be_3(OH)_3(HSO_4)_2(H_2O)]^+$, *m/z* 254 $[Be_3O(OH)(HSO_4)_2]^+$, *m/z* 156 $[Be_3O(OH)(HSO_4)_2]^+$ and *m/z* 334 $[Be_3O(HSO_4)_2]^+$ corresponding to various beryllium trimeric aggregates in the gas phase with increasing capillary exit voltages (CEV).

More energetic fragmentation of the mixed hydroxido/sulfato complexes (e.g. the dimeric ESI-MS ion $[Be_2OH(SO_4)(H_2O)_3]^+$ *m/z* 185 in Figure 2-12a), show preference for the loss of an acid molecule (H_2SO_4) to yield oxido/hydroxido bridged complexes (e.g. the $[Be_2OH(O)(H_2O)_2]^+$ *m/z* 87 in Figure 2-12a). The peak at *m/z* 87 increases in intensity continuously until it eventually dominates the spectrum as the base peak instead of the sulfato species. Other fragmentation pathways which have been illustrated in Figure 2-13 proceed by the loss or addition of other neutral species such as BeO or $Be(OH)_2$. Under elevated fragmentation conditions, CID of the dimeric ESI-MS ion $[Be_2OH(SO_4)(H_2O)_3]^+$ (*m/z* 185) solely yields the $[BeOH(H_2O)]^+$ species at *m/z* 44 alongside a minor peak of the trimer $[Be_3(OH)_3SO_4(H_2O)_3]^+$ at *m/z* 228 suggesting possible re-aggregation of the $[BeOH(H_2O)]^+$ fragment in the gas phase into the trimer. This supports the aggregation pathway in solution suggested to involve the linkage of the monomeric hydroxide to form $[BeOH]_n^{n+}$ where n = 3 yields the most prevalent oligomer.[48]

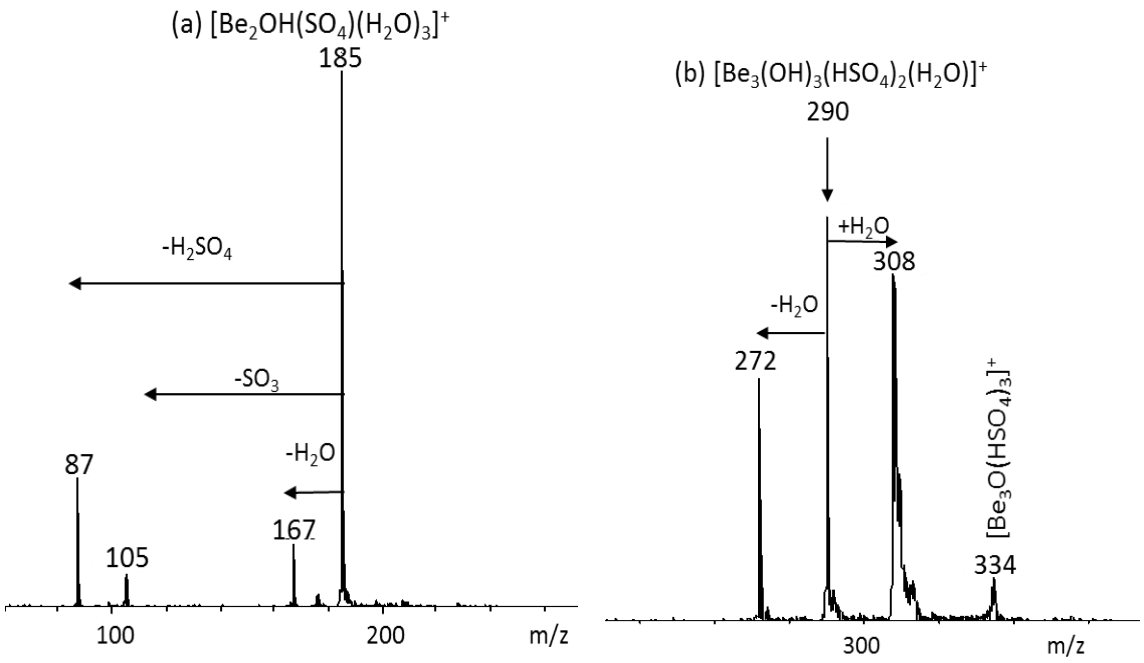

Figure 2-12 Fragmentation of ESI-MS ions using an ion trap mass spectrometer (a) $[Be_2OH(SO_4)(H_2O)_3]^+$ at *m/z* 185 showing the competing loss of acid and (b) $[Be_3(OH)_3(HSO_4)_2(H_2O)]^+$ at *m/z* 290 showing the sequential loss of water molecules and an early stage of rearrangement into the $Be_3(\mu_3\text{-}O)$ cluster in the gas phase.

The significance of the trimeric arrangements for beryllium hydroxido species in solution is also supported by the fragmentation of the trimeric ESI ion $[Be_3(OH)_3(HSO_4)_2(H_2O)]^+$ at *m/z* 290 (Figure 2-12b) which reveals a preference to substitute ligands and maintain a trimeric arrangement for the beryllium ions rather than the loss of simple neutral molecules. Interestingly, the eventual degradation of the trimer solely yields the monomeric hydroxide $[BeOH(H_2O)]^+$ skipping the dimeric species. Generally, under collision in the gas phase, the bridging hydroxido ligand in the trimer was deprotonated or substituted with sulfato ligands revealing a mixture of oxido, hydroxido and sulfato species such as $[Be_3(OH)O(HSO_4)_2]^+$ *m/z* 254. An increase in capillary exit voltage (CEV) also favoured the hydrogen sulfate species $[HSO_4]^-$ over the more highly charged SO_4^{2-}, therefore at voltages between 140 – 180 V, the trimeric ESI-MS ion was observed at *m/z* 290, 272 and 254 assigned as $[Be_3(OH)_3(HSO_4)_2(H_2O)]^+$, $[Be_3(OH)_3(HSO_4)_2]^+$ and $[Be_3(OH)_3(HSO_4)_2]^+$ respectively. These species, which were of relatively high

abundance (see Figure 2-12), show the stability of these other trimeric arrangements of the beryllium ion such as the $Be_3(\mu_3\text{-}O)$ which have also been observed in the solid state and NMR investigations.[49, 50] In this study, several ions such as $[Be_3O_2(HSO_4)]^+$ at *m/z* 156, $[Be_3(OH)O(HSO_4)_2]^+$ at *m/z* 254 and $[Be_3O(HSO_4)_3]^+$ at *m/z* 334 support a $Be_3(\mu_3\text{-}O)$ cluster with a symmetrical structure having similarities with that of basic beryllium acetate $Be_4O(O_2CCH_3)_6$ with 3 sulfato ligands bridging the beryllium ions in a near planar configuration. In an earlier study,[51] fragmentation of the nitrato species $Be_4O(NO_3)_6$ in electron ionisation mass spectrometry yielded the ions $[Be_4O(NO_3)_5]^+$, $[Be_4O_2(NO_3)_3]^+$ and $[Be_3O(NO_3)_3]^+$ and in this study with the sulfate anion, the analogous ions $[Be_3O(HSO_4)_3]^+$ at *m/z* 334 and $[Be_4O_2(HSO_4)_3]^+$ at *m/z* 359 were observed. However, $[Be_4O(HSO_4)_5]^+$ was absent, suggesting that the $[Be_3O(HSO_4)_3]^+$ species results from the rearrangement of the trimer $[Be_3(OH)_3(HSO_4)_2(H_2O)]^+$. This observation was also supported by the fragmentation path of $[Be_3(OH)_3(SO_4)(H_2O)_3]^+$, *m/z* 228. Essentially the trimeric cores of the beryllium complex at *m/z* 290 and *m/z* 228 are similar differing only from the number and protonation state of the sulfate ion, the transmutation of the $Be_3(OH)_3$ core into the $Be_3(\mu_3\text{-}O)$ core can be confidently justified. Furthermore, the $Be_3(\mu_3\text{-}O)$ core has also been observed by in a related study on bidentate diketonato ligands (see Chapter 3) indicating it could be another stable configuration within beryllium aggregates.

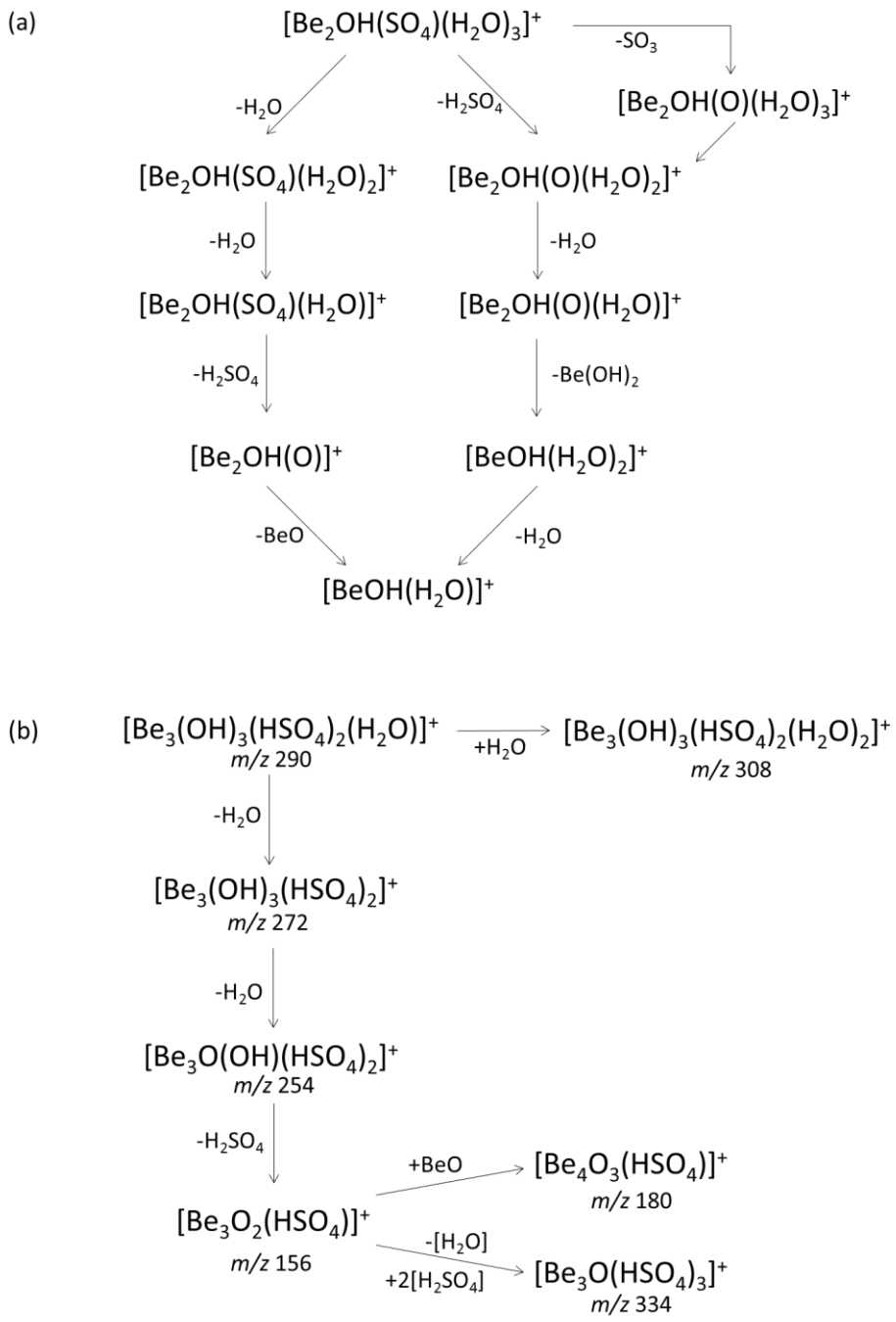

Figure 2-13 (a) Fragmentation scheme of the beryllium dimer $[Be_2(OH)SO_4(H_2O)_3]^+$ at *m/z* 185 and (b) the trimer $[Be_3(OH)_3(HSO_4)_2(H_2O)]^+$ at *m/z* 290

2.3 ESI-MS investigation of beryllium chloride solutions

Ion assignments for the positive- and negative-ion ESI-MS of aqueous beryllium chloride solution prepared by dissolution of beryllium metal in hydrochloric acid (see Chapter 7) are outlined in Table 2-4. As observed with the beryllium sulfate solution, ESI-MS speciation of the aqueous solution of beryllium chloride was equally influenced by the electrospray process as illustrated in Figure 2-5. This resulted in charge reduction of the pre-existing solution species with the chloride ions as displayed in Figure 2-14 for the beryllium trimer. However, it was observed that this charge reduction process was relatively less prevalent in the presence of the chloride as compared to the sulfate solution (for instance compare ion assignment in Table 2-1 and Table 2-4). This is in accord with other solution-based experimental reports which have observed higher level of inner sphere complexation in sulfate-containing solutions in comparison to those containing chloride ion.[21, 40]

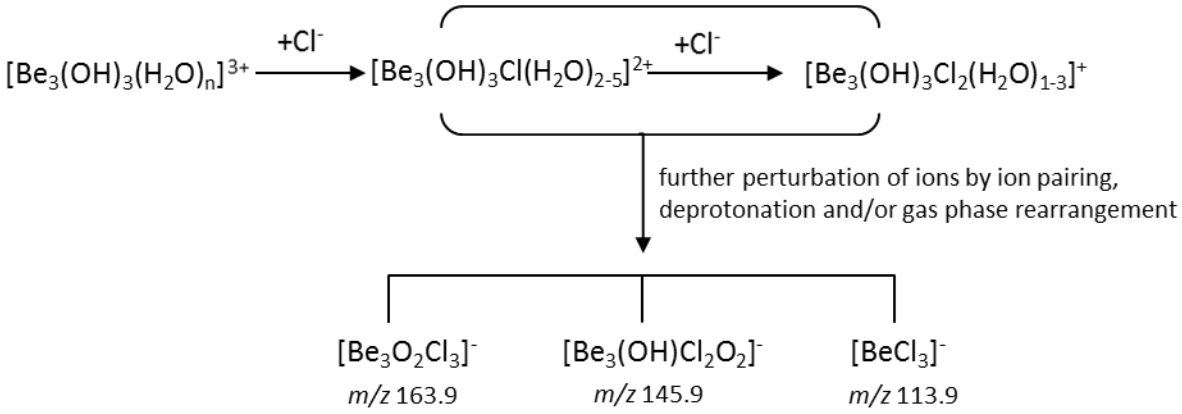

Figure 2-14 Correlation of the beryllium species in solution to the ESI-MS ions observed in the ESI-MS of aqueous beryllium chloride solution.

Table 2-4 Summary of ions observed in the positive ion ESI mass spectra of 2.2 x 10^{-3} mol L^{-1} aqueous beryllium chloride solutions at a capillary exit voltage of 60 V and pH 4.7.

Experimental *m/z*	**Theoretical** *m/z*	**ESI-MS ions**	**Experimental** *m/z*	**Theoretical** *m/z*	**ESI-MS ions**	**Experimental** *m/z*	**Theoretical** *m/z*	**ESI-MS ions**
		Positive ESI-MS ions						Negative ESI-MS ions
104.0831	*104.0824*	$[Be(OCH_3)(CH_3OH)_2]^+$	*137.0268*	*137.0123*	$[BeCl(H_2O)(BeO)_3]^+$	*113.9415*	*113.9181*	$[BeCl_3]^-$
148.0186	*147.9819*	$[Be_3(OH)_3Cl_2]^+$	*179.9962*	*180.0300*	$[BeCl(H_2O)_2(BeO)_4]^+$	*95.9120*	*95.9965*	$[BeOCl(H_2O)]^-$
166.0213	*165.9924*	$[Be_3(OH)_3Cl_2(H_2O)]^+$	*173.0323*	*173.0334*	$[BeCl(H_2O)_3(BeO)_3]^+$	*138.9505*	*138.9252*	$[Be_2OCl_3]^-$
183.9913	*184.0030*	$[Be_3(OH)_3Cl_2(H_2O)_2]^+$	*198.0175*	*198.0405*	$[BeCl(H_2O)_3(BeO)_4]^+$	*163.9678*	*163.9323*	$[Be_3O_2Cl_3]^-$
202.0011	*202.0136*	$[Be_3(OH)_3Cl_2(H_2O)_3]^+$	*241.0281*	*241.0582*	$[Be_6O(OH)_6Cl(OH)_2]^+$	*181.9429*	*181.9429*	$[Be_3O_2Cl_3(H_2O)]^-$
240.0131	*239.9429*	$[Be_3(OH)_3Cl_2(H_2O)_3(HCl)]^+$	*276.9798*	*276.9904*	$[Be_6O(OH)_6Cl_3]^+$	*206.9504*	*206.9500*	$[(BeO)_3BeCl_3(H_2O)]^-$
74.5318	*74.5168*	$[Be_3(OH)_3Cl(H_2O)_2]^{2+}$	*216.0352*	*216.0066*	$[Be_5O(OH)_4Cl_2OH]^+$	*244.9739*	*244.9267*	$[(BeO)_3BeCl_3(H_2O)(HCl)]^-$
83.5147	*83.5221*	$[Be_3(OH)_3Cl(H_2O)_3]^{2+}$	*259.0178*	*259.0243*	$[Be_6O(OH)_6Cl_2OH]^+$	*281.0384*	*280.9004*	$[(BeO)_3BeCl_3(H_2O)(HCl)_2]^-$
92.5194	*92.5273*	$[Be_3(OH)_3Cl(H_2O)_4]^{2+}$	*190.9890*	*190.9995*	$[Be_4O_3Cl(H_2O)_2HCl]^+$	*262.8915*	*262.8891*	$[(BeO)_3BeCl_3(HCl)]^-$
101.5282	*101.5326*	$[Be_3(OH)_3Cl(H_2O)_5]^{2+}$	*87.0349*	*86.9981*	$[Be_2(OH)_2Cl]^+$	*145.9947*	*145.9662*	$[Be_3(OH)Cl_2O_2]^-$
96.0348	*96.0256*	$[Be_3(OH)_3Cl(H_2O)_5BeO]^{2+}$	*105.0010*	*104.9642*	$[Be_2(OH)_2Cl(H_2O)]^+$			
227.0069	*226.9318*	$[Be_3(OH)_3Cl_2(BeCl_2)]^+$	*123.0130*	*122.9748*	$[Be_2(OH)_2Cl(H_2O)]^+$			
209.0051	*208.9656*	$[Be_3(OH)_3(OH)Cl(BeCl_2)]^+$	*141.0209*	*140.9853*	$[Be_2(OH)_2Cl(H_2O)_2]^+$			
119.0151	*119.0017*	$[Be_4O_3Cl]^+$						
130.0488	*130.0148*	$[Be_3(OH)_3(OH)Cl]^+$						
112.0405	*112.0052*	$[BeCl(H_2O)(BeO)_2]^+$						

2.3.1 Cationic ESI-MS ions

An illustrative positive ion mass spectrum of aqueous beryllium chloride solution is shown in Figure 2-15. Since pre-existing solution species were positively charged, they were readily transferred and detected in the mass spectrometer as cations often with distinct correlation to the well-established beryllium hydroxido species.[20] Consequently, despite the complexity of the spectra, the majority of the signals could be assigned by the simple correlation to pre-existing solution species employing the general formula $[Be_x(OH)_yCl_z(H_2O)_n]^+$ where n =1-2 and n= 0-4 (see Table 2-4). This highlights the good qualitative ESI-MS representation of pre-existing beryllium hydroxido species in an aqueous solution of beryllium chloride. For instance, the ESI-MS ion signals at *m/z* 105 and 123 which were assigned as $[Be_2OHCl_2]^+$ and $[Be_2OHCl_2(H_2O)]^+$ respectively correlate well with the beryllium hydroxide dimeric species $[Be_2(OH)]^{3+}$ in the solution. Furthermore, in agreement with the dominance of this beryllium hydroxido trimer, over 60% of all ESI-MS ions could be assigned from a beryllium trimeric species with the main ions including the monocation series $[Be_3(OH)_3Cl_2(H_2O)_{0-4}]^+$ and the dication series $[Be_3(OH)_3Cl(H_2O)_{1-5}]^{2+}$. In addition, other species of high nuclearity relatable to the trimer (perhaps as a result of gas phase aggregations) include the tetramers $[Be_3(OH)_3Cl(H_2O)_5BeO]^{2+}$ and $[Be_3(OH)_3Cl_2(BeCl_2)]^+$. Polynuclear beryllium species (of type Be_{5-6}) are also known to pre-exist in solution and are most likely the origin of the corresponding Be_{5-6} polynuclear ESI-MS ions such as $[Be_6O(OH)_{6-8}Cl_{1-3}]^+$. On the other hand, assignment of ion signals *via* a simplistic correlation to the known pre-existing beryllium hydroxido cores in solution was inapplicable to many other ESI-MS ions as a result of a more intense perturbation to the solution state. Such ions point out that in addition to the polymeric species in solution, a variety of gas phase polymerisation pathway are accessible to the Be^{2+} cation especially in association with the trimer arrangement (e.g. ions such as $[Be_4O_3Cl(H_2O)_{1-3}]^+$, $[Be_5O_4Cl(H_2O)_{1-3}]^+$.

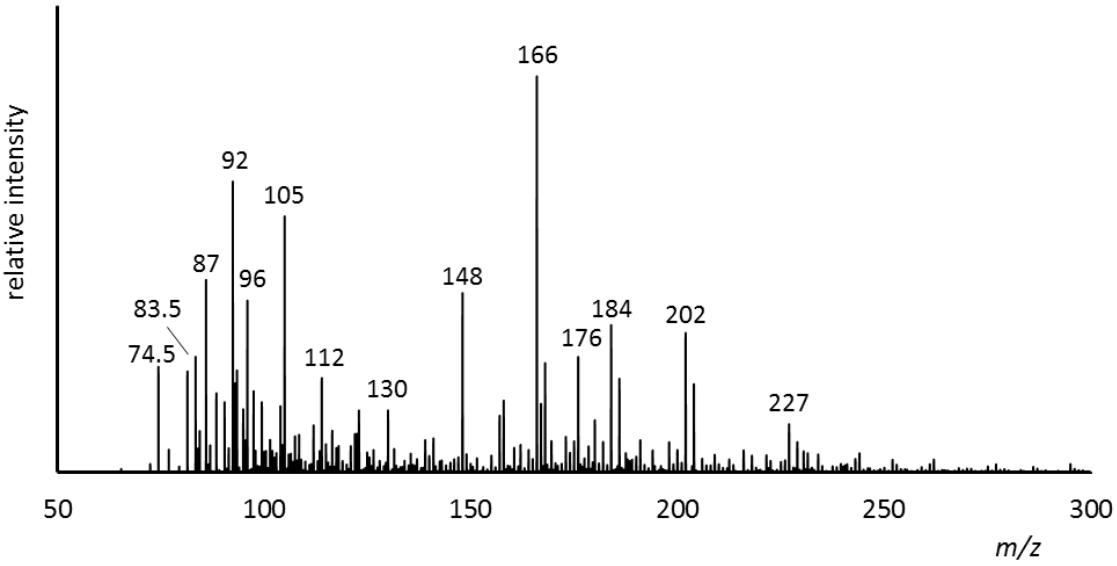

Figure 2-15 Positive ion ESI mass spectrum of 2.2 x 10^{-3} mol L^{-1} aqueous beryllium chloride solution at a capillary exit voltage (CEV) of 80 V and pH 4.7.

2.3.2 Anions

In comparison to the positive ion mass spectra, fewer and less intense signals were observed in the negative ion mode as illustrated in Figure 2-16. In addition, the negative ions reveal a less direct qualitative correlation to the solution speciation as shown in Figure 2-14. This is because the pre-existing cations in solution were expectedly more perturbed while being transformed into anionic ESI-MS ions (often involving a charge difference 3-4). Typically, a combination of deprotonation of the hydroxido core or coordination of Cl^- ion revealed a variety of anionic polynuclear beryllium complexes. The identified anionic ESI-MS ions shown in Table 2-4 were mainly singly charged containing one to four berylliums and were less hydrated.

2.3.3 OH^-/Cl^- substitution

One of the most noticeable features of the ion assignment in Table 2-2 is the obvious involvement of the chloride ion. The majority of the species in the ESI-MS of aqueous beryllium chloride solution were mixed beryllium chlorido/oxido/hydroxido complexes indicating an active involvement of the chloride anion in the gas phase although the same is not observed in aqueous

solution. For instance, EXAFS investigation of aqueous beryllium chloride solution indicated that only 10-15 % of inner sphere complexes pre-exist in solution.[52] Therefore, it is quite obvious that the increase in salt concentration and pH changes during the continuous shrinking of the droplet promotes the formation of most of the species in Table 2-4. However, compared to the sulfate ion, the chloride ion is a less versatile ligand for beryllium both in solution and in the gas phase. As a result, the ESI-MS ions from aqueous beryllium chloride solution generally revealed a higher hydration in comparison to the ESI-MS ion observed from beryllium sulfate under the same ionisation conditions.

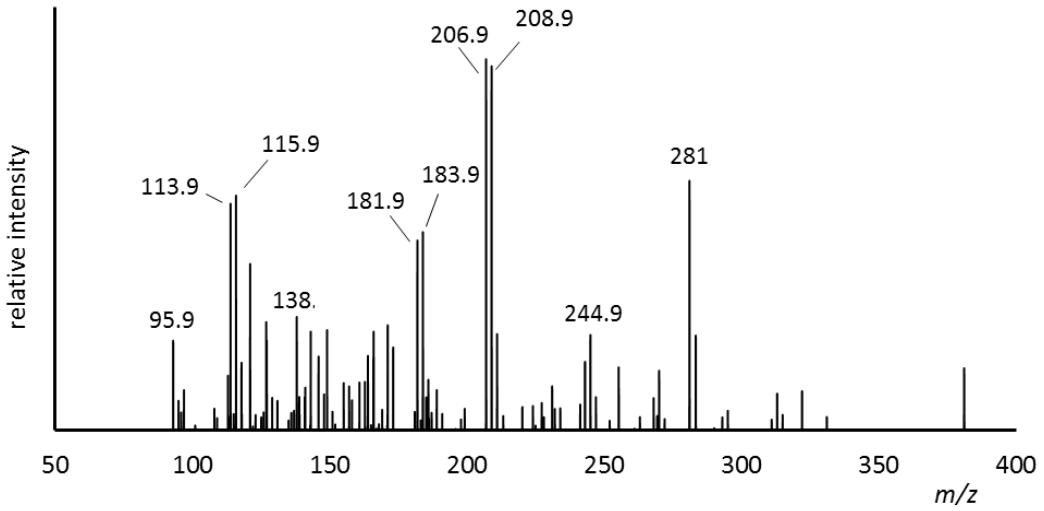

Figure 2-16 Negative ion ESI mass spectrum of 2.2 x 10^{-3} mol L^{-1} aqueous beryllium chloride solution at a capillary exit voltage (CEV) of 80 V and pH 4.7.

Secondly, it was also observed that the hydration of the beryllium chlorido complexes depended on the number of chloride ions in the complex. For instance in the ion series $[Be_3(OH)_3Cl_2(H_2O)_n]^+$ the number of water molecules observed was n=1-3 whereas for the series $[Be_3(OH)_3Cl(H_2O)_3]^{2+}$ a higher hydration was observed with n=2-5. This dependence of the level of microsolvation of the ESI-MS ion upon the number of Cl ions depicts the ligand exchange process which will be considered in more detail by employing computational simulation of beryllium complexes in an aqueous environment in the next Chapter.

2.4 Conclusions

This work has described the use of ESI-MS as an analytical tool for the investigation of beryllium speciation in solution. Using a qualitative and semi-quantitative approach, we have shown the ability of the ESI source to transfer beryllium hydroxide species from solution into the mass spectrometer thereby obtaining an approximate but quick screening of the hydrolytic tendencies in acidic solution of beryllium sulfate in agreement with present understanding of the beryllium species existing in solution. Additional insight into the role of the sulfato and chlorido ligand on beryllium hydrolysis was obtained justifying the possibility of inne-sphere complexes in beryllium solutions as a result of salt anions such as the sulfate to coordinate to the beryllium cation in a variety of modes. Furthermore, fragmentation of beryllium hydroxido species provided extra support for the stability and preference for a trimeric arrangements for the beryllium aggregate species. Although pre-existing solution species and hydrolytic trends in beryllium solutions were clearly preserved on transfer into the gas phase, careful correlation is required in deducing beryllium speciation in solution since the electrospray process and gas phase modifications were found to have a profound effect on the complexity of spectra. Nevertheless, these results have shown that the ESI-MS could provide an alternative, safe and sensitive solution-based technique for the investigation of beryllium speciation with other ligands of interest and this understanding of the ESI-MS behaviour of the Be^{2+} cation from this study would be a reference point in the microscale synthesis of beryllium complexes in solution for ESI-MS competition studies of beryllium ions with various ligands and other likely interfering metal cations.

2.5 References

1. M. E. Kolanz, *Applied Occupational and Environmental Hygiene*, 2001, **16**, 559-567.

2. K. A. Walsh and E. E. Vidal, *Beryllium Chemistry and Processing*, ASM International, Ohio, 2009.

3. G. M. Clayton, Y. Wang, F. Crawford, A. Novikov, B. T. Wimberly, J. S. Kieft, M. T. Falta, N. A. Bowerman, P. Marrack and A. P. Fontenot, *Cell*, 2014, **158**, 132-142.

4. C. Saltini and M. Amicosante, *The American Journal of the Medical Sciences*, 2001, **321**, 89-98.

5. C. Strupp, *Annals of Occupational Hygiene*, 2011, **55**, 43-56.

6. B. L. Scott, T. M. McCleskey, A. Chaudhary, E. Hong-Geller and S. Gnanakaran, *Chemical Communications*, 2008, **25**, 2837-2847.

7. T. M. McCleskey, D. S. Ehler, T. S. Keizer, D. N. Asthagiri, L. R. Pratt, R. Michalczyk and B. L. Scott, *Angewandte Chemie International Edition*, 2007, **119**, 2723-2725.

8. H. V. Diyabalanage, K. Ganguly, D. S. Ehler, G. E. Collis, B. L. Scott, A. Chaudhary, A. K. Burrell and T. M. McCleskey, *Angewandte Chemie International Edition*, 2008, **120**, 7442-7444.

9. O. Raymond, L. C. Perera, P. J. Brothers, W. Henderson and P. G. Plieger, *Chemistry in New Zealand*, 2015, **79**, 137-143.

10. S. P. Santoso, A. E. Angkawijaya, F. E. Soetaredjo, S. Ismadji and Y.-H. Ju, *Journal of Molecular Liquids*, 2015, **212**, 524-531.

11. C. S. Oh, C. W. Lee and J. Y. Lee, *Chemical Communications*, 2013, **49**, 3875-3877.

12. H. Matsumiya, H. Hoshino and T. Yotsuyanagi, *Analyst*, 2001, **126**, 2082-2086.

13. C. H. Stephan, M. Fournier, P. Brousseau and S. Sauvé, *Chemistry Central Journal*, 2008, **2**, 1-9.

14. C. H. Stephan, S. Sauvé, M. Fournier and P. Brousseau, *Journal of Applied Toxicology*, 2009, **29**, 27-35.

15. J. Akitt and R. H. Duncan, *Journal of the Chemical Society, Faraday Transactions 1*, 1980, **76**, 2212-2220.

16. P. G. Plieger, D. S. Ehler, B. L. Duran, T. P. Taylor, K. D. John, T. S. Keizer, T. M. McCleskey, A. K. Burrell, J. W. Kampf and T. Haase, *Inorganic Chemistry*, 2005, **44**, 5761-5769.

17. P. G. Plieger, K. D. John and A. K. Burrell, *Polyhedron*, 2007, **26**, 472-478.

18. P. G. Plieger, K. D. John, T. S. Keizer, T. M. McCleskey, A. K. Burrell and R. L. Martin, *Journal of the American Chemical Society*, 2004, **126**, 14651-14658.

19. K. J. Shaffer, R. J. Davidson, A. K. Burrell, T. M. McCleskey and P. G. Plieger, *Inorganic Chemistry*, 2013, **52**, 3969-3975.

20. L. Alderighi, P. Gans, M. Stefeno and A. Vacca, in *Advance in Inorganic Chemistry*, eds. A. G. Sykes and A. Cowley, H, Academic Press, Califorornia, 2000, vol. 50, pp. 109-197.

21. W. W. Rudolph, D. Fischer, G. Irmer and C. C. Pye, *Dalton Transactions*, 2009, 6513-6527.

22. K. J. Iversen, S. A. Couchman, D. J. Wilson and J. L. Dutton, *Coordination Chemistry Reviews*, 2015, **297**, 40-48.

23. D. Naglav, M. R. Buchner, G. Bendt, F. Kraus and S. Schulz, *Angewandte Chemie International Edition*, 2016, **55**, 10562-10576.

24. S.-W. A. Fong, J. J. Vittal, W. Henderson, T. S. A. Hor, A. G. Oliver and C. E. F. Rickard, *Chemical Communications*, 2001, 421-422.

25. W. Henderson and T. S. A. Hor, *Inorganica Chimica Acta*, 2014, **411**, 199-211.

26. W. Henderson and J. S. McIndoe, *Mass Spectrometry of Inorganic, Coordination and Organometallic Compounds: Tools, Techniques, Tips*, Wiley, Chichester, 2005.

27. E. Chinea, S. Dominguez, A. Mederos, F. Brito, A. Sánchez, A. Ienco and A. Vacca, *Main Group Metal Chemistry*, 1997, **20**, 11-18.

28. H. Schmidbaur, *Coordination Chemistry Reviews*, 2001, **215**, 223-242.

29. J. Bruno, *Journal of the Chemical Society, Dalton Transactions*, 1987, **10**, 2431-2437.

30. L. Alderighi, S. Dominguez, P. Gans, S. Midollini, A. Sabatini and A. Vacca, *Journal of Coordination Chemistry*, 2009, **62**, 14-22.

31. E. Bauer, D. Ehler, H. Diyabalanage, N. N. Sauer and T. M. McCleskey, *Inorganica Chimica Acta*, 2008, **361**, 3075-3078.

32. M. Peschke, A. T. Blades and P. Kebarle, *International Journal of Mass Spectrometry*, 1999, **185–187**, 685-699.

33. M. K. Beyer, *Mass Spectrometry Reviews*, 2007, **26**, 517-541.

34. A. T. Blades, P. Jayaweera, M. G. Ikonomou and P. Kebarle, *International Journal of Mass Spectrometry and Ion Processes*, 1990, **101**, 325-336.

35. I. I. Stewart and G. Horlick, *Analytical Chemistry*, 1994, **66**, 3983-3993.

36. M. Beyer, E. R. Williams and V. E. Bondybey, *Journal of the American Chemical Society*, 1999, **121**, 1565-1573.

37. T. Urabe, M. Tanaka, S. Kumakura and T. Tsugoshi, *Journal of Mass Spectrometry*, 2007, **42**, 591-597.

38. A. Sarpola, V. Hietapelto, J. Jalonen, J. Jokela, R. S. Laitinen and J. Rämö, *Journal of Mass Spectrometry*, 2004, **39**, 1209-1218.

39. W. Baldwin and D. Stranks, *Australian Journal of Chemistry*, 1968, **21**, 2161-2173.

40. W. W. Rudolph, *Journal of Solution Chemistry*, 2010, **39**, 1039-1059.

41. A. Sarpola, H. Hellman, V. Hietapelto, J. Jalonen, J. Jokela, J. Rämö and J. Saukkoriipi, *Polyhedron*, 2007, **26**, 2851-2858.

42. T. Urabe, T. Tsugoshi and M. Tanaka, *Journal of Mass Spectrometry*, 2009, **44**, 193-202.

43. N. V. Sidgwick and N. B. Lewis, *Journal of the Chemical Society*, 1926, **129**, 1287-1302.

44. R. B. Cole and A. K. Harrata, *Journal of the American Society for Mass Spectrometry*, 1993, **4**, 546-556.

45. R. B. Cole, *Electrospray and Maldi Mass Spectrometry:Fundamentals, Instrumentation, Practicalities, and Biological Applications*, Wiley, New Jersey, 2nd edn., 2010.

46. Z. Cheng, K. Siu, R. Guevremont and S. Berman, *Organic Mass Spectrometry*, 1992, **27**, 1370-1376.

47. P. Kebarle and L. Tang, *Analytical Chemistry*, 1993, **65**, 972A-986A.

48. D. A. Everest, *The Chemistry of Beryllium*, Elsevier, Amsterdam, 1964.

49. L. Ciavatta, M. Iuliano, R. Porto, P. Innocenti and A. Vacca, *Polyhedron*, 2000, **19**, 1043-1048.

50. R. Puchta, B. Neumüller and K. Dehnicke, *Zeitschrift für Anorganische Chemie*, 2011, **637**, 67-74.

51. N. Tuseev, V. Sipachev, R. Galimzyanov, A. V. Golubinskii, E. Zasorin and V. Spiridonov, *Journal of Molecular Structure*, 1984, **125**, 277-286.

52. P. E. Mason, S. Ansell, G. W. Neilson and J. W. Brady, *The Journal of Physical Chemistry B*, 2008, **112**, 1935-1939.

Chapter Three

Ab initio molecular dynamics investigation of beryllium complexes

3.1 Introduction

The greatest advantage of computational chemistry is that it enables the chemist to explore areas of scientific interest where experiments are difficult, expensive or impossible and one of such areas is the chemistry of beryllium. "Microgram for microgram",[1] beryllium has been described as the most toxic element in the periodic table as a result of the uncontrollable immune response of body white blood cells accompanying the inhalation of less than microgram portions of beryllium particles.[2-4]. Consequently, this has necessitated further studies on the aqueous solution chemistry of beryllium over the past two decades and an area of interest is the solvation of the beryllium ion and counterions from its salt solution.[5-7] Generally, it has been observed that the actual environment of the beryllium ion in aqueous solution of its salts involves fluctuating arrangements of hydration spheres and counterions especially in the presence of anions such as fluorides and sulfates.[8-10] This information is of high importance in view of the recently proposed toxicity route to beryllium sensitization involving an accompanying ion.[11] Moreover, the formation of these beryllium complexes in aqueous solution is of interest for a variety of other applications such as in environmental detection, wet chemical recycling and processing of the beryllium ores.[12, 13] Consequently, the modelling of the structure and speciation of these simple beryllium complexes in the virtual laboratory is very relevant to obtain important insights into beryllium-water and beryllium-anion interactions in a solvent environment.

In the previous Chapter, electrospray ionisation mass spectrometry was explored as a safe experimental technique to obtain rich information on the speciation and coordination environment of the Be^{2+} cation in aqueous solution. However, more and more researchers have turned to computational chemistry for the "safest" investigation of beryllium chemistry given that even tiny levels of

exposure have been reported to sensitise the white cells.[14] Already there exist far more computational investigations than experimental studies on the coordination chemistry of beryllium so leading to the recent emphasis on the complementation of computationally obtained results with those from supportive experimental techniques and *vice versa* as illustrated by the Plieger and coworkers.[15-18]

In addition, the electrospray ionisation mass spectrometric technique suffers from several unavoidable but well-documented drawbacks as a result of the change in the chemical environment as the solution species are transferred into the gas phase.[19] Consequently, both solution and gas phase phenomena can be represented in a mass spectrum in varying degrees and this thereby poses a challenge in fully understanding the role of the solvent on beryllium speciation by the ESI-MS technique. Therefore, in order to complement species observed by the ESI-MS (and indeed other experiment results reported in the literature), this chapter provides detailed insights into the dynamical structure of the beryllium aqua, sulfato, chloro and fluoro complexes as a function of the solvation environment, explored using *ab initio* molecular dynamics. By employing density functional theory (DFT) implemented in the Car-Parrinello method alongside suitable pseudopotentials, the solvent effect is modelled explicitly and further utilised to study the structure, speciation and ligand-substitution reactions of beryllium complexes in aqueous solution. In this chapter, Car-Parrinello molecular dynamics (CPMD) investigations were mainly concerned with the two phenomena associated with the ESI-MS behaviour of beryllium salt solutions observed in Chapter 2. These include the deprotonation of a coordinated water molecule and the coordination of the salt anion. Although these events are highly correlated to the charge reduction during the electrospray process, they have equally been reported in the aqueous solution chemistry of beryllium.[10] While the deprotonation of a coordinated water molecule and the resultant hydrolysis product of beryllium has been studied quite extensively, the occurrence of ion pairing in beryllium solution has received far less attention.[10, 20]

3.2 Results and discussion

3.2.1 Construction and validation of the beryllium pseudopotential

For the purpose of computational efficiency, the technique of *ab initio* molecular dynamics simulation is implemented in a pseudopotential/plane wave approach, which involves representing the nuclei and core electrons with a pseudopotential, while a plane wave basis set is used to represent the orbitals.[21] Therefore, a crucial prerequisite for any *ab initio* molecular dynamics simulation is the choice of pseudopotentials for the representation of the electrons within the core region of the atoms often determined by arriving at a compromise between accuracy of result and feasibility of computational effort. The pseudopotentials employed in this work were prepared by Professor Michael Bühl (University of St Andrews, UK) using a programme developed in-house by the Parrinello group.[22-24] While the pseudopotentials for the elements oxygen, fluorine, sulfur, hydrogen and chlorine employed in this study had previously been generated, tested and utilized in several simulations,[25, 26] an appropriate pseudopotential for beryllium had to be designed. For beryllium, a new pseudopotential was constructed following the procedure adopted previously for other metal nuclei.[25, 26] A relativistic atomic reference calculation was performed for the $[1s^2]2s^1$ state and a pseudopotential was created for the resulting core in brackets, using cut off radii of 1.1 a.u. for the *s*, *p*, and *d* channels together with non-linear core corrections on a Be^+ species.

Initial validation tests with this pseudopotential were performed for gaseous $[Be(H_2O)_4]^{2+}$ in a 12.8 Å box while testing the effects of the pseudopotential cut off radii (rc), wave function cut-off (Ry), and the non-linear corrections (NLCC).[21] The resulting parameters are collected in Table 3-1, together with the corresponding values for nonperiodic all-electron reference calculations at the BLYP-D/6-31G** and MP2/6-311+G** levels and in comparison with experimental data. Increasing the wavefunction cut-off beyond 80 Rydberg (Ry) resulted only in minor changes of the optimised Be-O distance (on the order of 0.006 Å). Likewise adjustment of the cut off radii between 1.0 to 1.2 a.u. yielded insignificant discrepancies in the Be-O bond lengths. However, slightly larger variations were observed for the energetics parameter which in this case was the binding energy of the fourth water

molecule in the tetraaquaberyllium $[Be(H_2O)_4]^{2+}$ cation calculated according to eqn (3-1).

$$[Be(H_2O)_3]^{2+} + H_2O \rightarrow [Be(H_2O)_4]^{2+} \quad (3\text{-}1)$$

Based on the correlation to the all-electron reference calculations as documented in Table 3-1, the pseudopotential PP6 was adopted for subsequent calculations. The atomic calculation was performed for a Be^+ state, and since the central Be in $[Be(H_2O)_4]^{2+}$ has a similar partial charge according to population analysis observed to be 1.17 from natural population analysis at the BLYP-D/6-311+G** level. Therefore the resulting pseudopotential is thus designed for cationic Be centres. Further validation studies for this pseudopotential were performed all through this study with other ligands which confirms its transferability and the consistency of the CP-opt data with other DFT methods. This pseudopotential for beryllium constructed for the use in CPMD simulation proved to furnish reliable results and would be a significant contribution in further studies of beryllium complexes by this technique.

Table 3-1 Validation of pseudopotentials.

Phase	Formulation details of electronic structure and pseudopotentials		r(Be-O)[a]	E[b] (kcal/mol)
gaseous	MP2/6-311+G**		1.667	-47.78
	BLYP/6-311+G**		1.672	-47.92
	CP-opt/ BLYP	$PP1_{(rc=1.2,\ Ry=80,\ s^1p^0)}$	1.648	-46.81
		$PP2_{(rc=1.2,\ Ry=100,\ s^1p^0)}$	1.649	-47.16
		$PP3_{(rc=1.2,\ Ry=120,\ s^1p^0)}$	1.649	-47.20
		$PP4_{(rc=1.1,\ Ry=80,\ s^1p^0)}$	1.651	-46.81
		$PP5_{(rc=1.1,\ Ry=80,\ s^{0.95}p^{0.05})}$	1.686	-108.14
		$PP6_{(rc=1.1,\ Ry=80,\ s^1p^0,\ NLCC)}$	1.654	-47.84
		$PP7_{(rc=1.0,\ Ry=80,\ s^1p^0,\ NLCC)}$	1.658	-48.04
	CPMD/ BLYP/PP6			-

[a] *Average (rBe-O) in the tetraaquaberyllium cation* $[Be(H_2O)_4]^{2+}$

[b] *Binding energy of the fourth water molecule calculated according to the equation* $[Be(H_2O)_3)]^{2+} + H_2O \rightarrow [Be(H_2O)_4)]^{2+}$

3.2.2 CPMD investigation of beryllium ion solvation in water and liquid ammonia

Chart 3-1 Tetraaquaberyllium cation **1a** and tetraammineberyllium cation **1b**

The organisation of solvent molecules around the beryllium ion has continually remained a subject of experimental and computational interest because of the small size and high charge density of this ion.[6] Following up on the pioneering CPMD/BLYP study of aqueous Be^{2+} in 31 water molecules by Marx, Sprik and Parrinello,[27] two unconstrained CPMD simulations of the tetraaquaberyllium cation **1a** were performed in 63 and 90 water molecules for a total of 18 ps in order to define the dynamical transition of the primary and secondary solvation around the Be^{2+} cation (see computational details in Chapter 7). The radial distribution functions, gBe-O(r) from CPMD simulation of Be^{2+} in 63 and 90 water molecules for the entire simulation period are given in Figure 3-1a.

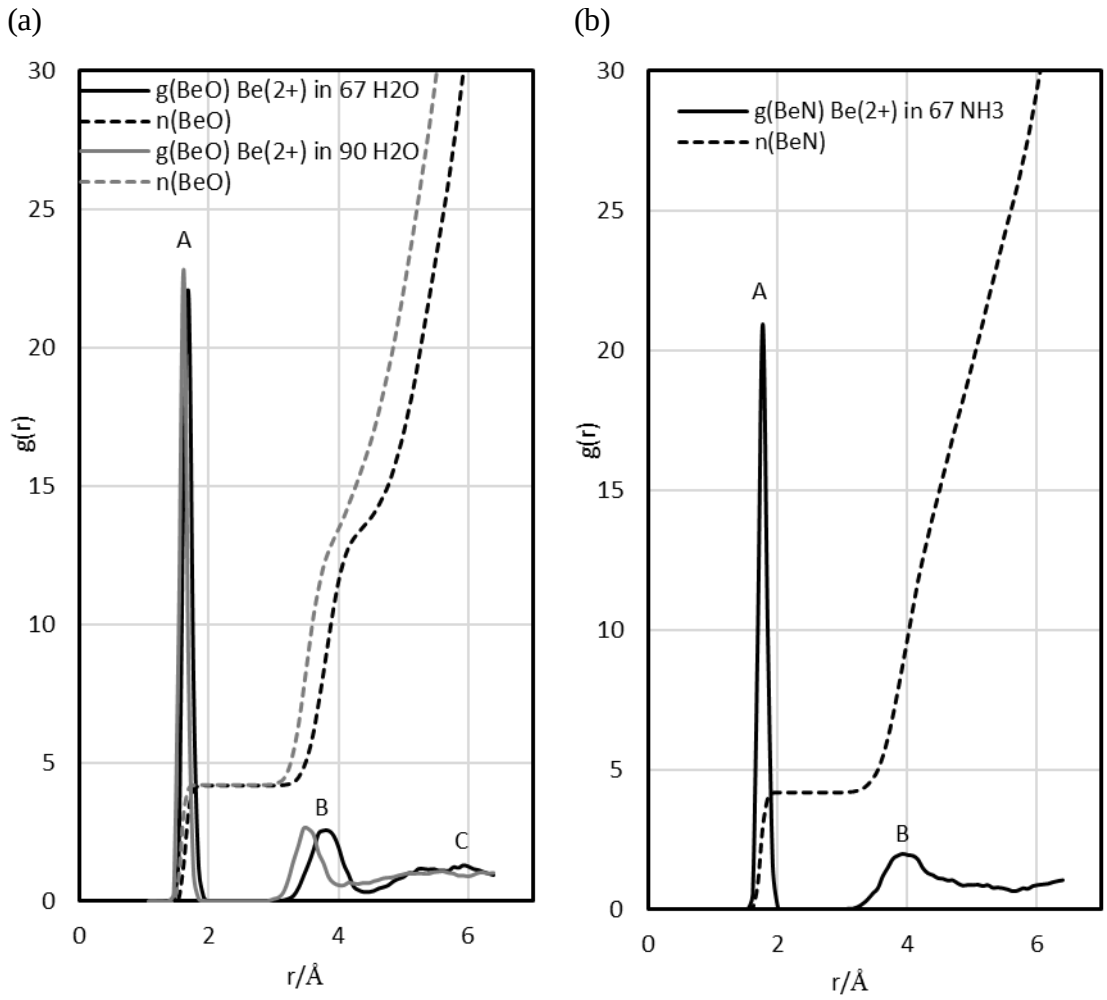

Figure 3-1 Be-O and Be-N radial distribution function of a) $[Be(H_2O)_4]^{2+}$ and b) $[Be(NH_3)_4]^{2+}$ in aqueous solution and liquid ammonia. (data collected after the first 3 ps)

In accordance with the preferred tetrahedral geometry of the beryllium ion, both simulations revealed a well demarcated first solvation shell corresponding to a sharp peak (point A) which integrates into 4 oxygen atoms. The average Be-O distance in the first hydration sphere was 1.647(6) Å and 1.643(4) Å for the Be^{2+} in 64 H_2O and Be^{2+} in 90 H_2O compared to the Be-O distance of 1.66 Å which was reported in 31 water molecules.[27] Interestingly, with the increasing number of water molecules, there is a trend of a slight shortening of the Be-O bond distances towards experimental values observed to lie between 1.60-1.63 Å. This highlights the subtle role of the second solvation sphere in computing the structural properties of the tetraaquaberyllium cation, as has been previously observed in static calculations.[28] CPMD simulations also revealed evidence of a well-defined second hydration sphere extending from 3.5 to 4.2 Å around the Be^{2+} cation observed at point B. As

shown in Figure 3-2 these water molecules in the second hydration sphere are clearly organised and form a distinct hydrogen bond network which further stabilises the species. From the integration of this peak, 9-11 water molecules reside in the second hydration sphere of a Be^{2+} where 9 is most predominant occupation number of water molecule from the sharper peak in the Be^{2+} in 90 H_2O. While no water exchange event was observed between the first and second hydration shells, interchange events were occasionally observed following the migration of water molecules between the second and the third hydration spheres as evident in the flattening of the RDF ongoing from point B to C in Figure 3-1.

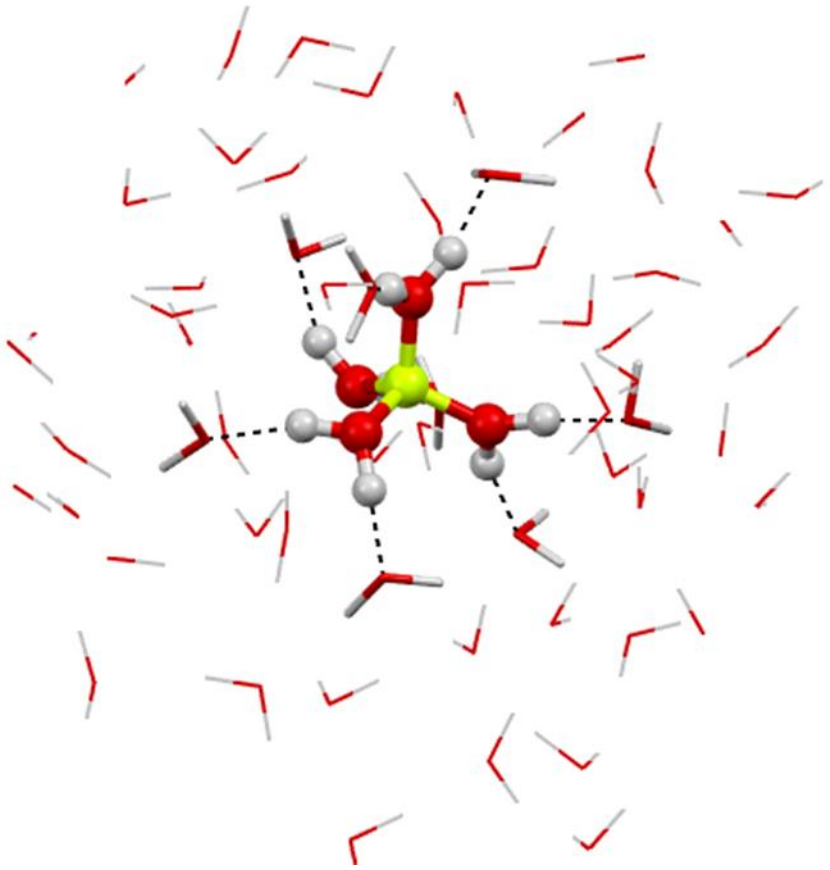

Figure 3-2 Snapshot showing the immediate coordination environment of the Be^{2+} ion in water revealing organisation of the primary solvation sphere (ball and stick model) and the hydrogen bonded network of secondary solvation sphere (tubes) from the CPMD simulation (green-beryllium, red-oxygen, grey-hydrogen).

Unlike the extensively studied tetraaquaberyllium complex **1a**, the sparse and inconclusive experimental details of the speciation of beryllium ion in liquid ammonia have led to the recent reinvestigation of beryllium complexes in liquid ammonia.[29, 30] Therefore, additional CPMD simulation of Be^{2+} was performed in

67 ammonia molecules for a total of 12 ps. The Be-N radial distribution functions and their integration numbers [n(r)] are shown in Figure 3-1b. The first peak observed at point A (which also integrates to 4 nitrogen atoms over a range of 1.694-1.849 Å) represents the first solvation shell of ammonia with an average Be-N distance of 1.7419 Å. This value is slightly elongated compared to the Be-N range of 1.725-1.733 Å in the recent X ray structure of **1b** but within the range of 1.710-1.74 Å from the neutron diffraction study of $[Be(ND_3)_4]^{2+}$.[29] In comparison to the aqueous system, the Be^{2+} cation similarly structured the ammonia molecule such that a second solvation sphere can be clearly observed at point B (see Figure 3-1b) but with an extended distance range from 3.6 - 4.8 Å which integrates into 8-11 nitrogen atoms. This finding suggests that not all the hydrogen atoms of the primary solvation shell are involved in hydrogen bonding, reflecting a weaker hydrogen bonding network in liquid ammonia in comparison to aqueous solution (see Figure 3-3). Lastly, the suitability of the CPMD/BLYP functional in describing the structural properties of beryllium complexes in both solutions have been subsequently compared to results for continuum models.

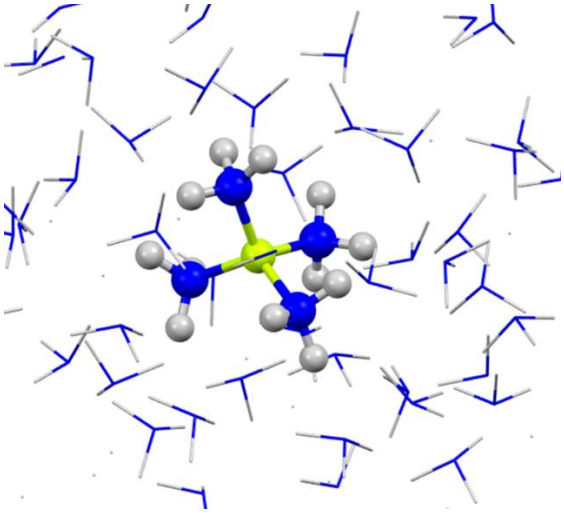

Figure 3-3 Snapshot of the tetraammineberyllium cation **1b** from CPMD simulation (green-beryllium, blue-nitrogen, grey-hydrogen).

3.2.3 CPMD investigation of the deprotonation of the tetraaquaberyllium cation and its trimeric hydrolysis product

From the ESI-MS speciation diagram in Chapter 2, the predominant species in aqueous solutions of beryllium salts at pH < 3 is the tetraaquaberyllium cation

1a. However, upon increasing the solution pH, hydrolytic reactions set in, firstly yielding the monohydroxide $[BeOH]^+$ (see eqn (3-2)) which quickly polymerizes into a complex mixture of oligomeric species $[Be_n(OH)_m]$ of varying compositions.[31]

$$\mathbf{1a} + H_2O \leftrightarrows [BeOH(H_2O)_3]^+ + H_3O^+ \qquad (3\text{-}2)$$

Due to the availability of useful experimental data, the deprotonation of the tetraaquaberyllium cation **1a** according to eqn (3-2), which marks the onset of the beryllium hydrolytic processes, provides an appropriate reaction for the extraction of microscopic observables for comparison with experiment and a gauge of the reliability of the CPMD methodology. Considering the strong solvation of the beryllium ion and the difference in charge between the reactant and product in equation (3-2), it would be rather difficult to accurately describe the solvation effects using simple PCM methods. However, CPMD simulations which are capable of modelling solvation as an actual dynamic ensemble around the reactant and product are expected to proffer better accuracy and have been used to reproduce pK_a values with accuracies of approximately 1-4 kcal/mol.[32] Additionally, CPMD simulations have been successfully employed to reproduce the acidity constant of the uranyl(VI) hydrate $[UO_2(H_2O)_5]^{2+}$ and the dissociation mechanism of formic acid.[33, 34]

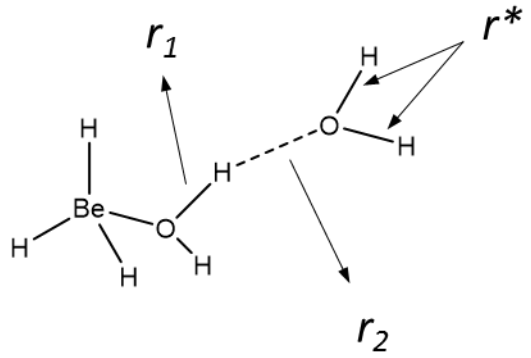

Figure 3-4 Tetraaquaberyllium cation **1a** solvated by a water molecule in the second solvation sphere revealing the O-H distances r_1 and r_2. (r* are the additional constraints imposed to prolong the reaction pathway)

To drive the deprotonation reaction forward according to eqn (3-2), constrained CPMD simulation was performed by taking a single O-H distance as

the constrained reaction coordinate (r_1 as shown in Figure 3-4). Then pointwise thermodynamic integration of the Helmholtz free energy along several fixed values of r_1 was propagated as the proton was extended away from the water molecule in a slow growth from 0.97 to 1.8 Å (see computational details in Chapter 7). To ensure sufficient convergence of the mean constraint force, each new step of r_1 was started up from a previous step and the simulation was carried on for 1.5-2 ps after 0.5 ps of equilibrations similar to the level of convergence previously reported.[33] The change in Helmholtz free energy evaluated according to eqn (3-3) afforded the free- energy profile shown in Figure 3-5.

$$\Delta A_{a\to b} = -\int_a^b \langle f(r_1)\rangle d(r_1) \qquad (3\text{-}3)$$

Along the simulation pathway at about r_1 = 1.4 Å, spontaneous proton transfer occurred onto the accepting water molecule in the second hydration sphere (Figure 3-4) followed by the well-known shuffling of the proton in CPMD simulations.[35] Therefore in order to further prolong the reaction path, additional constraints were imposed on the two OH distances in the accepting water molecule from this point on (as shown in Figure 3-4). To circumvent the slightly restrictive environment incurred from these additional constraints, the equilibration time at each integration point was thereafter increased to 1 ps. By r_1=1.8 Å, the leaving proton has effectively been transferred to a water molecule from the second hydration sphere in agreement with the values for the end-point of other similar proton transfer processes.[32-34] However, it is also worth pointing out that the end of the reaction coordinate does not correspond to the ideal standard state of infinite dilution represented by the experimental ΔG^0 term which will require continuously simulating the two product species in order to diffuse away from each other. Based on deductions from various experimental reports while at the same time putting into consideration the varying concentration and ionic strength, a recommended equilibrium constant of log β^0 = -5.4 has been pointed out for the reaction in eqn (3-2) from which a free energy of ΔG^0= 7.4 kcal/mol can be inferred at 298 K.[36] A similar value, 7.7 kcal/mol was also obtained in a potentiometric study of beryllium hydrolysis.[31] Comparing this to the CPMD free energy profile shown in Figure 3-5, the predicted difference in free energy between reactant and product taken from the near plateau region around r_1=1.6 Å is 9.6 kcal/mol. This is approximately 1.9

kcal/mol higher but still in good agreement with experimental values. The reason for the sustained rise in the free energy is perhaps due the constraining of both other OH bonds which may in fact be too over restrictive toward the reorientation of the solvation shell. Also, the accumulation of significant mean force on such additional constraints as r_1 increases and the calculated ΔA values have been previously reported.[25] Nevertheless, a plateau is apparent around r_1=1.5-1.7 Å while attempts to speed up the kinetics by firstly simulating the point at r_1 = >1.4 at 400 K (keeping all constraints) then restarting and running the simulation for another 2.5 ps with the thermostat set back to 320 K yielded only free energy ΔA values ca. 0.5 kcal/mol lower compared to the previous simulation.

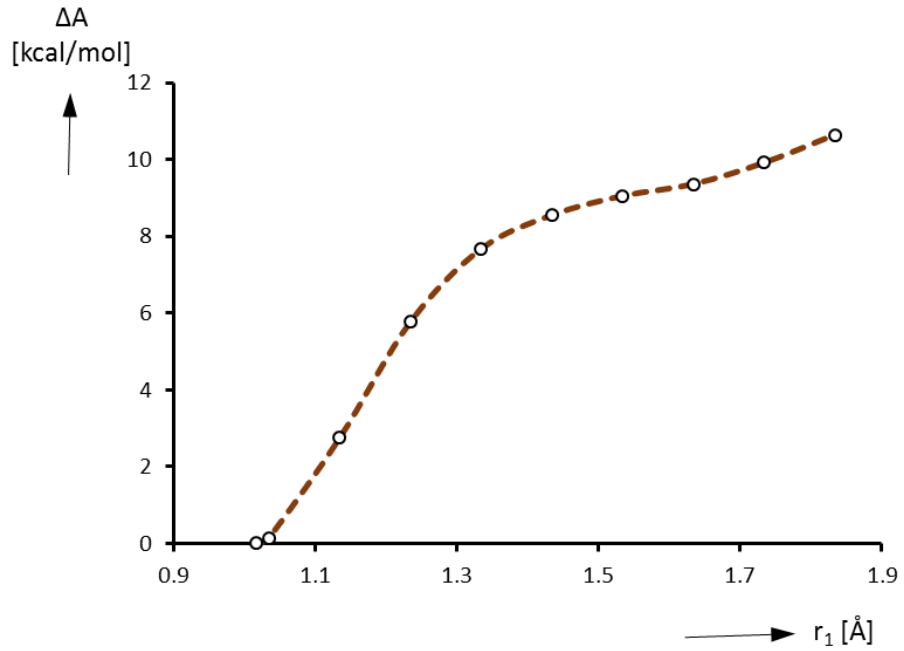

Figure 3-5 Computed free-energy profile for the deprotonation of the tetraaquaberyllium cation **1a** in aqueous solution.

In a further attempt to assess the validity of the choice of reaction coordinate, a plot of the mean distance of the leaving proton (r_2) to the accepting water as a function of the constrained value r_1 is displayed in Figure 3-6. The desirable smooth transition of the leaving proton to the accepting water molecule with no discontinuities in the reaction pathway is observed showing that there was no rapid process that could have rendered this path unacceptable due to significant bias. However, several literature reports have shown other possible and perhaps more sophisticated reaction coordinates such in the constraining of coordination

numbers but they have equally been reported to yield very similar results.[33, 37] In practice, the greatest source of error and drawback in the present day CPMD simulation and pointwise thermodynamic integration technique of this type is related to the inherent limitation applicable to the corresponding DFT-functional. Also, the inexorable finiteness of the system forces the use of a limited number of integration points and simulation times. Nevertheless, within these limitations, the computation of the acidity constant of the tetraaquaberyllium cation **1a** within typical accuracy of DFT-based methods underscores the potential and applicability of the CPMD approach in the study of beryllium complexes in solution. This can be of value in probing other beryllium hydroxido species such as the beryllium trimer $[Be_3(OH)_3]^+$.

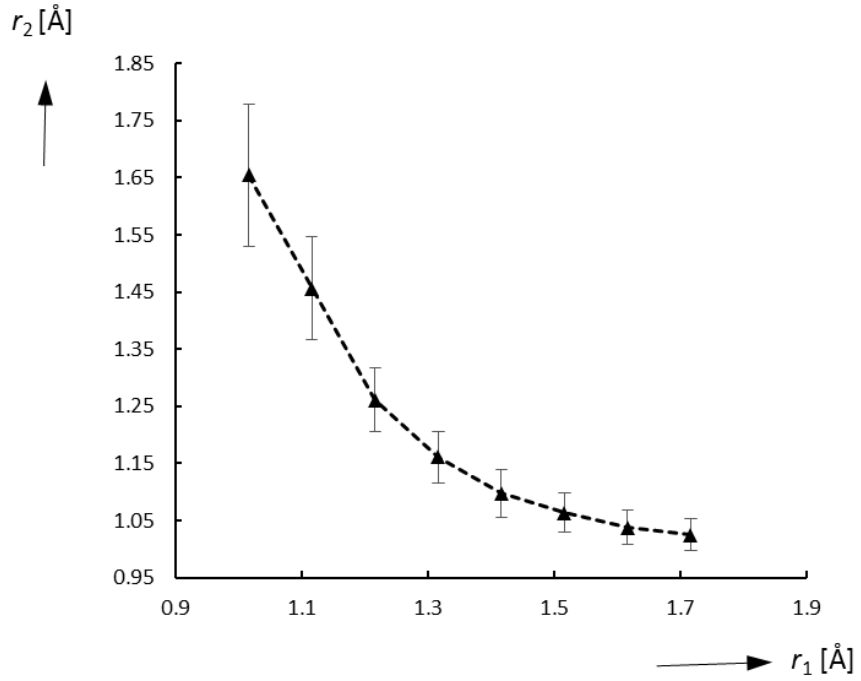

Figure 3-6 Plot of the bond distance of the leaving proton to the accepting water (r_2) versus the constrained O-H distance (r_1) (see Figure 3-4 for definition); mean values of r_2 are shown as triangles and the standard deviations (with respect to the mean value) as vertical bars.

In aqueous solution, the resultant mononuclear beryllium hydroxido species formed by the deprotonation reaction of eqn (3-2) is short lived and quickly polymerises into a range of polynuclear hydrolysis products of which the beryllium trimer $[Be_3(OH)_3]^+$ is the most commonly occurring.[10, 31] This species has been extensively characterised in the solid state and in the gas phase (see Chapter 2).

Employing an unconstrained CPMD simulation, this species was immersed in a box of 90 water molecules in a simulation for 6 ps. Figure 3-7 displays the Be-OH bond distances of the beryllium trimer which were found to oscillate around 1.5-1.69 Å. The most obvious deduction from this simulation is the stability of the cyclic arrangement for the beryllium species which was also found intact in the gas phase (see Chapter 2).

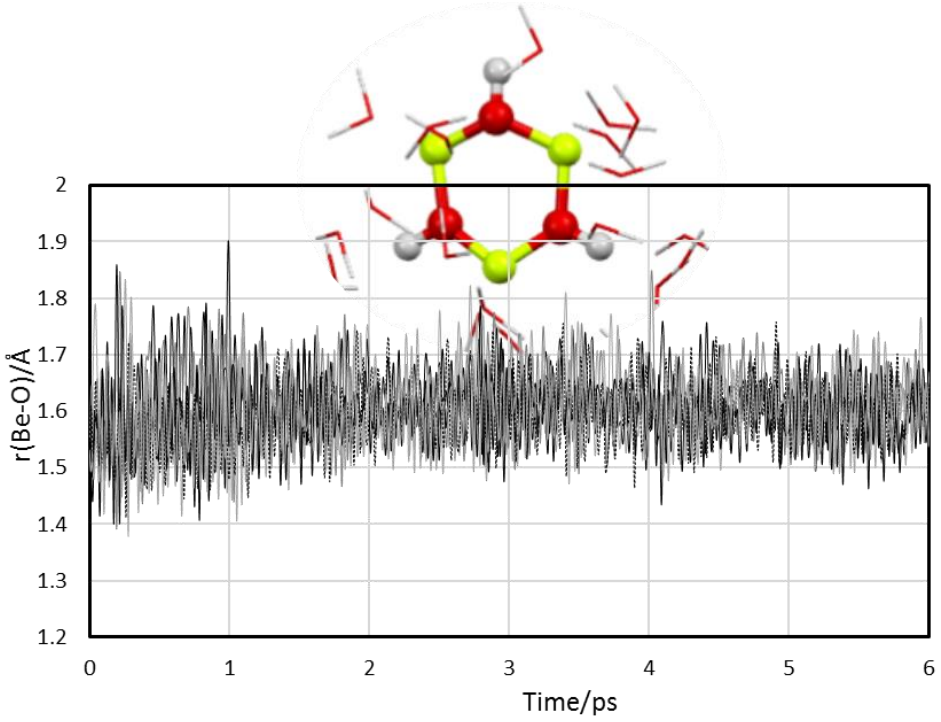

Figure 3-7 Time-evolution of Be-O distances (in Å) for the beryllium hydroxido trimer $[Be_3(OH)_3]^{3+}$ in aqueous solution for 6 ps (including representative snapshot from the 3 ps region)

3.2.4 CPMD investigation of Be^{2+} and counter ions in aqueous solution

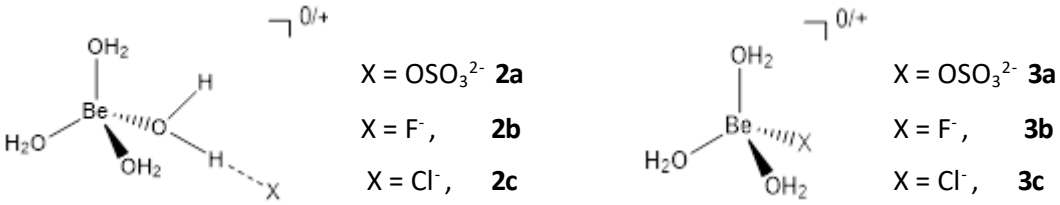

Chart 3-2 Outer sphere complexes (OSC) **2a-2c** and inner sphere complexes (ISC) **3a-3c** of beryllium complexes with sulfate, fluoride and chloride ions.

For an initial simplistic interaction of beryllium with the counter ions in solution the monomeric complexes sketched in Chart 3-2 have been proposed reflecting the possibility of outer sphere or inner sphere coordination of the sulfate, chloride and fluoride anions to the metal centre.

(a)

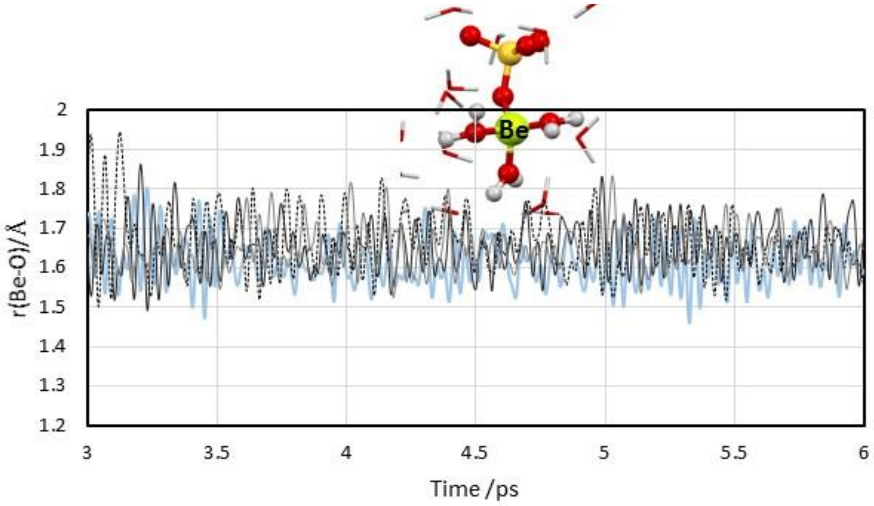

(b)

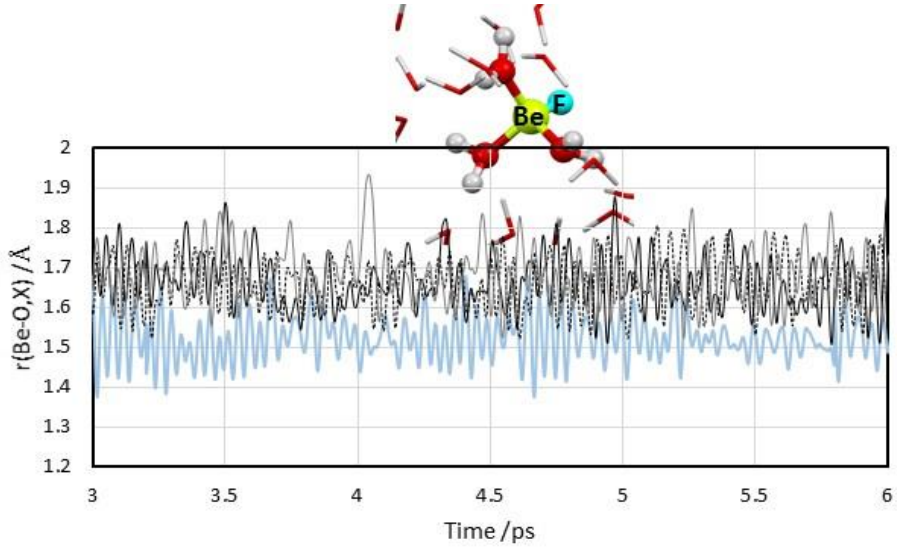

(c)

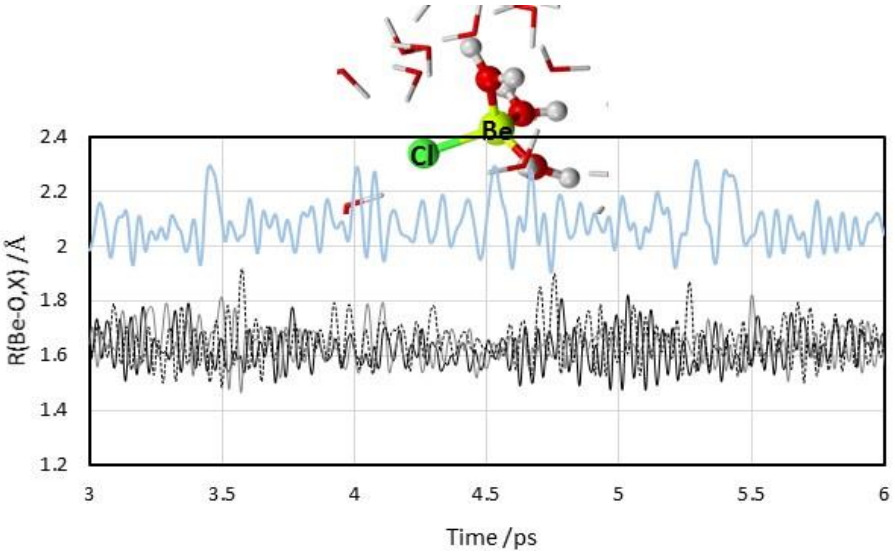

Figure 3-8 Time evolution of Be-O and Be-X distances (blue) in Å, for (a) complex **3a** (b) complex **3b** (c) complex **3c**

It is also worth highlighting that ESI-MS data (see Chapter 2) equally pointed to the existence of these species especially the inner sphere complexes, hence a more detailed investigation of structural arrangement corresponding to the stoichiometric composition from the mass spectra is herein provided. Clearly, both coordination modes would immensely alter the structural properties of the complexes in solution. Hence detailed structural and energetics properties of the complex **2** and **3** (see Chart 3-2) were examined. Optimised geometrical parameters of complexes **2** to **3** are collected in Table 3-2 and Table 3-3 alongside available experimental data. In addition, structural data from unconstrained CPMD simulations were reported therein in the gas phase and in aqueous solution of 63 water molecules for 6 ps where the CPMD simulation in solution corresponded to a 1 mol L^{-1} $BeSO_4$, and $BeCl_2$ and BeF_2 solution in which the second halide ion was left to migrate freely in the bulk solution (see computational details in Chapter 7).

Firstly, the gas phase static optimised geometries are considered. All complexes could be characterised as minima in the gas phase and in a polarisable continuum of aqueous solution each revealing a C_1 symmetry. Going from the BLYP to the B3LYP functional, Table 3-2 and Table 3-3 reveal that there is a trend of a slight shortening of bond distances by ca. 0.01-0.02 Å for the Be-O bonds and by ca. 0.01-0.03 Å for the Be-X bond distances. The inner sphere coordination of

the chloride, fluoride and sulfate ions evidently weakened the bonding strength of the coordinated aqua ligands as observed by their elongated Be-O distances. Also, in the complex **3a**, one of the Be-O bonds was shortened due to hydrogen bonding with the sulfato ligands. This is in agreement with an earlier reported observation that sulfate ions tend to catalyse the hydrolytic tendency of the beryllium cation in solution.[38] Also, this process tends to explain the extensive beryllium hydroxide/sulfato speciation observed in Chapter 2. For the outer sphere complexes **2a-c**, the sulfate and fluoride ion provided the most structural perturbation to the tetraaquaberyllium cation **1a** which involved shortening of the Be-O bond distance of a coordinated water molecule due to hydrogen bonding to an anion in the second solvation sphere.

Table 3-2 Geometrical parameters (bond distances in Å) of complexes **2a-c**.

Type of complex	Comp.	Bond	BLYP	B3LYP	PCM	B3LYP-D3	MP2	Cp-opt	$CPMD_{gas}$	$CPMD_{aq}$	Expt
Outer Sphere complex	**2a**	r(Be-O)	1.80 1.78 1.55 1.57	1.79 1.77 1.54 1.54	1.71 1.70 1.53 1.64	1.76[1.71] 1.76[1.71] 1.56[1.53] 1.53[1.64]	1.79[1.71] 1.77[1.70] 1.54[1.53] 1.54[1.64]	1.77 1.70 1.51 1.65	1.80(6) 1.62(1) 1.51(27) 1.71(61)	1.64(9) 1.66(23) 1.63(33) 1.67(36)	1.60-1.69[b]
		r(Be···OSO_3)	3.01	3.41	3.57	3.01[3.56]	3.39[3.51]	3.17	3.49(44)	3.99(86)	3.57[b]
	2b	r(Be-O)	1.71 1.73 1.68 1.52	1.70 1.72 1.51 1.67	1.65 1.67 1.55 1.67	1.72[1.67] 1.70[1.68] 1.50[1.54] 1.67[1.68]	1.72[1.68] 1.74[1.68] 1.69[1.68] 1.51[1.54]	1.72 1.73 1.65 1.52	1.73(59) 1.73(9) 1.68(30) 1.52(15)	1.64(11) 1.66(28) 1.63(11) 1.66(70)	
		r(Be-F)	3.08	3.06	3.12	3.06[3.13]	3.12[3.14]	3.05	3.01(18)	3.61(15)	
	2c	r(Be-O)	1.66 1.66 1.66 1.67	1.64 1.64 1.64 1.66	1.62 1.66 1.62 1.66	1.69[1.65] 1.69[1.65] 1.60[1.63] 1.59[1.63]	1.65[1.65] 1.64[1.65] 1.64[1.63] 1.64[1.63]	1.72 1.65 1.73 1.51	1.75(83) 1.73(66) 1.68(67) 1.50(10)	1.64(64) 1.64(44) 1.67(9) 1.65(0)	1.60-1.61[c]
		r(Be-Cl)	3.09	3.06	3.74	3.41[3.65]	3.01[3.55]	3.55	3.60(23)	4.16(59)	

[a]In square brackets are values commuted in the PCM model for the corresponding functional. In parentheses are standard deviations over the CPMD trajectories. [b]ref [6] (XRD, neutron and X-ray diffraction techniques). [c]ref 39

Table 3-3 Geometrical parameters (bond distances in Å) of complexes **3a-c**, **4a**.

Type of complex	Comp.	Bond	BLYP	B3LYP	PCM	B3LYP-D3	MP2	Cp-opt	$CPMD_{gas}$	$CPMD_{aq}$	Expt.
Inner Sphere complex	**3a**	r(Be-O) r(Be-OSO_3)	1.73 1.75 1.54 1.62	1.71 1.73 1.75 1.53	1.71 1.67 1.55 1.64	1.72 [1.71] 1.71 [1.67] 1.53 [1.55] 1.61 [1.64]	1.71 [1.67] 1.72 [1.71] 1.53 [1.55] 1.60 [1.64]	1.68 1.68 1.57 1.65	1.66(49) 1.71(02) 1.69(88) 1.56(33)	1.65(93) 1.67(12) 1.66(42) 1.63(27)	
	3b	r(Be-O) r(Be-F)	1.70 1.70 1.70 1.43	1.72 1.71 1.68 1.46	1.70 1.70 1.70 1.43	1.70 [1.68] 1.67 [1.69] 1.70 [1.70] 1.46 [1.47]	1.71 [1.70] 1.66 [1.70] 1.71 [1.69] 1.44 [1.47]	1.71 1.70 1.70 1.42	1.73(04) 1.73(5) 1.73(3) 1.42(87)	1.66(31) 1.66(41) 1.69(81) 1.53(2)	
	3c	r(Be-O) r(Be-Cl)	1.70 1.70 1.70 1.88	1.70 1.69 1.70 1.88	1.70 1.70 1.70 1.88	1.70 [1.67] 1.70 [1.67] 1.70 [1.67] 1.88 [1.93]	1.70 [1.68] 1.70 [1.68] 1.70 [1.68] 1.86 [1.91]	1.69 1.71 1.69 1.89	1.72(8) 1.73(52) 1.73(43) 1.89(37)	1.65(82) 1.64(92) 1.63(53) 2.07(35)	2.2[b]
	4a	r(Be-O) r(Be-O_2SO_2)	1.72 1.72 1.58, 1.58	1.70 1.70 1.57, 1.57	1.66 1.66 1.63, 1.63	1.70 [1.63] 1.70 [1.63] 1.57 [1.66] 1.57 [1.66]	1.70 [1.63] 1.70 [1.63] 1.58 [1.66] 1.58 [1.66]	1.66 1.66 1.64, 1.64	1.67 1.67 1.65, 1.65		

[a]*In square brackets are values commuted in the PCM model for the corresponding functional. In parentheses are standard deviations over the CPMD trajectories.* [b]*ref* 7.

However, with the chloride ion in complex **2c**, all four Be-O distances were almost equivalent signifying a lesser disruption of the primary solvation corresponding to lesser propensity for the formation of inner sphere complexes in comparison to the other anions. Moving on to the solution phase, most of the above structural trends were retained upon solvation of complexes **2 - 3** via a polarisable continuum except that the Be-OH_2 bond distance was observed to decrease by ca. 0.03 Å (for instance compare BLYP gas and BLYP PCM for **3** in Table 3-3). Also for the outer sphere beryllium complexes, shortening of the Be-O bonds due to hydrogen bonding of the water molecule to the counter ion is diminished by ca 0.04 Å for the $Be(H_2O)_4F$ complex since solvation would greatly reduce the charge density on the fluoride ion.

Comparison of the optimisation by CPMD/BLYP (denoted as Cp-opt) with other DFT methods especially BLP reveals closely related bond distances to each other thereby lending more credence to the effectiveness of the beryllium pseudopotential. But going from Cp-opt geometries to dynamic average from unconstrained CPMD simulations in the gas phase, all bond distances increased (for instance compare Cp-opt and CPMD entries in Table 3-2 and Table 3-3). Also, it could be observed that the most significant bond increase occurred with the Be⋯X bond in the outer sphere complexes **2a-c**, although rearrangement of the species was not observed during the simulations. Moving on to the CPMD in aqueous solution, the radial distribution functions, gBe-O(r) from CPMD simulation of the complexes **2 - 3** are given in Figure 3-9. In accordance with the preferred tetrahedral geometry of the beryllium ion, RDF of species **2a-c** revealed Be-O coordination integrating into 3 suggesting that the inner sphere complex of beryllium remained stable and undetached throughout the entire simulation. Also, visualisation of the simulation supported the earlier suggestion from the RDF plots that the complexes **2a-c** remained intact during the 6 ps simulation, thereby attesting the existence of the inner sphere coordination complexes in solution involving the sulfate, fluoride and chloride anions in agreement with experimental evidence.[7, 9, 10] However, the only structures that can be structurally compared to experiment were **3a**, **3c** and **2a, 2c**. In the solid state, the Be⋯OSO_3 bond distance of the outer sphere complex in **2a** was significantly elongated by ca. 0.3 Å when immersed in solution whereas

CPMD simulations in the gas phase revealed a shortening by ca. 0.1 Å. However, the solvation effect on the sulfato inner sphere complex **3a** increases the Be-OSO_3 bond distance by ca. 0.01 Å in comparison to the values observed in the structures of the disulfato beryllium anion $[Be(SO_4)_2(H_2O)_2]^{2-}$.[40] In addition, aqueous CPMD simulation of **3c** reveals an average Be-Cl distance of 2.1 Å in reasonable comparison to EXFAS measurements[7] at 2.2 Å whereas static optimisation employing a polarisable continuum differed by a much higher value of 0.27-0.3 Å depending on the functional.

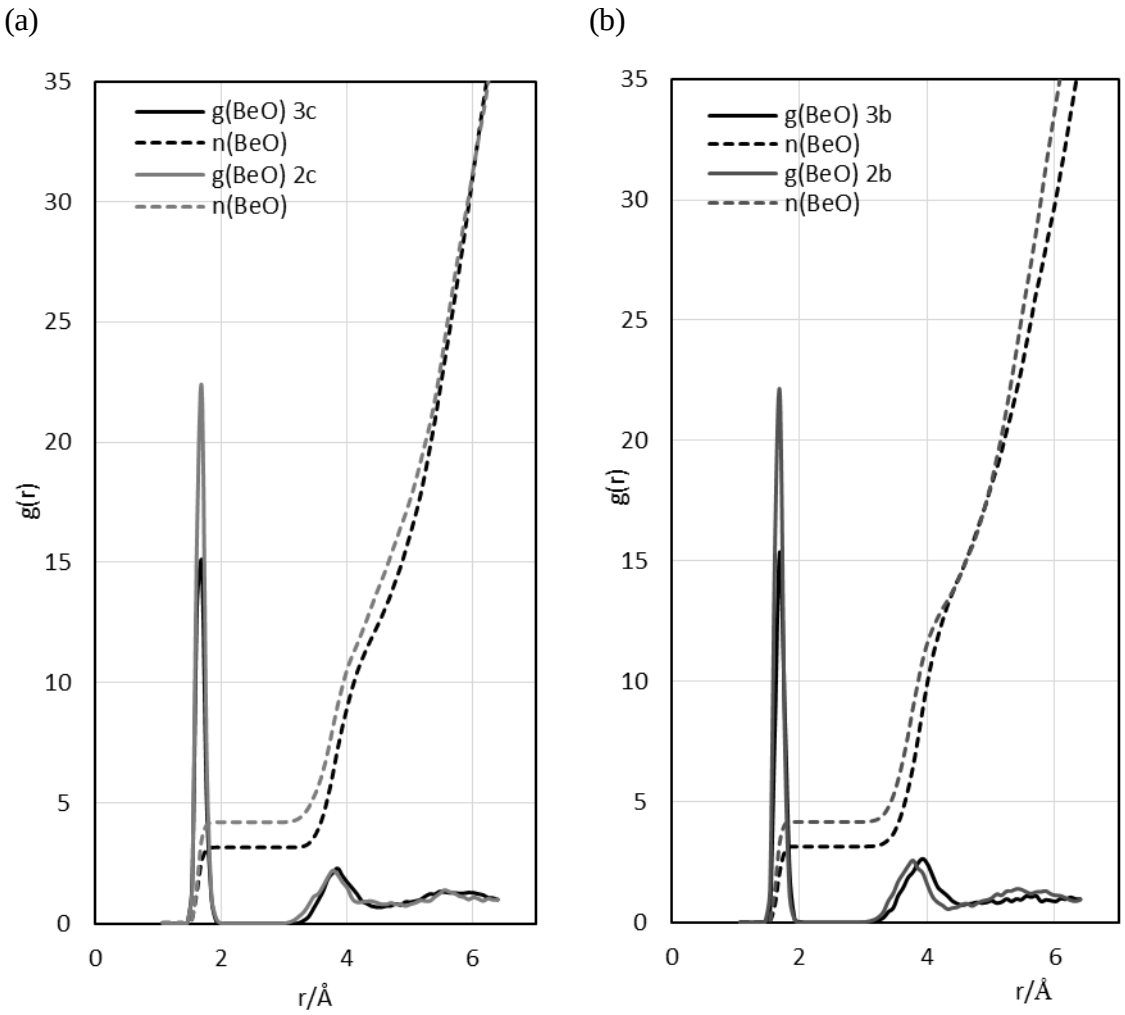

Figure 3-9 Be-O radial distribution function of a) beryllium chlorido complexes **2c** and **3c** b) beryllium fluorido complexes **2b** and **3b**.

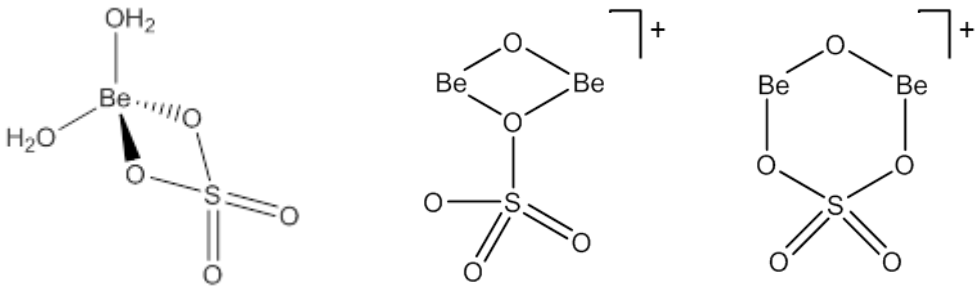

4a **4b** **4c**

Chart 3-3 Coordination modes of the sulfato ligand

The binding modes of the sulfate ion are, shown in Chart 3-3. CPMD simulations reveal that κ^2-SO_4 coordination to beryllium as shown in **4a** is unstable in aqueous solution. In a simulation for 6 ps, one of the κ^2-SO_4 bonds in the complex **4a** lengthens to about 3.5 Å and eventually decoordinates from the primary solvation sphere while simultaneously letting in a water molecule from the secondary coordination sphere, which leads to the collapse of **4a** into **3a** after 4.75 ps (see

Figure 3-10). Nevertheless, a minimum on the potential energy surface was obtained for the species **4a** in the gas phase and in the polarisable continuum model. While it has been suggested that a κ^2-SO_4 coordination to beryllium could exist in beryllium sulfate melts,[9] it is clear that chelation from the four member ring and the small bite size of the sulfate ion cannot compete favourably with the ion solvation thus monodentate and bridging coordination modes are preferred.

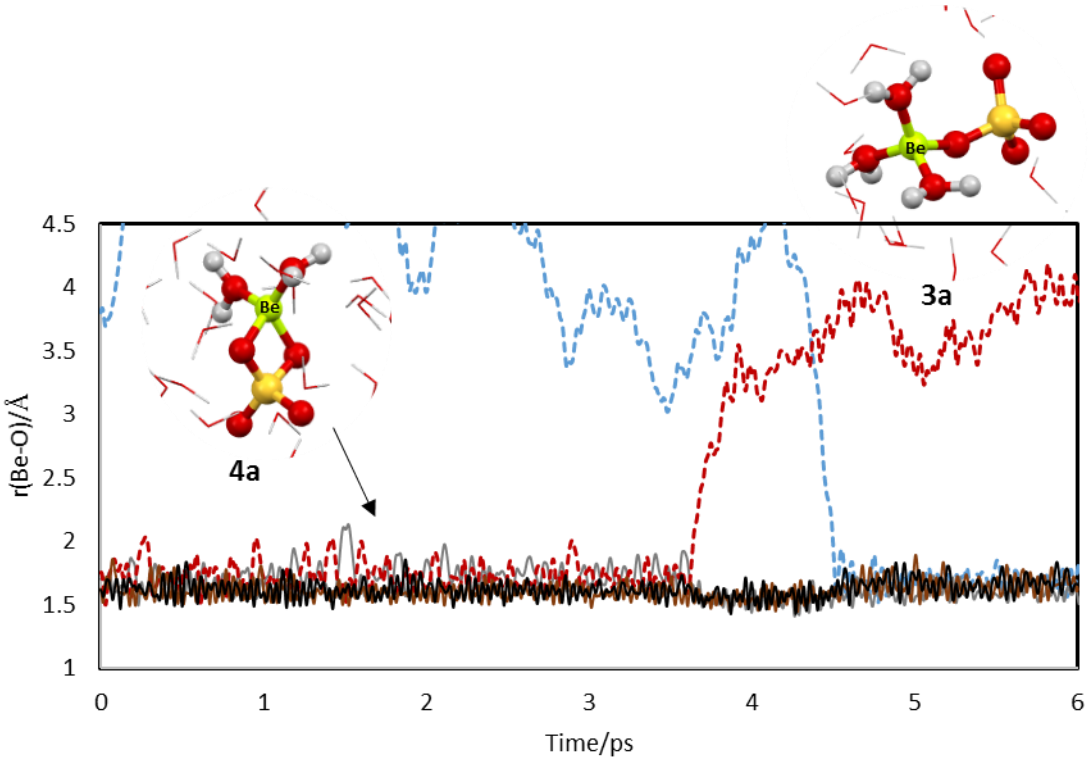

Figure 3-10 Time evolution of Be-O distances in complexes **4a** and **3a** (in Å) showing the lengthening of a Be-OSO_3 bond distance (red) and the entering of a water molecule in to the primary coordination sphere (blue).

Furthermore, structural inference from the stoichiometric composition supplied by ESI mass spectra have suggested mixed beryllium sulfato/hydroxido complexes proposed as complexes **4b** and **4c** illustrating additional coordination modes of the sulfato ligands. To investigate these species in an aqueous environment, CPMD simulation of **4b** and **4c** were followed for a total of 6 ps in solution. The sulfato ligand appeared to be quite flexible and during the first 2 ps, the κ-OSO_3 bonding mode in **4b** gradually approaches the κ^2-O_2SO_2 bonding mode in complex **4c**. Also a similar but faster rotation of the sulfato ligands was observed in a simulation starting from **4c** but both systems remain stable and unchanged throughout the simulations. The relative stability of both complexes (with the remaining coordination site of the beryllium ion filled with aqua ligands) was then examined by employing static calculation in the gas phase and PCM. It was observed that the structure in **4b** was relatively more stable compared to **4c** by 6.2 kcal/mol and 5.2 kcal/mol in PCM and gas phase respectively. This indeed hints at the preference of the monodentate coordination mode of the sulfate in aqueous

systems. In comparison to the stable bridging coordination mode of the sulfate ion, CPMD simulation of the corresponding complexes employing bridging chlorido and fluorido ligands reveals that a halide would generally coordinate to the beryllium in a monodentate fashion in agreement with evidence from the NMR coupling which pointed out the absence of splitting of the due to a bridging fluoride.[20]

3.2.5 Further investigation on the structural arrangements of beryllium hydroxido/sulfato inner sphere complexes observed in the ESI-MS

With an increasing number of beryllium atoms, there exist many possibilities for the arrangements of the beryllium sulfato complexes. ESI-MS data (see Chapter 2) have revealed stoichiometric compositions corresponding to several beryllium sulfato/hydroxido mixed complexes such as the series in which hydrogensulfato ligands progressively replace the hydroxido ligands to yield the ions $[Be_3O_2(HSO_4)]^+$, $[Be_3OHO(HSO_4)_2]^+$, and $[Be_3O(HSO_4)_3]^+$. Although these are gas phase species, the reduced hydrolytic tendencies of beryllium in its sulfate solutions and the observation of the Raman stretching modes for an inner shere complex $[Be\text{-}OSO_3(H_2O)]^+$ at 498 cm^{-1} distinguished them from the fully hydrated species $[Be\text{-}(OH_2)_4]^{2+}$ at 1014 cm^{-1} and have emphasized the existence of such mono and bidentate inner sphere sulfato complexes.[8, 41] Therefore on the basis of the chemical compositions of ions observed in ESI-MS, further theoretical investigation on the role and binding mode of the sulfato ligand was carried out. Illustrative minimum energy structures of monomeric, dimeric and trimeric ESI-MS ions are shown in Figure 3-11. A general feature of the sulfato ligand is its ability to coordinate to the beryllium cation in bridging positions as a monodentate or bidentate ligand depending on the number of aqua ligands in the complex. Inner sphere coordination of the sulfato ligands altered the structural properties of the beryllium hydroxido complex. For instance the coordination of the sulfato ligand to the cyclic trimeric hydroxido species in the ESI-MS ion $[Be_3(OH)_3(HSO_4)_2(H_2O)_2]^+$ *m/z* 308 distorts the near planar configuration of the trimer causing one of the bridging hydroxyl ligands to fold in and assume a position central to the trimeric arrangement of the beryllium ions. This structural

arrangement is plausible as it reveals how a $Be_3(\mu_3\text{-}OH)$ trimeric core transforms to a $Be_3(\mu_3\text{-}O)$ configuration under elevated conditions as observed in the ESI-MS ion $[Be_3O(HSO_4)_3]^+$ *m/z* 334 (Figure 3-11). Also in the gas phase, ESI-MS ions prefer bridging and bidentate sulfato ligand arrangements. The optimised dimeric ion $[Be_2OH(HSO_4)_2(H_2O)_2]^+$ (Figure 3-11) favoured a cage structure involving the sulfato ligands in bidentate and/or bridging positions thereby allowing beryllium to attain a tetrahedral coordination in the absence of water molecules. Once again, this is observed in the monomeric ion $[Be(HSO_4)(H_2O)_n]^+$ n = 2 whereby the bidentate sulfato ligand configuration which completes the tetracoordination to the Be cation is more stable by about 7 kcal/mol in comparison to a monodentate sulfato ligand configuration. However, this is not entirely representative of the solution state as a comparison between the binding energies of ESI-MS ions $[Be(HSO_4)(H_2O)_n]^+$ n = 2 and 3 at *m/z* 142 and 160 reveals that contrary to peak intensities, the more hydrated sulfato complexes are more stable (see Chapter 2). Also, this has been rightly depicted by the CPMD technique pointing out this technique as a promising alternative in reproducing solvent effects.

Lastly, to summarize this section, it can be seen that the aqueous solution of beryllium sulfate is certainly more complicated in its speciation than the present simple understanding of beryllium hydroxido species in aqueous solution. CPMD simulations points out that the versatility and competitive bridging ability of the sulfato ligand will result in increased occurrence of inner sphere complexes with this anion especially at high temperatures and sulfate concentration.

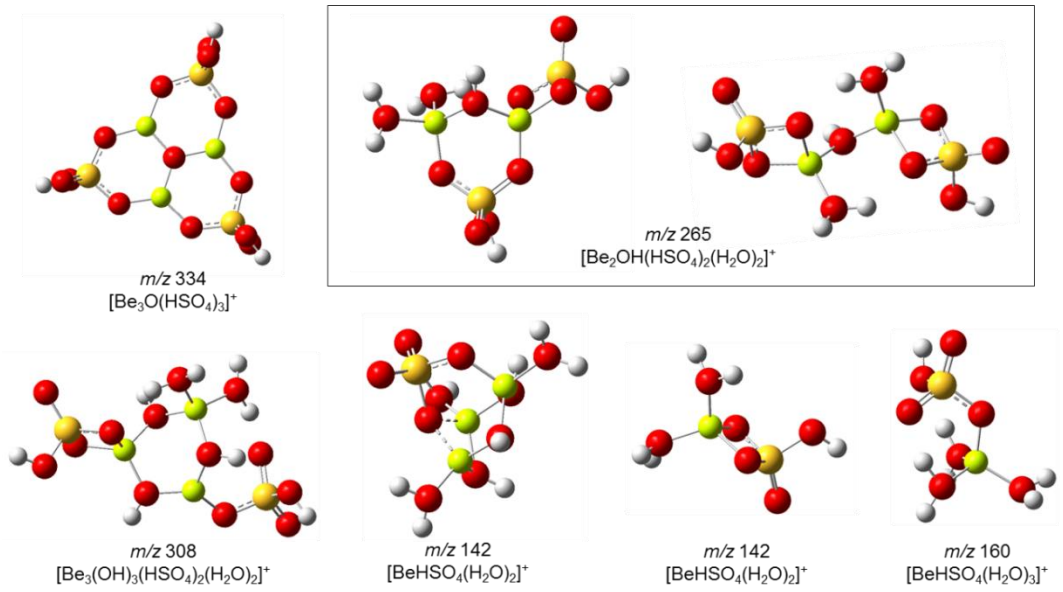

Figure 3-11 Optimized geometric structures of the energetically most stable configurations of selected monomeric, dimeric and trimeric ions observed by ESI-MS. (red-oxygen, green-beryllium, yellow-sulfur, grey-hydrogen)

3.2.6 Relative energies

To answer the question of the likelihood of outer vs inner coordination of counter ions to the beryllium ion, the affinities of the beryllium ion to the sulfate, fluoride and chloride ions were assessed by following the energetics of the sequential substitution for aqua ligands in comparison with experimental data where available. Although it is important to note that apart from the individual affinities of the counter ions towards the beryllium ion, the prevalent species in solution would be dependent on the ion concentrations in solution. Salient data of the energetic parameters computed at various DFT levels involving static PCM optimisations and single point energy evaluations according to eqn (3-4) where X = F^-, Cl^- are summarized in Table 3-4 and Table 3-5.

$$[Be(H_2O)_4]^{2+} + nX^- \leftrightarrows [BeX_n(H_2O)_{4-n}]^{(2-n)+} + nH_2O \qquad (3\text{-}4)$$

Although simple and straightforward, these computations in the gas phase and the continuum solvation (both of which are without hydrogen bond considerations) for the derivation of thermodynamic data impressively reproduced the qualitative finding in which the binding of the beryllium cation and the counter ions are smaller in water than in the gas phase. This is depicted in the observed

trend in the sequential binding of the fluoride ion to Be^{2+} in the gas phase which pinpoints binding energies of ca. -260 to -415 kcal/mol whereas in PCM this value is significantly reduced to ca 12 to -67 kcal/mol while employing the B3LYP functional. Also similar energetics data were reproduced at the BLYP level according to Table 3-4 which also revealed a slightly lower value by within 4-14 kcal/mol.

Table 3-4 Computed energies according to eqn (3-4) for the fluoride ion ($X=F^-$) in kcal/mol

	B3LYP				ΔG
n	ΔE (gas)	ΔE PCM	ΔG PCM	ΔE [ΔE^{cp}] PVQZ/PCM	Expt[a]
1	-260.4	15.1	12.5	-46.0 [-46.2]	-6.68
2	-423.0	-19.0	-23.8	-80.3 [-80.6]	-5.13
3	-491.8	-65.9	-72.0	-102.7 [-103.2]	-3.8
4	-415.2	-59.3	-66.9	-119.4 [-120.0]	-1.94
	BLYP				ΔG
n	ΔE (gas)	ΔE PCM	ΔG PCM	ΔE [ΔE^{cp}] PVQZ/PCM	Expt[a]
1	-256.4	17.76	15.1	-42.8 [-43.4]	-6.68
2	-415.3	-15.9	-19.9	-76.0 [-77.6]	-5.13
3	-481.1	-62.1	-68.5	-98.1 [100.2]	-3.8
4	-401.1	-54.9	-62.9	-113.2 [-115.8]	-1.94

[a]ref 1

On the other hand, the binding energy of the beryllium and chloride ions predicted with the BLYP and B3LYP functional revealed lower values in comparison to the fluoride ions. Clearly, the association of two opposite and highly charged Be^{2+} and the F^- or Cl^- ions will invariably attract each other strongly in the gas phase but to a lesser extent in solution due to solvation. However, the PCM model for water seems also to yield overestimated binding affinities in comparison to the experimental values. For instance, assuming n=2 in eqn (3-4), a significantly more negative value was obtained for the driving forces of the aqua substitution reaction but again dependent on the functional (see ΔE for n=2 in Table 3-4). It must be pointed out, however that, although the incorporation of the solvent dielectric constant is of great importance in the charge stabilization, accounting for

hydrogen bonding in the computation of strong order forming ions such as the Be^{2+} is essential.

Table 3-5 Computed energies according to eqn (3-4) for the chloride ion ($X=Cl^-$) in kcal/mol.

		B3LYP		
n	ΔE (gas)	ΔE PCM	ΔG PCM	ΔE [ΔE^{cp}] PVQZ/PCM
1	-161.8	45.1	42.9	-12.8 [-12.7]
2	-335.4	37.9	34.2	-17.8 [-17.7]
3	-361.3	19.3	13.1	-16.4 [-16.3]
4	-299.2	36.8	28.6	-14.4 [-14.2]
		BLYP		
n	ΔE (gas)	ΔE PCM	ΔG PCM	ΔE [ΔE^{cp}] PVQZ/PCM
1	-201.6	46.4	44.3	-11.9 [-11.8]
2	-310.8	38.8	34.5	-17.6 [-18.1]
3	-324.6	18.6	12.2	-16.5 [-17.0]
4	-249.5	36.3	27.7	-15.0 [-15.4]

This is evident in the disagreement of the PCM results with the experimental trend. Moreover, from the experimental trend according to Table 3-4, the binding of additional fluoride ion is expected to be less favourable however, this trend is not comprehensively captured either in the gas phase or in a polarisable continuum. Instead the opposite trend prevails wherein higher stability is designated to the increasing number of counterions substituting for the aqua ligand. Nevertheless, in credit to the PCM model the high magnitude of the binding energy between the beryllium ion and both the fluoride and chloride ion in the gas phase is well attenuated upon repeating the calculation in a polarisable continuum representing aqueous solution. Furthermore, calculation in the PCM model also captured the well-known stronger binding interaction between the beryllium ion and the fluoride in comparison to beryllium ion and a chloride. Indeed due to the high affinity of beryllium for the fluoride ion and its favourable nuclear properties, ^{19}F NMR measurements of beryllium fluoride solutions has been an area of fruitful research.[10, 20] Increasing the basis set does not improve the PCM result very much therefore, it

is obvious from the above result that the reliability of these computations of the energetics of ligand exchanges (of simple ligands) on the beryllium centre is not only dependent on the treatment of the electron-correlation but perhaps, on the solvation effects. More so, the transition between the outer sphere and inner sphere complexes would entail changes in the assemblage of the solvation sphere as a result of the charge reduction making the solvation effect crucial in accounting for the energetics of this reaction. In recognition of this, various methods have been employed to account for this solvation effect around the beryllium ion and its effects on the computation of the energetics of the substitution reaction on the metal centre. Generally, the most widely embraced approach is the polarisable continuum model introduced by Tomasi and co-workers[42] which embeds the species in a cavity in a solvent medium. While this modest approach provides very impressive results on most occasions, its intrinsically implicit nature tends to limit the role of ion-molecule interactions such that the continuum model can sometimes yield abysmally poor results. Another basic way to improve on result involves the explicit incorporation of a limited number of solvent molecules to yield microsolvated clusters which can be calculated either in the gas phase or further in the PCM. However, since the PCM energy is quite sensitive to the cavity containing the molecule, it has been observed in this study (and of course in the literature) that such microsolvated clusters are quite difficult to optimise in a polarisable continuum. Furthermore, the existence of too many possible minima that have to be considered would render this approach too cumbersome for studying ligand exchange processes at the beryllium ion centre.

A way around this (albeit involving more computational demanding resources) is explicit incorporation of the solvent effect using the method of *ab initio* molecular dynamics. Since this method bridges quantum chemistry and classical molecular dynamics it particularly offers the advantage providing a more realistic solvent environment towards simulating chemical reactions such as ligand substitution reactions. Furthermore this technique has gained increased popularity as it is widely employed to reproduce the free binding energies of metal complexes in solution.[25, 26] Therefore, going beyond the simple static PCM calculation, the free energies of ligand substitution on the beryllium ion was further derived in a dynamic ensemble of explicitly solvated complexes by means of constrained

CPMD simulations along reaction paths designed to mimic the ligand substitution of a beryllium coordinated aqua ligand by X where X=F^- and SO_4^{2-} ligands. This would essentially involve a transition from the outer sphere complexes **2a-b** to the inner sphere complexes **3a-b.**

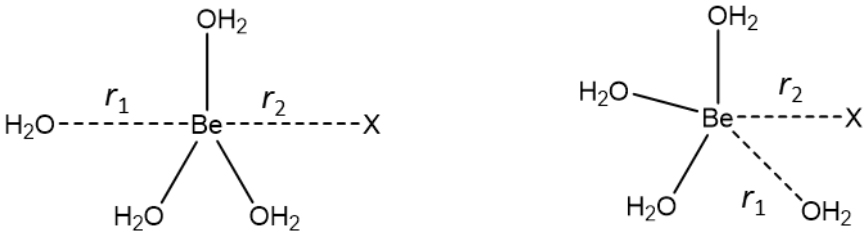

Figure 3-12 Transition state in a frontside and backside attack revealing O-Be-X constraint employed in the constrained CPMD simulation of the ligand substitution on the tetraaquaberyllium cation **1a**. ($\Delta r = r_1$-r_2 where r_1 = Be-X and r_2 = Be-O)

Following previous experimental and computational propositions[5, 43] modelling of the ligand substitution *via* a dissociative pathway was not attempted. Besides, preliminary CPMD simulation of a tri-coordinated beryllium centre tends to accept a fourth water molecule to complete its coordination within 0.5 ps of simulation. Therefore, the ligand exchange was enforced by constraining the X-Be-OH_2 bond distances as reaction coordinates and fixing the difference $\Delta r = r_1$-r_2 where r_1 = Be-X and r_2 = Be-O bonds (see Figure 3-12). Importantly, fixing the difference in distance is less restrictive compared to individually fixing the two distances (r_1 and r_2) simultaneously as it allows a higher degree of motion such that the true nature of the TS region can be probed ($O \cdots\cdots Be \cdots X \Rightarrow O \cdots Be \cdots X \Rightarrow O \cdots Be \cdots\cdots X$).

The ligand substitution reaction was undertaken by fixing the difference Δr at successively larger values in steps sizes of 0.3 Å and propagating the system at each point until the mean constrained force $\langle f(r) \rangle$ was sufficiently converged. The Helmholtz free energy at each point was evaluated *via* numerical integration according to eqn (3-5), generally, the system was found to be converged within 1.5 to 2.5 ps after 0.5 ps of equilibration time, similar to the degree of convergence previously reported.[25, 26]

$$\Delta A_{a\to b} = -\int_a^b \langle f(\Delta r)\rangle d(\Delta r) \qquad (3\text{-}5)$$

Firstly, CPMD simulations of the fluoride exchange on the beryllium cation (ie X=F^-) are considered. Starting from the minimum at Δr = -2.18 Å and increasing the distance difference Δr the leaving fluoride ion is gradually transferred to the outer coordination sphere. It subsequently accepts hydrogen bonds from other aqua ligand while a distant aqua ligand enters the inner coordination sphere to form a contact ion pair with beryllium while passing through a transition state at Δr = 0.21 Å. A second minimum is reached at Δr = 2.01 Å at which the mean constraint force basically is zero. Thus the free energy difference between the two points which constitutes the total driving force for the fluoride binding is computed to be 6.2 kcal/mol by the CPMD based approach which agrees favourably with the experimental value of 6.68 kcal/mol. It should also be noted that the CPMD simulation does not correspond to the idea state of infinite dilution and as such the order of accord between simulation and experimental can possibly differ further. Nevertheless, the CPMD method certainly constitutes improvement over the results from static calculation employing the BLYP/PCM (compare with Table 3-4).

On the other hand, the above CPMD simulation is more comparable to the transition from an outer sphere complex **2b** to the inner sphere complex **3b** in the last stage of a ligand substitution process according to the Eigen-Wilkins mechanism.[6] Using a conductrimetric stopped-flow technique, the experimental activation energy barrier for this process in the aqua substitution by a fluoride has been reported as 8.9±0.8 kcal/mol.[44]

By employing the CPMD approach, and assuming the outer sphere complex (at the product side in Figure 3-13) to be set at zero, the activation energy barrier for the substitution of a water molecule by the fluoride ion is reproduced as 11.7 kcal/mol. This barrier though a bit overestimated and somewhat uncharacteristic for GGAs, is still in good agreement with the experimental value by ca 2.8 kcal/mol; an acceptable value for calculation with the present day DFT method. Furthermore, in consideration of the level of uncertainty from the experimental value, the congruity between experiment and CPMD simulations could possibly improve.

E4r

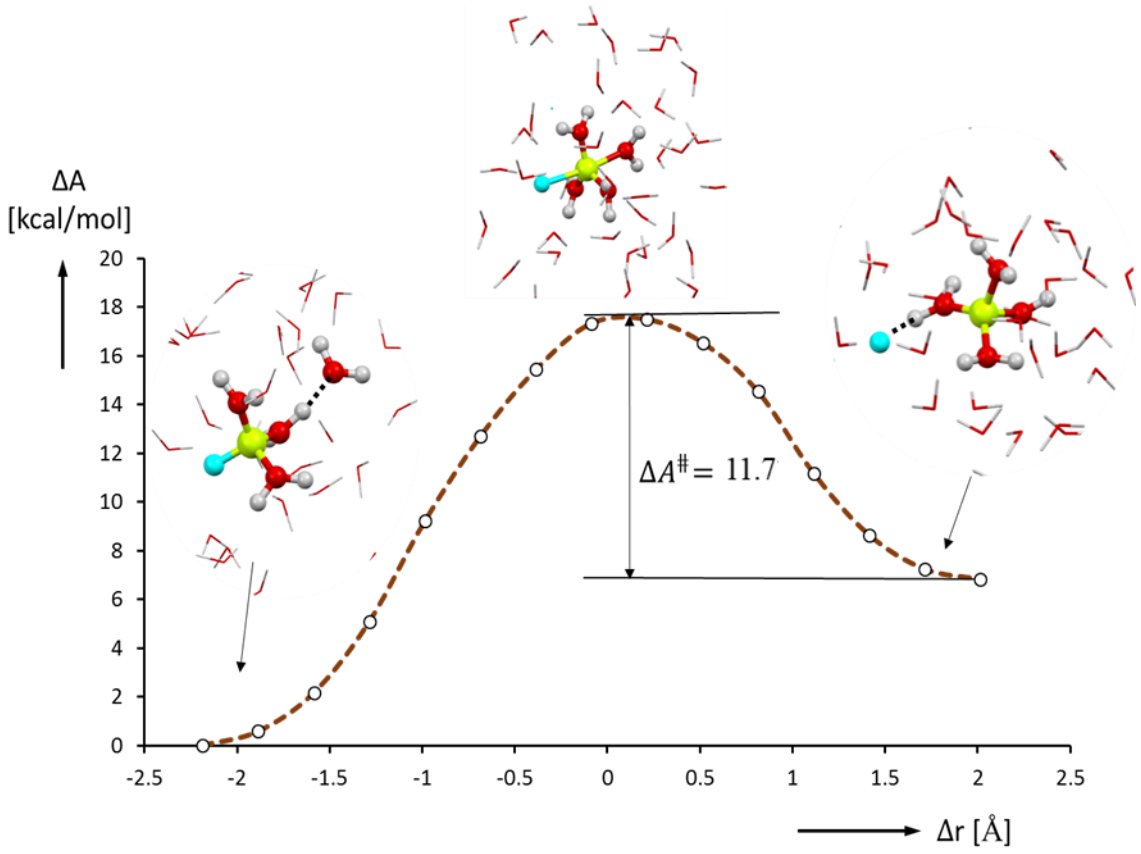

Figure 3-13 Calculated change in Helmholtz free energy, Δ*A*, for the substitution of an aqua ligand by a fluoride ion as obtained from constrained CPMD simulations and thermodynamic integration, including representative snapshots from the indicated region. (reaction coordinate: O-Be-F distance).

Since free energy is essentially a state function, the driving force for the reaction corresponding to the difference between the start and endpoint of the integration paths should be independent of the path followed, whereas the simulated activation energy barrier would be much more sensitive to the proper minimum energy pathway. Therefore, in order to scrutinize the reaction path for possible lower activation energy barriers, the transition state was examined. In principle, the simulation constraint should be flexible enough so that the system can reorient to the most favourable angle of attack although this might require much longer simulation times. To speed up any possible reorientation process CPMD simulation of the transition state at Δr = 0.21 Å was performed at 400 K for an additional 2 ps. Thereafter, the endpoint of the simulation was employed to retrace the CPMD trajectory using the same step sizes and slow growth in the positive and negative

direction of the transition state while maintaining the same constraint as before. Essentially, this also provided a means to probe for any hysteresis effect which can potentially upset such constrained CPMD simulations (due to the finite integration points along the reaction path). Generally, no huge deviation from the previous simulation was observed and the resultant average activation energy barrier from both simulation was 11.9 kcal/mol.

Following the O···Be···F angles of the atoms involved in the constraint confirms that the transition state corresponds to a backside attack (that is resembling the S_N2 transition state in organic chemistry mechanism as shown in Figure 3-12) in which the O···Be···F angle ranges between 162-178°. Furthermore, the transition state at Δr = 0.21 Å was again simulated using the same constraint but with the respective value for the O···Be···F angle corresponding to a frontside attack (see Figure 3-12). Evidently, the small size of the beryllium ion highly disfavours a potential transition state in a frontside attack and this transition state species reorients into complex **2b** within 3 ps of simulation.

Certainly, the greatest limitation of present day *ab initio* molecular dynamics simulation lies in its treatment of the electronic structure commonly implemented by the Kohn-Sham DFT formalism of which only a couple of GGA functional have been shown to generally provide a better description of liquid water.[45] To further investigate the effect of the functional on the activation energy barrier and driving force for the reaction, a snapshot of the complex in the transition state region with zero FE gradient at Δr = 0.21 Å, was extracted and used as a starting input to locate a transition state using static calculations and implicit solvation using the PCM model (see Figure 3-14). Ongoing from BLYP to B3LYP and MP2 the driving force for the reaction tend to increase by 0.3 to 0.5 kcal/mol whereas the barrier of the reaction is decreased by 0.2-0.6 kcal/mol. Comparing the CPMD results to PCM data, it can be seen that the activation energy barrier is much more overestimated than the free energy difference between the two points. While static calculations at BLYP level predicted an activation energy barrier of 12.9 kcal/mol, employing the CPMD/PTI technique with the same functional yields an activation energy of 11.7 kcal/mol which is closer to the experimental value. More disparate results between PCM and CPMD are even obtained in the calculation of the driving force of the reaction whereby the PCM static calculation pinpoints the

reaction energy as 12.0 kcal/mol in comparison to 6.2 kcal/mol obtained from CPMD simulations.

From these data, it is clearly observed that the large driving force for the formation of the inner sphere complex in the gas phase would be well attenuated in solution but this is difficult to describe by simple continuum models. It must also be conceded that solvation effects are not the only concern in the computation of these beryllium complexes and the description of the electronic structure is also of high importance. For instance, the highly parameterised M06-2X functional was found to yield static calculation result in PCM closest to experimental results while differing from other functional by 0.4 – 1 kcal/mol for the activation energy barrier and 1.2 – 1.7 kcal/mol for the driving force of the reaction. This is consistent with the recommendation for this functional in the commutation of thermodynamics of the main group elements.

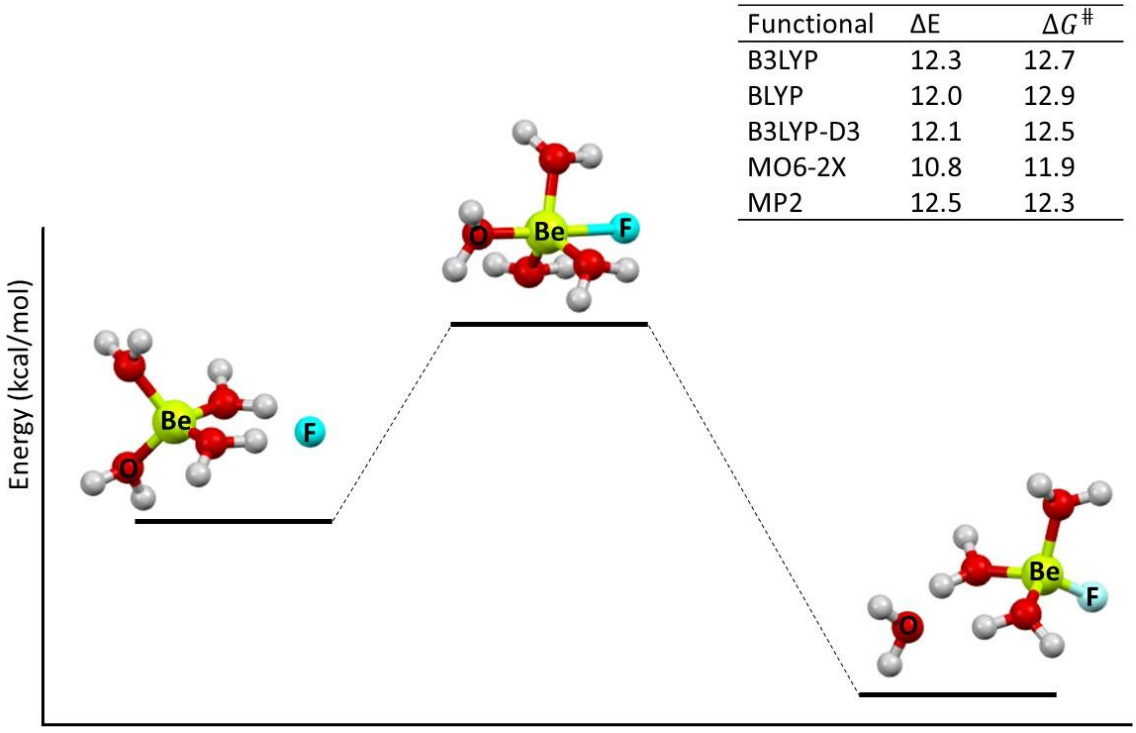

Functional	ΔE	$\Delta G^{\ddagger}$
B3LYP	12.3	12.7
BLYP	12.0	12.9
B3LYP-D3	12.1	12.5
MO6-2X	10.8	11.9
MP2	12.5	12.3

Figure 3-14 Free energy profile for the structural transition between the outer sphere and inner sphere structural arrangements of beryllium fluorido complex.

Finally, the same CPMD-based technique has been used to evaluate the activation energy barrier involved in the ligand substitution of a water molecule by the sulfate ion in the tetraquaberyllium cation **1a** using the corresponding

$H_2O\cdots Be\cdots SO_4$ bond distance as reaction coordinate. In the resulting free-energy profile depicted in Figure 3-15 starting from the outer sphere sulfato complex $Be(H_2O)_4.SO_4$ at Δr = -2.1 Å, a second but slight higher minimum is apparent at the end of the simulation at Δr = 1.7 Å corresponding to the inner sphere complex $BeSO_4.(H_2O)_3.H_2O$. According to Figure 3-15, the activation free energy barrier for this reaction is obtained as 16 kcal/mol. Several measurements of the activation energy for the ligand substitution of the aqua ligand by a sulfate ion have been reported with varying degrees of agreement.[38, 46] However the activation energy barrier of 13.2±0.6 kcal/mol, reported by Strehlow and Knoche by employing a pressure jump relaxation technique to re-examine other previously published data appear to be more reliable.[38] CPMD simulation in this study has reproduced this the activation energy barrier within 2.8 kcal/mol (see Figure 3-15).

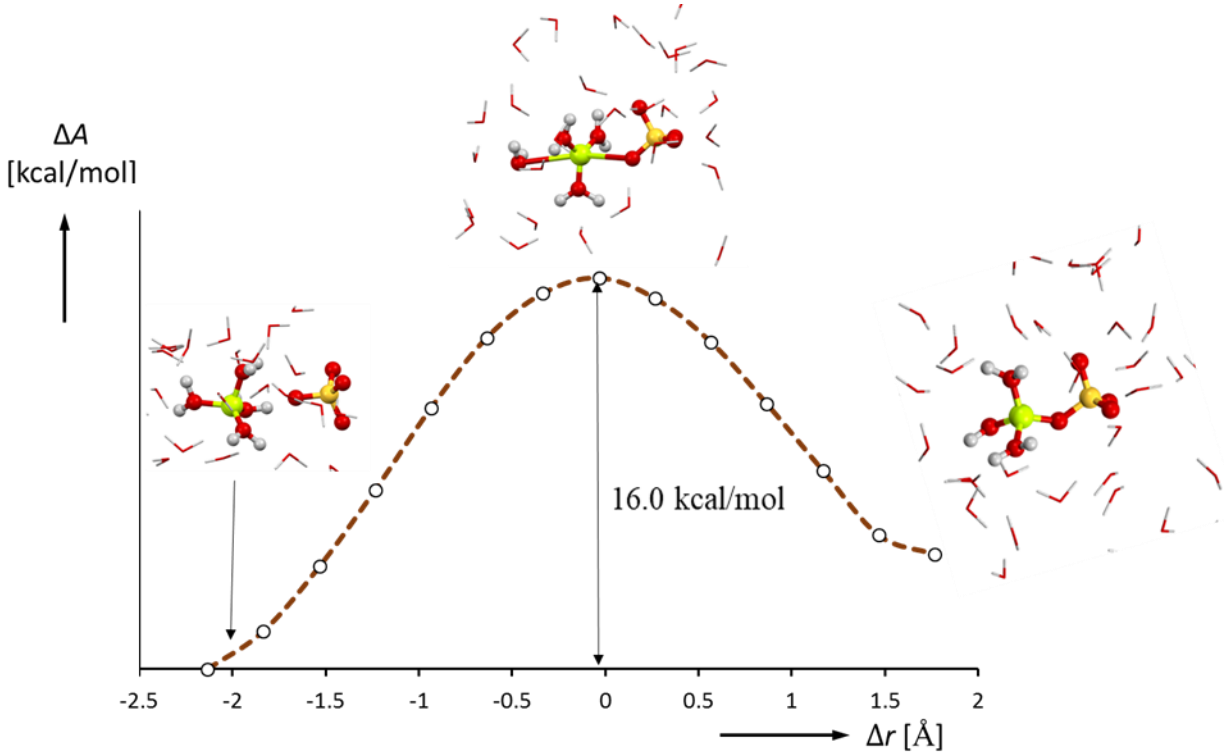

Figure 3-15 Calculated change in free energy, ΔA, for the substitution of an aqua ligand by a sulfato ligand as obtained from constrained CPMD simulations in aqueous solution and thermodynamic integration, including representative snapshots from the indicated region. (reaction coordinate: O-Be-F distance).

To further look into the effect of the solvent, the ligand substitution path of the sulfate ion for a water molecule was followed in the gas phase. Similar CPMD simulations were again set up employing the same constraint and the resultant free-

energy profile is depicted in Figure 3-16. Judging from the difference in ΔA between the two curves in Figure 3-15 and Figure 3-16, the stabilization of the inner sphere sulfato complex in the gas phase amounts to 4.7 kcal/mol. Moreover, it can be observed that the larger driving force of the formation of the inner sphere beryllium sulfato complex in the gas phase is attenuated in solution. This is in complete accord with the observation of the beryllium sulfato complex ubiquitously in the ESI-MS of beryllium sulfate solution and in further agreement of the proposed route of charge reduction during the ESI-MS process (see Chapter 2). Additionally, it is should also be noted that the substitution of the aqua ligand by a sulfato ligand is catalysed by the OH^- ion thereby suggesting other pathways leading to the inner sphere complex.[38]

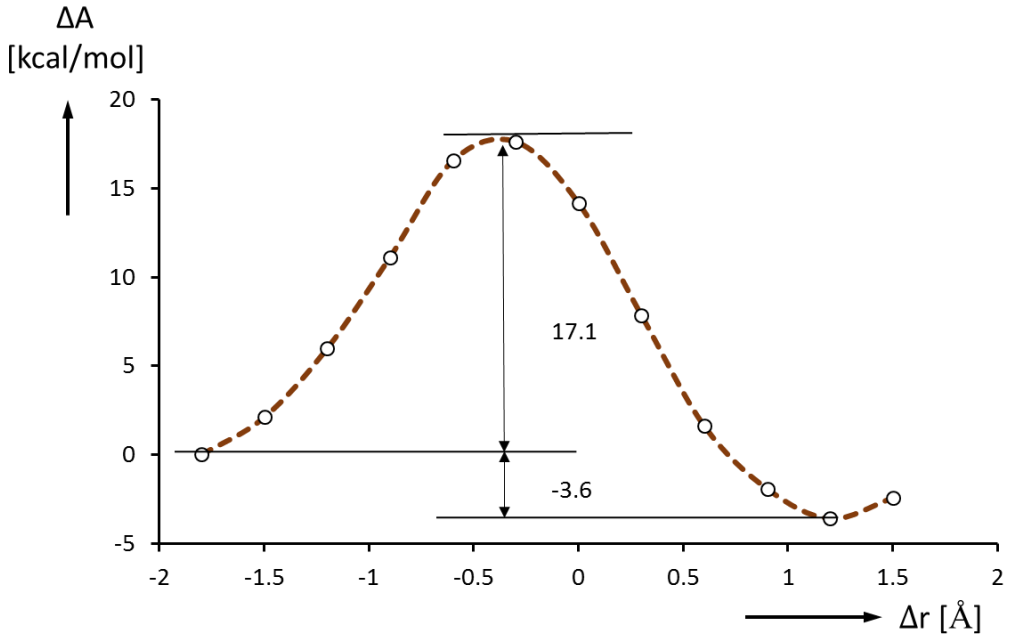

Figure 3-16 Calculated change in free energy, ΔA, for the substitution of an aqua ligand by a sulfato as obtained from constrained CPMD simulations in the gas phase and thermodynamic integration (reaction coordinate: O-Be-F distance).

3.2.7 Mechanism of counterion exchange process with an aqua ligand on the solvated beryllium cation

The water exchange on the tetraaquaberyllium cation **1a** has previously been studied both experimentally and computationally in some detail.[5, 6, 43] The consensus classification for the water exchange between the first and second coordination spheres of the beryllium ion with aqua ligand is a limiting associative

or associative interchange mechanism according to the high negative activation volume of -13.6 cm^3 mol^{-1} relative to other water exchange processes. On the other hand, computational results of Putchta *et al* appear to provide evidence for the interchange mechanism as predominant in water exchange.[47] This result is consistent with previous mechanistic study involving water exchanges. Computationally, the preference for a mechanism is often rationalized by examining key species, especially the transition state species. For the substitution mechanisms for simple ligands such as fluoride ions on $[Be(H_2O)_4]^{2+}$, tracing the reaction energy trajectory for the exchange mechanism by the CPMD/PTI technique passes through a trigonal bipyramidal penta-coordinated complex. The occurrence of the transition state at r=0 points out that both the entering and the leaving groups have considerable bonding to the beryllium centre which is a clear indication of an interchange type of mechanism. Realistically, an interchange associative Ia mechanism would be challenging to distinguish from an interchange mechanism since it lies in between both. However, while the associative mechanism produces an intermediate of which all the bonds to the beryllium ion are within the expected range as in the reactants and products and thus can be characterized by the absence of any imaginary vibrational frequency the interchange mechanism reveals a transitional state. The static optimisation of this trigonal bipyramidal penta-coordinated beryllium complex for the fluoride exchange could be characterized as a true transition state by the presence of exactly one imaginary vibrational frequency in agreement with an interchange associative mechanism.

Furthermore, it is obvious that the small size of the beryllium ion will strongly disfavour a five coordinate species with similar bond distances as would be required to form a true intermediate. Rather, inspection of the Be-O and Be-X ($X=F^-$, SO_4^{2-}) bond distances of the entering and leaving ligands reveal that their bond distances are 0.3-0.8 Å longer than the Be-O/Be-X bonds not directly involved in the exchange process. This is more obvious with the sulfate exchange compared to the fluoride ion possibly due to steric factors. However, for the sulfate substitution, attempts to optimise a transition state failed though this does not necessarily indicated the absence of a transition state. Obviously, the agreement of the CPMD results from this study with experimental data reveal that the mechanism

for the fluoride and sulfate substitution with aqua ligands proceeds *via* an interchange mechanism.

3.3 Conclusion

In summary, this Chapter has employed static DFT calculations and Car-Parrinello molecular dynamics to elucidate the precise coordination environment about the beryllium ion in mixed aquo, fluorido and sulfato complexes as proposed from stoichiometry data assessed from electrospray ionisation mass spectrometry. It was established that in the presence of counter ions such as fluoride, sulfate and chloride, inner sphere complexes exist in solution in agreement with the observation made in earlier discussed mass spectra. The sulfate and fluoride ion were particularly prone to the formation of such species in comparison to the chloride. In addition the multidentate nature of the sulfate facilitated various polynuclear structural arrangement of beryllium sulfato complexes. Furthermore, the role of the solvation on geometric and energetic parameters of beryllium complexes were illustrated pointing out that the accurate description of the solvent effect is particularly challenging for simple continuum models but yield fairly reasonable results. On the other hand, the computationally demanding technique of *ab initio* molecular dynamics, involving the treatment of the whole solution as a dynamic ensemble has provided more agreement with experimental data thereby highlighting the role played by the hydrogen bond interactions with the solute which are critical but which, unfortunately, cannot be captured by a continuum solvation. Finally, it has been shown that the beryllium speciation in aqueous solution could involve independent hydrated metal ions as well as inner and outer sphere complexes depending on the binding affinity of the counterion and its concentration in solution. This insight into the speciation of beryllium in a solvent environment using the CPMD/PTI methodology as well as the impressive reproduction of the energetics of the ligand substitution reaction on the beryllium cation would be a reference point in subsequent *ab initio* molecular dynamics simulations of beryllium interactions with important binding sites of other ligands of interest.

3.4 References

1. L. S. Newman, *Chemical & Engineering News*, 2003, http://pubs.acs.org/cen/80th/beryllium.html. Accessed June, 2017.

2. T. M. McCleskey and B. L. Scott, *Journal of Occupational and Environmental Hygiene*, 2009, **6**, 751-757.

3. H. A. Schroeder, *Medical Clinics of North America*, 1974, **58**, 381-396.

4. J. Borak, *Journal of Occupational and Environmental Medicine*, 2016, **58**, e355-e361.

5. R. Puchta, E. Pasgreta and R. van Eldik, *Advances in Inorganic Chemistry*, 2009, **61**, 523-571.

6. D. T. Richens, *The Chemistry of Aqua Ions: Synthesis, Structure, and Reactivity : A Tour Through the Periodic Table of the Elements*, Wiley, Chichester, 1997.

7. P. E. Mason, S. Ansell, G. W. Neilson and J. W. Brady, *The Journal of Physical Chemistry B*, 2008, **112**, 1935-1939.

8. W. W. Rudolph, *Journal of Solution Chemistry*, 2010, **39**, 1039-1059.

9. W. W. Rudolph, D. Fischer, G. Irmer and C. C. Pye, *Dalton Transactions*, 2009, 6513-6527.

10. L. Alderighi, P. Gans, M. Stefeno and A. Vacca, in *Advance in Inorganic Chemistry*, eds. A. G. Sykes and A. Cowley, H, Academic Press, Califorornia, 2000, vol. 50, pp. 109-197.

11. G. M. Clayton, Y. Wang, F. Crawford, A. Novikov, B. T. Wimberly, J. S. Kieft, M. T. Falta, N. A. Bowerman, P. Marrack and A. P. Fontenot, *Cell*, 2014, **158**, 132-142.

12. M. J. Brisson and A. A. Ekechukwu, *Beryllium: Environmental Analysis and Monitoring*, Royal Society of Chemistry, United Kingdom, 2009.

13. K. A. Walsh and E. E. Vidal, *Beryllium Chemistry and Processing*, ASM International, Ohio, 2009.

14. P. F. Infante and L. S. Newman, *The Lancet*, 2004, **363**, 415.

15. A. Agrawal, J. Cronin, J. Tonazzi, T. M. McCleskey, D. S. Ehler, E. M. Minogue, G. Whitney, C. Brink, A. K. Burrell and B. Warner, *Journal of Environmental Monitoring*, 2006, **8**, 619-624.

16. P. G. Plieger, K. D. John and A. K. Burrell, *Polyhedron*, 2007, **26**, 472-478.

17. P. G. Plieger, K. D. John, T. S. Keizer, T. M. McCleskey, A. K. Burrell and R. L. Martin, *Journal of the American Chemical Society*, 2004, **126**, 14651-14658.

18. K. J. Shaffer, R. J. Davidson, A. K. Burrell, T. M. McCleskey and P. G. Plieger, *Inorganic Chemistry*, 2013, **52**, 3969-3975.

19. R. B. Cole, *Electrospray and Maldi Mass Spectrometry:Fundamentals, Instrumentation, Practicalities, and Biological Applications*, Wiley, New Jersey, 2nd edn., 2010.

20. H. Schmidbaur, *Coordination Chemistry Reviews*, 2001, **215**, 223-242.

21. D. Marx and J. Hutter, *Ab Initio Molecular Dynamics:Basic Theory and Advanced Methods*, Cambridge University Press, New York, 2009.

22. G. Bachelet, D. Hamann and M. Schlüter, *Physical Review B*, 1982, **26**, 4199.

23. D. Hamann, *Physical Review B*, 1989, **40**, 2980.

24. D. Hamann, M. Schlüter and C. Chiang, *Physical Review Letters*, 1979, **43**, 1494.

25. M. Bühl, N. Sieffert, V. Golubnychiy and G. Wipff, *The Journal of Physical Chemistry A*, 2008, **112**, 2428-2436.

26. M. Bühl, N. Sieffert and G. Wipff, *Chemical Physics Letters*, 2009, **467**, 287-293.

27. D. Marx, M. Sprik and M. Parrinello, *Chemical Physics Letters*, 1997, **273**, 360-366.

28. C. W. Bock and J. P. Glusker, *Inorganic Chemistry*, 1993, **32**, 1242-1250.

29. F. Kraus, S. A. Baer, M. R. Buchner and A. J. Karttunen, *Chemistry: A European Journal* 2012, **18**, 2131-2142.

30. F. Kraus, S. A. Baer, M. Hoelzel and A. J. Karttunen, *European Journal of Inorganic Chemistry*, 2013, **2013**, 4184-4190.

31. G. Schwarzenbach and H. Wenger, *Helvetica Chimica Acta*, 1969, **52**, 644-665.

32. B. L. Trout and M. Parrinello, *Chemical Physics Letters*, 1998, **288**, 343-347.

33. M. Bühl and H. Kabrede, *ChemPhysChem*, 2006, **7**, 2290-2293.

34. J.-G. Lee, E. Asciutto, V. Babin, C. Sagui, T. Darden and C. Roland, *The Journal of Physical Chemistry B*, 2006, **110**, 2325-2331.

35. D. Marx, *ChemPhysChem*, 2006, **7**, 1848-1870.

36. C. F. Baes and R. E. Mesmer, *Hydrolysis of cations*, Wiley, New York, 1976.

37. M. Sprik, *Chemical Physics*, 2000, **258**, 139-150.

38. H. Strehlow and W. Knoche, *Berichte der Bunsengesellschaft für Physikalische Chemie*, 1969, **73**, 427-432.

39. W. Massa and K. Dehnicke, *Zeitschrift für Anorganische und Allgemeine Chemie*, 2007, **633**, 1366-1370.

40. M. Georgiev, M. Wildner, D. Stoilova and V. Karadjova, *Journal of Molecular Structure*, 2005, **753**, 104-112.

41. D. A. Everest, *The Chemistry of Beryllium*, Elsevier, Amsterdam, 1964.

42. J. Tomasi, B. Mennucci and R. Cammi, *Chemical reviews*, 2005, **105**, 2999-3094.

43. P. A. Pittet, G. Elbaze, L. Helm and A. E. Merbach, *Inorganic Chemistry*, 1990, **29**, 1936-1942.

44. W. Baldwin and D. Stranks, *Australian Journal of Chemistry*, 1968, **21**, 2161-2173.

45. A. Bankura, V. Carnevale and M. L. Klein, *The Journal of Chemical Physics*, 2013, **138**, 014501.

46. H. Strehlow and S. Kalarickal, *Berichte der Bunsengesellschaft für Physikalische Chemie*, 1966, **70**, 139-143.

47. R. Puchta, N. van Eikema Hommes and R. van Eldik, *Helvetica Chimica Acta*, 2005, **88**, 911-922.

Chapter Four

ESI-MS microscale screening and characterisation of beryllium complexes with important classes of ligands

4.1 Introduction

Ever since an electrospray device was successfully coupled to a mass analyser about 3 decades ago, the technique of electrospray ionisation mass spectrometry has gained huge popularity as a means of probing solution speciation with a broad spectrum of applications across many scientific fields including inorganic and organometallic chemistry.[1-3] An essential feature of this technique in application to inorganic and organometallic systems is its ability to directly provide stoichiometric information on metal-ligand complexation and reactivity in solution.[2, 4, 5] In addition, the ESI-MS technique can also be employed in quantifying the abundance of representative ions in the mass spectra as a means to examine metal-ligand binding affinity and selectivity in solution.[6, 7] While this requires a careful consideration of the peculiarities in the system involved, numerous studies have revealed good agreement of ESI-MS speciation data with other solution-based techniques.[1, 8-10] However, the greatest advantage of the ESI-MS technique lies in its robust and straightforward nature with the ability to handle complex mixtures involving tiny amounts of sample in solutions to the extent that the technique is amendable for rapid microscale screening of solution species. This advantage has been well harnessed by Henderson and co-workers[2] who pioneered a "combinatorial-type" approach in the ESI-MS survey of metalloligand chemistry in inorganic and organometallic systems. Worthy of mention is their utilization of this strategy in the conservation of rather expensive metals and starting material prior to macroscale characterisation using other techniques such as X-ray crystallography and NMR.[2, 5, 11, 12] Indeed, a similar limitation is encountered in the coordination chemistry of beryllium as a result of its high toxicity. Therefore, it is

even more desirable to work on a microscale hence this strategy was adopted and replicated for the first time in the relatively uncharted territory of the coordination chemistry of beryllium.[13, 14] Most importantly, the utilisation of tiny amounts of material in solution essentially minimizes any exposure to beryllium dust while at the same time gaining rich information on beryllium species present in various solutions.

In resemblance to the grossly understudied chemistry of beryllium highlighted in Chapter one, the mass spectrometry of beryllium compounds is equally sparse, although older ionisation techniques such as electron ionisation (EI) and fast atom bombardment (FAB) mass spectrometry have previously been employed in a few fragmentation studies.[15-19] This relegated role of mass spectrometry is not unexpected since in addition to its toxicity, beryllium is monoisotopic and exhibits only one stable oxidation state (+2). Consequently, very little is portrayed in terms of isotopic information in comparison to other more interesting isotope-rich metals. (The isotopic pattern of beryllium complexes with organic ligands essentially involves only one major peak except in the presence of heavier isotopes of salt anions such as the chlorides). Nonetheless, the general research interest in the chemistry of beryllium is currently being rejuvenated in response to burgeoning production output and diversification of applications involving this element across many industries.[20, 21] Since an area of frontline interest in this field is the interaction of beryllium with important classes of ligands, this chapter aims to project the technique of ESI-MS as an alternative and safer methodology suitable for investigating the solution speciation of toxic beryllium ion.

Following up the ESI-MS behaviour of beryllium ion in the presence of simple inorganic ligands such as the sulfate (see Chapter two), this Chapter considers the ESI-MS ionisation and fragmentation behaviour of beryllium complexes with various classes of organic ligands. This will serve as reference data both for other chemically-interesting interactions unique to this metal or other inorganic systems of interest. In addition, the well-established power of the electrospray technique is employed in sampling a number of previously-synthesised and well-characterised thermodynamically stable beryllium complexes containing important classes of ligands including salicylaldimines,[22] diketonate,[23] mono-

/dicarboxylates,[24, 25] citrate[26] etc. These complexes which were synthesised *in situ* and subjected to detailed characterisation by ESI-MS will serve to identify any ligand exchange and/or solvolysis processes arising as a result of ligand lability, and will contribute to the present knowledge of factors that influence the stability of the beryllium complexes (see Chapter 7 for the general ESI-MS methodology and microscale syntheses of these beryllium complexes). For example the chelate effect and polynuclear binding via bridging phenolic groups have already been pointed out as playing a major role in stabilising beryllium complexes.[27, 28]

4.2 Results and discussion

4.2.1 ESI-MS of Be^{2+} and acetic acid

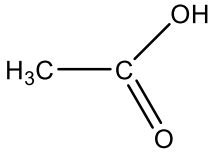

Acetic acid (HOAc)

Although equilibrium constants[23] for the interaction of the monocarboxylate ligands with the beryllium ion in solution suggests that these ligands poorly complex beryllium, they are well-known to form a variety of beryllium complexes of which the tetraberyllium μ_4–oxo-acetato complexes $Be_4O(O_2CCH_3)_6$ have been characterised both in the solid and gas phases.[15, 23] While the tetraberyllium μ_4–oxo-acetato complex is one of the oldest structurally characterized beryllium coordination complexes known, there is as yet no evidence for its existence in solution as a complex ion.[16, 17, 25, 29-32] Elsewhere, the very narrow peak in the ^{9}Be NMR chemical shift ranging between 2.36 to 3.14 ppm led to the conclusion of a Be_4O core unit in a few sterically encumbered monocarboxylato beryllium complexes.[15] However, at the time of this ESI-MS study, there is still no prior speciation study on the interaction of the beryllium and the acetate ion in solution or evidence for the Be_4O cores in solution. Therefore, the interactions of the Be^{2+} ion with the acetate anion (OAc^-) will be examined using the ESI-MS technique.[33] Importantly, very soft ionisation conditions are employed by using a low capillary exit voltage of 60 V to facilitate the effective transmission of pre-existing beryllium acetate species from solution into the gas phase with minimal perturbation noting

that the tetraberyllium μ_4 –oxo-acetato species is very labile.[25] An illustrative positive ion mass spectrum of a 2:3 molar mixtures of beryllium sulfate solution and acetic acid in 1:1 methanol-water (neutralized to a pH of 5.5-6.5 with sodium hydroxide and left standing for 24 hours for proper equilibration) is shown in Figure 4-1 and the assignments of the majority of ions have been compiled in Table 4-1.

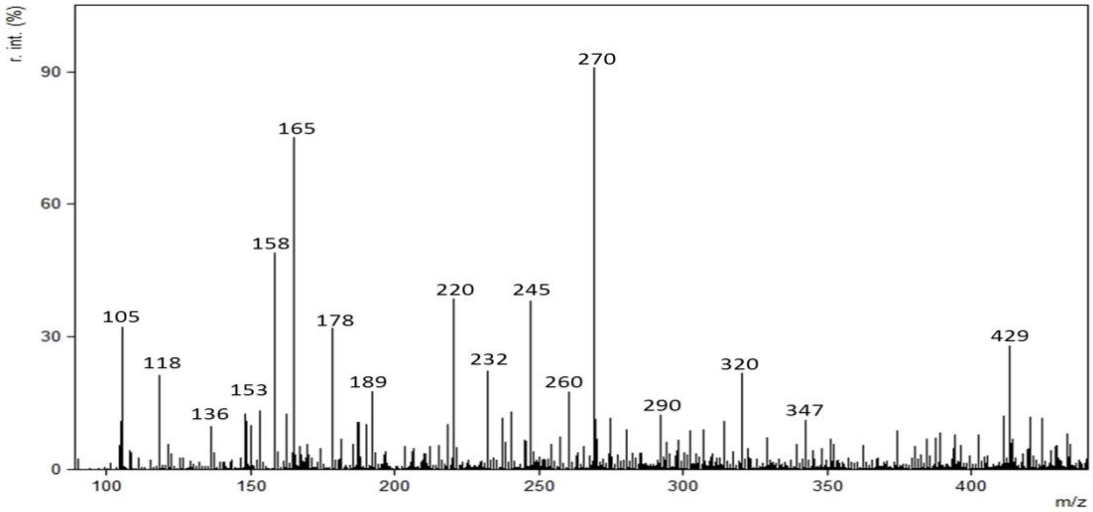

Figure 4-1 Positive ion ESI mass spectrum of beryllium sulfate and acetate ion in 1:1 methanol-water solution showing the presence of the sodium adduct of the basic beryllium acetate complex $[Be_4O(OAc)_6Na]^+$ at *m/z* 429. Sodium hydroxide was used to adjust the solution pH to 5.5-6.5.

The positive ion spectra were relatively complex, with peaks revealing a variety of ions because as a weak ligand, the acetate is in competition with solvent ligands and the sulfate ion in solution. This is consistent with the observation of species with various degree of solvation often revealing a series in the mass spectra such as $[Be_3(OH)_3(OAc)_2(CH_3OH)_n]^+$ where n = 1-3 observed at *m/z* 228, 260, 292 and $[Be_2OH(OAc)_2(H_2O)_2]^+$ where n = 0-2 observed at *m/z* 153, 171, 189 as shown in Table 4-1. In contrast, the negative ion mode predominantly revealed the bisulfate ion $[HSO_4]^-$ at *m/z* 97 as the most abundant ESI-MS ion. Since the *m/z* value of the acetate ion $[OAc]^-$ (*m/z* 59.01) falls within the lower mass region for which the poor sensitivity of the time of flight mass analyser is known, the abundance of this ion in the mass spectra was quite insignificant.

Table 4-1 Summary of ions observed in the positive ion ESI mass spectra of 2.2×10^{-3} mol L^{-1} aqueous beryllium sulfate solutions and actetate ion across pH 5.5 – 6.5 and capillary exit voltages of 60 – 180 V.

Experimental *m/z*	**Theoretical** *m/z*	**ESI-MS ions**	**Experimental** *m/z*	**Theoretical** *m/z*	**ESI-MS ions**
153.0911	153.0531	$[Be_2OH(OAc)_2]^+$	168.0792	168.0385	$[Be(OAc)_2(H_2O)Na]^+$
171.1060	171.0637	$[Be_2OH(OAc)_2H_2O]^+$	186.0446	186.0491	$[Be(OAc)_2(H_2O)_2Na]^+$
189.0733	189.0742	$[Be_2OH(OAc)_2(H_2O)_2]^+$	150.0732	150.0280	$[Be(OAc)_2Na]^+$
214.0901	214.0813	$[Be_3(OH)_3(OAc)_2H_2O]^+$	118.091	118.0617	$[Be(OAc)(CH_3OH)(H_2O)\ ]^+$
232.0921	232.0919	$[Be_3(OH)_3(OAc)_2(H_2O)_2]^+$	158.0892	158.0759	$[Be_3(OH)_3(OCH_3)H_2O]^+$
228.0884	228.0970	$[Be_3(OH)_3(OAc)_2(CH_3OH)]^+$			
260.1905	260.1232	$[Be_3(OH)_3(OAc)_2(CH_3OH)_2]^+$		Negative ions	
292.1121	292.1494	$[Be_3(OH)_3(OAc)_2(CH_3OH)_3]^+$	96.9987	96.9967	$[HSO_4]^-$
270.0704	270.0303	$[Be_3(OH)_3(H_2O)(OAc)HSO_4]^+$	157.1151	156.99	$[(HOAc)HSO_4]^-$
220.0780	220.0708	$[Be_3O(OH)_3(OAc)_3]^+$	119.0411	119.0375	$[(HOAc)(OAc)_2]^-$
203.0309	203.0899	$[Be_4O_2(OAc)_2OH/Be_2OH(OAc)_2(H_2O)_2]^+$	223.0394	223.0985	$[(BeO)_4(OAc)(CH_3OH)\ ]^-$
245.0286	245.0779	$[Be_4O(OAc)_3O]^+$	109.0199	109.0269	$[(BeO)_2(OAc)\ ]^-$
429.1527	429.1126	$[Be_4O(OAc)_6Na]^+$	126.9859	127.0374	$[(BeO)_2(OAc)H_2O]^-$
320.8991	320.9704	$[Be_4O_2(HSO_4)_2(OAc)\ ]^+$	141.0423	141.0531	$[(BeO)_2(OAc)CH_3OH]^-$
347.1212	347.1096	$[Be_4O(OAc)_5]^+$	173.0688	173.0793	$[(BeO)_2(OAc)(CH_3OH)_2]^-$
178.1077	178.0602	$[Be_3O(OAc)_2OH]^+$	166.0491	166.0602	$[(BeO)_3(OAc)CH_3OH]^-$
105.0112	104.9981	$[(HOAc)Na]^+$			
132.1104	132.0773	$[Be(OAc)(CH_3OH)_2]^+$			
100.0017	100.0511	$[Be(OAc)CH_3OH]^+$			

However, adducts of the acetate ligand with slightly higher *m/z* value such as $[(HOAc)HSO_4]^-$ and $[(HOAc)(OAc)_2]^-$ were observed at *m/z* 157 and 119 respectively at relatively high abundances (see Figure 4-2). Generally, the beryllium-containing acetate species observed in the negative ion mass spectra were in low abundance (<30%) and included various solvated analogues of the $[OAc(BeO)_n]^-$ ion series where n = 2-4 such as $[OAc(BeO)_2CH_3OH]^-$ *m/z* 141, $[OAc(BeO)_2(CH_3OH)_2]^-$ *m/z* 173 and $[OAc(BeO)_3CH_3OH]^-$ *m/z* 166. As a result of this poor representation of Be^{2+} and acetate in the negative ion mode, subsequent ESI-MS investigations of the beryllium actetate species in solution were carried out in positive ion mode.

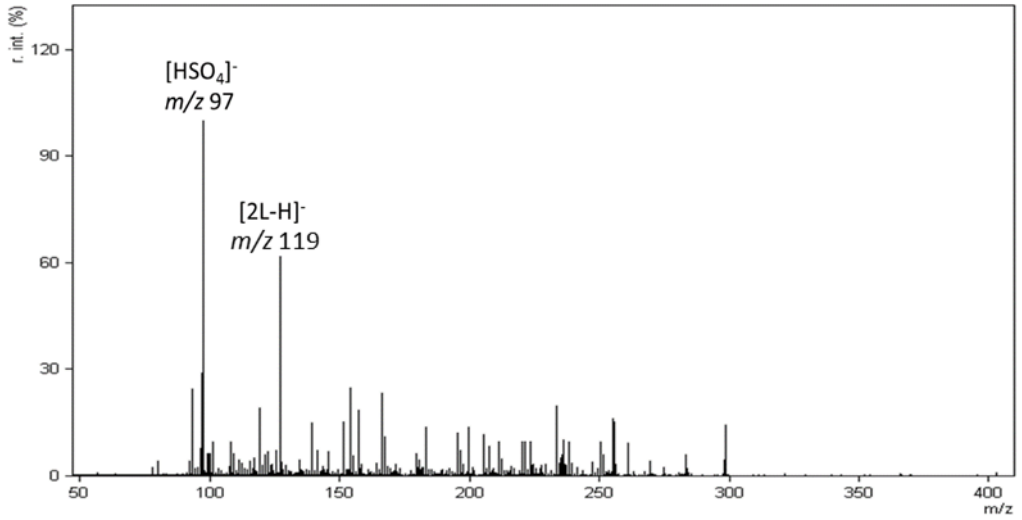

Figure 4-2 Negative ion ESI mass spectrum of Be^{2+} and acetate ion in 1:1 methanol-water solution showing the predominance of the hydrogen sulfate ion $[HSO_4]^-$ at *m/z* 97 and the acetate ion $[(HOAc)(OAc)_2]^-$ at *m/z* 119.

The major cationic complexes in the ESI-MS spectra contained the oligomeric hydrolyzed species well-known to exist in beryllium solutions at the pH range of the injected beryllium acetate solutions (pH 5.5-6.5) and previously observed in the ESI-MS of beryllium sulfate solutions described in Chapter 2. However, the ion pairing observed in the ESI-MS of beryllium sulfate solution was attenuated as the acetate ion sufficiently coordinated to the metal centre (at least as a monodentate ligand) to effectively reduce the high charge density on these beryllium hydroxido cores. This results in ion series consisting of the dimeric and trimeric beryllium cores such as $[Be_2OH(OAc)_2(solv)_n]^+$ and

$[Be_3OH_3(OAc)_2(solv)_n]^+$ (where solv = CH_3OH, H_2O or both) in the mass spectra. Nevertheless, the most abundant ion signal which was observed at *m/z* 270 due to $[Be_3(OH)_3(H_2O)_2(OAc)SO_4]^+$ presents a beautiful picture of the most probable situation in solution wherein beryllium complexation by the ligand is in competition with the notorious hydrolysis of the beryllium ion as well as the previously reported ion pairing with the sulfato ligands (see Chapter 2). This is understandable in consideration of the fact that all the potential ligands in this system (OH^-, CH_3COO^-, SO_4^{2-}) are oxygen donor ligands. Although the acetato and sulfato anions can potentially adopt a bidentate coordination mode, the narrow bite size and the resultant strained four-membered chelate ring would make this coordination mode highly unfavorable (as shown in Chapter 3 for the sulfato ligand). Therefore, all the ligands involved (OH^-, CH_3COO^-, SO_4^{2-}) are invariably monodentate and at best bridging ligands. Herein lies the advantage of the acetate ion which is capable of stabilizing the Be_4O core via extensive bridges forming a highly symmetrical beryllium complex as observed in the X-ray structures.[15, 32] This also explains the predominance of the tetraberyllium μ_4 –oxo-acetato and triberyllium μ_4 –oxo-acetato species in the gas phase.[25] Moreover, the possibility of numerous interactions of the beryllium ion with the bridging ligands increases forming a variety of polynuclear species in the mass spectra especially at elevated ionisation conditions (Table 4-1).

For the monomeric ESI-MS ions in the mass spectra, 1:1 and 1:2 beryllium acetato complexes of the type $[Be(OAc)(solv)_n]^+$ for n = 2-3 and $[Be(L)_2(solv)_nNa]^+$ for n = 0-2 were observed. This includes the ions at *m/z* 150, 168, 118 due to $[Be(OAc)_2Na]^+$, $[Be(OAc)_2(H_2O)Na]^+$, and $[Be(OAc)(CH_3OH)(H_2O)]^+$ respectively. The presence of these species which apparently retained the molecules of the solvent ligands (solv= H_2O, CH_3OH or both) transferred from the solution phase into the gas phase, further pointed out that the acetate ligand is mainly monodentate in solution such that the remainder of the coordination sites in the metal centre are filled up by the solvent ligands. Another significant observation in the ESI-MS of Be^{2+}/acetate mixtures is the absence of the monomeric species $[BeOH]^+$ and $[BeHSO_4]^+$ which were observed to be stabilized in a H_2O/DMSO solvent system.[14, 34] While the monomeric $[BeOH]^+$ is known to be transient and polymerizes into the higher oligomeric species, the absence of the

$[BeHSO_4(solv)_n]^+$ species is also an affirmation that the acetate ion binds beryllium ahead of the sulfato ligand. However, since the solvent molecule is not excluded deprotonation and subsequent hydrolysis is not completely prevented.

In addition, the occurrence of the oligomeric beryllium oxido/hydroxido cores in solution is noteworthy, since it involves no actual fragmentation of the parent complex. This phenomenon becomes significant with the observation of other possible beryllium cores for which the most notable is the well-known Be_4O and the Be_3O. Analysis of the ESI-MS spectra reveals a moderately strong signal observed at an experimental *m/z* 429.15 (calc *m/z* 429.11) which fits well to a signal due to the $[Be_4O(OAc)_6Na]^+$ species. This ion, which corresponds to the sodium adduct of the tetrameric beryllium acetate complex $Be_4O(CH_3COO)_6$, suggests that this well-known species equally exists in solution from ESI-MS data. Furthermore, the observation of a signal at *m/z* 347 due to $[Be_3O(OAc)_5]^+$ (which has also been identified as a fragment of the tetraberyllium μ_4 –oxo-acetato complex using electron ionisation mass spectrometry) is consistent with the formation and pre-existence of the $Be_4O(CH_3COO)_6$ in solution.[25] Unfortunately, the assignment of several other signals which could lend more support to the Be_4O core were ambiguous due to the complexity of the spectra at the desired low capillary exit voltage (60 V). For instance, the signal at *m/z* 203 which could be due to $[Be_4O_2(OAc)_2OH]^+$ or $[Be_2OH(OAc)_2(H_2O)_2]^+$ cannot be confidently distinguished from each other although the Be_4O core is actually a combination of the beryllium dimer with the elimination of a water molecule according to eqn (3-6)

$$2Be_2(OH)^{3+} \rightarrow Be_4O^{6+} + H_2O \qquad (3\text{-}6)$$

Certainly, the acetate ligand is unable to counter the hydrolytic and oligomeric trends of the beryllium ion in solution hence the formation of interesting polynuclear beryllium cores of the beryllium acetate complexes. However, it appears that in aqueous solutions of beryllium acetates, the dominant hydroxido cores such as $[Be_2OH]^{3+}$ and $[Be_3(OH)_3]^{3+}$ persist alongside the oxido-bridged cores (Be_4O and Be_3O core unit) which are more popular with the monocarboxylates. In fact it likely that the trimeric beryllium hydroxido cores supersede in solution but the poorly chelating acetate ion renders them unfavorable during crystallization in comparison to the $Be_4O(CH_3COO)_6$ complex. However, it has been shown

elsewhere that ligands containing an additional carboxylate groups that are able to chelate the metal centres can be employed to isolate the $[Be_3(OH)_3]^{3+}$.[24] This further explains the preferential isolation of the $Be_4O(CH_3COO)_6$ complex ahead of a complex containing the $[Be_3(OH)_3]^{3+}$ trimer core. Importantly, it also points out that species predominant in beryllium solution may not similarly be obtainable in the solid state. Hence the relevance of the ESI-MS technique cannot be overemphasised as a guide in understanding the solution state. In addition, the ESI-MS characterisation of the Be^{2+} and acetate ion mixtures in solution is unprecedented and these data astutely emphasise the strengths of the electrospray ionisation mass spectrometry technique as the softest ionisation technique for the intact transfer of pre-existing solution species.

In a series of early works,[29] the tetraberyllium μ_4–oxo-acetato complex was investigated using electron impact mass spectrometry and the finding is best summarized by the author's statement - "None of the spectra contains molecular ions; the heaviest and as a rule most intense ions are generated by the elimination of RCO_2 or OR from the M^+". Also, a subsequent investigation of related tetraberyllium μ_4-oxo-arylcarboxylato complexes by the relatively softer FAB-MS was quite successful in transferring the intact parent ion to the gas phase in an appreciable abundance.[15] However, it is worth pointing out that none of these techniques traditionally handle the characterization of complexes from the mother solutions but required the successful isolation of pure compounds prior to any analysis. This is a huge deterrence in the exploration of beryllium chemistry as the exposure and inhalation hazard involved in handling of solid compounds of beryllium increases. Preferentially, such a hazard could effectively be controlled by employing the ESI-MS methodology of this thesis as a very sensitive solution-based technique to eliminate handling larger quantities of toxic beryllium compounds.

Unfortunately because reaction mixtures are employed, a major disadvantage of this strategy is that in the presence of poorly complexing ligands, a huge variety of species could be obtained (including the complex beryllium hydroxido species) thereby rendering the ion assignment cumbersome. Nevertheless, since such complex mass spectra are merely a reflection of the state of beryllium's interaction in solution the patterns of behavior of these systems under the various ESI ionisation conditions deserves further considerations.

It is possible to ramp the ESI-MS ionisation condition in a controllable manner so that the technique can equally be used for fragmentation and structural elucidation. ESI-MS experiments across capillary exit voltages from 60 to 180 V afforded a change of relative intensity trends among the fragmentation series. Typically, a loss or exchange of the acetate ligand with the solvent ligand alongside gas phase rearrangement were the most common phenomena observed under elevated ionisation conditions. Consequently, the intensity of the ions such as $[Be_3O(OH)_3(HOAc)_3]^+$ *m/z* 220, $[Be_4(HOAc)_3O_2]^+$ *m/z* 245 become increased and the latter emerges as the base peak at capillary exit voltages above 120 V.

4.2.2 ESI-MS of Be^{2+} and acetylacetonate

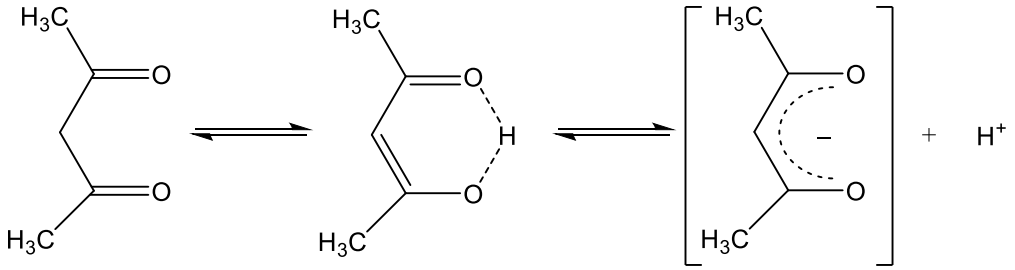

Hacac acac$^-$

Scheme 4-1 Acetylacetone and the acetylacetonate anion

The 1,3-diketones such as acetylacetone and its corresponding anion (see Scheme 4-1) are important ligands in the coordination and analytical chemistry of beryllium as they are widely employed as chelating agents in the extraction of the beryllium ion in numerous analytical procedures and mineral processing.[35-37] Given the numerous practical applications of the beryllium diketonates, extensive ESI-MS investigation has been carried out on these complexes especially with the parent acetylacetonate ligand. Positive and negative ESI-MS were recorded at a range of low, medium, and high capillary exit voltages for mixtures of $BeSO_4$ and acetylacetone in the molar ratios 1:0.5, 1:1, 1:2 and 1:4 in 1:1 methanol-water solution. Illustrative spectra for a varying molar mixture of $BeSO_4$ and acetylacetone at various metal-ligand molar ratios are shown in Figure 4-3. The spectra suggest the predominant species present as $[Be(acac)(CH_3OH)]^+$, $[Be(acac)(CH_3OH)_2]^+$, $[Be(acac)_2H]^+$, $[Be_2(acac)_3]^+$ at *m/z* 140, 172, 208, and 315

in varying order of abundance. The small size of the Be^{2+} cation and its inability to exercise a coordination number greater than four implies that the solvent ligands and acetylacetonate ligand have to compete for the four available coordination sites. The observation of these competitive interactions provides further evidence that the ESI-MS behaviour of beryllium resembles the situation in solution. The ESI-MS spectra of Be^{2+}/Hacac at ratios below 1:0.5 reveal a mix of the species $[Be(OCH_3)(CH_3OH)_3]^+$, $[BeOH(H_2O)_2(CH_3OH)]^+$, $[(Be_2OH)SO_4(CH_3OH)_3]^+$, $[Be_3(OH)_3SO_4]^+$, and $[Be(acac)(CH_3OH)]^+$ reflecting the presence of beryllium hydrolysis species at a low concentration of acetylacetone. Further increase of the acetylacetonate ligand ratio increased the abundance of the $[Be(acac)_2H]^+$ (*m/z* 208) species but only a few differences were observed between the spectra of Be^{2+}/Hacac at 1:2 and 1:4. The ESI-MS spectra of Be^{2+}/Hacac at a 1:1 molar ratio reveals a base peak at *m/z* 140 which is assignable to the species $[Be_3(OH)_3(OCH_3)_2]^+$ or $[Be(acac)(CH_3OH)]^+$. However, the behaviour of the ion signal at *m/z* 140 on going from ESI-MS experiment in 1:1 methanol-water to a similar experiment in acetonitrile-water solvent mixes, pointed to out the latter species as being the most probable assignment.

A simple ESI-MS experiment employed to illustrate such confirmation of ion assignments is to run the same experiment in any other suitable solvent system such as acetonitrile-water solution as shown in Figure 4-4. ESI-MS analysis of Be^{2+} and acetylacetone in acetonitrile-water solution reveals the corresponding $[Be(acac)(CH_3CN)]^+$ species at *m/z* 149. In addition, the $[Be(acac)(CH_3CN)_2]^+$ species was also observed at *m/z* 190 suggesting that the acetonitrile equally coordinated to beryllium ion strongly in the gas phase. It is interesting that acetonitrile competes very successfully with water especially since nitrogen is a softer donor atom than oxygen. Nevertheless, the preferential solvation of metal cations in the gas phase has previously been reported,[38] and the emergence of the mixed solvated species $[Be(acac)(CH_3CN)(H_2O)]^+$ *m/z* 167 (which was absent in the 1:1 methanol-water solvent system) points out a lesser preference of Be^{2+} by acetonitrile molecules in the gas phase as compared to the gas phase preference of the methanol ligand (see Chapter 2).

Since the beryllium cation is known to be strongly solvated in solution it is not surprising that the solvated species $[Be(acac)(CH_3OH)]^+$ *m/z* 140 seems to

compete favourably with the expected parent ion $[Be(acac)_2H]^+$ even at the higher concentrations of acetylacetonate. The formation of the $[Be(acac)_2H]^+$ species involves acetylacetonate (a monoanionic bidentate ligand) displacing two solvent ligands to produce the species observable in the ESI mass spectra as the $[Be(acac)(CH_3OH)]^+$ peak before the formation of the bis(acetylacetonato) beryllium complex, observed as a protonated species $[Be(acac)_2H]^+$ at *m/z* 208. It should also be noted that due the ionisation mode of the ESI-MS, this observation could also be because of the competition between the loss of a ligands and the gain of a proton. While this utilisation of the ESI-MS technique to provide information on the progress of inorganic reactions and the intermediates formed is well known,[2] it is yet to be applied extensively in any beryllium experiments.

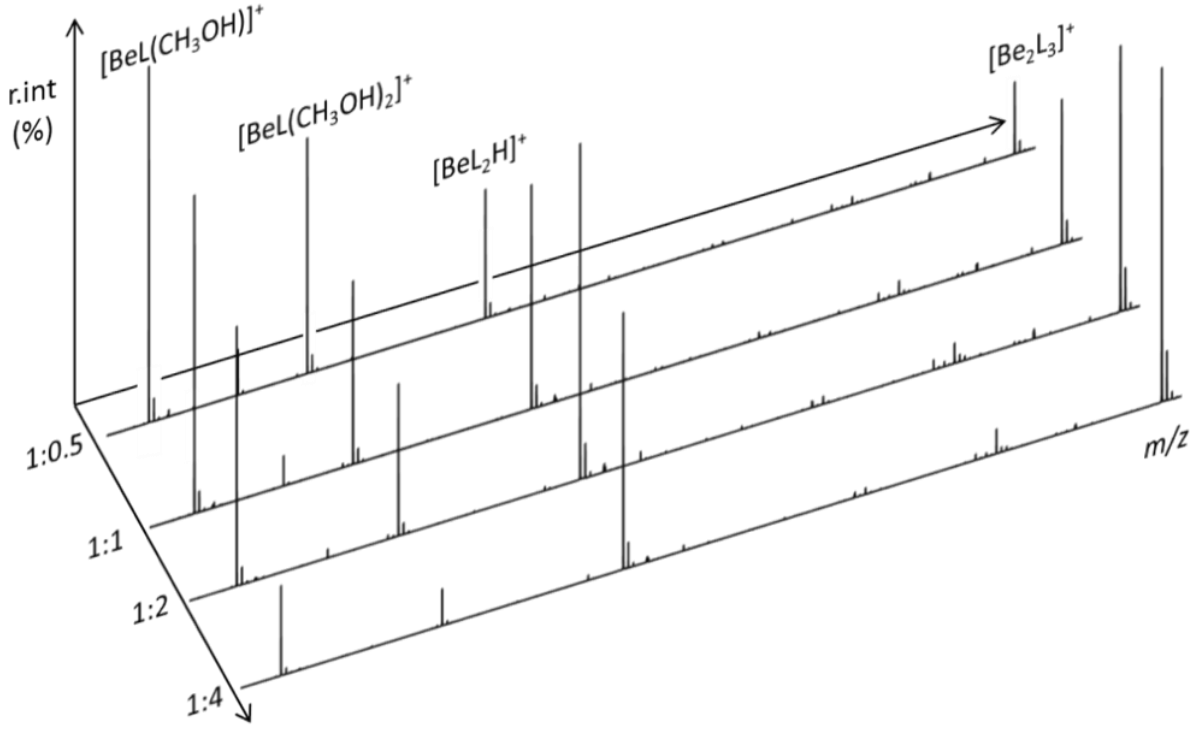

Figure 4-3 Positive-ion ESI-MS spectra for 1:1, 1:2, 1:3 and 1:4 molar mixtures of Be^{2+} and acetylacetone L = $[CH_3COCHCOCH_3]^-$ in 1:1 methanol-water solution at a low capillary exit voltage of 40 V. (No alkali metal cation was added).

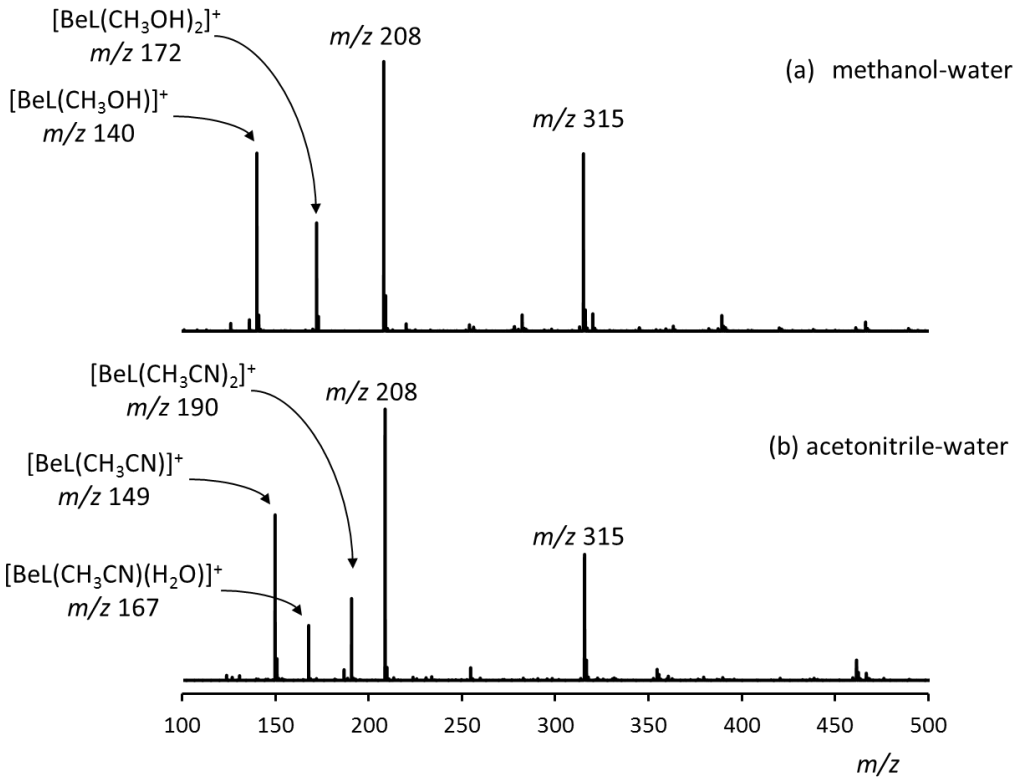

Figure 4-4 Positive ion ESI mass spectra of 1:2 Be^{2+} and acetylacetonate L = $[CH_3COCHCOCH_3]^-$ in (a) 1:1 methanol-water (b) acetonitrile-water solution at capillary exit voltage of 40 V displaying the change in ion signals corresponding to the solvated species.

The X-ray structure of the bischelated complex of acetylacetonate with Be^{2+} is known[39] and the assignment of the $[Be(acac)_2H]^+$ (*m/z* 208) ion is further supported by spiking with sodium and potassium ions which revealed the corresponding $[Be(acac)_2Na]^+$ and $[Be(acac)_2K]^+$ ions at *m/z* 230 and *m/z* 246 respectively. An additional interesting feature in these mass spectra is the dominance of the peak at *m/z* 315 corresponding to the dinuclear species $[Be_2(acac)_3]^+$. While this complex has not been characterized previously, a possible explanation involves the $Be(acac)_2$ complex acting as a metalloligand toward the $[Be(acac)]^+$ species as depicted in Figure 4-5. This is further supported by the existence of this ion even at high capillary exit voltages whereas the suggested constituents $[Be(acac)(CH_3OH)]^+$ *m/z* 208 and $[Be(acac)_2H]^+$ *m/z* 140 respectively disappeared completely. The stability of this ion beyond mild ESI conditions (where aggregates are commonly observed) supports a structure of one acetylacetonate ligand bridging the two metal centres; a well-known factor that

increases the binding strength of ligands to beryllium. This study also supports the fact that the addition of a bridging unit (beryllium oxide or a bridging ligand) leads to the formation of a suitable polynuclear species that could be explored for strong beryllium binding. Also for this reason, the ESI-MS is invaluable for investigating beryllium species in solution being able to represent the stoichiometry composition of polynuclear beryllium complexes.

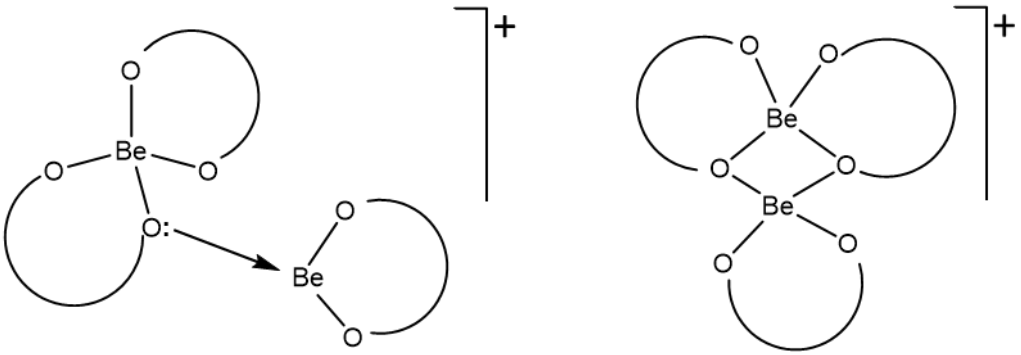

Figure 4-5 Proposed formation of the dinuclear species $[Be_2(acac)_3]^+$ observed at *m/z* 315 by the aggregation of $Be(acac)_2$ and $[Be(acac)]^+$ species.

Structural information through fragmentation can be obtained in an ESI-TOF-MS experiment by changing the capillary exit voltage which is the voltage between the capillary exit and the first skimmer. Positive ion ESI mass spectra for Be^{2+} and the acetylacetone mixtures recorded at a range of capillary exit voltages (CEV) are shown in Figure 4-6. At a low CEV, the spectrum is dominated by the bischelated beryllium complex $[Be(acac)_2H]^+$ at *m/z* 208. There is also a significant abundance of the $[Be(acac)(CH_3OH)_2]^+$ ion at *m/z* 172. However, a solvent in this complex is readily stripped off so that this signal disappears entirely at moderately high CEV of 80 V (see Figure 4-6). Similarly, the slightly harsher ionisation condition strips away an acetylacetonate ligand so that the $[Be(acac)(CH_3OH)]^+$ ion at *m/z* 140 now dominates the spectrum at a CEV of 180 V.

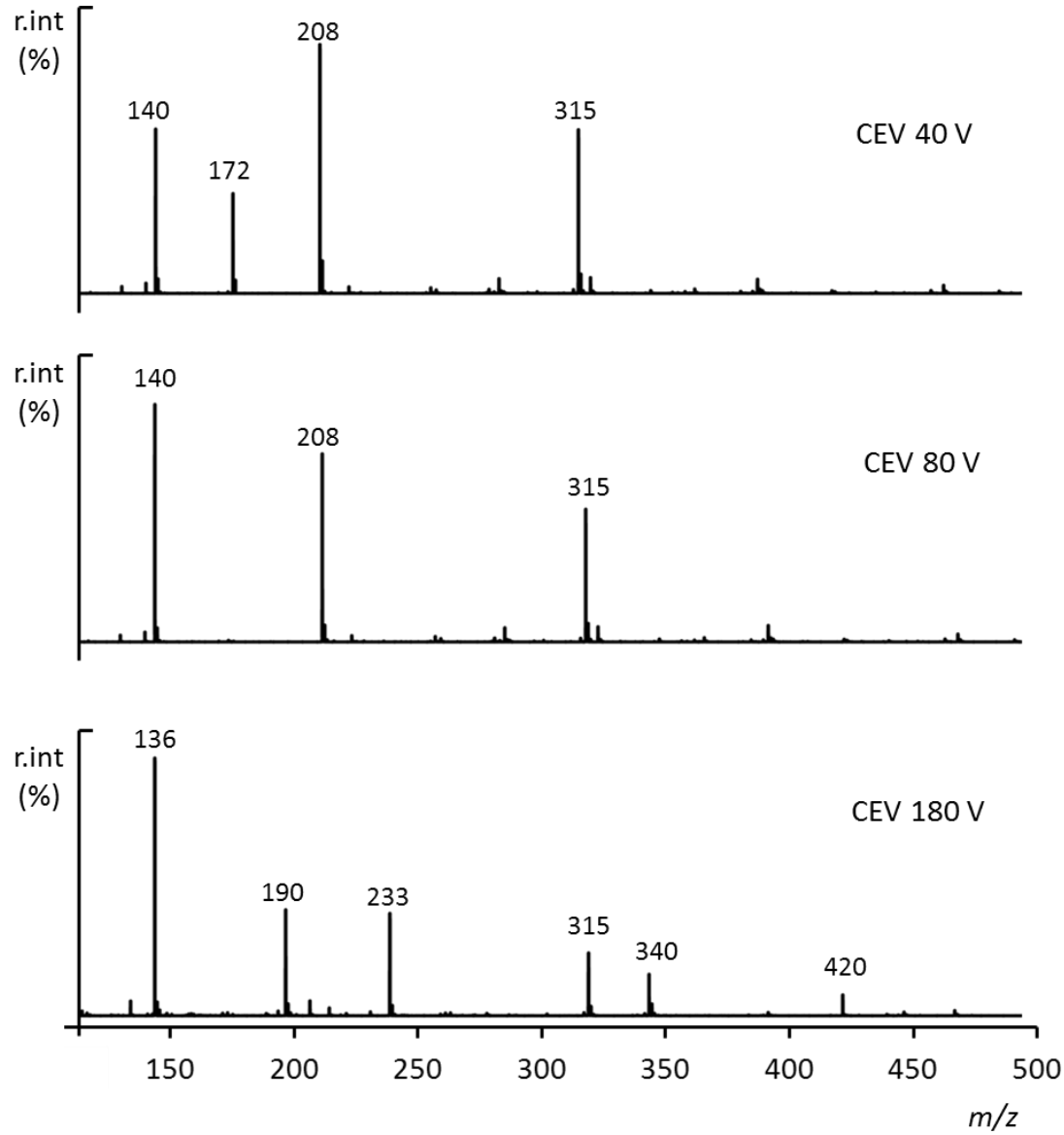

Figure 4-6 The ESI-MS behaviour of 1:2 molar mixtures of Be^{2+} and acetylacetone in 1:1 methanol-water solution at a range of capillary exit voltages of 40, 80 and 180 V (pH unadjusted).

At a high capillary exit voltage (180 V), new peaks emerge revealing ligand fragmentation and other aggregates as shown in Table 4-2. Collision induced dissociation by the high capillary exit voltage results in the observation of more fragment ions. Consequently, a high capillary exit voltage is expected to strip away solvent molecules to give a dominant peak for the species $[Be(acac)]^+$ but the signal corresponding to this species at *m/z* 108 remained insignificant suggesting that the acetylacetonate ligand cannot sufficiently stabilise the high charge density of Be^{2+}

cation to form an ESI-MS ion. Instead a more stable ESI-MS ion $[Be_2OH(acac)_2]^+$ *m/z* 233 is formed by the hydroxido bridging of two $[Be(acac)]^+$ species. Clearly, aggregation is beryllium's preferred response to an increase in capillary exit voltages. Figure 4-7 shows a graphical evaluation of the relative intensity of the ratio of polymeric beryllium species to monomeric species against the capillary exit voltage from the ESI-MS spectra of Be^{2+} and acetylacetone mixtures. The observed increase in polymeric species over monomeric species suggests better stability of polymeric beryllium ESI-MS ions. This could have partially originated from the instrument parameter but again it correlates well with beryllium's strong tendency to form polymeric species in solution. Also there is a reversal in the solvation preference of beryllium species across the capillary exit voltages as only water clusters are observed at higher capillary exit voltage as seen in the base peak at high capillary exit voltage is the species $[Be_3O_3(CH_3CO)(H_2O)]^+$ *m/z* 136 which additionally depicts the presence of a beryllium trimeric core. The acetylacetonate ligand forms the fragment ion $[CH_3CO]^+$ which coordinated to the trimeric beryllium oxido species.

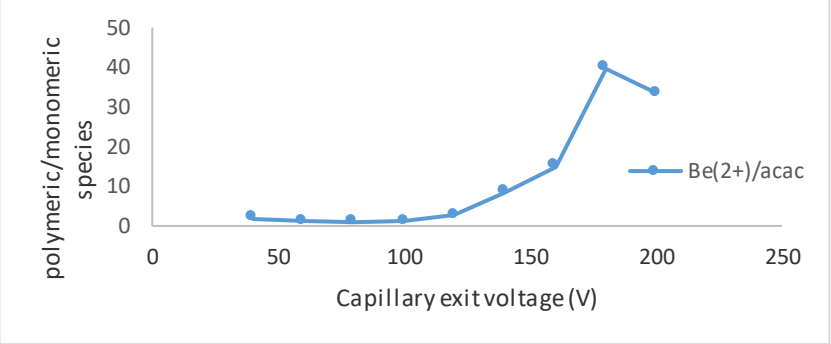

Figure 4-7 Ion abundances of polymeric and monomeric species in the ESI-MS spectra of 1:2 molar mixture of Be^{2+} and acetylacetonate L = $[CH_3COCHCOCH_3]^-$ as a function of capillary exit voltage.

4.2.3 Comparison with the ESI-MS of aluminium acetylacetonate

The ESI-MS spectra of aluminium sulfate and acetylacetonate mixtures under the same experimental conditions reveal simpler speciation in comparison with Be^{2+}. The species $[Al(acac)_2]^+$ *m/z* 225 appears as the base peak in the spectrum while the $[Al(acac)_3H]^+$ ion *m/z* 325 displayed a low intensity. Aluminium acetylacetonate appears to ionize favourably by the loss of an acetylacetonate ligand

to form a stable species $[Al(acac)_2]^+$ unlike the beryllium counterpart which showed increased stability by the addition of a bridging ligand to form polynuclear species. This may be attributable to the larger size and coordination number of aluminium. Although aluminium and beryllium have similar size to charge ratios, aluminium is a trication and prefers a coordination number of 6 thereby accommodating two bidentate monoanionic acetylacetonate to form suitable electrospray friendly species. The ESI-MS spectra of Al^{3+} and acetylacetonate mixtures do not reveal any prominent solvated species which could be an indication that the Be^{2+} cation is solvated more strongly in the gas phase than the Al^{3+}. However, a more distinct difference in the ESI-MS behaviour of these two metal cations is observed at high capillary exit voltage where several beryllium oxido species were observed (see Table 4-3) while no such species could be identified with the Al^{3+} cation although fragmentation patterns were closely related and in agreement with previously reported electron ionisation mass spectra.[19] This includes fragment species observed $[Al(acac)(CH_3COCH_2)_2]^+$ at *m/z* 183 and $[Al(CH_3COCH_2)_2]^+$ at *m/z* 141. The absence of aluminium oxido or hydroxido species suggests a lesser tendency for aluminium to hydrolyse in solution or its stronger binding with an acetylacetonate in comparison to beryllium. Noteworthy in the comparison of the ESI-MS behaviour of these two metals is that no informative peak was obtained in the negative ESI-MS spectra of Al^{3+} and acetylacetonate mixtures whereas, the ESI-MS of Be^{2+} and acetylacetonate solution gave several informative peaks assigned in Table 4-3. In particular, the negative ion mass spectra of beryllium diketonates were consistent with the observation in the positive ion mode providing support for the ion assignment and beryllium's behaviour under ESI-MS conditions. The most significant negative ESI-MS ions supportive of the beryllium speciation in Be^{2+}/Hacac mixture was the sulfate adduct of the BeL species which was observed as $[Be(acac)SO_4]^-$ at *m/z* 204.

Table 4-2 Positive ESI-MS ion data for 1:2 Be^{2+}/Hacac and Be^{2+}/Hdbm molar mixtures in 1:1 methanol-water solution (pH unadjusted).

Be^{2+}/acetylacetone (Hacac) L= $[CH_3COCHCOCH_3]^-$					Be^{2+}/dibenzoylmethane (Hdbm) L = $[C_6H_5COCHCOC_6H_5]^-$				
m/z	Positive ions	Relative ion intensity (%) with capillary exit voltage			*m/z*	Positive ions	Relative ion intensity (%) with capillary exit voltage		
		Low 40 V	Medium 80 V	High 180 V			Low 40 V	Medium 80 V	High 180 V
101	$[H_2acac]^+$	2	-	-	105	$[C_6H_5CO]^+$	-	2	95
108	$[Be(acac)]^+$	-	-	2	225	$[H_2dbm]^+$	5	-	-
126	$[Be(acac)(H_2O)]^+$	-	10	6	250	$[Be(dbm)(H_2O)]^+$	-	3	15
136	$[Be_3O_3(CH_3CO)(H_2O)]^+$	-	35	100	264	$[Be(dbm)(CH_3OH)]^+$	43	17	-
190	$[Be_3O_3(CH_3CO)(H_2O)_4]^+$	-	3	45	282	$[Be(dbm)(CH_3OH)(H_2O)]^+$	5	-	-
140	$[Be(acac)(CH_3OH)]^+$	40	10	-	296	$[Be(dbm)(CH_3OH)_2]^+$	4	-	-
158	$[Be(acac)(CH_3OH)(H_2O)_2]^+$	4	-	-	456	$[Be(dbm)_2H]^+$	100	100	35
172	$[Be(acac)(CH_3OH)_2]^+$	10	-	-	513	$[Be_2OH(dbm)(CH_3OH)]^+$	3	5	16
166	$[Be_5O_4(CH_3COCH_2)]^+$	-	25	2	687	$[Be_2(dbm)_3]^+$	15	15	50
208	$[Be(acac)_2H]^+$	75	40	6	481	$[Be_2OH(dbm)_2]^+$	-	2	13
212	$[Be_2(acac)(SO_4)]^+$	-	-	3	712	$[Be_3O(dbm)_3]^+$	-	-	5
233	$[Be_2OH(acac)_2]^+$	-	6	40	792	$[Be_3(dbm)_3SO_4]^+$	1	3	20
315	$[Be_2(acac)_3]^+$	100	100	25	260	$[Be_5O_4(C_6H_5COCH_2)(CH_3OH)]^+$	-	40	100
340	$[Be_3(acac)_3O]^+$	-	2	6					
420	$[Be_3(acac)_3SO_4]^+$	-	2	2					
445	$[Be_3(acac)_3(SO_4)BeO]^+$	-	2	2					
461	$[Be_4O(OH)(HSO_4)_2(acac)_2]^+$	-	2	-					

Table 4-3 Assignment of ions observed in the negative ESI-MS of 1:2 Be^{2+}/Hacac and 1:2 Be^{2+}/Hdbm mixture

Negative ions	Be^{2+}/acetylacetone (Hacac) L= $[CH_3COCHCOCH_3]^-$	Be^{2+}/dibenzoylmethane (Hdbm) L=$[C_6H_5COCHCOC_6H_5]^-$
	Experimental *m/z*	Experimental *m/z*
$[HSO_4]^-$	96.9962	96.9951
$[L]^-$	98.9898	223.1445
$[BeOHSO_4]^-$	122.0092	-
$[BeO(L)]^-$	123.9663	247.9130
$[BeSO_4(L)]^-$	204.0738	328.1340
$[BeSO_4(L)(H_2O)]^-$	222.0888	346.1488
$[BeSO_4(L)(CH_3OH)]^-$	236.1081	360.1683
$[Be(HSO_4)_2(L)]^-$	302.0645	-
$[Be_2(L)(SO_4)_2]^-$	309.0553	433.1243
$[Be_3(L)_3(SO_4)_2]^-$	516.2120	-
Unidentified	194.9893	-

4.2.4 ESI-MS of Be^{2+} and other 1,3-diketonates

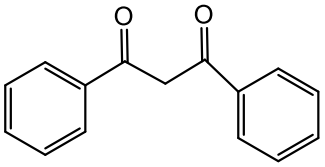

Dibenzoylmethane (Hdbm)

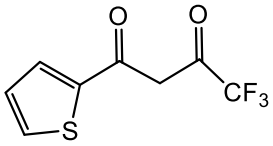

Thenoyl trifluoroacetylacetone (Htta)

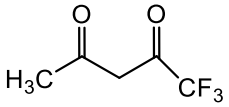

Trifluoroacetylacetone (Htfac)

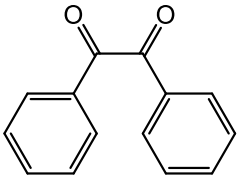

Benzil

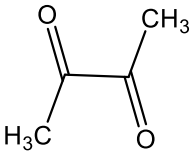

Diacetyl

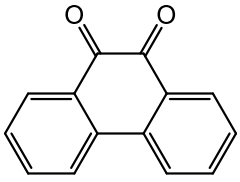

Phenanthrenequinone

The ESI-MS spectra of the mixtures of Be^{2+} and other 1,3-diketones are shown in Figure 4-8. The major peaks observed are the set of three major species $[Be(L)(CH_3OH)]^+$, $[Be(L)_2H]^+$, $[Be_2(L)_3]^+$ (L=dbm, tta, and tfac) but with a remarkable difference in their dominance. While the ESI-MS spectra of beryllium and the bulkier dibenzoylmethane (see Figure 4-8a) reveals the base peak as $[Be(dbm)_2H]^+$ *m/z* 456 the other diketones revealed a prominent abundance of the $[BeL]^+$ ion. In addition, the acetylacetonate (which is a less bulkier diketone), tends to aggregate more easily in the gas phase. For instance, the polynuclear species $[Be_2L_3]^+$ is observed as the base peak in the ESI-MS of Be^{2+}/Hacac at 80 V but with the Be^{2+}/Hdbm under the same conditions, the corresponding species is observed at 15% intensity.

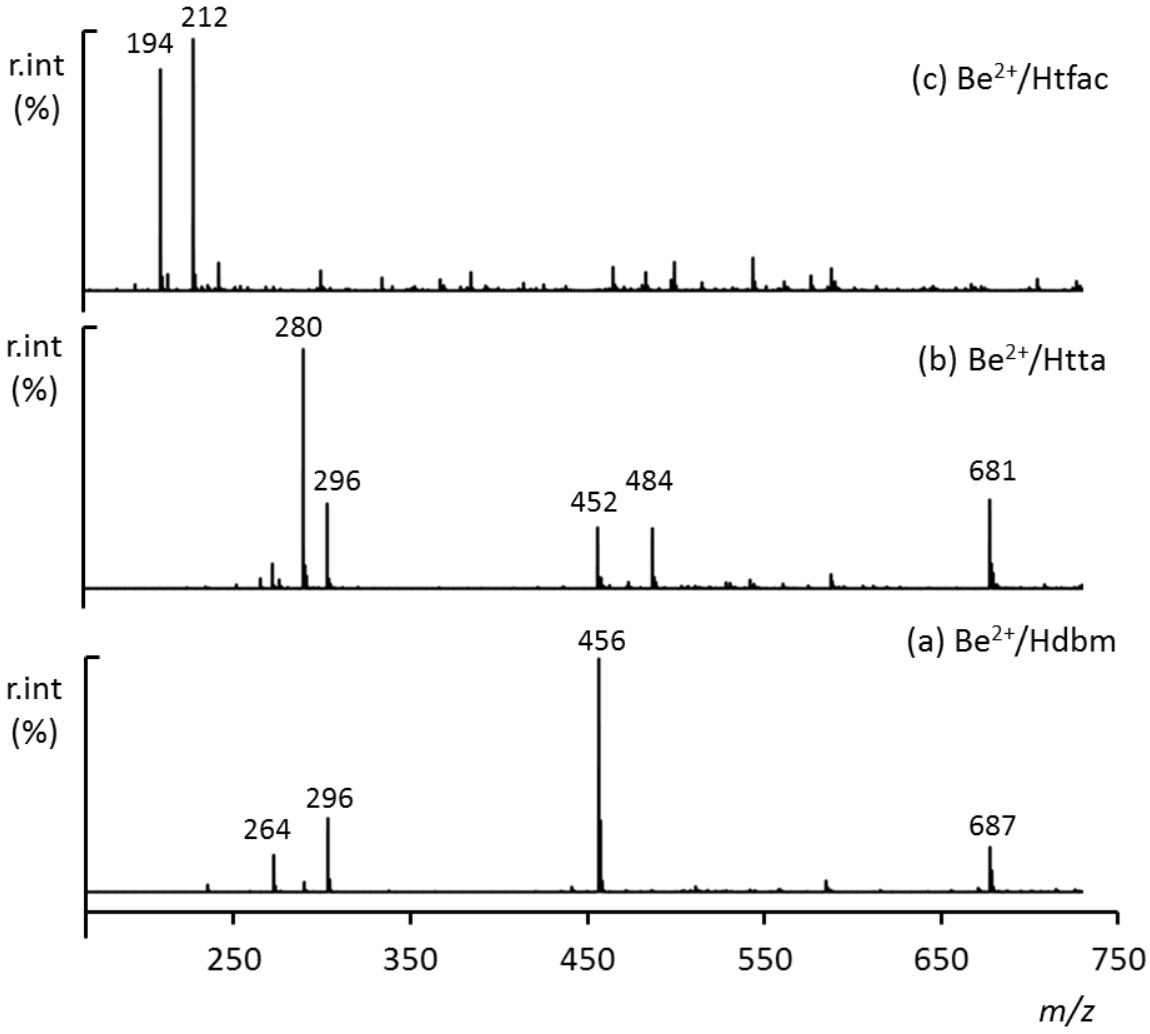

Figure 4-8 Positive-ion ESI mass spectra for 1:2 molar mixtures of beryllium sulfate and (a) dibenzoylmethane (Hdbm) (b) thenoyl trifluoroacetylacetone (Htta) and (c) trifluoroacetylacetone (Htfac) in 1:1 methanol-water solution at capillary exit voltage 100 V.

This is further illustrated in Figure 4-9 which reveals a less rapid increase in the abundance of polymeric beryllium species in the ESI-MS of beryllium sulfate solution with acetylacetonate and dibenzoylmethanate ligands respectively. This points out that under harsher ESI-MS conditions, the bis(dibenzoylmethanato) beryllium complex tends to be more stable to fragmentation and also resisted the polymerisation of beryllium better.

(a)

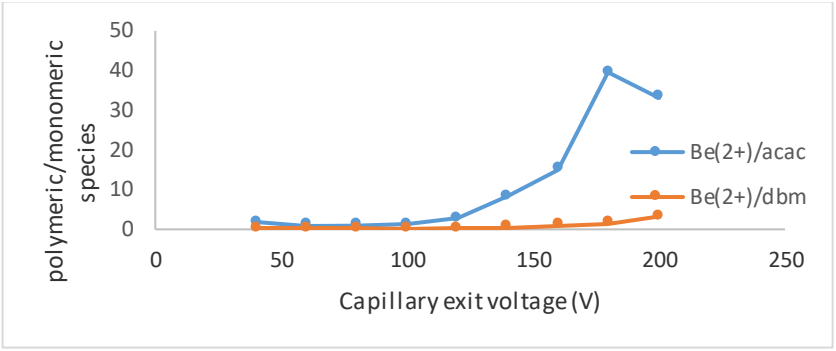

(b)

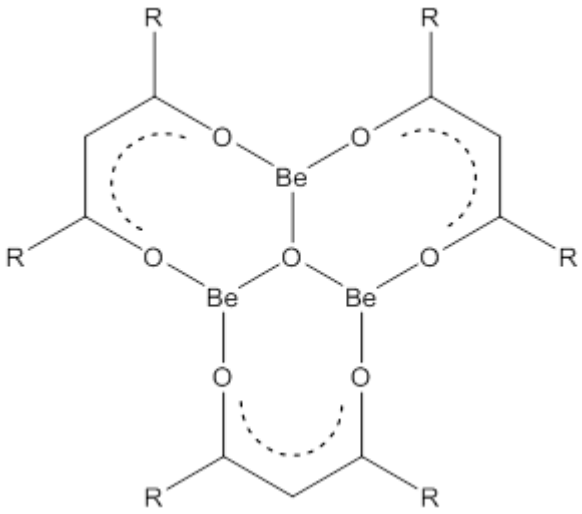

Figure 4-9 (a) Ion abundances of polymeric and monomeric species in the ESI-MS spectra of 1:2 molar mixture of Be^{2+}/acac and Be^{2+}/dbm as a function of capillary exit voltage. (b) Proposed structural arrangement of the $[Be_3(L)_3O]^+$ ion observed in the ESI-MS of 1:2 molar mixture of Be^{2+} and 1,3-diketonate ligands at high CEV (>120 V)

However, the spectra of Be^{2+} and all 1,3-diketones in this study (except Htfac) suggest the presence of a beryllium trimer which was observed as $[Be_3(L)_3SO_4]^+$ and $[Be_3(L)_3O]^+$ (where L= acac, dbm, tta). This is likely formed from the diketonate ligands substituting each bridging hydroxido ligand from the $[Be_3(OH)_3]^{3+}$ species in solution. From the abundance of these ions, it appears the ESI-MS ion $[Be_3(L)_3O]^+$ is the more stable species compared to the $[Be_3(L)_3SO_4]^+$

ion. This is probably because in the former, the oxido group occupies a central bridging position to three metal centres in forming the well-known trimer and planar structural arrangement analogous to the basic beryllium acetate (see Figure 4-9). This structure has also been proposed with other monoanionic ligand such as the nitrate,[17] monocarboxylates[15] and the sulfate anions.[14]

ESI-MS spectra of Be^{2+} and the partially fluorinated 1,3-diketonates (CF_3COCH_2COR where R=methyl or thenoyl groups) are shown in Figure 4-8b-c while a collection of the ion assignment is presented in Table 4-4. Again the spectra employing the more robust thenoyltrifluoroacetyacetonate ligand show a better interaction with beryllium observable in the $[Be(tta)_2H]^+$ ion signal at *m/z* 452 which is almost absent with the trifluoroacetylacetonate. The absence of the species $[Be_2(tfac)_3]^+$ and a low intensity ion signal corresponding to the $[Be(tfac)_2H]^+$ species in the ESI-MS spectra of Be^{2+} and the trifluoroacetylacetonate (Figure 4-8c) tends to suggest it has the weakest interaction with beryllium in this study most likely due to the electron withdrawing effect of the fluorides reflecting the acidity of the different ligands since the pH was not strictly controlled. This is further supported by the even poorer interaction of the Be^{2+} and hexafluoroacetylacetone (Hhfac) which did not reveal either the $[Be(hfac)CH_3OH]^+$ or $[Be(hfac)_2H]^+$ species in the mass spectra. In addition, the fluorinated 1,3-diketonate metal complexes of beryllium and aluminium are known to be very volatile and readily fragmented in the gas phase by the loss of a CF_2 group and migration of a fluorine to the metal.[18, 40] While the mechanism involved in the fragmentation and rearrangement reactions among the beryllium diketonates is an area of fruitful mass spectrometric research (especially employing the electron ionisation mass spectrometry), its lies outside the interest of this thesis. However, it is worth pointing out that as an additional advantage of the ESI-MS technique is its ability to impact a much more controlled energy on the ions in the gas phase for related fragmentation and mechanistic studies. In addition, ions observed in the ESI mass spectra of beryllium sulfate and the fluorinated diketonates (especially at high capillary exit voltages) were consistent with the previously proposed fragmentation pathway.

Table 4-4 Ion assignments for 1:2 molar mixture of beryllium sulfate and diketone ligands (L= tta, tfac and benzil)

Ion Assignment	Be^{2+}/Htta Experimental *m/z*	Be^{2+}/Htfac Experimental *m/z*	Ion Assignment	Be^{2+}/Benzil Experimental *m/z*
$[Be(L)BeO]^+$	255.0813	-	$[L+Na]^+$	233.0649
$[Be(L)(CH_3OH)]^+$	262.0631	194.0672	$[L+H]^+$	211.0817
$[Be(L)(H_2O)]^+$	266.0610	-	$[L+K]^+$	249.0389
$[Be(L)(CH_3OH)(H_2O)]^+$	280.0821	212.0798	$[2L+Na]^+$	443.1392
$[Be(L)(CH_3OH)_2]^+$	294.0972	226.1208	$[2L+H]^+$	421.1818
$[Be(L)_2H]^+$	452.0639	316.0725	$[2L+K]^+$	459.1133
$[Be(L)_2CH_3OH]^+$	484.0863	-	$[BeL_2]^{2+}$	214.5824
$[Be_2(L)_3]^+$	681.0732	-	$[BeL_3]^{2+}$	319.6180
$[C_4H_3SCO]^+$	111.0190	-	$[BeL_4]^{2+}$	427.1178
$[BeF(L\text{-}CF_3)]^+$	180.0417	112.0168	$[BeLCH_3OH]^{2+}$	141.5714
$[BeL(C_4H_3SCOCHCO)]^+$	382.0534	246.0758	$[Be_2LSO_4]^+$	146.0706
$[Be_2OH(L)_2]^+$	477.0769	341.1188		
$[Be_3(L)_3O]^+$	706.0944	-		
$[Be_3(L)_3SO_4]^+$	786.0583	-		

Other diketonate ligands such as the 1,2-diketones except benzil showed poor interactions with beryllium since they essentially involve neutral oxygen donors and five-membered chelate rings. Thus the ESI-MS screening of the Be^{2+} cation with diacetyl, and phenanthrenequinone revealed only signals attributed to the potassium adduct $[L+K]^+$ and a lesser signal due to the $[L+Na]^+$ ion despite the fact that the solutions were spiked with sodium ion illustrating these ligands' preference for large cations. However, benzil showed good interaction with Be^{2+} in solution as revealed in the spectra of a 1:2 mole ratio mixture of beryllium sulfate and benzil at capillary exit voltages of 60 and 120 V (see Figure 4-10). Since benzil is a neutral diketone and unable to reduce the charge of the beryllium ion in the gas phase (due to the lack of a readily acidic proton), the multiply charged complex formed was therefore expected to be charge reduced by the coordination of the sulfato anion or deprotonation of a coordinated solvent ligand to form hydroxido or methoxido species. This was observed in ESI-MS ions such as $[BeLCH_3OH]^{2+}$ *m/z* 141.5 and $[Be_2LSO_4]^{2+}$ *m/z* 146 but at low intensities (<15%). On the other hand, the ESI-MS spectra of Be^{2+}/benzil mixtures revealed a series of beryllium

complexes $[BeL_n]^{2+}$ for n = 2-4 at *m/z* 214.5, 319.6 and 427.0 respectively. As a result of the double charge on these ions, the spectra revealed a significant isotopic pattern which was in good agreement with theoretically calculated *m/z* value and isotope patterns. This observed ability of the benzil ligand to exclude the solvent and counter ions (which have been shown to bind to beryllium quite strongly) suggests a favourable complexation of the Be^{2+} which can be related to the unique structural difference between the benzil ligand and 1,2-diketones such as diacetyl and phenanthrenequinone. Unlike diacetyl and phenanthrenequinone which are essentially planar with the oxygen donors unsuitably positioned for chelating the tetrahedral beryllium cation, structural investigations of the benzil ligand have pointed out a relatively long carbon-carbon bond length between the keto groups.[41] Furthermore, its predominant structural conformation in which the O=C-C=O torsion angle is 116.9° and the benzoyl substituent are twisted with respect to each other reduces steric crowding while providing a near perfect fit for the Be^{2+} cation.[41] Nevertheless, it is more likely that at least one of the benzil ligands is coordinated to the beryllium ion in a monodentate fashion indicated from the observation of an intense ion signal due to $[BeL_3]^{2+}$ at *m/z* 319.6. Meanwhile, at higher capillary exit voltages, the spectrum is considerably simplified such that the ion $[BeL_2]^{2+}$ at *m/z* 214.5 becomes the only prominent peak in the spectrum. This stabilization of such a highly charged Be^{2+} metal centre in the presence of suitable charge-reducing ions such as OH^- and SO_4^{2-} is often rare and could be of practical application in preserving highly charged beryllium solution species and transferring into the gas phase. However, this ligand has poor selectivity for beryllium in the presence of larger alkali metal ions due to the significant abundance of ion signals corresponding to the $[L+K]^+$ and $[2L+K]^+$ at *m/z* 249 and 459 respectively.

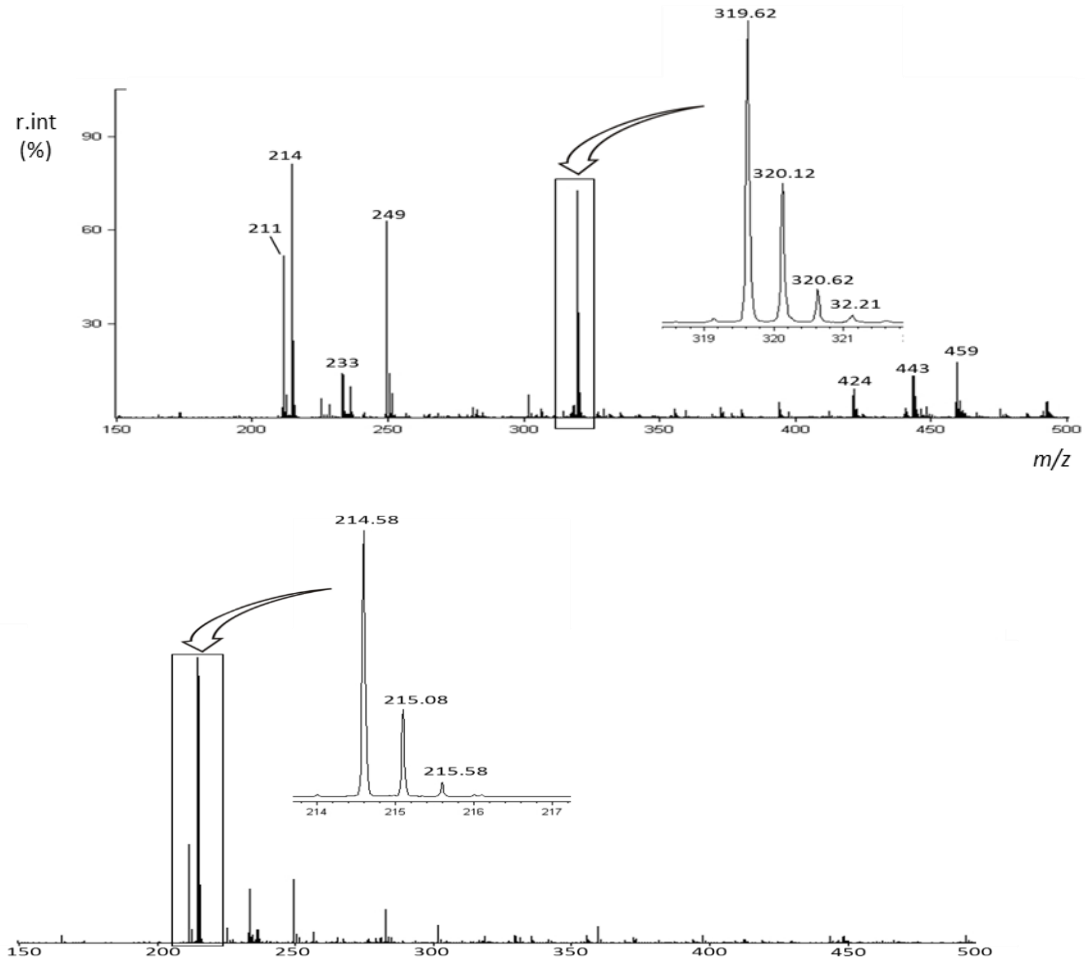

Figure 4-10 Positive ion ESI-MS of Be^{2+} and benzil (HL) in 1:1 methanol-water solution at two different capillary exit voltages. While the $[BeL_4]^{2+}$ ion at *m/z* 319.6 is the base peak at CEV of 60 V (top), the $[BeL_2]^{2+}$ ion at *m/z* 214.5 emerges as the base peak with at a higher voltage of 120 V (bottom). Inset are the isotope pattern confirming the dicationic nature of the ions.

4.2.5 ESI-MS of Be^{2+} and hydroxy keto ligands and other keto ligands

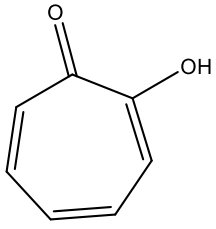

Tropolone (Htrop)

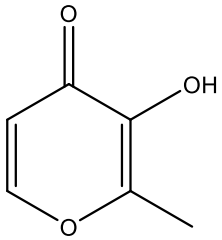

Maltol (Hmal)

The tropolone ligand and its corresponding tropolonate anion reveal a system very similar to the 1,3-diketonates and therefore yield closely related ESI-MS ionisation trends although subtle differences could be identified. Figure 4-11

displays the ESI-MS spectrum of a 1:2 molar mixture of Be^{2+} and tropolone in 1:1 methanol/water solution (without adjusting the pH). The spectrum shows that there were prominent ions at *m/z* 123, 252 and 381 corresponding to the ions $[H_2trop]^+$, $[Be(trop)CH_3OH]^+$, $[Be(trop)_2H]^+$ with relative abundances of 40%, 100% and 95% respectively (see Table 4-5). On comparing the ESI-MS behaviour of these beryllium complexes observed in the ESI-MS spectra of Be^{2+}/Htrop mixtures with that of the Be^{2+}/diketone mixtures, a few important differences are seen to exist. These differences include a relatively higher intensity of the dinuclear complex $[Be_2(trop)_3]^+$ as well as the free ligand $[H_2trop]^+$, which suggests that the tropolonate is more apt at forming oligomeric bridges due to the formation of five-membered chelate rings.

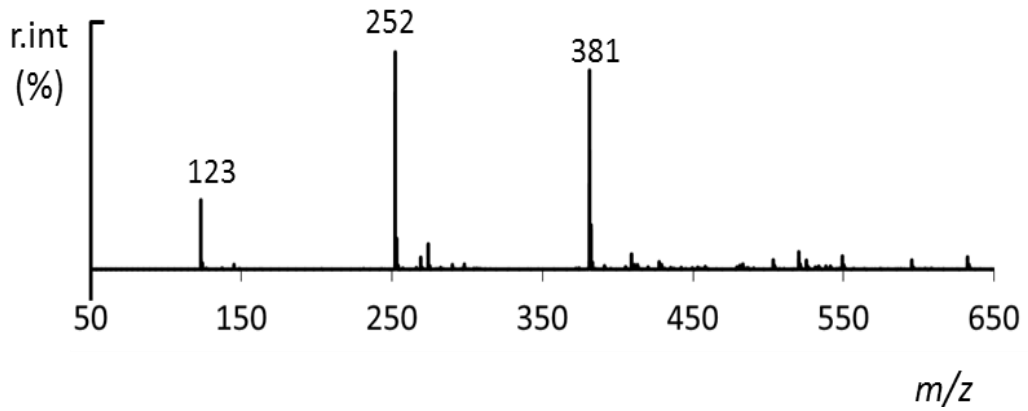

Figure 4-11 Positive ESI-MS mass spectrum for 1:2 molar mixture of beryllium sulfate and tropolone in 1:1 methanol-water solution at capillary exit voltage 100 V. (pH was not adjusted)

With the maltol ligand, ESI-MS behaviour of the resultant beryllium complexes also tends to be relatively straightforward. The major signal observed in the positive ESI mass spectra of a 1:2 mixture of beryllium sulfate and this ligand occurred at *m/z* 127, 166 and 260 due to the ions $[H_2mal]^+$, $[Be(mal)CH_3OH]^+$, and $[Be(mal)_2H]^+$ as observed in Figure 4-12a. This is similar to the ESI-MS behaviour of beryllium mixtures with monoanionic ligands as revealed in previous sections, except for the notable absence of a corresponding signal due to the $[Be_2L_3]^+$ ion. Further comparison to the ESI-MS behaviour of the Be^{2+}/diketones at higher capillary exit voltages shows that the $[BeL_2H]^+$ ion of L=maltol is considerably more stable toward dissociation and ligand fragmentation in the gas phase than any of the diketonates which is likely due to the more rigid and robust pyrone heterocyclic ring.

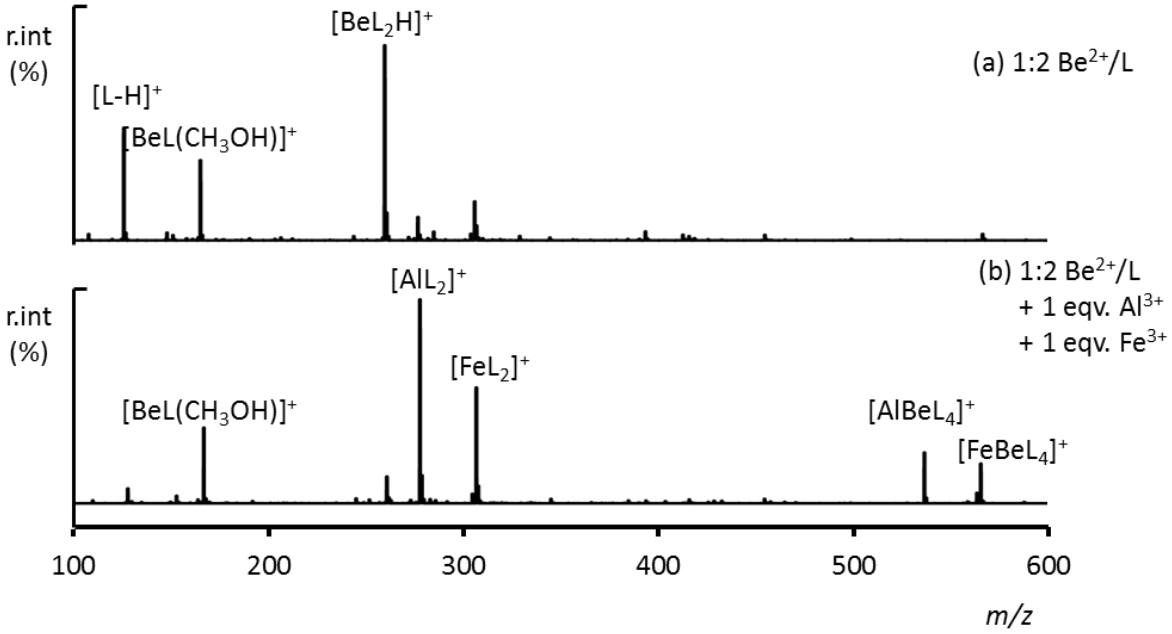

Figure 4-12 Positive ion ESI mass spectra for (a) 1:2 mole mixtures of beryllium sulfate and maltol (b) 1:2 mole mixtures of beryllium sulfate and maltol with Al^{3+} and Fe^{3+} added in 1:1 methanol-water solution at capillary exit voltage of 100 V. (pH was not adjusted)

A major feature of ligands containing the hydroxyl and keto functional groups is their affinity for the Al^{3+} and Fe^{3+} cations such that they are popularly employed as chelating ligands in the treatment of metal ion overload.[42] In agreement with this, Figure 4-12a displays low intensity ion signals at *m/z* 277 and *m/z* 303.9 which were assigned to $[Al(mal)_2]^+$ and $[Fe(mal)_2]^+$ respectively indicating the ligand's propensity to complex adventitious Al^{3+} and Fe^{3+} cations in the ion source (arising from other ESI-MS usage or Fe^{3+} from the stainless steel capillary which has been observed before). To further examine the selectivity of maltol for the Be^{2+} cation in the presence of Al^{3+} and Fe^{3+} by the ESI-MS technique, the spectra of a 1 mole equivalent of each of Al^{3+}, Fe^{3+} was added to a well-equilibrated 1:2 mole mixture of Be^{2+} and maltol and the ESI mass spectrum was also recorded. The general ESI-MS features for this ternary system are illustrated in Figure 4-12b. Firstly the addition of Al^{3+} and Fe^{3+} cations clearly disrupts the complexation of beryllium by maltol which is well indicated by the huge decline in the $[Be(mal)_2H]^+$ ion intensity. However, more important is the change in the base peak to the $[Al(mal)_2]^+$ ion suggesting the order of maltol binding to the three cations as Al^{3+}> Fe^{3+}> Be^{2+}. Also, mixed metal complexes were observed at *m/z* 536 and 565 due to the $[AlBe(mal)_4]^+$ and $[FeBe(mal)_4]^+$ species.

Table 4-5 Summary of ions observed in the ESI-MS spectra of Be^{2+}/Hmal and Be^{2+}/Htrop with interfering metal ions (Al^{3+} and Fe^{3+})

Type of species	Positive ions	Experimental *m/z*	
		Be^{2+}/Hmal	Be^{2+}/Htrop
Free ligand	$[LH]^+$	127.0376	123.0454
	$[2LH]^+$	253.0809	-
	$[LNa]^+$	149.0150	-
Beryllium complexes	$[BeLCH_3OH]^+$	166.0556	-
	$[BeL_2H]^+$	260.0617	252.0739
	$[Be_2L_3]^+$	-	381.3035
	$[AlBeL_4]^+$	536.0318	520.1218
Complexes of	$[FeBeL_4]^+$	565.0493	549.3006
interfering cations	$[AlL_2]^+$	277.0231	-
	$[AlL_3H]^+$	403.0537	-
	$[FeL_3H]^+$	432.0063	-

4.2.6 ESI-MS of Be^{2+} and dicarboxylate/dihydroxyl ligands

The hard oxygen donors of the carboxylate and hydroxyl functional groups alongside the formation of six-membered chelate ring in beryllium complex make ligands such as malonate and chromotropate very good chelating agents for beryllium. In addition, these ligands alongside their beryllium complexes are best detected in the negative ion mode due to the easily deprotonated groups. Negative ion ESI-MS of 1:2 beryllium sulfate and malonic acid and 1:2 beryllium sulfate and chromotropic acid mixtures in aqueous solution at pH 6.5 are shown in Figure 4-13. Generally, both spectra reveal the free ligand as the base peak alongside an overall low intensity due to the poor ion transmission in the negative ESI-MS mode as a result of the electrical (corona) discharge phenomena in negative ion operation (especially with aqueous solutions).[43] However, ions in these spectra indicate the presence of dinuclear beryllium complexes with chromotropate ligands which includes the ions due to $[Be_2O(L\text{-}4H)]^{2-}$ and $[Be_2SO_4(L\text{-}4H)]^{2-}$ at *m/z* 174.9 and 214.9 in addition to the free ligand $[L\text{-}2H]^{2-}$ observed at *m/z* 158.9. In contrast, the spectrum of 1:2 beryllium sulfate and malonate mainly revealed mononuclear beryllium complexes which included the ions; $[BeOH(L\text{-}2H)(H_2O)]^-$ *m/z* 146, $[BeOH(L\text{-}2H)]^-$ *m/z* 128, $[Be(L\text{-}H)(L\text{-}2H)(H_2O)]^-$ *m/z* 232, and $[BeHSO_4(L\text{-}2H)]^-$

m/z 232. While the protonation state of these ions in solution at equilibrium may differ and will highly depend on the solution pH, the stoichiometric information of these species is certainly in agreement with potentiometric species distribution of the 1:2 beryllium sulfate-malonate system which indicated the dominance of the BeL and $[BeL_2]^{2-}$ species between pH 2-6.[24]

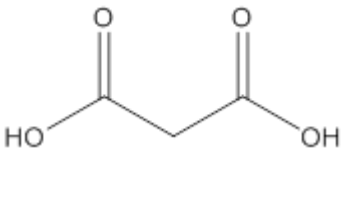

Malonic acid

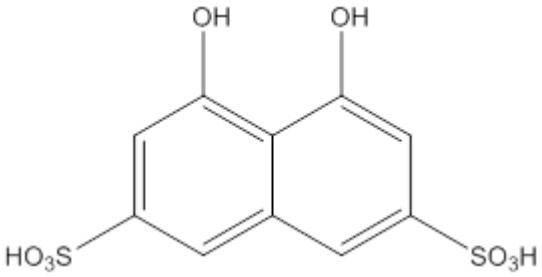

Chromotropic acid

Although no studies have confirmed the structure of beryllium complexes with chromotropate, the ligand has been widely investigated as a fluorogenic chelator for beryllium in aqueous solutions.[44] The ions observed in the mass spectra suggests a dinuclear beryllium complex but this could be as a result of the gas phase interaction of the Be^{2+} cation with the sulfonate substituent groups.

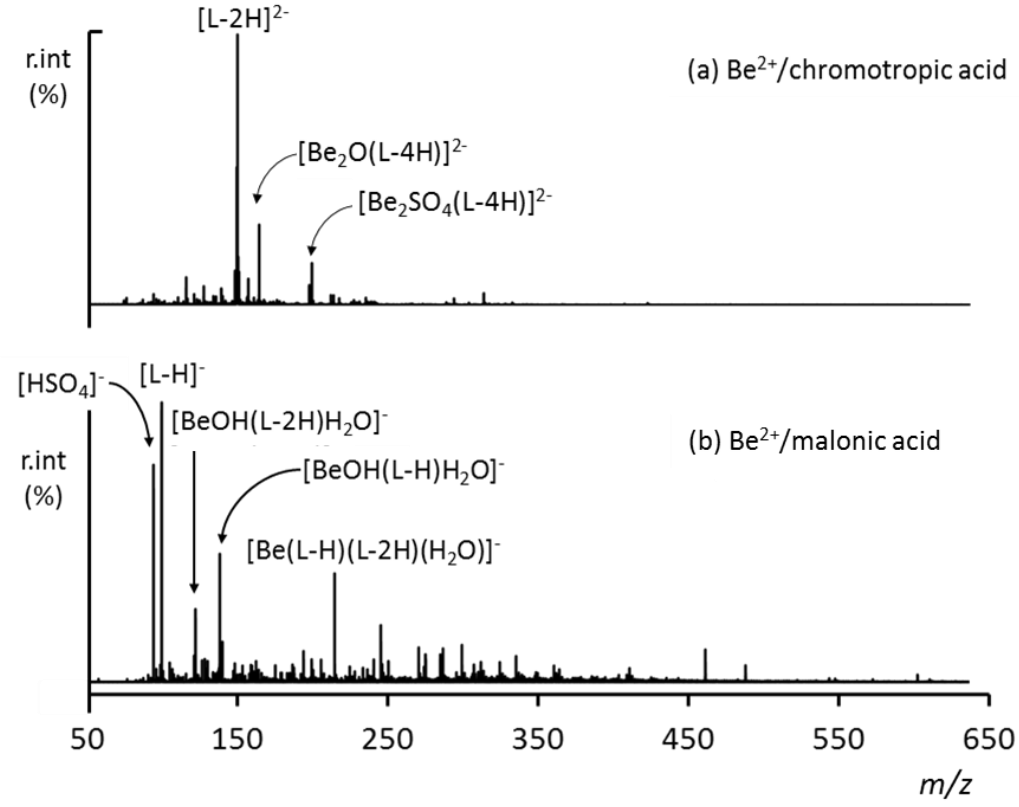

Figure 4-13 Negative ion ESI mass spectra of (a) 1:1 Be^{2+} and chromotropic acid and (b) 1:2 Be^{2+} and malonic acid at a capillary exit voltage of 80 V and pH adjusted to 6.5 using sodium hydroxide.

4.2.7 ESI-MS of Be^{2+} and *N,O* donor bidentate chelating ligands

The tendency of beryllium to form complexes with *N,O* donor ligands of suitable geometry such as the picolinate and salicylamide ligands is well known.[22, 45] On the other hand, *N,O* donor ligands such as 8-hydroxyquinoline are also of great significance as they show greater affinity for Al^{3+} in comparison to the Be^{2+} cation.[46] Therefore, they are employed in analytical procedure to separate other ions from the beryllium cation before sampling.[46] This was also illustrated in an ESI-MS experiment of Al^{3+} and 8-hydroxyquinoline in methanol solution which revealed very intense signal for the ions corresponding to $[AlL_2]^+$ at *m/z* 315 whereas a similar experiment using Be^{2+} and 8-hydroxyquinoline showed no ion signal attributable to complexation with the Be^{2+} cation.

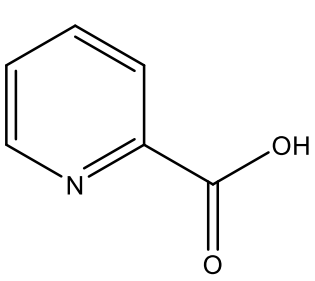

Picolinic acid

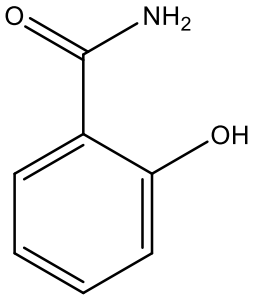

Salicylamide

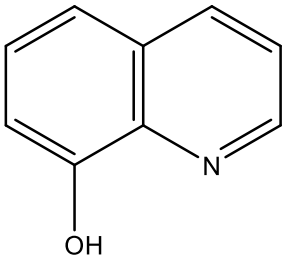

8-Hydroxyquinoline

The ESI-MS of Be^{2+} and the monoanionic salicylamide and picolinate behaved broadly the same way as the other monoanionic ligands mainly because, as has been pointed out earlier, the charge of the preexisting species in solution is a strong determinant of the behavior of the ESI ions. However, it is worthy of note that the salicylamide ligand is capable of *O,O* as well as *N,O* chelation to beryllium although *N,O* chelation has been structurally elucidated in a BeL_2 complex.[22] While the preferred binding mode cannot be distinguished by mass spectrometry, existence of the beryllium complex can certainly be discovered by the ESI-MS technique. Illustrative positive ion spectra pointed out that these ligands complexed the Be^{2+} cation strongly enough to suppress hydrolysis and formed species of the type $[BeL]^+$ and $[BeL_2]$. Nonetheless, this feature is less probable for picolinate

which showed the presence of the trimeric beryllium core in a species such as $[Be_3(OH)_3(L\text{-}H)_2]^+$ observed at *m/z* 322 (see Figure 4-14b). This correlates very well with the $[Be_3(OH)_3L_3]$ beryllium hydroxido picolinate complex which interestingly was the first complex for which an X-ray structure of the cyclic nature of the beryllium trimer was structurally confirmed.[45]

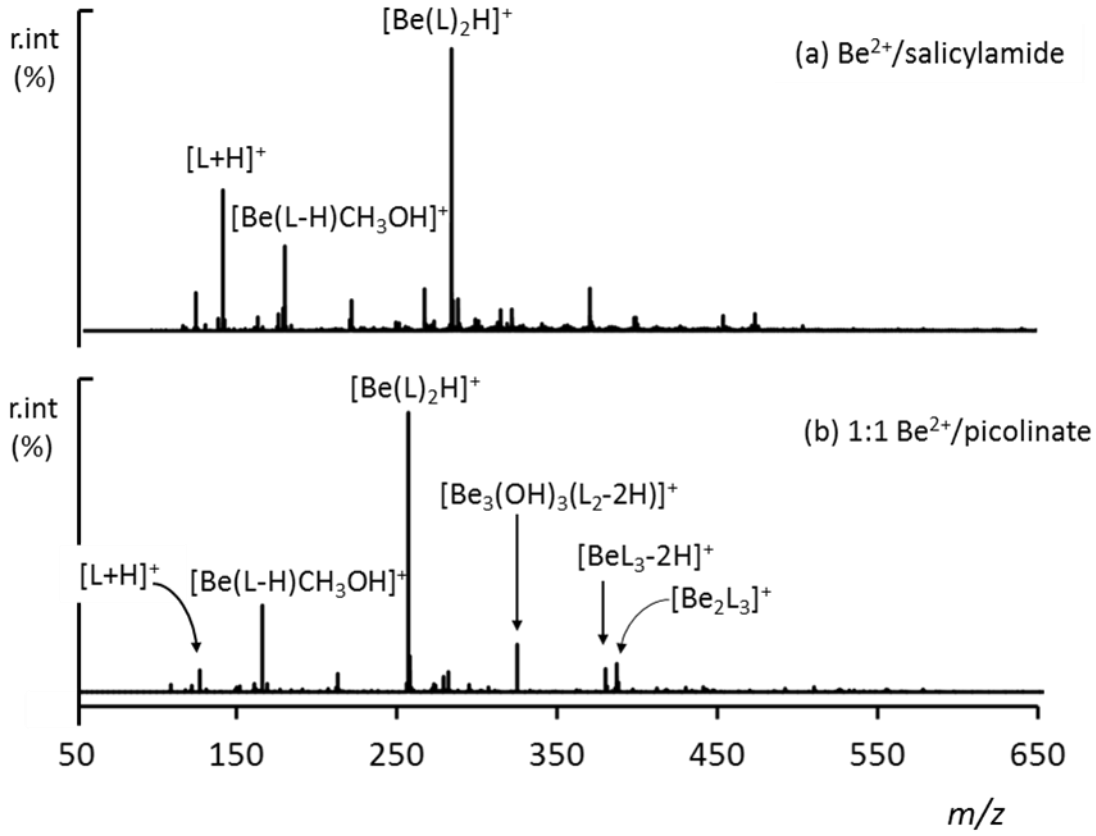

Figure 4-14 Positive ion ESI-MS of (a) 1:2 Be^{2+} and salicylamide (pH unadjusted) (b) 1:2 Be^{2+} and picolinate (pH adjusted to 5.7) in 1:1 methanol-water solution at capillary exit voltage of 80 V.

4.2.8 ESI-MS of Be^{2+} and citrate

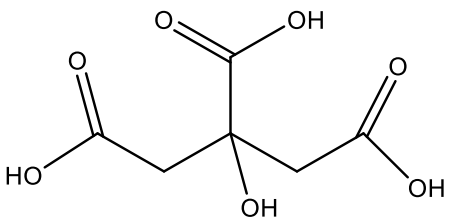

Citric acid

Hydroxycarboxylate ligands such as citrate are crucial ligands which model a strong beryllium binding motif *via* strong hydrogen bonding suspected to be

present in hydroxyl-bearing proteins and other biomolecules.[47, 48] Despite the excellent binding of beryllium by citrate, the coordination of beryllium citrate is rather poorly defined. To date, the only beryllium citrate structure obtained by X-ray crystallography is a beryllium aluminium citrate complex which reveals that the alcohol functional group of the citrate is involved in beryllium coordination and is in fact capable of bridging several metal centres.[49] The present interest in expounding beryllium interaction with ligands using the ESI-MS technique led to the investigation of beryllium citrate speciation in aqueous solutions noting that elsewhere, the ESI-MS technique has provided invaluable supportive as well as additional data for the complicated interactions of citrate with other highly charged ions including Fe^{3+} and Al^{3+}.[4, 50-52] Since the beryllium citrate complexes in solution are mainly anionic, the negative ion ESI-MS was the most appropriate mode to record the mass spectra of the species in solution. However, it is worth pointing out that because the negative ion mode is not the better ionisation mode of the ESI-MS for purely aqueous solutions, highly charged species will certainly be protonated during the electrospray process hence interpretation and correlation of ESI-MS results to previous reports will best be limited to stoichiometric compositions of species in solution.

Table 4-6 Ion assignment of species observed in the ESI-MS of Be^{2+} and citric acid (L) in solution at pH 6.7.

m/z	Ion Assignments	*m/z*	Ion Assignments
214.0010	$[Be_4O(L\text{-}4H)_2]^-$	111.04	$[Be_2O(L\text{-}4H)]^{2-}$
201.5211	$[Be_3(L\text{-}4H)_2]^{2-}$	129.06	$[Be_2O(L\text{-}4H)(H_2O)]^2$
302.9352	$[Be_2HSO_4(L\text{-}3H)]^{2-}$,	223.02	$[Be_2HSO_4(L\text{-}3H)]^{2-}$
335.0056	$[Be_2HSO_4(L\text{-}3H)CH_3OH]^{2-}$	198.01	$[Be(L\text{-}3H)]^-$

Illustrative ESI mass spectra of a 2:1 Be^{2+} and citrate solution recorded at CEV 80 V and pH 6.7 is displayed in Figure 4-15 and a summary of the assigned ions recorded in Table 4-6. Negative ion ESI mass spectra of Be^{2+}/citrate showed major peaks corresponding to the free ligand $[L\text{-}H]^-$ at *m/z* 191 and the species $[Be_2O(L\text{-}4H)]^{2-}$ at *m/z* 111.04. This is due to the fact that the envisaged dominant species in beryllium citrate solution is a neutral 2:1 Be_2L complex which would be poorly ionized. However, the signal of intensity 90% which was observed at *m/z* 111.04 due to $[Be_2O(L\text{-}4H)]^{2-}$ clearly supports the dinuclear beryllium complex

with citrate. Other signals corresponding to the Be_2L species in solution were observed at *m/z* 129, 302.9, 223 and 335 corresponding to $[Be_2O(L\text{-}4H)(H_2O)]^{2-}$, $[Be_2OH(L\text{-}4H)_2]^{-}$, $[Be_2HSO_4(L\text{-}3H)]^{2-}$, $[Be_2HSO_4(L\text{-}3H)CH_3OH]^{2-}$. Therefore ESI-MS supports earlier data on the speciation of the Be^{2+} cation with citrate. Furthermore, additional species observed at *m/z* 198, 214 and 201.5 which were assigned as $[Be(L\text{-}3H)]^{-}$, $[Be_4O(L\text{-}4H)_2]^{2-}$, $[Be_3(L\text{-}4H)]^{2-}$ respectively have pointed out the existence of other mononuclear and polynuclear species in solution. In summary, ESI-MS data tend to suggest that the speciation of beryllium citrate in solution is more complicated than the present picture of a 2:1 Be_2L complex.

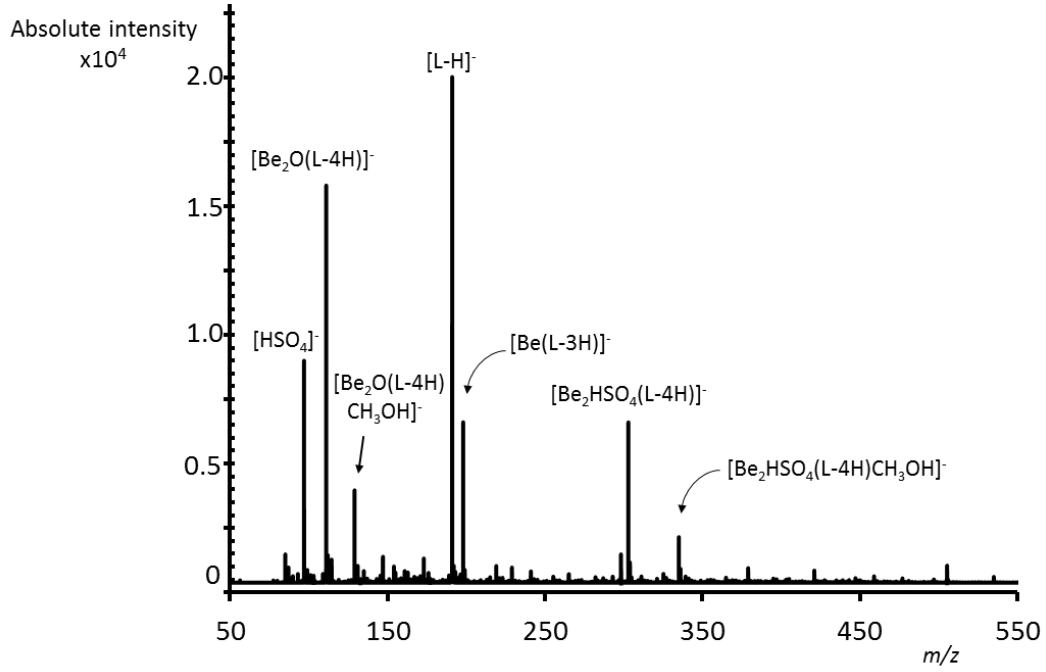

Figure 4-15 Positive ion ESI-MS of Be^{2+} and citric acid in 1:1 methanol-water solution at capillary exit voltage of 80 V and pH 6.7.

4.2.9 ESI-MS of Be^{2+} and crown ether and cryptand ligands

The crown ether complexes of beryllium have been elaborately characterized in the solid state and the X-ray structures of beryllium complexes with 12-crown-4, 15-crown-5 and 18-crown-6 have all been reported.[16, 32, 53] Ironically, corresponding solution-based speciation of beryllium complexation by crown ethers have never been explored either by ESI-MS or any solution based technique. Although ion extraction studies with the benzo-9-crown-3 ligand and its naphthalene derivative reveal good complex formation with beryllium to the extent that the benzo-9-crown-3 is a component of a beryllium selective membrane

electrode.[54] In contrast, a considerable number of studies has used the ESI-MS technique to explore the interactions of crown ethers with the neighbouring alkali, alkaline earth and other divalent metal ions supporting the correlation between the size of the cation and the effective radius of the cavity of the crown ether. Therefore, the mixtures of Be^{2+} and crown ether ligands were re-examined in aqueous solution to identify the representative species occurring in solution as well as the potential of the crown ethers as beryllium chelators (see Chart 4-1). Closely related to the crown ethers are the cryptand ligands such as the cryptand[2.2.2] which possess a larger cavity size and as a result tend to complex oxido/hydroxide-bridged metal centres.[42]

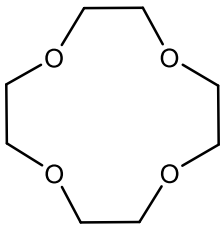

12-crown-4 [12C4]

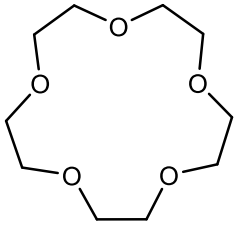

15-crown-5 [15C5]

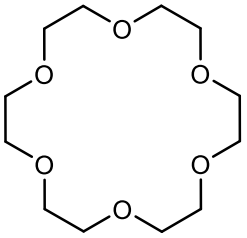

18-crown-6 [18C6]

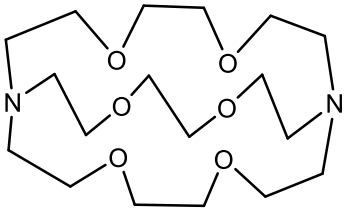

Cryptand[2.2.2]

Chart 4-1 Macrocyclic ligands investigated for beryllium complexation using ESI-MS

The positive ion ESI-MS of 12-crown-4, 15-crown-5 and 18-crown-6 and cryptand[2.2.2] in 1:1 methanol-water phase ran as a blank test revealed expected peaks corresponding to H^+, Na^+, or K^+ adducts depending on the availability of the alkali metal in solution and most importantly the cavity size of the ligands. The ESI-MS data and behaviour of the crown ether and cryptand ligands and their binding selectivity trend with the alkali metal have been described elsewhere.[2] ESI mass spectra observed upon addition of $BeCl_2$ are shown in Figure 4-16 while the corresponding ion assignments are given in Table 4-7. It is worth pointing out that neither K^+ or Na^+ were added to the reaction but the well-known affinity of these ligands for the group I metals resulted in their scavenging of Na^+ and K^+ cations

from various possible sources (such as the glassware, instrument electrospray capillary etc).

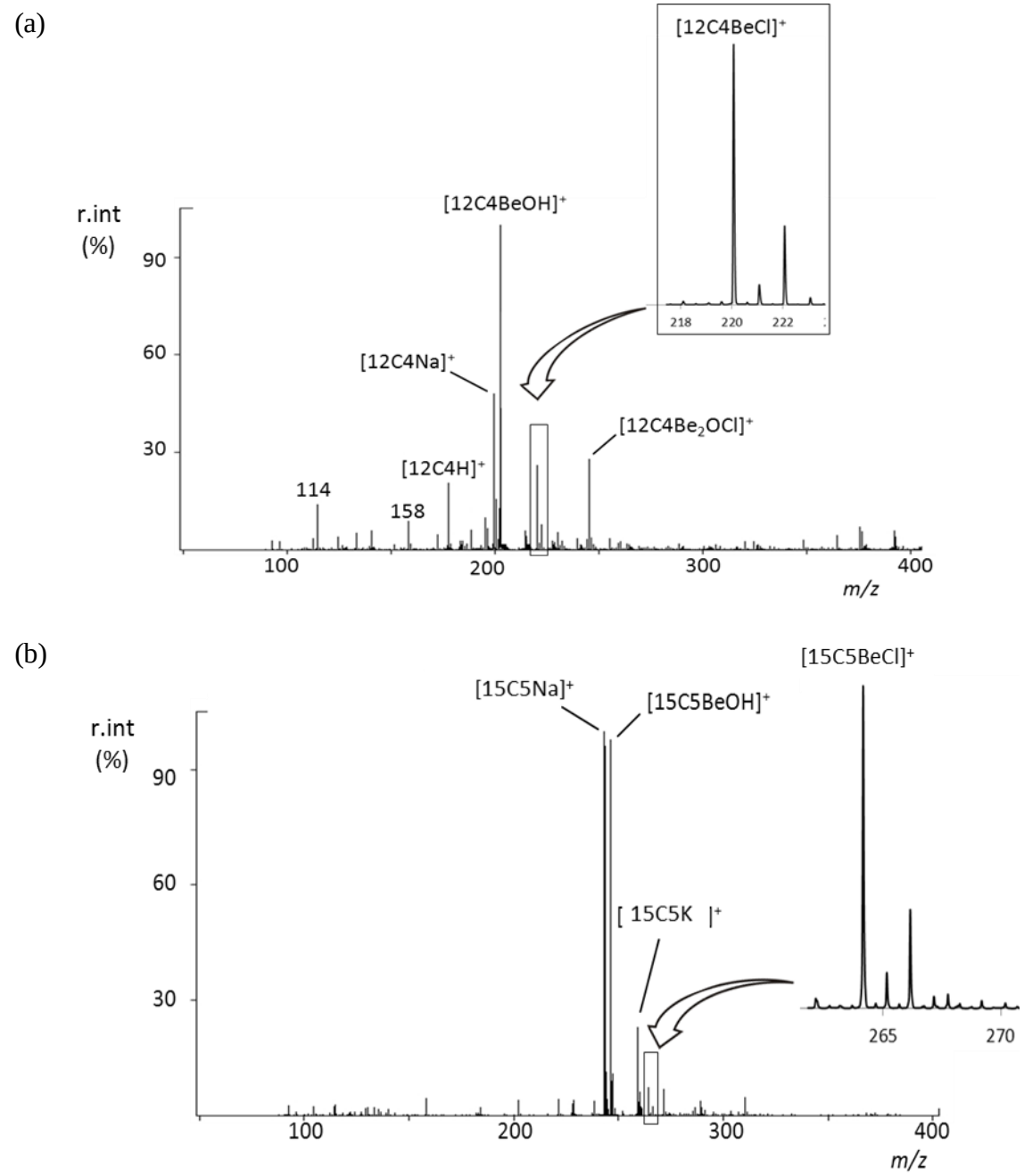

Figure 4-16 Positive ion ESI mass spectra of 2:1 molar mixtures of Be^{2+} and (a) 12-crown-4 (12C4) and (b) 15-crown-5 (15C5) in methanol-water solution and at capillary exit voltage of 80 V (with no alkali metal added). Inset shows the isotope pattern of the chloride complex species.

A striking observation in the ESI-MS behaviour of Be^{2+} with these ligands is that with the increase in cavity size and progressive mismatch for the Be^{2+} from

12-crown-4 to 18-crown-6 and cryptand[2.2.2], the resultant ESI mass spectra became exceedingly simplified such that the 12-crown-4 revealed the most complex spectra. Indeed, the observation of more ions containing Be^{2+} could be accepted as a prime indicator of the greater interactions of the 12-crown-4 with the Be^{2+} in comparison with other crown ethers. For instance, ESI mass spectra of a 2:1 molar mixture of Be^{2+} and the cryptand[2.2.2] ligand revealed only the K^+, Na^+, and H^+ adducts at *m/z* 415, 399 and 377 respectively without any sign of beryllium coordination as shown in Figure 4-17. Further increase in the Be^{2+}/cryptand[2.2.2] molar ratio up to 4:1 still revealed no beryllium-containing ion. Clearly, the ESI mass spectrum is in reflection of the abysmally poor interaction of this ligand with beryllium which have been shown to possess cavities more suited to the much larger potassium and rubidium cations.[55]

Table 4-7 Summary of ions observed in the positive ion ESI mass spectra of a 2:1 molar mixtures of beryllium chloride and macrocyclic ligands (no alkali metal added) in 1:1 methanol-water solution and at capillary exit voltage of 80 V.

Ion assignments	12-crown-4	15-crown-5	18-crown-6	Cryptand[2.2.2]
$[LBeOH]^+$	202.1171 (100%)	246.1157 (90%)	290.2306 (20%)	-
$[LBeOCH_3]^+$	216.1129 (15%)	-	-	-
$[LBeCl]^+$	220.0808 (30%)	264.1342 (20%)	308.2167 (5%)	-
$[LBe_2(OH)_2]^{2+}$	114.0648 (20%)	-	-	-
$[LBeOH(BeO)]^+$	227.1210 (30%)	-	-	-
$[LBeCl(BeO)]^+$	245.0875 (30%)	-	-	-
$[LBe]^{2+}$	92.5535 (5%)	114.5899 (10)	-	-
$[LBe(H_2O)]^{2+}$	101.5576 (5%)	-	-	-
$[LNa]^+$	199.0811 (50%)	243.1542 (100%)	287.1981 (100%)	399.3070 (100%)
$[LH]^+$	177.1082 (25%)	221.1689	-	377.3229 (100%)

$[LK]^+$	-	259.1375 (25%)	303.1712 (20%)	415.2815 (20%)
Beryllium hydroxido species (0-20%)				
$[Be_3(OH)_3(OCH_3)_2]^+$ *m/z* 158, $[Be_2(OH)(OCH_3)_2(H_2O)_2]^+$ *m/z* 133, $[Be_3(OH)_3(Cl)_2H_2O]^+$ *m/z* 166				

However, for the crown ethers, ESI mass spectral data provide unequivocal evidence of a variety of beryllium interactions and complexes in solution. The mass spectra revealed the existence of beryllium complexes at *m/z* 220 (30%) due to $[BeCl(12C4)]^+$, *m/z* 264 (20%) due to $[BeCl(15C5]^+$ species and *m/z* 308 (5%) due to $[BeCl(18C6]^+$. These chloride containing species could further be characterized by their distinct isotope pattern (see inset in Figure 4-16). These complexes match directly with previous vibrational and X-ray structural investigations of the monomeric crystalline products [BeCl(12-crown-4)][$SbCl_4$] and [$BeCl_2$(15-crown-5)] from non-aqueous media.[56] In addition, the dinuclear complex [$(BeCl_2)_2$(18C6)] is known.[57]

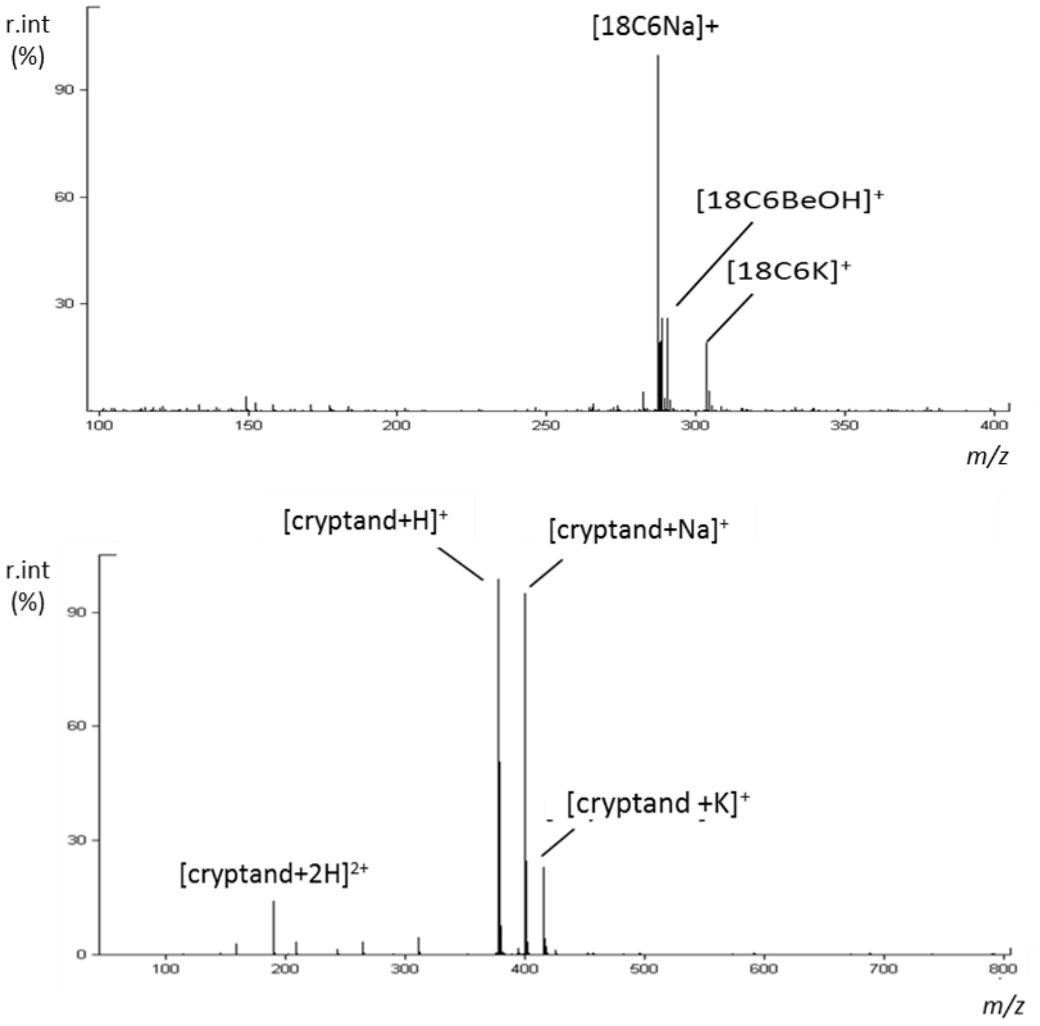

Figure 4-17 Positive ion ESI mass spectra of 2:1 molar mixtures of Be^{2+}/18-crown-6 (top) and Be^{2+}/cryptand [2.2.2] (bottom) revealing no sign of beryllium complexation by the cryptand ligand.

From ESI data, it is obvious that in aqueous or methanolic solutions of beryllium chloride and crown ethers, the $[LBeX]^+$ species where X=OH, OCH_3 are predominant for all crown ethers as illustrated by the ions at *m/z* 202 (100%) due to [BeOH(12C4)]+, *m/z* 246 (90%) due to $[BeOH(15C5)]^+$ and *m/z* 290 (20%) due to $[BeOH(18C6)]^+$ respectively. The observation of the analogous $[LBeOH]^+$ complex in comparison to the previously reported $[LBeCl]^+$ in non-aqueous media highlights the potential of ESI-MS in providing stoichiometric information of beryllium complexes in solution. Also, the $[LBeX]^+$ stoichiometric composition of the dominant beryllium species with the crown ether ligands indicate a partial encapsulation of the Be^{2+} cation whereby the multidentate crown ether ligands do not completely tetracoordinate to beryllium rather bi- and tri-dentate coordination take place. Thus, the crown ethers are confirmed incapable of a full encapsulation of beryllium. In the present system, it has to compete with the solvent ligands and counterion for one or more coordination site on the metal centre as observed in the ES-MS data. This is imperative in view of the ligand geometry of the crown ethers for which the donor atoms are poorly situated to 'wrap round' a tetrahedral cation. Moreover, the neutral donor oxygen atoms in the crown ethers which are inherently less basic in comparison to the negative oxygen donor of the (deprotonated) hydroxy group compete less favourably against the well-known hydrolytic tendency of the Be^{2+} cation. Therefore, additional peaks, especially those corresponding to the major beryllium hydroxido dimeric and trimeric cores such as $[Be_3(OH)_3(OCH_3)_2]^+$, $[Be_2(OH)(OCH_3)_2(H_2O)_2]^+$, $[Be_3(OH)_3(Cl)_2H_2O]^+$, at *m/z* 158, 133 and 166 respectively, were observed.

Another commonly observed property of the crown ether ligands is their propensity to act as second coordination sphere ligands. Thus an X-ray-determined structure have shown that the trimeric beryllium hydroxide $[Be_3(OH)_3(H_2O)_6]^{3+}$ can be crystallised alongside the 18-crown-6 ligand hydrogen bonded to its water molecules. ESI-MS data are also in support of this as the mass spectra have revealed dimeric beryllium hydroxido cores such as $[LBe_2(OH)_2]^{2+}$ *m/z* 114, $[LBeOH(BeO)]^+$ *m/z* 227, $[LBeCl(BeO)]^+$ *m/z* 245 where L = 12-crown-4. Although the actual structures of such species involving 12-crown-4 are unknown,

it likely involve the inner sphere coordination oxido/hydroxido bridging of the two metal centres since under ESI-MS conditions the evaporation of the solvent ion will bring the beryllium hydroxido cores in closer coordination proximity with the crown ethers.

Finally, while it can be deduced with certainty from these ESI-MS data and previous X-ray structure that full encapsulation of a tetrahedral cation such as the Be^{2+} cation is rarely achieved due to the ligand geometry of the crown ethers, other complexes have been shown to exist in solution at varying degrees of abundance which might be suitably stable towards the selective extraction of the Be^{2+} cation as displayed by the benzo-9-crown-3 ligand.[54]

4.3 Conclusion

This work has so far applied electrospray ionisation mass spectrometry to the study of some of the more important beryllium complexes with ligands of interest including acetate, mono-/dicarboxylates, citrate and the crown ethers. Using a "combinatory type" approach, ESI mass spectral data were acquired from solution mixtures of the Be^{2+} and important classes of ligands in order to outline the behaviour patterns of these compounds toward the application of modern mass spectrometry to other beryllium specialist areas of interest. On most occasions, the ESI mass spectra revealed solution speciation and ESI behaviour consistent with previously established chemistry and binding affinity trends of beryllium with all types of ligands. For instance, ions corresponding to predominant bischelated beryllium complexes known to be formed with monoanionic ligands such as the diketonates, salicylamide were observed in the mass spectra; depicting the ESI-MS technique as a powerful tool for the investigation of the interaction of beryllium with ligands in solutions. Using this technique solution speciation of beryllium in the presence of solvent and 1,3-diketonate ligands were observed and the results corroborate the tendency of beryllium to form stable polynuclear species with oxido, hydroxido or diketonato ligands bridging the metal centres. On the contrary, the Al^{3+} cation (although chemically similar to Be^{2+}), showed more straightforward ESI-MS spectra and interaction with diketonate ligands, a notable difference being the absence of polynuclear, oxido and solvent cluster species. This correlates well with the smaller size and slightly higher charge-density of the beryllium cation. In addition, ESI-MS mass spectra well represented the competition between the

solvent and ligands for beryllium binding while stoichiometric information from the assignment of ESI-MS ions provided more information on the nuclearity of additional beryllium species the presence of which tend to be overlooked due to their low abundance or the nature of the solvent/counter ion involved. An example is the beryllium citrate system which could be relevant in deciphering the underly interactions of beryllium with ligands in biological systems. Clearly, ESI data point out that the existent species in equilibrium mixtures of beryllium and citrate across various pH and molar ratios are more complicated than the 2:1 Be:L stoichiometry currently portrayed.

Lastly, the idea and practical consideration in employing ESI-MS for investigation speciation in mixtures of metal ions and ligands in solution have been provided. It has therefore been proven that by employing suitable experimental conditions, representative data can be obtained from the ESI mass spectra data thereby rendering the microscale requirement of the ESI-MS an extremely useful advantage for a quick but approximate screening of potential ligands of interest toward beryllium complexation.

4.4 References

1. R. B. Cole, *Electrospray and Maldi Mass Spectrometry:Fundamentals, Instrumentation, Practicalities, and Biological Applications*, Wiley, New Jersey, 2nd edn., 2010.

2. W. Henderson and J. S. McIndoe, *Mass Spectrometry of Inorganic, Coordination and Organometallic Compounds:Tools, Techniques, Tips*, Wiley, Chichester, 2005.

3. J. B. Fenn, *Angewandte Chemie International Edition*, 2003, **42**, 3871-3894.

4. W. R. Harris, Z. Wang and Y. Z. Hamada, *Inorganic Chemistry*, 2003, **42**, 3262-3273.

5. W. Henderson and T. S. A. Hor, *Inorganica Chimica Acta*, 2014, **411**, 199-211.

6. M. J. Keith-Roach, *Analytica Chimica Acta*, 2010, **678**, 140-148.

7. V. B. Di Marco and G. G. Bombi, *Mass Spectrometry Reviews*, 2006, **25**, 347-379.

8. J. S. Brodbelt, *International Journal of Mass Spectrometry*, 2000, **200**, 57-69.

9. J. M. Daniel, S. D. Friess, S. Rajagopalan, S. Wendt and R. Zenobi, *International Journal of Mass Spectrometry*, 2002, **216**, 1-27.

10. E. Reinoso-Maset, P. J. Worsfold and M. J. Keith-Roach, *Rapid Communications in Mass Spectrometry*, 2012, **26**, 2755-2762.

11. W. Henderson, S. H. Chong and T. S. A. Hor, *Inorganica Chimica Acta*, 2006, **359**, 3440-3450.

12. J. S. L. Yeo, J. J. Vittal, W. Henderson and T. S. A. Hor, *Inorganic Chemistry*, 2002, **41**, 1194-1198.

13. O. Raymond, L. C. Perera, P. J. Brothers, W. Henderson and P. G. Plieger, *Chemistry in New Zealand*, 2015, **79**, 137-143.

14. O. Raymond, W. Henderson, P. J. Brothers and P. G. Plieger, *European Journal of Inorganic Chemistry*, 2017, **2017**, 2691-2699.

15. R. J. Berger, M. A. Schmidt, J. Jusélius, D. Sundholm, P. Sirsch and H. Schmidbaur, *Zeitschrift für Naturforschung B*, 2001, **56**, 979-989.

16. V. A. Sipachev and Y. S. Nekrasov, *Journal of Mass Spectrometry*, 1988, **23**, 809-812.

17. V. A. Sipachev, N. I. Tuseev, Y. S. Nekrasov and R. Galimzyanov, *Polyhedron*, 1982, **1**, 820-822.

18. J. C. Kunz, M. Das and D. T. Haworth, *Inorganic Chemistry*, 1986, **25**, 3544-3545.

19. C. MacDonald and J. Shannon, *Australian Journal of Chemistry*, 1966, **19**, 1545-1566.

20. K. J. Iversen, S. A. Couchman, D. J. Wilson and J. L. Dutton, *Coordination Chemistry Reviews*, 2015, **297**, 40-48.

21. D. Naglav, M. R. Buchner, G. Bendt, F. Kraus and S. Schulz, *Angewandte Chemie International Edition*, 2016, **55**, 10562-10576.

22. F. Cecconi, E. Chinea, C. A. Ghilardi, S. Midollini and A. Orlandini, *Inorganica Chimica Acta*, 1997, **260**, 77-82.

23. L. Alderighi, P. Gans, M. Stefeno and A. Vacca, in *Advances in Inorganic Chemistry*, eds. A. G. Sykes and A. Cowley, H, Academic Press, Califorornia, 2000, vol. 50, pp. 109-197.

24. P. Barbaro, F. Cecconi, C. A. Ghilardi, S. Midollini, A. Orlandini, L. Alderighi, D. Peters, A. Vacca, E. Chinea and A. Mederos, *Inorganica Chimica Acta*, 1997, **262**, 187-194.

25. Y. S. Nekrasov, S. Y. Sil'vestrova, A. I. Grigo'ev, L. N. Reshetova and V. A. Sipachev, *Journal of Mass Spectrometry*, 1978, **13**, 491-494.

26. T. S. Keizer, N. N. Sauer and T. M. McCleskey, *Journal of Inorganic Biochemistry*, 2005, **99**, 1174-1181.

27. T. S. Keizer, *Journal*, 2005, **1**, 338-342.

28. T. S. Keizer, N. N. Sauer and T. M. McCleskey, *Journal of the American Chemical Society*, 2004, **126**, 9484-9485.

29. A. Grigor'ev and V. Sipachev, *Inorganica Chimica Acta*, 1976, **16**, 269-279.

30. V. A. Sipachev and Y. S. Nekrasov, *Journal of Mass Spectrometry*, 1988, **23**, 813-815.

31. N. Tuseev, V. Sipachev, R. Galimzyanov, A. V. Golubinskii, E. Zasorin and V. Spiridonov, *Journal of Molecular Structure*, 1984, **125**, 277-286.

32. W. Bragg and G. T. Morgan, *Proceedings of the Royal Society of London. Series A, Containing Papers of a Mathematical and Physical Character*, 1923, **104**, 437-451.

33. S.-W. A. Fong, J. J. Vittal, W. Henderson, T. S. A. Hor, A. G. Oliver and C. E. F. Rickard, *Chemical Communications*, 2001, 421-422.

34. E. Chinea, S. Dominguez, A. Mederos, F. Brito, A. Sánchez, A. Ienco and A. Vacca, *Main Group Metal Chemistry*, 1997, **20**, 11-18.

35. M. J. Brisson and A. A. Ekechukwu, *Beryllium: Environmental Analysis and Monitoring*, Royal Society of Chemistry, United Kingdom, 2009.

36. A. Fairhall, *The Radiochemistry of Beryllium*, National Academies, Washington D.C, 1960.

37. K. A. Walsh and E. E. Vidal, *Beryllium Chemistry and Processing*, ASM International, Ohio, 2009.

38. B. J. Duncombe, J. O. Rydén, L. Puškar, H. Cox and A. J. Stace, *Journal of the American Society for Mass Spectrometry*, 2008, **19**, 520-530.

39. J. Stewart and B. Morosin, *Acta Crystallographica Section B: Structural Crystallography and Crystal Chemistry*, 1975, **31**, 1164-1168.

40. C. Reichert, G. Bancroft and J. Westmore, *Canadian Journal of Chemistry*, 1970, **48**, 1362-1370.

41. Q. Shen and K. Hagen, *Journal of Physical Chemistry*, 1987, **91**, 1357-1360.

42. A. E. Martell and R. D. Hancock, *Metal Complexes in Aqueous Solutions*, Springer Science & Business Media, New York, 1996.

43. R. B. Cole and A. K. Harrata, *Journal of the American Society for Mass Spectrometry*, 1993, **4**, 546-556.

44. B. K. Pal and K. Baksi, *Microchimica Acta*, 1992, **108**, 275-283.

45. R. Faure, F. Bertin, H. Loiseleur and G. Thomas-David, *Acta Crystallographica Section B: Structural Crystallography and Crystal Chemistry*, 1974, **30**, 462-467.

46. H. B. Knowles, *National Bureau of Standards Journal of Research*, 1935, **15**, 87-96.

47. T. M. McCleskey, D. S. Ehler, T. S. Keizer, D. N. Asthagiri, L. R. Pratt, R. Michalczyk and B. L. Scott, *Angewandte Chemie International Edition*, 2007, **119**, 2723-2725.

48. T. M. McCleskey and B. L. Scott, *Journal of Occupational and Environmental Hygiene*, 2009, **6**, 751-757.

49. T. S. Keizer, B. L. Scott, N. N. Sauer and T. M. McCleskey, *Angewandte Chemie International Edition*, 2005, **44**, 2403-2406.

50. V. B. Di Marco, G. G. Bombi, M. Ranaldo and P. Traldi, *Rapid Communications in Mass Spectrometry*, 2007, **21**, 3825-3832.

51. I. Gautier-Luneau, C. Merle, D. Phanon, C. Lebrun, F. Biaso, G. Serratrice and J. L. Pierre, *Chemistry–A European Journal*, 2005, **11**, 2207-2219.

52. A. M. Silva, X. Kong, M. C. Parkin, R. Cammack and R. C. Hider, *Dalton Transactions*, 2009, 8616-8625.

53. V. A. Sipachev and I. P. Gloriozov, *Journal of Mass Spectrometry*, 1979, **14**, 29-30.

54. M. R. Ganjali, A. Moghimi and M. Shamsipur, *Analytical Chemistry*, 1998, **70**, 5259-5263.

55. A. F. Cotton, G. Wilkinson, M. Bochmann and C. A. Murillo, *Advanced inorganic chemistry*, Wiley, 1999.

56. B. Neumueller and K. Dehnicke, *Zeitschrift für Anorganische und Allgemeine Chemie*, 2006, **632**, 1681-1686.

57. R. Putcha, R. Kolbig, F. Weller, B. Neumüller, W. Massa and K. Dehnicke, *Zeitschrift für Anorganische und Allgemeine Chemie*, 2010, **636**, 2364-2371.

Chapter Five

ESI-MS microscale screening, macroscale syntheses and characterisation of beryllium complexes with potentially encapsulating ligands

5.1 Introduction

One area of major interest in the chemistry of beryllium is its coordination to uniquely designed ligands with the ability to sequester the metal for applications in therapies for exposed individuals.[1, 2] Generally, beryllium poisoning is less common in comparison with intoxication from the heavier metals like Pb, As and Cd. However, the absence of a well-defined dose-related toxicity level as well as newly emerging risk of exposure have progressively increased biomedical interest in the toxicology of beryllium.[3-5] Chelation therapy is the mainstay medical procedure in the treatment of metal poisoning and it involves the administration of a suitable chelating ligand to extract or deplete the metal dosage in the body. Among the commonest group of chelating agents employed are the polyaminocarboxylate ligands such as ethylenediaminetetraacetic acid (EDTA), nitrilotriacetic acid (NTA) and diethylenetriaminepentaacetic acid (DTPA).[6, 7] These multidentate ligands also form highly stable complexes with other metal ions as a result of the cumulative chelate effect inherent in a single ligand's encapsulation of the metal ion in an appropriate coordination geometry.[8, 9] As a consequence, the majority of the polyaminocarboxylic acids reveal poor interaction with the beryllium cation due to the distinct features of the Be^{2+} cation in terms of charge density, size and coordination preference.[10-12] Hence little work has been reported on the possibility of chelation treatment of beryllium intoxication by these ligands.[7, 13]

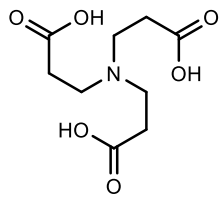

Nitrilotripropionic acid NTP

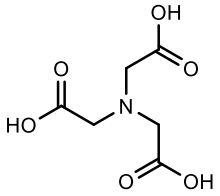

Nitrilotriacetic acid NTA

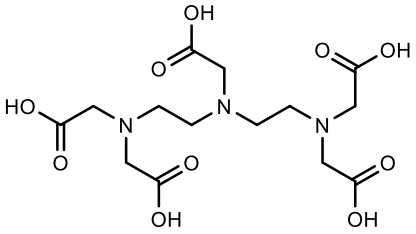

Diethylenetriaminepentaacetic acid DTPA

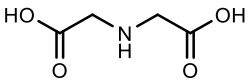

Iminodiacetic acid IDA

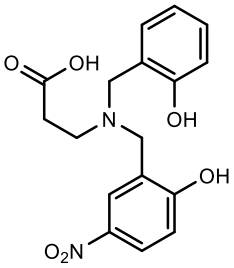

L1

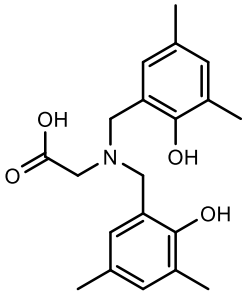

L2

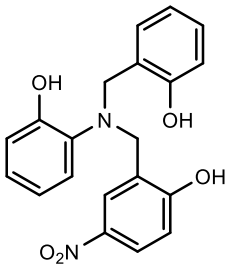

L3

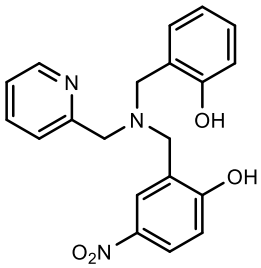

L4

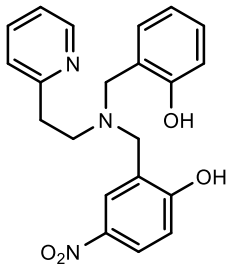

L5

Figure 5-1 Multidentate ligands investigated for their ability to potentially encapsulate beryllium ions via tetrahedral binding.

Nevertheless, recent experimental results from *in vivo* animal testing as well as potentiometric titrations have identified nitrilotripropionic acid (H_3NTP) as a potentially useful chelating agent for beryllium.[1, 10] Nitrilotripropionic acid is a very interesting tripodal polyaminocarboxylic acid which forms a strong complex with

beryllium (log k = 9.24) through binding with a nitrogen atom and oxygen atoms from 3 carboxylate pendant arms so that the beryllium ion is completely encapsulated in a tetrahedral pocket.[10] Since beryllium is the only metal cation observed to possess a stronger affinity for nitrilotripropionic acid ahead of the analogous but more popular nitrilotriacetic acid, the former chelating group has also been proposed for use in the analytical determination of Be^{2+} ion.[14] Furthermore, Mederos and co-workers have systematically examined the increase in binding affinity while following the effect of the encapsulating pendant arms from a five-membered chelating acetate group to a six-member ring-forming propionate group.[15] More recently, Plieger and co-workers sought to improve the binding affinity and selectivity of the polyaminocarboxylate ligands towards beryllium by synthesizing a series of more pre-organized phenolic analogues based on the NTP encapsulating motif.[16, 17] Given the prospects of applying these ligands as environmental and biomedical chelating agents for beryllium, this chapter explores speciation studies involving electrospray-generated gas phase ions (see Chapter 7 for the ESI-MS methodology and instrument conditions in generating these beryllium complexes in the gas phase) as a representation of solution species from the complexation of beryllium by the polyaminocarboxylic acids and other related ligands. Lastly, selected beryllium-ligand combinations were characterized by 'traditional' techniques (NMR and single crystal X-ray diffraction) to further support and check ESI-MS results.

5.2 Results and discussion

5.2.1 Preliminary ESI-MS investigations of the polyaminocarboxylate ligands

The ligands investigated in the first section of this study are displayed in Figure 5-1. Firstly, the ESI-MS of the free polyaminocarboxylate ligands were investigated particularly to characterize the ligands **L1-L5** which were resynthesized according to literature procedures[16, 17] and to ascertain the purity of other purchased ligands. The main observation was that the ESI-MS behaviour of these ligands is closely related to the nature of their functional groups. Since all the ligands possess basic amino groups and carboxylate/phenol groups, the ligands readily ionized in the positive and negative mode to yield intense signals due to $[M+H]^+$ and $[M-H]^-$ ions respectively. Occasionally, the $[2M+H]^+$ ion series were

observed in the positive ion mode especially at high ligand concentration in solution and at low capillary exit voltages. The ligands in this first section have been divided according to the maximum number of ionisable protons present. This includes dianionic, trianionic and the DPTA ligand which has five ionisable protons.

5.2.2 ESI-MS studies of beryllium complexation by IDA, and L4-L5 in solution

The dianionic ligands IDA, **L4** and **L5**, which were expected to form neutral beryllium complexes were observed to be fairly well ionized both in the positive and negative ESI-MS ion mode. The major signals observed in the positive and negative ion ESI-MS of 1:1 molar mixtures of beryllium sulfate and the ligands IDA, **L4** and **L5** are summarized in Table 5-1.

Starting firstly with the ESI-MS analysis of the Be^{2+}/IDA system, the negative ion mass spectra of beryllium sulfate and iminodiacetic acid reveals peaks corresponding to the ESI-MS ions $[L_{-2H}BeHSO_4]^-$ and $[L_{-2H}BeOH]^-$ at *m/z* 236.99 (50%) and *m/z* 157.01 (60%) respectively (L_{-2H} is the doubly deprotonated dianionic ligand). Additional ions include the $[L_{-H}]^-$ and the $[HSO_4]^-$ ion at *m/z* 132 and *m/z* 97 respectively while the signal at *m/z* 97 was observed as the most prominent ion as shown in the illustrative mass spectrum in Figure 5-2. Importantly, the ESI mass spectra on the speciation in the Be^{2+}/IDA system is in good agreement with potentiometric speciation data which have shown the $[L_{-2H}BeOH]^-$ species to be the most prominent species when employing the beryllium perchlorate salt as the source of Be^{2+}.[18, 19] Contrary to the perchlorate ion ClO_4^-, the sulfate ion SO_4^{2-} has been well observed (both in this research and in other literature) to bind strongly to the beryllium cation.[20-22] Other ions detected in the negative ion mode at lower intensities include the ions and $[BeL_{-3H}]^-$ and $[Be(L_{-H})(L_{-2H})]^-$ at *m/z* 139 and 272 respectively. These species, which were only observed at higher capillary exit voltages (>120 V). In contrast, positive ion mass spectra of beryllium sulfate and iminodiacetic acid was less informative revealing only a prominent signal corresponding to the free ligand $[L+Na]^+$ at *m/z* 156 as shown in Figure 5-2. This is expected since the prominent beryllium complexes in solution are negatively charged. Nevertheless, a few beryllium containing species were observed which includes $[BeL_{-H}(CH_3OH)]^+$, $[Be(L)(L_{-H})]^+$ and $[Be_2O(L_{-H})(CH_3OH)]^+$ at *m/z* 173,

274 and 198 respectively. The latter (which is a dinuclear species) signifies that hydrolytic reactions might equally be occurring in solution.

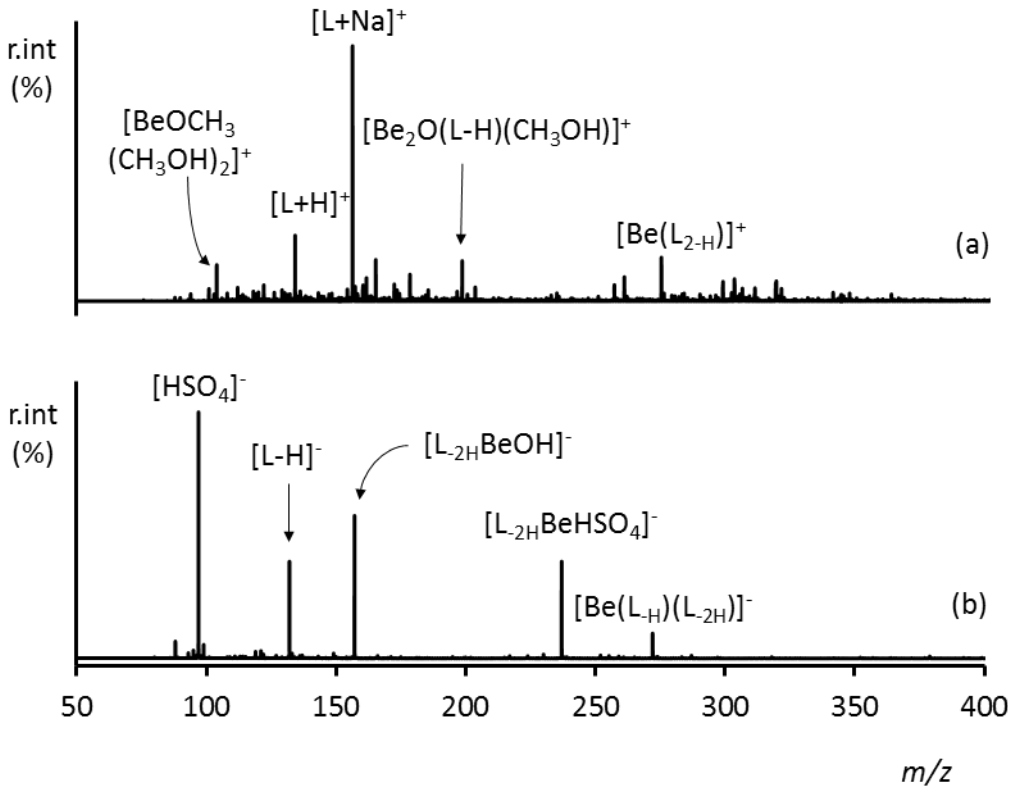

Figure 5-2 ESI mass spectra of $BeSO_4$ and iminodiacetic acid (L) in methanol-water solution at capillary exit 60 V (a) positive ion mode (b) negative ion mode. pH was adjusted to 6.7 using sodium hydroxide.

Although no X-ray structure for the beryllium complex with iminodiacetate ligand has yet been reported, it has rigorously been shown employing potentiometric data that the IDA ligand is able to break up the cyclic beryllium trimer by partially encapsulating the Be^{2+} cation *via* tridentate coordination from two acetates and the imine group.[22] It is apparent that the unavailability of donor atoms for a complete tetrahedral coordination to beryllium (as observed in the IDA ligand) results in a partially encapsulated beryllium centre and the concomitant incorporation of a second ligand (see Figure 5-3). While structural information cannot be concluded from the ESI-MS data, the coordination of a second ligand (usually OH^-, HSO_4^-, Cl^-) to the beryllium centre (which is readily detected from stoichiometric information provided by the ESI-MS technique as shown in Figure 5-3) can provide complementary information on the interaction of the Be^{2+} cation

with potentially encapsulating multidentate ligands. Therefore the ESI-MS ion behaviour of the beryllium complex with IDA could be employed as a simple model towards inferring the probable coordination mode adopted by the other dianionic ligands such as **L4** and **L5** due to the presence of an additional weakly coordinating nitrogen donor atom in these ligands in direct comparison to the nitrilotripropionate ligand.

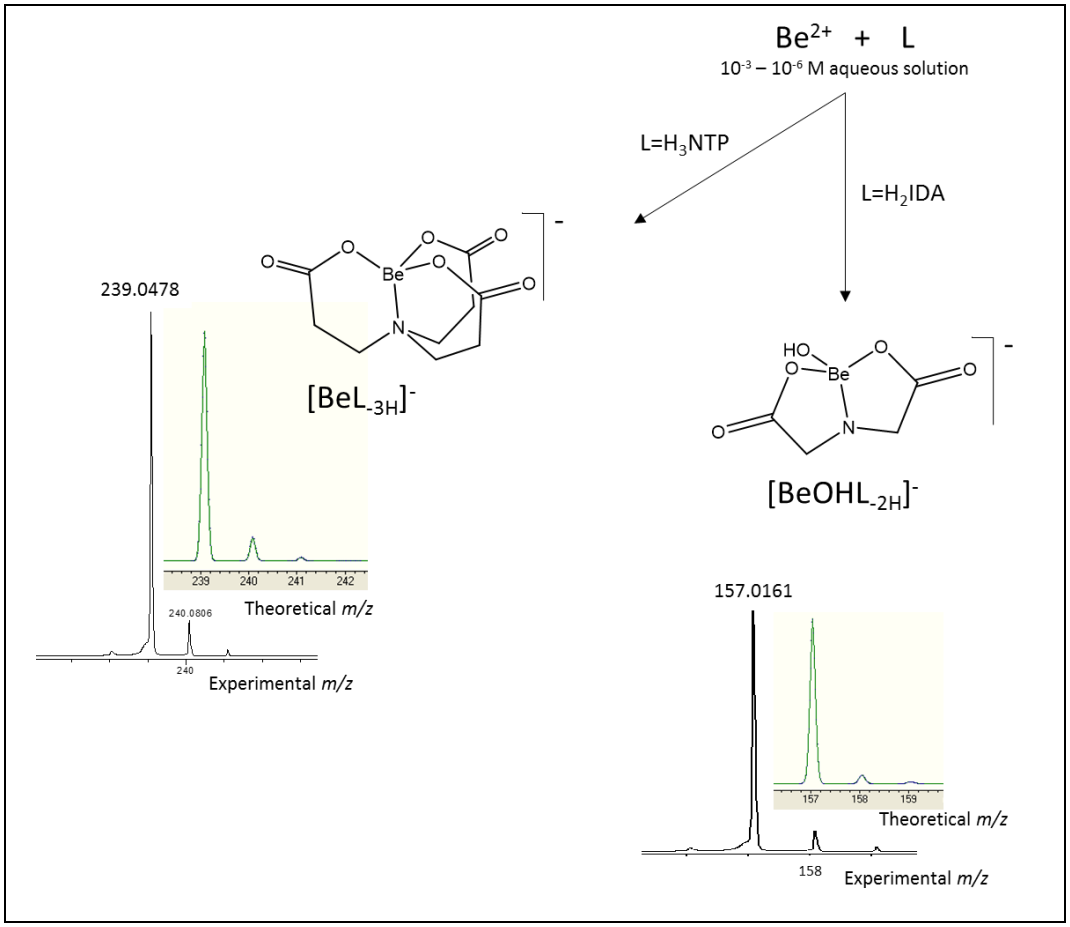

Figure 5-3 Illustration of supportive stoichiometric information on the full encapsulation of the Be^{2+} cation for ESI-MS screening of beryllium-ligand solutions at low concentrations.

The negative ion mass spectra of beryllium sulfate and ligands **L4**-**L5** reveal peaks corresponding to the ESI-MS ions $[L_{-H}BeHSO_4]^-$ for **L4** (*m/z* 469 100%) and **L5** (*m/z* 483 72%), $[(L_{-2H})_2Be_2HSO_4]^-$ for **L4** (*m/z* 841 20%) and **L5** (*m/z* 869 10%), $[Be(L_{-H})(L_{-2H})]^-$ for **L4** (*m/z* 736 25%) and **L5** (*m/z* 764 5%). The beryllium containing ions in the positive mass spectra include $[Be(L)(L_{-H})]^+$ observed at *m/z* 373 (5%) for **L4** and *m/z* 387 (15%) for **L5**. The $[Be(L_{-H})(L_{-2H})]^-$ species tends to suggest that these ligands could also adopt a bidentate coordination mode to the beryllium cation as such complexes with the ligand **L5** appear to be formed more abundantly compared to **L4** (see Table 5-1). Furthermore, comparison to the

nitrilopropionic acid suggests that full encapsulation of beryllium by **L4** or **L5** would be relatively weaker as a result of the additional nitrogen donor atom. Due to the extreme oxophilicity of the Be^{2+} cation, the pyridine nitrogen donor (in **L4** and **L5**) would compete less favourably with water or other oxygen donor ligands and this is clearly indicated by the observation of the $[LBeX]^-$ ion where X= OCH_3^-, HSO_4^- (see Figure 5-4)

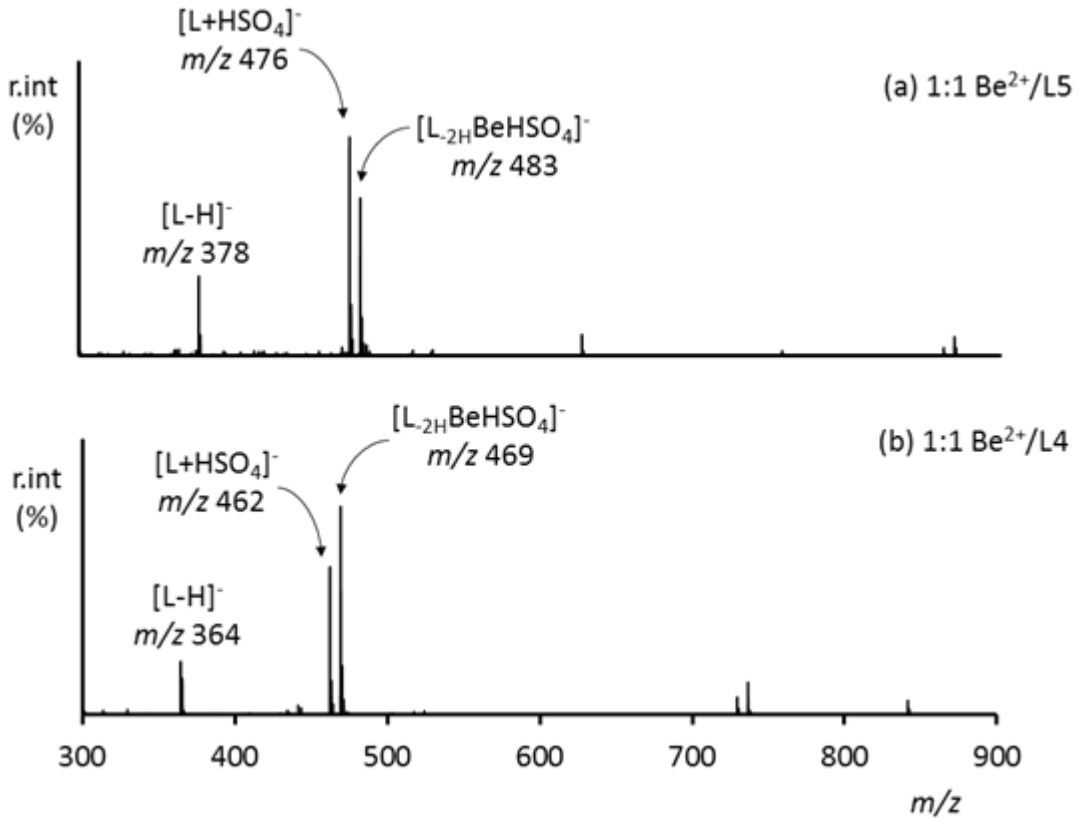

Figure 5-4 Negative ion ESI mass spectra of mixtures of beryllium sulfate and the ligands (a) **L4** and (b) **L5** in methanol-water solution at capillary exit 60 V. pH was adjusted to 7.2 using sodium hydroxide.

This is in accord with a conclusion previously reported from calculated and experimental ^{9}Be NMR chemical shifts observed for the beryllium complexes of ligands **L4**-**L5** synthesized *in situ* in a DMF solvent. It was observed that the solvent molecule (DMF) completed the tetracoordination of beryllium instead of the pyridine nitrogen donor of the ligands.[17] Lastly, there is also a possibility that the adduction of a sulfate group is a reflection of the ionisation mode of the beryllium complex with this group of dianionic ligands. However, ESI-MS ions such as $[LBeOH]^-$ highlight the competition of complexation of the hydroxide over the full

encapsulation of the beryllium ion by tetradentate coordination as shown in Figure 5-3. This was also observed with the crown ethers (see Chapter 4). Therefore, the relative ease of formation of the $[LBeOH]^-$ species in the mass spectra (as revealed by the species abundance) pointed out the existence of competition from other oxygen donor ligands in solution. In that case and based on the ESI-MS data (see Table 5-1), the ligand **L4** is expected to be more suited to adopt the $[LBeX]^-$ coordination mode proposed in Figure 5-3 as a result of its combination of a weakly coordinating nitrogen donor and a five membered chelate ring within an encapsulating arm. Further examination of the relative intensities in the ESI mass spectra support this idea as Table 5-1 reveals that the $[L_{-2H}BeHSO_4]^-$ ion is formed in higher abundance for **L4** in comparison to **L5**.

Table 5-1 Summary of ions observed in the negative ion ESI mass spectra of 1:1 molar solution of beryllium sulfate and the ligands IDA and **L4**-**L5** across pH 6.5 – 7.2 and capillary exit voltage of 100 V.

ESI-MS solutions	Negative ions	Experimental *m/z*	Theoretical *m/z*	i^a *(%)*	Positive ions	Experimental *m/z*	Theoretical *m/z*	i^a *(%)*
Be^{2+} + IDA	$[L_{-H}]^-$	132.0371	132.0291	40	$[L+Na]^+$	156.0279	156.0267	100
	$[BeHSO_4L_{-2H}]^-$	236.9924	236.9930	50	$[BeL_{-H}(CH_3OH)]^+$	173.0509	173.0675	20
	$[[BeOHL_{-2H}]^-$	157.0161	157.0362	60	$[Be(L)(L_{-H})]^+$	274.0752	274.0788	20
	$[BeOL_{-2H}(CH_3OH)]^{2-}$	94.0170	94.0270	10	$[BeL_{-H}]^+$	141.0413	141.0413	10
	$[BeL_{-3H}]^-$	139.0197	139.0256	5	$[Be_2O(L_{-H})(CH_3OH)]^+$	198.0626	198.0746	10
	$[Be(L_{-H})(L_{-2H})]^-$	272.0631	272.0637	15	$[L_H]^+$	134.0312	134.0245	25
Be^{2+} + **L4**	$[LHSO_4]^-$	462.1567	462.0965	70	$[L_H]^+$	366.0565	366.1448	100
	$[BeHSO_4L_{-2H}]^-$	469.1681	469.0930	100	$[Be(L)(L_{-H})]^+$	373.0431	373.1413	5
	$[Be(L_{-H})(L_{-2H})]^-$	736.3729	736.2632	25				
	$[(BeL_{-2H})_2HSO_4]^-$	841.3535	841.2271	20				
Be^{2+} + **L5**	$[LHSO_4]^-$	476.2706	476.1122	100	$[L_H]^+$	380.1463	380.1604	100
	$[Be(L_{-H})(L_{-2H})]^-$	764.2511	764.3279	5	$[Be(L)(L_{-H})]^+$	387.1398	387.1570	15
	$[BeHSO_4L_{-2H}]^-$	483.2619	483.1322	72				
	$[(BeL_{-2H})_2HSO_4]^-$	869.5338	869.2932	10				

i^a = relative intensity

5.2.3 ES-MS studies of beryllium complexation by NTA, NTP and L1-L3

The major signals observed in the positive and negative ion ESI-MS of 1:1 solution mixtures of beryllium sulfate and ligands NTA, NTP and **L1-L3** are summarized in Table 5-2. These trianionic ligands readily formed monoanionic beryllium complexes which were transferred into the mass spectrometer with good efficiency. In the positive ion mode the pre-existing monoanionic beryllium complexes of **L1-L3** are poorly ionized, leading to the emergence of ESI-MS signals of the protonated free ligand $[L_H]^+$ as the most intense signal for all the ligands and often the only signal except for **L1** for which the ESI-MS ion $[BeL_{-H}]^+$ was observed at *m/z* 354 (40%). Despite increasing the Be/L molar ratio to 3:1, the intense $[L_H]^+$ signal still persisted due to the high electrospray ionisation efficiency of the amine group. Therefore subsequent investigation of this group of ligands was conducted in the negative ion mode. Nevertheless, the few other beryllium containing ESI-MS ions observed in the positive ion mode, although occuring at very lower intensity (<20%), highlighted the existence of other coordination modes. For instance a tetradentate coordination to beryllium can be ruled out in the complexes of 1:2 beryllium ligand stoichiometry observed in species such as $[Be(L_{-H})_2H]^+$ at *m/z* 692 for **L2**, and *m/z* 738 for **L3**.

In the negative ion mode, ESI-MS of beryllium complexes with all ligands revealed singly charged ESI-MS ions $[L_{-H}]^-$ and $[BeL_{-3H}]^-$ corresponding to the free ligand and beryllium complex in solution. The ESI-MS ions $[BeL_{-3H}]^-$ corresponding to a 1:1 beryllium/ligand stoichiometry for NTA, NTP and **L1-L3** were observed at *m/z* 197.12, 239.04, 352.10, 349.17, 372.12 respectively as the most abundant ESI-MS ion in a 1:1 beryllium sulfate/ligand solution mixture. This supports the dominance of the $[BeL_{-3H}]^-$ complex in solution for which the Be^{2+} ion is most likely in a tetrahedral coordination mode from one ligand in agreement with the related tetradentate nitrilotripropionate (NTP) ligand.[10] Previous investigation of the ESI-MS behaviour of these beryllium complexes have shown that the tetracoordination of beryllium ion (which is maintained in solution by the coordination of solvent molecule(s) is often transferred into the gas phase under relatively soft ionisation conditions.[23] However, signals corresponding to solvated

ions, adducts and other polynuclear hydroxido species well-known to exist in beryllium solutions (especially the beryllium trimer) were absent revealing the ability of these ligands to completely exclude the solvent molecules from binding in the beryllium primary coordination sphere thereby suppressing the well-known hydrolytic tendency of Be^{2+}.[24] This is in agreement with previous studies on these ligands in which experimental and predicted ^{9}Be NMR chemical shifts showed good correlation for a fully encapsulated Be^{2+} cation by tetracoordination from ligands **L1**-**L3** as has been structurally authenticated for the $[BeNTP]^{-}$ complex in the solid state.[10, 17] Importantly, such insight into the beryllium complexes in solution gleaned from a combinatorial and quick ESI-MS microscale screening can be an invaluable tool for preliminary investigation of beryllium complexes in solution.

Table 5-2 Summary of ions observed in the positive and negative ion ESI mass spectra of 1:1 molar solutions of beryllium sulfate and the ligands NTA, NTP, and **L1**-**L3** at pH 6.5 and capillary exit voltage 100 V.

ESI-MS solutions	Negative ions	Experimental *m/z*	Theoretical *m/z*	i^a	Positive ions	Experimental *m/z*	Theoretical *m/z*	i^a
Be^{2+} + NTA	$[L_{-H}]^-$	190.0317	190.0424	30	$[L_H]^+$	192.0615	192.0502	100
	$[BeL_{-3H}]^-$	197.0322	197.0311	100				
Be^{2+} + NTP	$[L_{-H}]^-$	232.0496	232.0815	100	$[L_H]^+$	234.1143	234.0972	100
	$[BeL_{-3H}]^-$	239.0478	239.0781	30	$[BeL_{-3H}H]^+$	241.1056	241.0937	35
	$[Be(L_{-2H})_2H]^-$	472.1466	472.1680	10	$[Be(L_{-H})_2H]^+$	474.2567	474.1836	10
	$[BeHSO_4L]^-$	337.1471	337.1471	5				
Be^{2+} + **L1**	$[L_{-H}]^-$	345.1039	345.1081	0	$[L_H]^+$	347.1275	347.1237	100
	$[BeL_{-3H}]^-$	352.1046	352.1060	100	$[BeL_{-H}]^+$	354.1051	354.1071	45
Be^{2+} + **L2**	$[L_{-H}]^-$	342.1530	342. 1699	10	$[L_H]^+$	344.2197	344.1699	100
	$[BeL_{-3H}]^-$	349.1730	349. 1665	100				
	$[Be(L_{-2H})_2H]^-$	692.3459	692.3448	5				
Be^{2+} + **L3**	$[L_{-H}]^-$	365.1299	365.1131	80	$[L_H]^+$	367.1443	367.1288	100
	$[BeL_{-3H}]^-$	372.1274	372.1097	100				
	$[Be(L_{-2H})_2H]^-$	738.2733	738.2313	5				

i^a= relative intensity

5.2.4 pH dependence of $[BeL]^-$ complexes and fragmentation in the gas phase

To investigate the behaviour of ESI-MS signals due to the $[BeL_{-3H}]^-$ complexes in solution, the effects of solution pH, capillary exit voltage and the ESI-MS drying gas temperature on the ionisation of these complexes were assessed. The electrospray ionisation of the $[BeL_{-3H}]^-$ species were seldom affected by changes in the drying gas temperatures between 140-200 ^oC although lower temperatures only diminished the overall signal intensity of the spectra yet no solvated species was observed. On the other hand, an increase in the instrument's capillary exit voltage (which corresponds to a shift into harsh ionisation) firstly resulted in an increased signal intensity of the ion up to a capillary exit voltage of 120 V after which fragment species prominently emerge. Therefore, except where fragmentation of the beryllium complex was desired, a moderately low CEV of 80 V was utilised and this revealed optimal intensity for the $[BeL_{-3H}]^-$ ion signal without fragmentation peaks. The fragmentation of the $[BeL_{-3H}]^-$ ions for **L1**-**L2** proceeded through the cleavage of the phenol-bearing encapsulating arm revealing peaks assigned as $[Be(L\text{-}CH_2Ph\text{-}OH)]^-$ at *m/z* 246 for **L1** and *m/z* 215 for **L2**. Interestingly, no ESI-MS ion was found corresponding to a cleavage of the carboxylate-bearing arm in the $[BeL_{-3H}]^-$ complex of ligands **L1** and **L2** perhaps due to a relatively stronger binding of beryllium with a carboxylate in comparison to a hydroxyl oxygen donor.[9] At capillary exit voltages greater than 140 V, the fragment species $[Be(L\text{-}CH_2Ph\text{-}OH)]^-$ became the dominant beryllium complexes in the gas phase as shown in Figure 5-5.

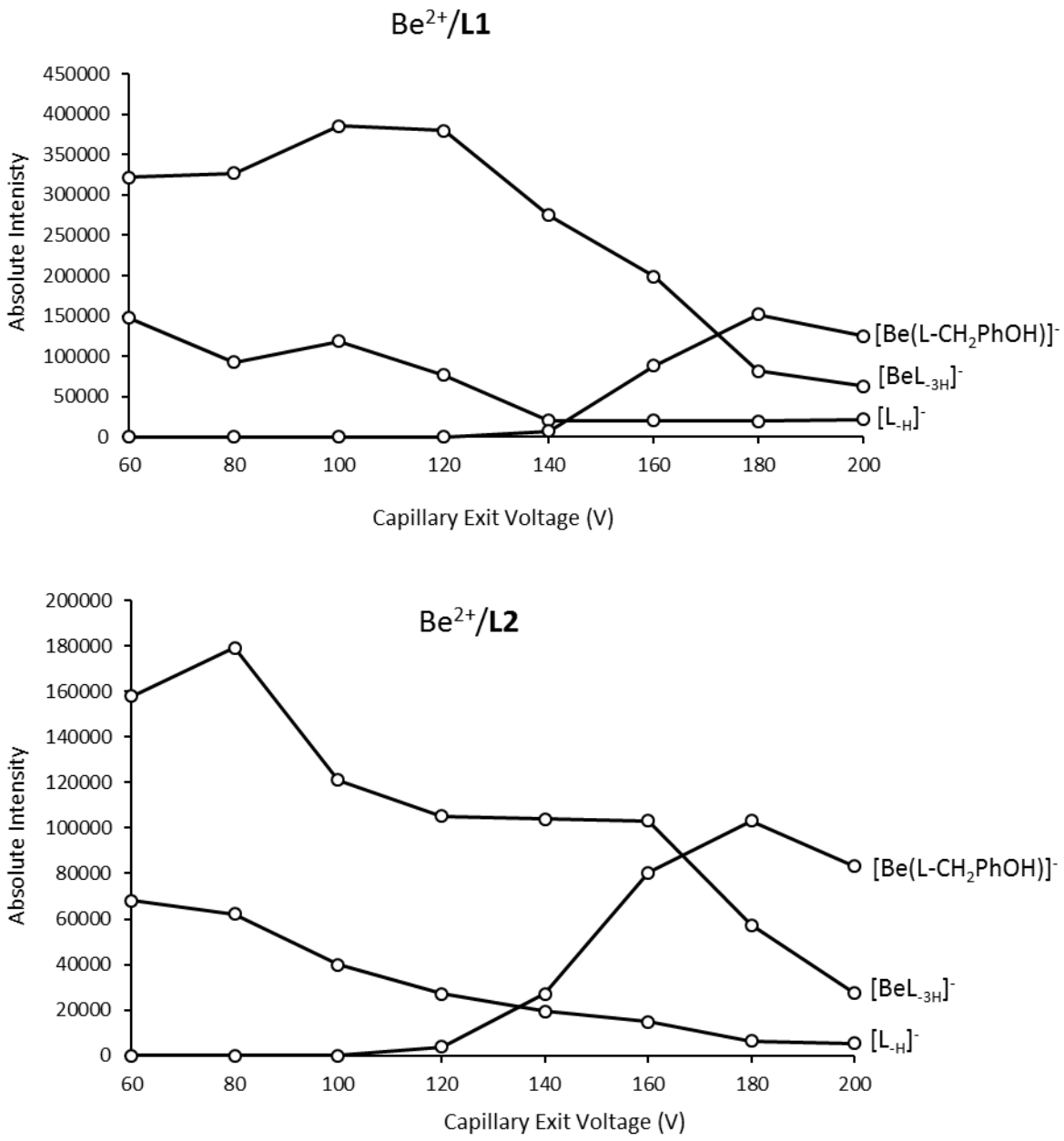

Figure 5-5 Influence of capillary exit voltages on the ionisation of the BeL complexes.

Further assessment of the representative $[BeL_{-3H}]^-$ ion signal in the ESI-MS spectra across the pH range of 2.5-8.5 reveals that the encapsulation of Be^{2+} is pH dependent and the $[BeL_{-3H}]^-$ complexes were hardly formed at acidic pH. Rather, complexation of beryllium is optimized between pH values of 6.5-7.9 as shown in Figure 5-6. Understandably, the ligands which would be poorly deprotonated in acidic media were preferentially ionized in the ESI-MS revealing ions corresponding to the hydrogen sulfate adduct with the free ligands $[L+HSO_4]^-$ at *m/z* 443 for **L1**, *m/z* 440 **L2**, and *m/z* 463 for **L3** respectively. For the $[BeNTP]^-$

complex in solution prominent signals corresponding to the $[BeL_{-3H}]^-$ ESI-MS ion only appeared at pH 4.5 and increased steadily until its highest absolute intensity at pH 6.9 while further increase in pH up to 7.9 resulted in the diminishing of the $[BeL_{-3H}]^-$ signal absolute intensity in good agreement with the potentiometric titration of the Be-NTP system which found pH 6.5 to be the optimal pH for the complexation of beryllium by NTP.[10] Although the inherent droplet shrinkage during the electrospray process in the ESI-MS technique can in some cases induce equilibrium shifts in metal-ligand reactions,[25, 26] potentiometric investigation of the related Be-NTP system suggest high stability involving slow kinetic equilibrium changes which have been shown to be well monitored using the ESI-MS technique.[10] ESI-MS of equimolar solution mixtures of beryllium sulfate and ligands **L1-L3** at various pHs have also revealed similar pH dependence although the $[BeL_{-3H}]^-$ complex is more strongly formed across a much wider pH range in comparison to NTP and NTA.

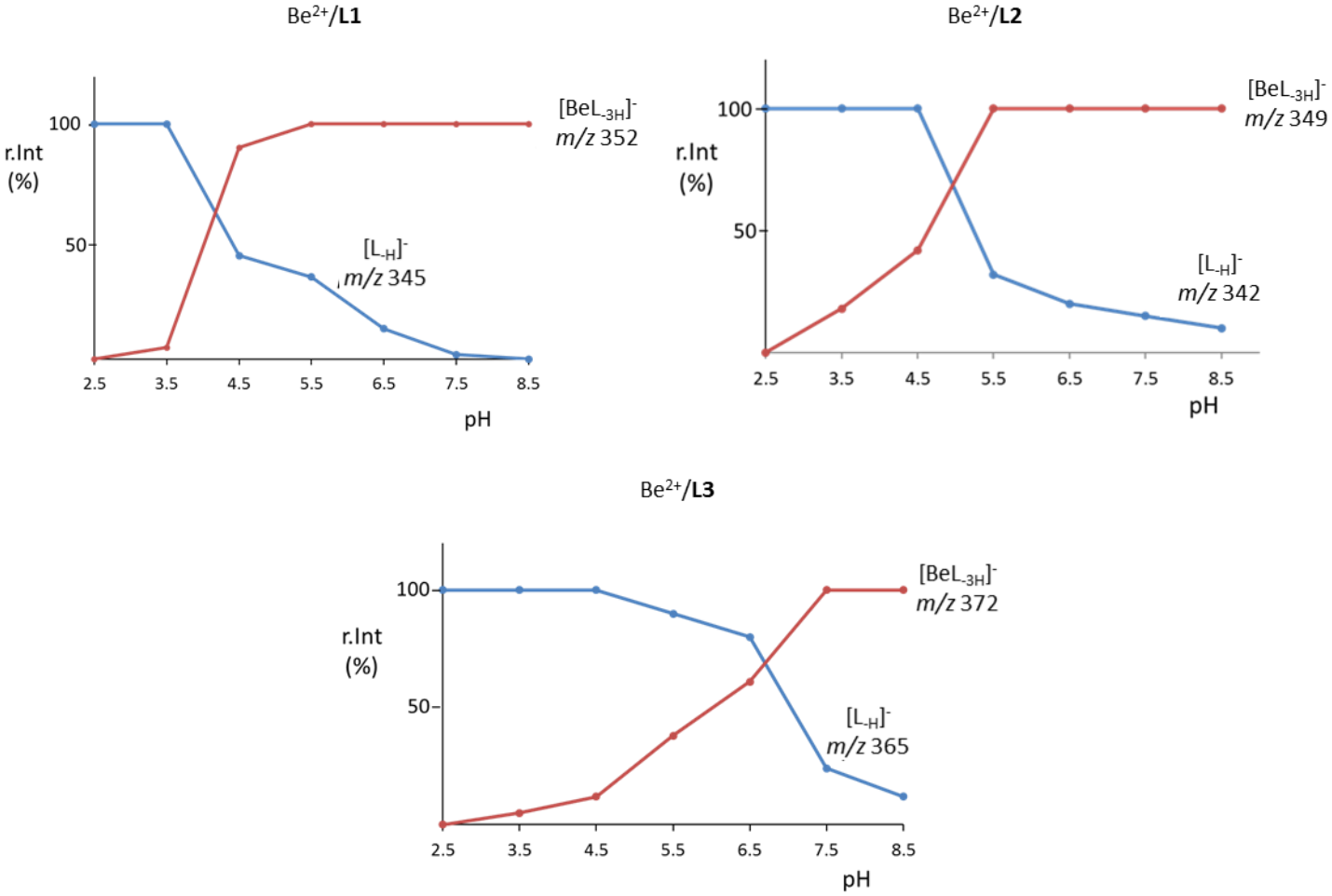

Figure 5-6 Influence of pH in solution on the ionisation of the BeL complexes.

5.2.5 Competitive interactions of ligands towards the encapsulation of the Be^{2+} cation

5.2.5.1 NTP vs NTA

Having obtained representative qualitative data of beryllium complexes in solution, the ability of the ESI-MS technique to quantitatively represent beryllium speciation was further assessed in order to identify relative binding affinity trends from the microscale screening of various beryllium-ligand systems. Firstly, an illustrative experiment to justify the potential of the ESI-MS technique in a ternary systems involving beryllium complexes is considered by employing the well-described Be-NTP and NTA systems. Having observed similar ionisation efficiency of 1/0.94 for the ESI-MS signal intensities of $[NTA]^-/[NTP]^-$ from the ESI-MS spectra of equimolar mixtures of both ligands in the negative ion mode, the corresponding ion intensities of their respective complexes can be expected to be approximately the same, enabling direct monitoring of beryllium chelation in a Be/NTA:NTP ternary system. The relative intensity behaviour of signals corresponding to the free ligands and BeL complexes in an ESI-MS experiment with Be-NTA/NTP at increasing NTA/NTP mole ratio from 1:0.125 to 1:1 according to Figure 5-7 shows the expected metal-ligand exchange reactions. Based on their formation constants the beryllium complex of NTP (log *k* 9.2), is expected to be more stable compared to NTA (log *k* 6.8). As a result, the latter will be progressively displaced by the coordination of NTP to the beryllium ion. Accordingly, the addition of NTP to a well-equilibrated solution mixture of beryllium sulfate and NTA results in the decrease of the $[BeNTA]^-$ signal while the subsequent complexation by the stronger donor (NTP) increasingly show more intense $[BeNTP]^-$ signal in accordance with the binding affinity of both ligands for beryllium. Also, the ability of ESI-MS in the study of ternary systems is also of benefit in the investigation of ligand selectivity for Be^{2+} and potential interfering cations such as Mg^{2+}. For instance, ESI-MS of a Mg-NTA/NTP ternary system with limited Mg^{2+} shows that the NTA ligands bind Mg^{2+} ahead of NTP thus the corresponding signal due to the $[MgNTA]^-$, $[MgNTP]^-$ ions at *m/z* 212 and 254 have relative abundances of 40% and 5% respectively. Upon the addition of Be^{2+} to the system, the NTP ligand solely complexes with beryllium revealing a corresponding signal at *m/z* 239 while the $[MgNTA]^-$ signal diminishes only slightly. This is again

consistent with results from potentiometric titration which have shown that NTP is capable of the selective uptake of beryllium in the presence of the Mg^{2+} cation.[10]

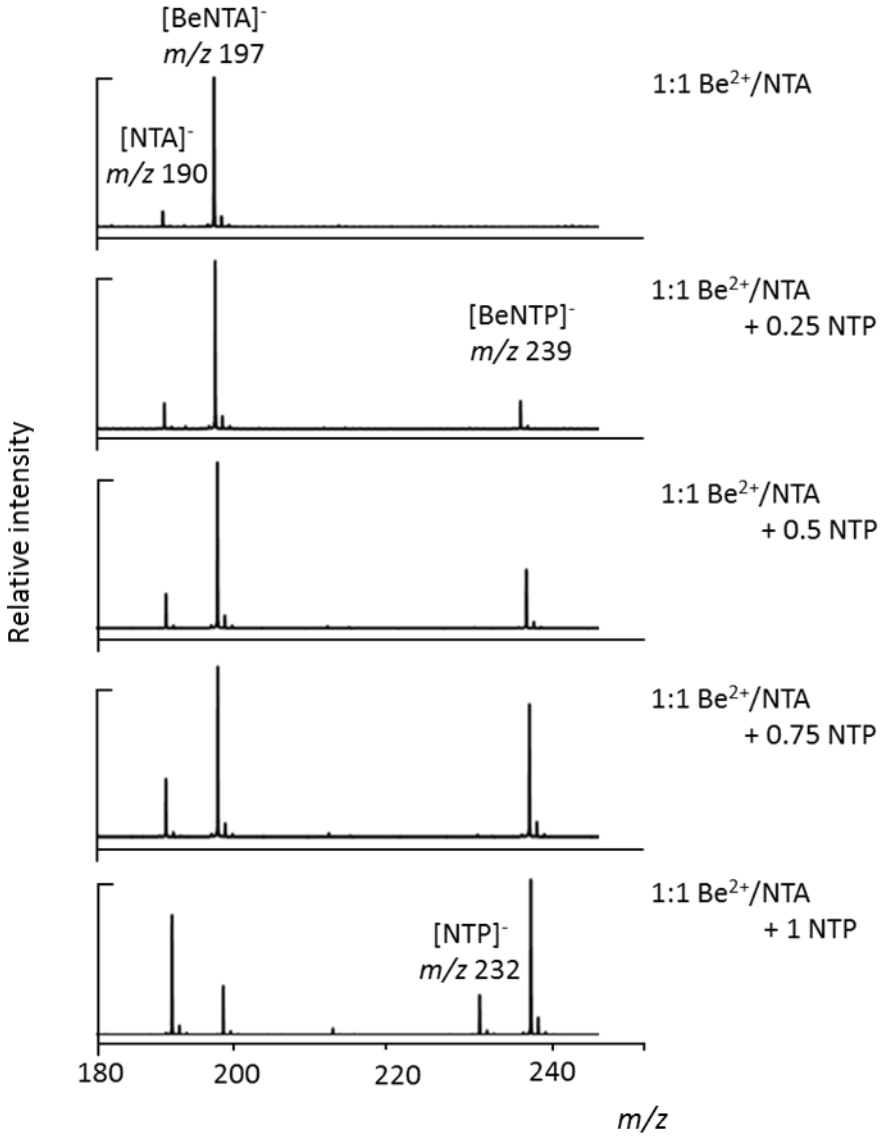

Figure 5-7 Negative ESI mass spectra of a ternary system comprising of 2.2 x 10^{-3} mol L^{-1} aqueous beryllium sulfate solutions and 2.2 x 10^{-3} mol L^{-1} methanol solutions of NTA with varying amounts of NTP.

5.2.5.2 Ligands L1-L3

Preliminary screening of equimolar concentrations of the ligands **L1-L3** showed varying ESI response for their corresponding ESI-MS signals $[L_{-H}]^-$ in the order **L3**>**L2**>**L1** which was clearly due to the differences in substituent groups. The implication of this observation is that unlike the NTA/NTP system, the $[BeL_{-3H}]^-$ complexes for ligands **L1-L3** will be sufficiently different such that a direct ternary investigation of the relative binding affinity of these ligands towards beryllium as achieved between the NTP and NTA would be inappropriate. A more

rigorous quantitative assessment of ion signal intensities would require adding a fixed concentration of a reference compound in all ESI-MS experiments from which ion signal intensities are standardized. In the present experiments, the following are conditions for a suitable reference compound to standardize the ion intensity:

i) The ligands must not have appreciable affinity for beryllium in a way that disturbs the $[BeL_{-3H}]^-$ equilibrium in solution

ii) The ligand must ionize in the same ESI-MS ion mode of investigation

iii) The ligand should be structurally similar to the ligands in solution such that both ligands would possess a approximately similar but not 100% exact ESI-MS ion response

A suitable reference investigated was the tetraphenylborate anion because it is expected to show no interaction with beryllium in solution and possess similar phenyl rings as ligand **L1**-**L3**. Unfortunately, a suitably linear calibration curve could not be obtained within the working concentration range for the beryllium experiments. Therefore other strategies were developed to identify binding trends from the ESI mass spectra. This involved the incorporation of a competitively binding ligand in a strategy initially proposed by Brodbelt and co-workers[27] while the second technique was to generally assess the relative formation of the $[BeL_{-3H}]^-$ complexes as reflected by the $[BeL_{-3H}]^-$ /$[L_{-H}]^-$ relative intensity ratio with increasing metal concentration in a series of ESI-MS experiments shown in Figure 5-8.

Valuable information on the relative binding affinity trends among the ligands **L1**-**L3** can be obtained from individual ESI-MS investigation of solution mixtures of Be^{2+}/ligand in molar ratios from 0.25 to 1. Following the electrospray ionisation behaviour of the $[L_{-H}]^-$ and $[BeL_{-3H}]^-$ ion signals, as revealed in Figure 5-8, with increasing molar ratio of the Be^{2+} cation, the BeL complex for the ligand **L1** appears to be formed most strongly in comparison to the other ligands. However, for the ligand **L3**, the $[L_{-H}]^-$ and $[BeL_{-3H}]^-$ ion signals reveal a relatively high abundance of the free ligands in solution even at a 1:1 metal ligand mole ratio. Additionally, this is more clearly illustrated as a comparison of the $[BeL_{-3H}]^-/[L_{-H}]$ relative intensity ratio for ligand **L1**-**L3** shown in Figure 5-9a. From these data the order of formation of the BeL complexes in solution is suggested as **L1**>**L2**>**L3**

which is consistent with the binding preference for beryllium complexation wherein 6 membered chelate rings as formed by **L1** are more stable than five membered chelate rings (as formed by **L2**, **L3**). However, it should be noted that the difference in these trends is expected to be very small as has been observed between the nitrilotripropionic acid (NTP) and nitriloaceticdipropionic acid (NTA).

To further examine this trend, the displacement of beryllium from the respective BeL complexes by the NTP ligand was investigated in a competitive type assessment.[27] Addition of NTP to a well-equilibrated solution of Be^{2+} ion and the individual ligands **L1**-**L3** in equimolar proportions results in the displacement of the Be^{2+} cation and can be directly observed as a diminution of the $[BeL_{-3H}]^-$ ion signal of the BeL complexes in the ESI mass spectra. Figure 5-9b displays the $[BeL_{-3H}]^-/[L_{-H}]$ relative intensity ratio for ligand **L1**-**L3** upon the addition of NTP.

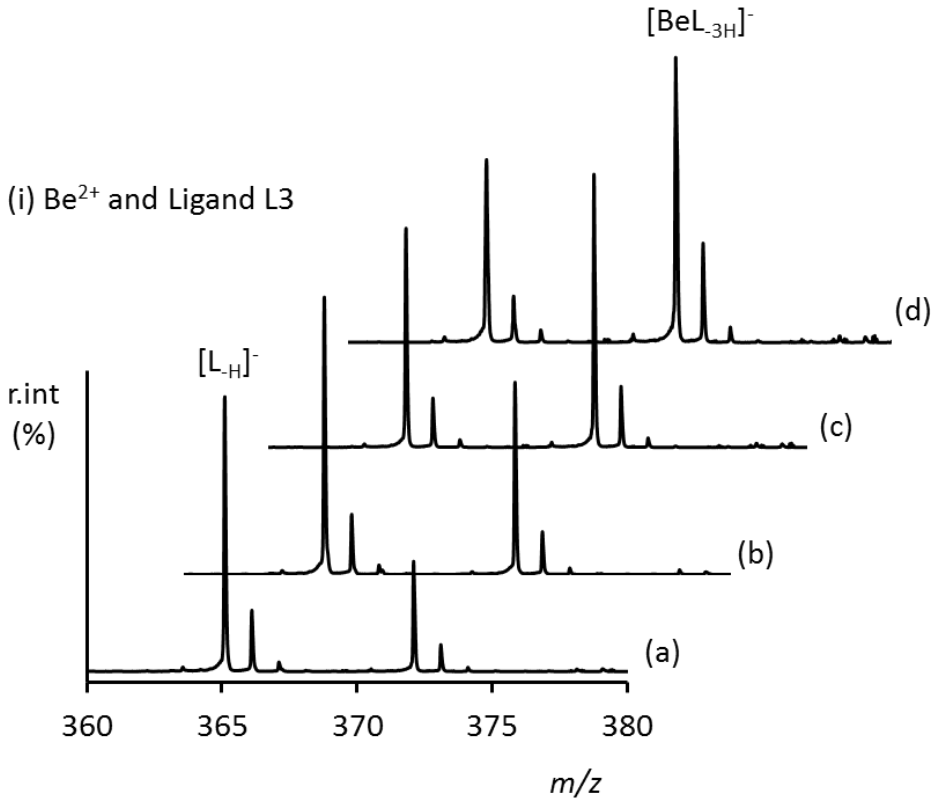

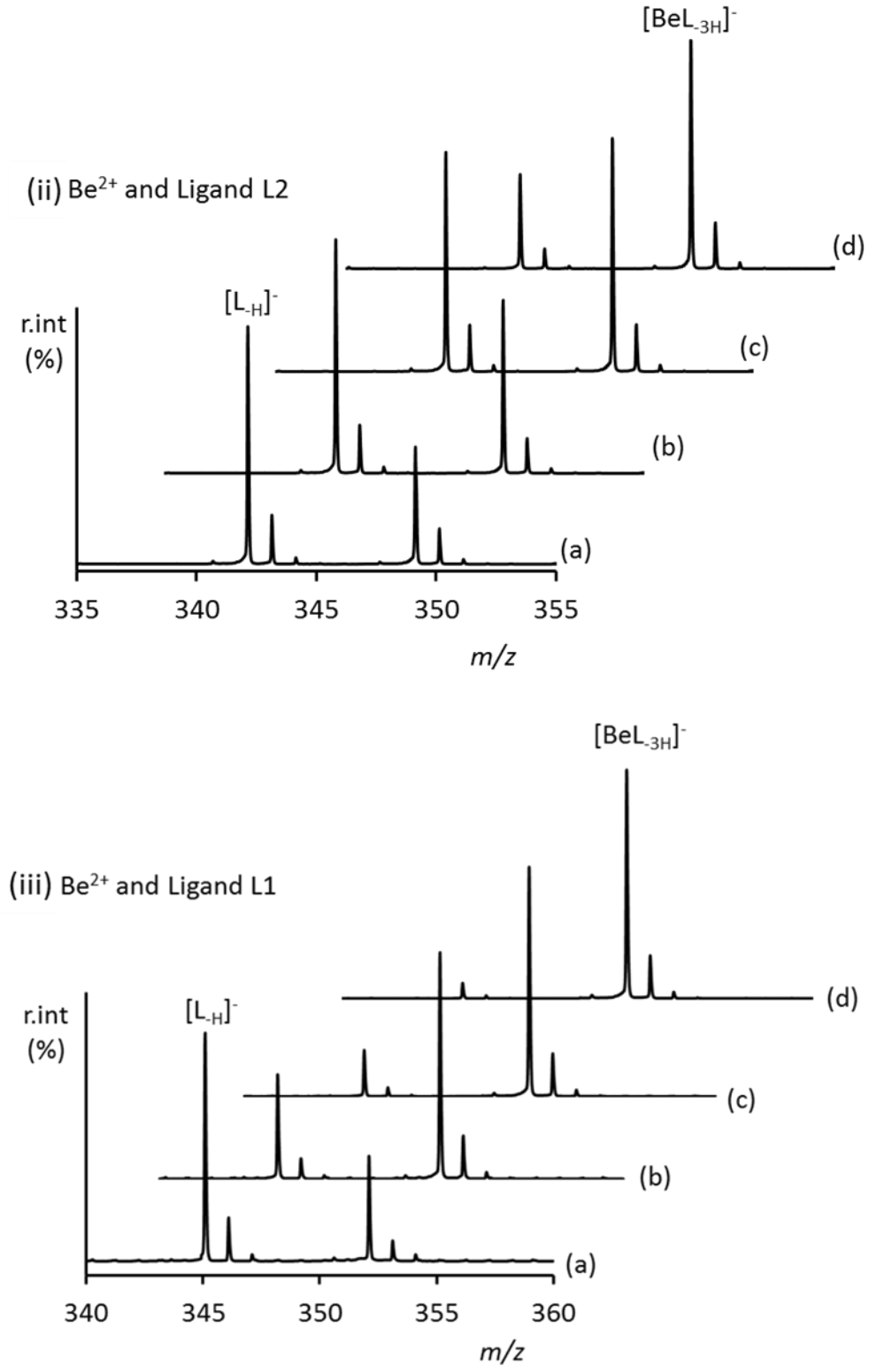

Figure 5-8 Negative ESI mass spectra of $BeSO_4$ and (i) **L3** (ii) **L2** (iii) **L1** in methanol-water and capillary exit voltage of 80 V at different Be^{2+} / L molar mixtures of (a) 0.25 (b) 0.5 (c) 0.75 (d) 1.

Again the trend in Figure 5-9b supports the previously established binding affinity trend of **L1**>**L2**>**L3** in solution. However, it was also observed that perhaps due to

the rigidity of the pendant arm in **L3**, the ligand was more successful in shielding the Be^{2+} cation from exchange with NTP in comparison with **L1** and **L2** which reveal a more significant change in the $[BeL]^-/[L\text{-}_H]$ relative intensity ratio between the Be-L system and the **L1-L3** and NTP ternary system.

(a)

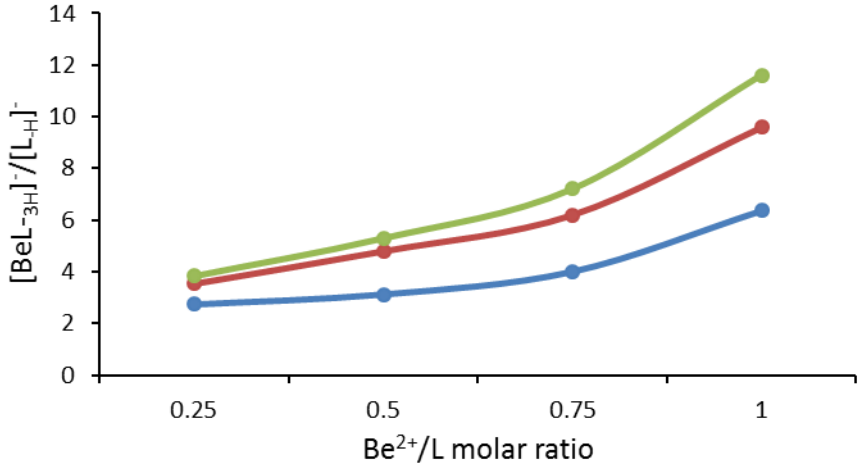

(b)

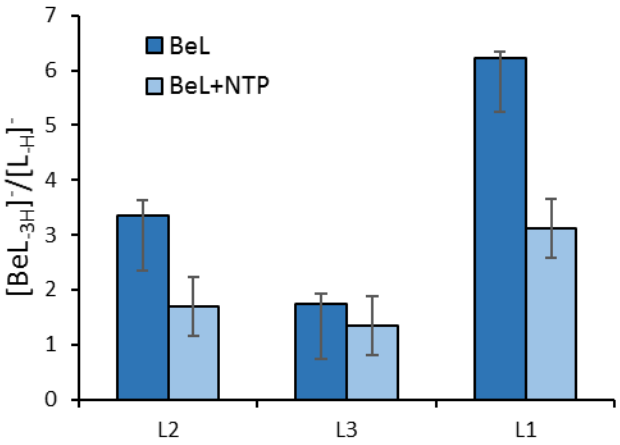

Figure 5-9 Ion signal intensity ratio of the $[BeL_{-3H}]^-$ complex and the free ligands $[L_{-H}]^-$ in 2.2 x 10^{-3} mol L^{-1} aqueous beryllium sulfate solutions and 2.2 x 10^{-3} mol L^{-1} methanol solutions of ligands **L1-L3** (a) as a function of Be^{2+}/Ligand ratio (b) with 1 molar equivalent of NTP ligand.

In biological systems, the complexation of beryllium will be in competition with endogenous metal binding agents such as citrate and amino acids in proteins. Since these binding sites will exist in high abundance in the natural systems the purpose of chelation therapy is to maximize the stability and selectivity of ligands towards a desired metal cation over biological binding sites. Therefore, changes in the ESI-MS ion signal of the free ligand and the beryllium complex with the addition of citrate were evaluated for the ligand NTA, NTP and **L1-L3**. In view of

the ESI-MS behaviour of beryllium citrate which reveals several peaks in the mass spectra (see Chapter 3), the effect of citrate on the stability of the beryllium complex formed by these ligands were best monitored indirectly. Due to the strong chelating ability of citrate for beryllium ion, the citrate ligand almost completely extracts the encapsulated Be^{2+} cation from the beryllium complexes with the ligands **L1-L3**, NTP and NTA. This is significant as it points out the poor performance of polyaminocarboxylates in general as chelating agents in a biological environment. Nevertheless, from this ternary system, the binding affinity trends among these ligands NTA, NTP and **L1-L3** is evident (see Figure 5-10).

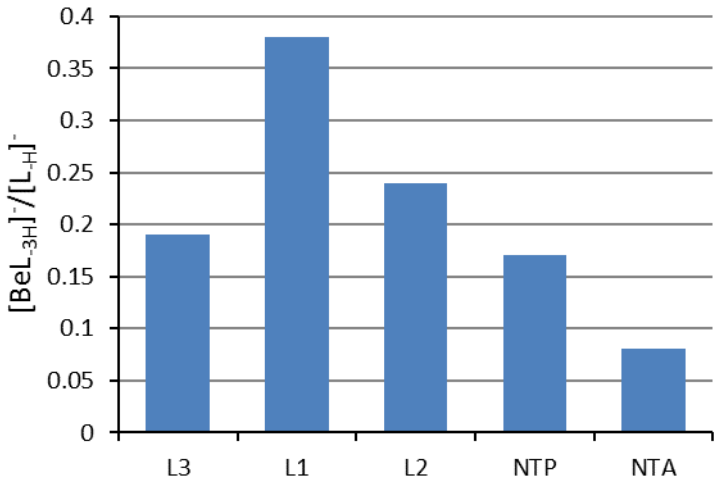

Figure 5-10 Ion signal intensity ratio of the $[BeL_{-3H}]^-$ complex and the free ligands $[L_{-H}]^-$ in 2.2 x 10^{-3} mol L^{-1} aqueous beryllium sulfate solutions and 2.2 x 10^{-3} mol L^{-1} methanol solutions of ligands NTA, NTP and **L1-L3** with 1 molar equivalent of citrate.

Addition of the citrate ligands to a pre-equilibrated 1:1 mixture of beryllium sulfate and individual ligands NTA, NTP, **L1-L3** in solution to obtain a metal/ligand/citrate ratio of 1:1:1 reveals that the previously intense $[BeL_{-3H}]^-$ ion signal (see Table 5-2) is largely diminished while the signal of the free ligand intensifies. However, a closer look at the relative interference of the citrate ligand on the $[BeL_{-3H}]^-$ ion signal for L = **L1-L3**, NTA, NTP shown in Figure 5-10 suggest the relative binding affinity trend to be **L1**>**L2**>**L3**>**NTP**>**NTA**. These data is also in accordance with the affinity of NTA and NTP for beryllium determined by potentiometric titration.[15] Therefore from these relative binding trends, it can be inferred that the absolute binding affinity of these ligand **L1-L3** would lie somewhere above the binding affinity of NTP but certainly below the log *k* value of the citrate.

5.2.5.3 Exchange reactions of $[BeL]^-$ complexes with metal ions (Al^{3+}, Co^{2+}, Zn^{2+} and Mg^{2+})

The selectivity of the ligands **L1-L3** for Be^{2+} in the presence of potentially interfering cations including Zn^{2+}, Co^{2+}, Cu^{2+}, Mg^{2+}, and Al^{3+} were measured. Besides the divalency of most of the selected cations, these ions were chosen because of most of them (apart from Mg^{2+}) can adopt tetrahedral coordination geometry easily. It is also important to point out that the toxicity route of the beryllium ions in the body could as well be through the ability of Be^{2+} cation to displace some of these ions essential to the body functions. For instance, beryllium is capable of inhibiting enzymes which require the Mg^{2+} cation to function.[28] The metal exchange in solution was followed by monitoring the $[BeL_{-3H}]^-/[L_{-H}]^-$ relative intensity ratio to provide an insight into the desired relative trend. A summary of the ESI-MS data on the exchange reactions of the corresponding $[BeL_{-3H}]^-$ complexes for **L1-L3** with Zn^{2+}, Co^{2+}, Cu^{2+}, Mg^{2+} and Al^{3+} are shown in Figure 5-11. The ESI-MS experiments of the ternary systems comprising of Be^{2+}/ligand and M^{2+} in equimolar ratio reveal only insignificant peaks corresponding to the $[ML_{-3H}]^-$ species for M=Zn^{2+}, Co^{2+}, Cu^{2+}. Also, additional species corresponding to the $[ML(CH_3CN)]^-$ and $[ML(CH_3OH)]^-$ ions were observed for M^{2+} = Zn^{2+}, Co^{2+}, Cu^{2+} and L = **L1-L3**.

According to Figure 5-11, the ligands **L1** and **L2** showed fairly similar trends in the interference of the $[BeL_{-3H}]^-$ ion signal by the larger cations such as Zn^{2+}, Co^{2+}, Cu^{2+}. The addition of these interfering cations revealed only slight disruption of the complexation of beryllium as is evident from the small reduction in the $[BeL]^-/[L_{-H}]^-$ relative intensity ratio. In contrast, **L3** appeared to be the least beryllium selective ligand of the three as it also showed good complexation to the Mg^{2+} cation which resulted in the diminishing of the $[BeL]^-/[L_{-H}]^-$ relative intensity ratio as magnesium complexes were formed. This is also consistent with potentiometric results which have shown six-member chelate ring formation to be a key factor in discriminating Be^{2+} from the Mg^{2+} cation.[10] Furthermore, ESI results shows that beryllium complexation by the ligand **L3** is reasonably impeded in the presence of Cu^{2+} ions.

Furthermore, all the ligands **L1-L3** revealed poor performance in distinguishing Al^{3+} from beryllium ion in solution as reflected by the strongly diminished $[BeL]^-/[L_{-H}]^-$ ratio upon the addition of Al^{3+}. The closely related

chemical properties of aluminium and beryllium is a major challenge encountered in the chemistry of beryllium since the early days of the periodic table, noting that beryllium was once erroneously placed above aluminium among the group 13 elements (in place of boron) due to its remarkable chemical similarity with aluminium. In the field of coordination chemistry, this diagonal relationship between both elements often results in unsuccessful chelation of beryllium ions ahead of the Al^{3+} cation such that no beryllium specific chelator is yet known to bind beryllium selectively in the presence of interfering Al^{3+} ion. However, a few unique and very interesting examples exist in which the subtle differences between the Be^{2+} and the Al^{3+} results in outstanding differences in the interactions of both metals with ligands. Two of such examples include beryllium's interaction with EDTA and the yet unidentified binding site in the body which results in chronic beryllium disease. While the actual mechanism and the elusive binding site involved in the beryllium toxicity route in the body is unknown, it is obvious that such a ligand successfully distinguishes beryllium from aluminium ions since similar exposure to aluminium in any quantity whatsoever does not trigger the escalating immune response as observed in the case of beryllium. On the other hand, the factors which contribute to the dramatic difference in binding affinity of the EDTA for Al^{3+} (log k =18) and Be^{2+} (log k =6) is less abstruse. This is can be related to the capability of the EDTA to support octahedral geometry to the extent that fitting in a small tetrahedral cation such as beryllium destabilizes any resultant complex ion formed. Since the structure of the $[BeNTP]^-$ complex in the solid state suggests a closely knit tetrahedral binding pocket for beryllium, it was expected that reinforcing the pendant arms in related ligands such as **L1-L3** would strengthen these ligands' selectivity for beryllium. However, ESI-MS data have shown that while a selectivity over larger was achieved, Al^{3+} could still not be reliably distinguished from Be^{2+}. Noteworthy is the fact that a similarly good interaction between NTA with the Al^{3+} cation has also been reported elsewhere from ESI mass spectra wherein a dominant $[Al(F)NTA]^-$ ion at *m/z* 234 was observed.[29] Nevertheless, the relatively poor complexation of beryllium by EDTA in comparison to aluminium has found useful applications. For instance, with EDTA being able to strongly bind Al^{3+} and other interfering ions but not Be^{2+}, the current strategy employed to selectively complex beryllium is to remove the Al^{3+} or any

expected interfering ion with EDTA prior to beryllium chelation by beryllium complexing ligands.

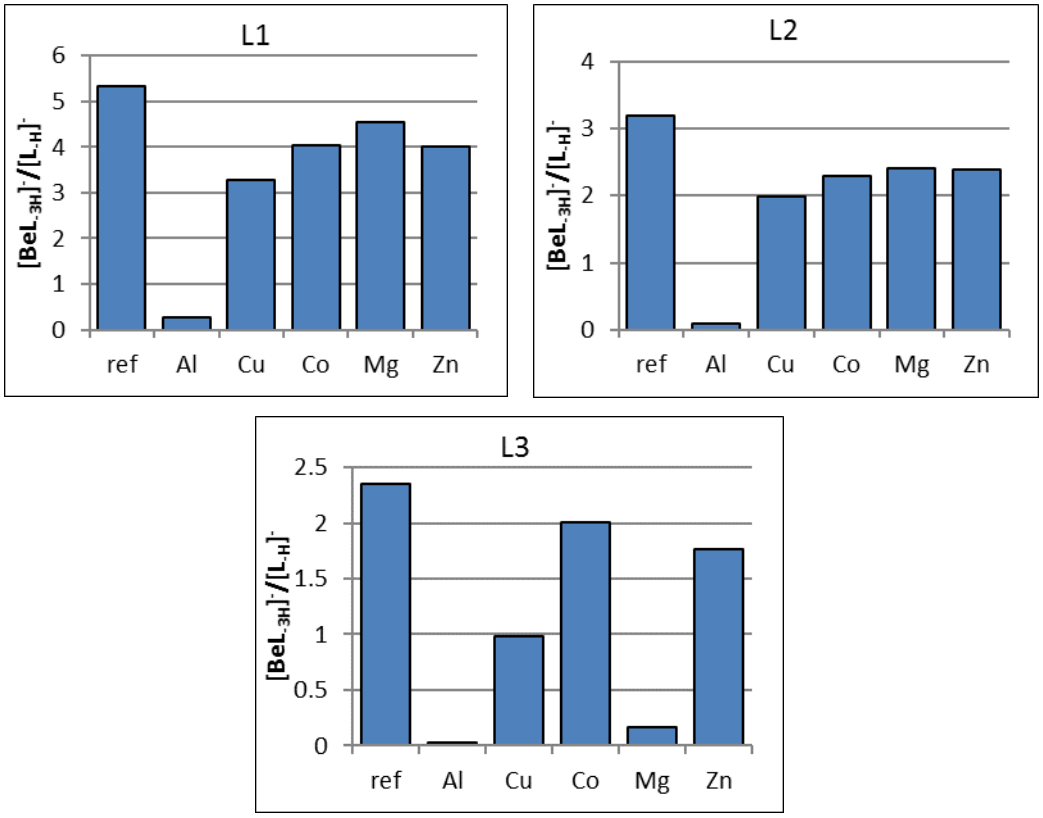

Figure 5-11 Ion signal intensity ratio of the BeL complex and the free ligands in solution for ligands NTA, NTA and **L1**-**L3** in the presence of interfering metal cations

More importantly, this representation of exchange processes in solution in a simple mass spectrum is of immeasurable potential for the rapid microscale screening of ligands of interest toward beryllium complexation prior to macroscale characterisation which require the isolation of solids. Evident from the trial experiments above, ESI-MS can further provide valuable and insightful quantitative data on the abundance in solution. Although the treatment of these data is simplistic and straightforward, its combination with previously established data on beryllium speciation with NTP and NTA as reference systems shows profound insight into the ESI-MS behaviour and binding affinity trends for the new set of ligands (**L1**-**L5**). Moreover, the restriction of the data analysis and subsequent deduction to relative binding trends clearly eliminates the well-known shortcoming of ESI-MS, namely signal quantitation and ion suppression problems. Nevertheless a major assumption in this study is that the ESI-MS ion response of the free ligand ion [L-

$_H]^-$ and the beryllium complex $[BeL_{-3H}]^-$ would be very similar. This is a safe approximation since at a relatively basic solution, both species are monoanionic differing only in by the coordination of a metal cation and the trend in binding affinity from such a ternary system are well-known.[30, 31]

5.2.5.4 ESI-MS study of the interactions of DTPA with beryllium ion

As a result of its sequestering effects, the diethylenetriaminepentaacetic acid (DTPA) like other polyaminocarboxylic acids is an important ligand in the chelation of metal ions and its medical applications are well developed such as its use in the removal of plutonium and other actinides from the body.[9] Given the effective applications of this ligand in biological systems, extensive ESI-MS investigation has been carried out on its complexes with the beryllium ion in solution especially the effect of potential interfering cations. Generally, DTPA is preferentially administered as its calcium or zinc salt to counteract resultant depletion of essential metal ions since the calcium or zinc ions are released, as the metal ion of interest in chelated.[9]

Negative ion ESI mass spectra were recorded at a range of low, medium, and high capillary exit voltages for mixtures of $BeSO_4$ and DTPA in the molar ratios 1:1, 1:2 and 1:3 in methanol-water solution at a pH of 5.9. Due to the acidic groups, the DTPA is expected to form anionic beryllium complexes in solution which will ionise more appropriately in the negative ion mode. Illustrative mass spectra for mixtures of $BeSO_4$ and DTPA at various metal-ligand molar ratios are shown in Figure 5-12. The spectra reveal prominent ion signals at *m/z* 195, 199, 392, and 399 which have been assigned as $[L_{-H}]^-$, $[L_{-2H}]^{2-}$, $[BeL_{-3H}]^-$ and $[BeL_{-4H}]^{2-}$ respectively. The latter two species correspond to a 1:1 metal/ligand stoichiometry in solution differing only in their charge state. Hence adjacent peaks in the isotopic pattern corresponding to the ion at *m/z* 199 are separated by 0.5 *m/z* consistent with the assigned double charge on the ion. Though the nature of the beryllium interaction with DTPA cannot be confirmed from mass spectral data, ESI-MS results tend to suggest that the DTPA ligand coordinates to the beryllium ion in a tetradentate fashion thereby excluding the solvent or hydroxido ligands as with the other polyaminocarboxylates. Nevertheless, the observation of the ion at *m/z* 406 assigned as $[Be_2L_{-5H}]^-$, suggest that other bonding modes and stoichiometry persist in solution. The ions intensity signal of the dinuclear $[Be_2L_{-5H}]^-$ species at *m/z* 406

tends to increase steadily on going from a metal/ligand molar ratio of 1:1 to 3:1 which signifies that the ligand can possibly coordinate several beryllium ions particularly at high metal concentrations. This is further illustrated with the detection of a $[Be_3OL_{-5H}]^-$ species at *m/z* 431. At elevated capillary exit voltages, the $[BeL_{-3H}]^-$ and $[BeL_{-4H}]^{2-}$ species at *m/z* 199 and 399 fragment by the loss of by a carboxylate group to signals corresponding to $[BeL_{-4H}\text{-}COOH]^-$ and $[BeL_{-3H}\text{-}COOH]^{2-}$ at *m/z* 177 and 355 respectively.

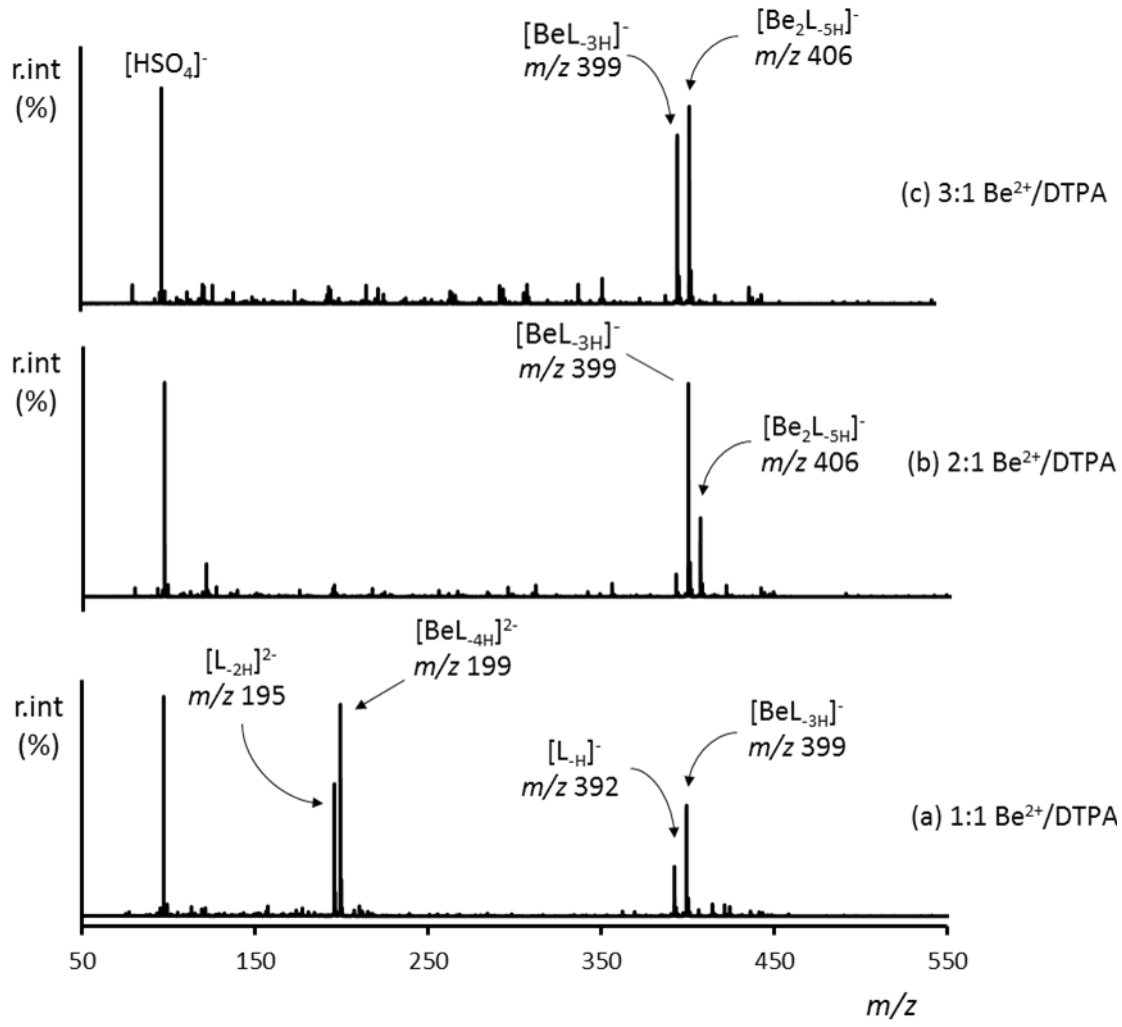

Figure 5-12 Negative ion ESI mass spectra of $BeSO_4$ and DTPA in methanol-water solution at a capillary exit of 60 V and pH 5.9 for Be^{2+}/L ratio of (a) 1:1 (b) 2:1 (c) 3:1.

Furthermore, the interaction of DTPA with beryllium in the presence of another cation was investigated in consecutive ESI-MS experiments of ternary system consisting of 1:1 Be^{2+}/DTPA with added metal cation M=Zn^{2+}, Co^{2+}, Cu^{2+}, Mg^{2+}, Al^{3+}. In these experiments, ESI-MS ion signal intensities were compared

directly because it has been previously observed that with large ligands such as DTPA, the effect of the metal cations on the electrospray efficiency are expected to be negligible (see section 5.2.5.1). As displayed in Figure 5-13, Al^{3+} and Mg^{2+} cations strongly interfered with formation of the beryllium complexes in solution which is signified by the prominently observed signal of the corresponding metal complex. The Al^{3+} cation in particular displaces all beryllium, forming two signals at *m/z* 416 and 441 corresponding to $[AlL_{-5H}]^-$ and $[AlBeOL_{-5H}]^-$. Generally, the additional ESI-MS ions detected in the presence of other cations include the $[ML_{-H}]^-$ for Cu^{2+} *m/z* 453, Co^{2+} *m/z* 449, and Zn^{2+} *m/z* 454 (see Figure 5-13).

It is evident from these results that the DTPA shows good interaction with beryllium even in the presence of transition metal ions such as copper and zinc although other ions including aluminium and magnesium appear to successfully compete more favourably with beryllium ion toward binding of the DTPA ligand. However, this situation presents an improvement over the analogous EDTA which is popularly known to ligate beryllium poorly in comparison to other ions. Clearly, this is not unrelated to their difference in structural arrangement of donor atoms. The structure of DTPA comprises of an EDTA structure with an expanded 5 carbon chain possessing an iminoacetate group at a central position thereby making this ligand more suitable for the coordination of a tetrahedral cation but not finely tailored for the exclusion of larger cations. Based on this, attempts were made to design and synthesise additional ligating agents with a more suitable arrangement of donor atoms toward tetradentate coordinating cations such as the beryllium ion.

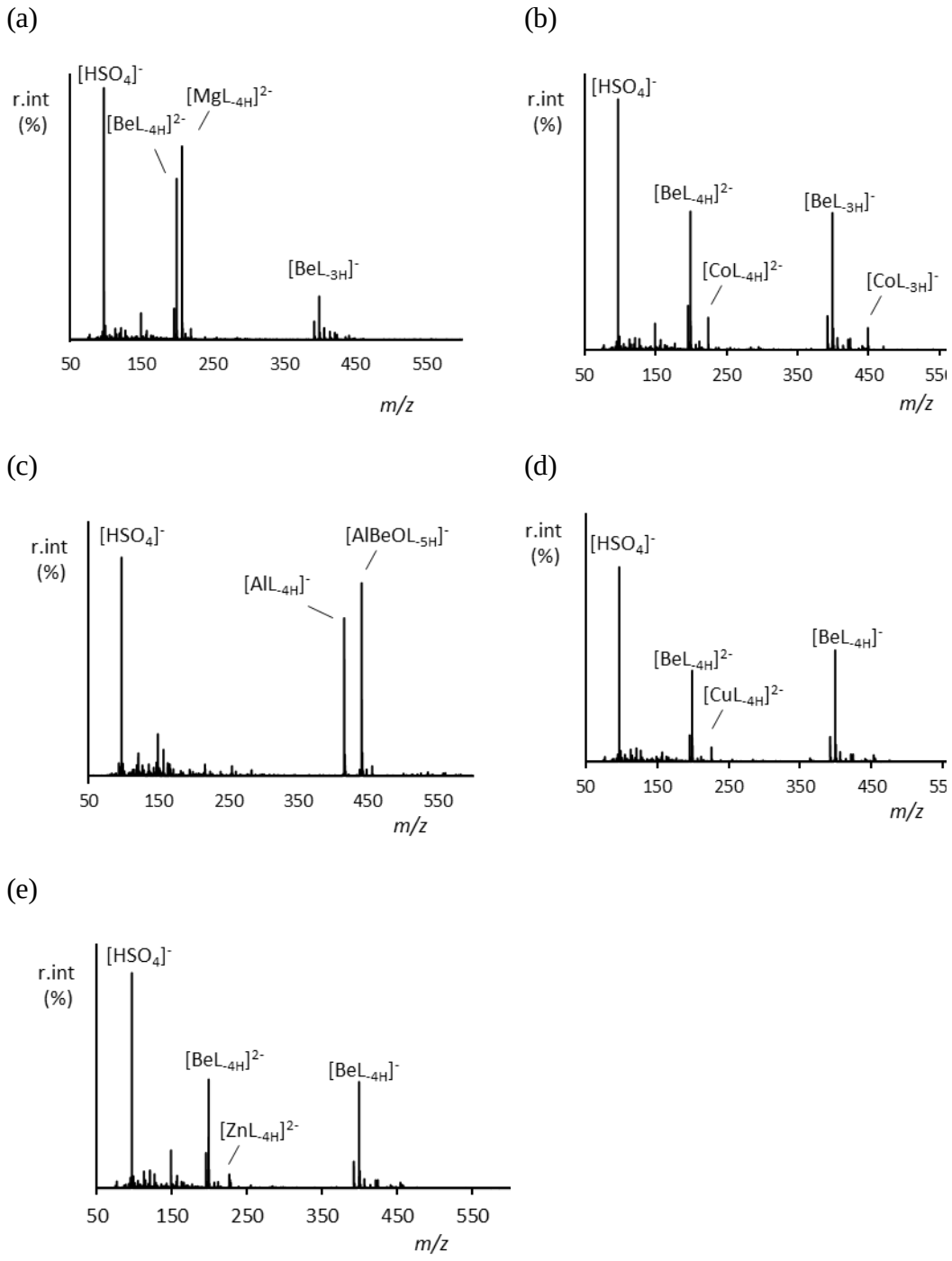

Figure 5-13 Negative ion ESI mass spectra of $BeSO_4$ and DTPA in methanol-water solution at capillary exit 60 V in the presence of interfering cations at Be^{2+}/M/L ratio of 1:1:1 for (a) Mg^{2+} (b) Co^{2+} (c) Al^{3+} (d) Cu^{2+} (e) Zn^{2+}

5.2.6 Design and synthesis of newly targeted tetradentate ligands L6 – L8 towards beryllium encapsulation

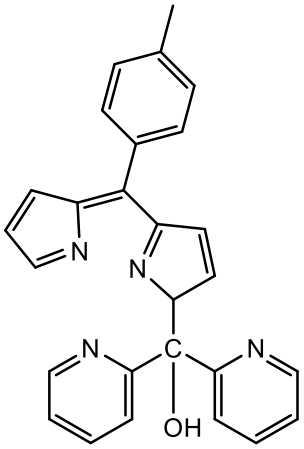

L6

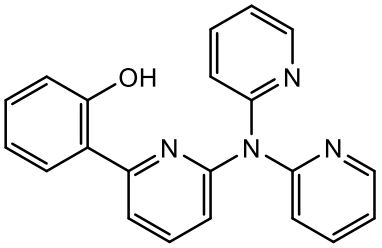

L7

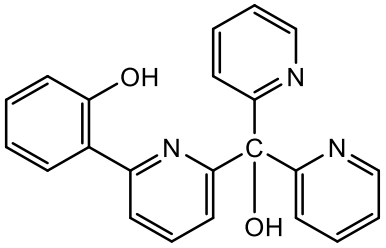

L8

Figure 5-14 Newly targeted tetradentate ligands for beryllium chelation

What is evident from the ESI-MS results so far in this thesis is the fact that achieving strong and perhaps more selective binding of beryllium is a demanding task requiring a careful consideration of the small size and high charge density of this metal ion which adopts tetrahedral geometry. While the unique properties of the Be^{2+} cation such as its small size and high charge density can ultimately be relied upon to discriminate the Be^{2+} ions from larger cations, it is not so helpful in distinguishing it from closely related metal cations such as Al^{3+} and Mg^{2+}. However, since the Al^{3+} and Mg^{2+} cations both prefer an octahedral geometry, a highly pre-organised and rigid tetrahedral arrangement of donor atoms would significantly improve such a new ligand's selectivity for beryllium. This is the overall aim of a tri-university collaborative research project of which this present PhD work is an integral part of. Based on these propositions, the tetradentate ligands outlined in Figure 5-14 were designed by incorporating a mixture of phenolate, carboxylic acid,

pyridine or imidazole donors around a substituted di-pyridyl scaffold to satisfy the requirements for the selective encapsulation of beryllium. Elsewhere, it has been indicated that ligands based around such substituted di-pyridyl group can guarantee a tetrahedral arrangement of donor atoms toward the chelation of metal cations.[16, 32] The encapsulation of beryllium in a tetrahedral pocket and 6-membered chelate rings provided by three pyridine nitrogen donor and a phenolic oxygen donor can be seen in Figure 5-15.

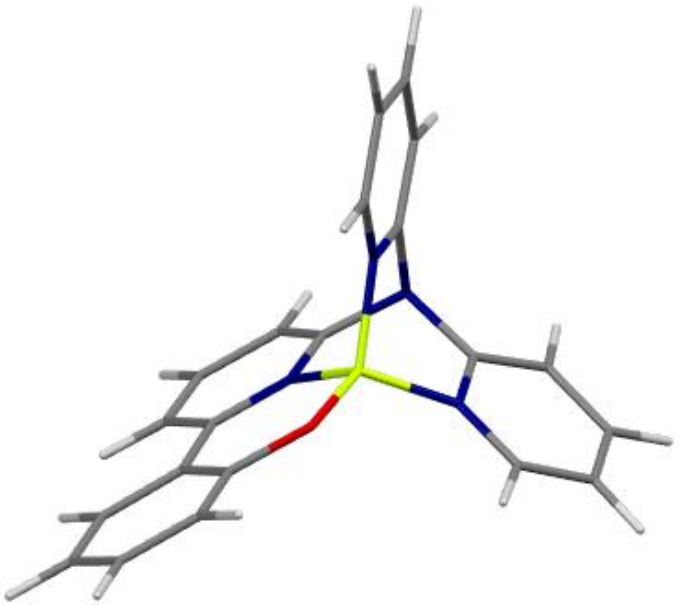

Figure 5-15 Geometric optimized structural illustration of the binding pocket for the ligand **L6** upon tetradentate encapsulation of the beryllium ion. (beryllium- green, nitrogen-blue, oxygen-red, carbon-grey, hydrogen-lighter grey)

Besides the requirement of a tetrahedral pocket and 6-membered chelate rings which were the main rationale for the development of these ligands, other features of interest can be readily incorporated into the ligands. In addition, the ligands feature a variety of monoanionic or dianionic groups resulting in beryllium complexes which will be either cationic or neutral respectively thereby enabling the binding of the complexes in a range of solvent media which is relevant for the selective extraction of beryllium as well as the ionisation process in the ESI MS technique. Further enhancements, such as the incorporation of sulfonic acid groups or other derivative R can also be targeted to impart aqueous solubility and luminescent properties. More so, the incorporation of hydrogen bond donors (and

potentially other non-hydrogen bonding groups) at the di-pyridyl scaffold pyridine groups will influence the size of the resulting binding pocket. Such groups will hydrogen bond with the N- or O-atom in the apical coordination site, creating an attractive interaction that will draw the three arms closer together, altering the coordination angles and size of the coordination pocket. This additional, outer-sphere interaction can be thought of as a buttress, further supporting the binding site and enhancing the strength of binding for a small cation. Similar outer-coordination sphere hydrogen-bonding effects have been explored for tuning the selectivity for copper in extractants for hydrometallurgic applications.[33]

The synthetic pathways to these ligands were designed and carried out by collaborators at the University of Auckland and Massey University. Although several more ligands have been targeted for synthesis, only the ligands L6-L8 were available as of the time of writing this thesis.

5.2.7 ESI-MS microscale screening of newly target tetradentate ligands (L6-L8)

The positive ESI mass spectrum of ligand **L6** revealed a peak at *m/z* 419 due to the species $[L+H]^+$ (100%) so confirming the synthesis and purity of this ligand. Other minor peaks observed include $[L+2H]^{2+}$and $[Cu(L_{-H})]^+$ at *m/z* 210 and 481 respectively. The latter involves a commonly observed phenomenon in ESI mass spectra whereby ligands pick up copper ion from the electrospray needle during the electrospray process especially under elevated ionisation conditions.[34] This is also a prescient of the ligand's preference to complex copper ion instead of beryllium ion as observed in Figure 5-16a. Under mild fragmentation, the $[L+H]^+$ ion undergoes a loss of water molecule to yield the peak $[(L+H)-H_2O]^+$ at *m/z* 401. ESI-MS experiment of 1:1 molar mixtures of beryllium sulfate and ligand **L6** in methanol showed signal of any beryllium complex. However, in the presence of excess Be^{2+} cation (metal/ligand ratio < 3:1), familiar beryllium hydroxide species peaks emerged. This reflects a poor binding of beryllium by this ligand perhaps due to a stronger affinity for a proton. Indeed, since ligand **L6** is an all nitrogen donor ligand, it is expected to compete less favourably for beryllium in the presence of water molecules. A similarly poor metal-ligand interaction was observed with aluminium and magnesium except for the observation of small peak (<10%)

corresponding to $[Al(OH)L_{-H}]^+$ at *m/z* 462. However, ESI-MS of 1:1 metal/ligand molar mixtures of ligands **L6** and metal cations M=Cu^{2+}, Co^{2+} and Zn^{2+} showed moderately intense peaks due to the corresponding $[ML_{-H}]^+$ ion indicating the **L6** ligand's preference for the larger size cations.

For ligand **L7**, preliminary ESI-MS screening immediately revealed that the ligand synthesised was not in fact the target ligand depicted in Figure 5-14 because the ESI-MS spectra revealed an isotope-rich signal at *m/z* 342. Further attempts to rationalise the actual product from ESI-MS data alone was frustratingly futile as this experimental *m/z* was in disagreement with the beryllium complexes expected in solution. Nevertheless, the successful crystallisation of a beryllium complex from the solution mixtures of this ligand with beryllium chloride (see Section 5.2.11) provided insight for the assignment of the ESI-MS ion at *m/z* 342. On the other hand, the targeted ligand **L8** was synthesised successfully albeit with a major side product (for the ion assigned as $[L+BOH]^+$) suspected to be a boron compound due to the boron isotope pattern as shown in Figure 5-16b. Meanwhile complexation of this ligand with beryllium revealed the $[BeL_{-H}]$ signal at *m/z* 348 (see Figure 5-16b) pointing out the suitability of this ligand for more beryllium experimentation if purified.

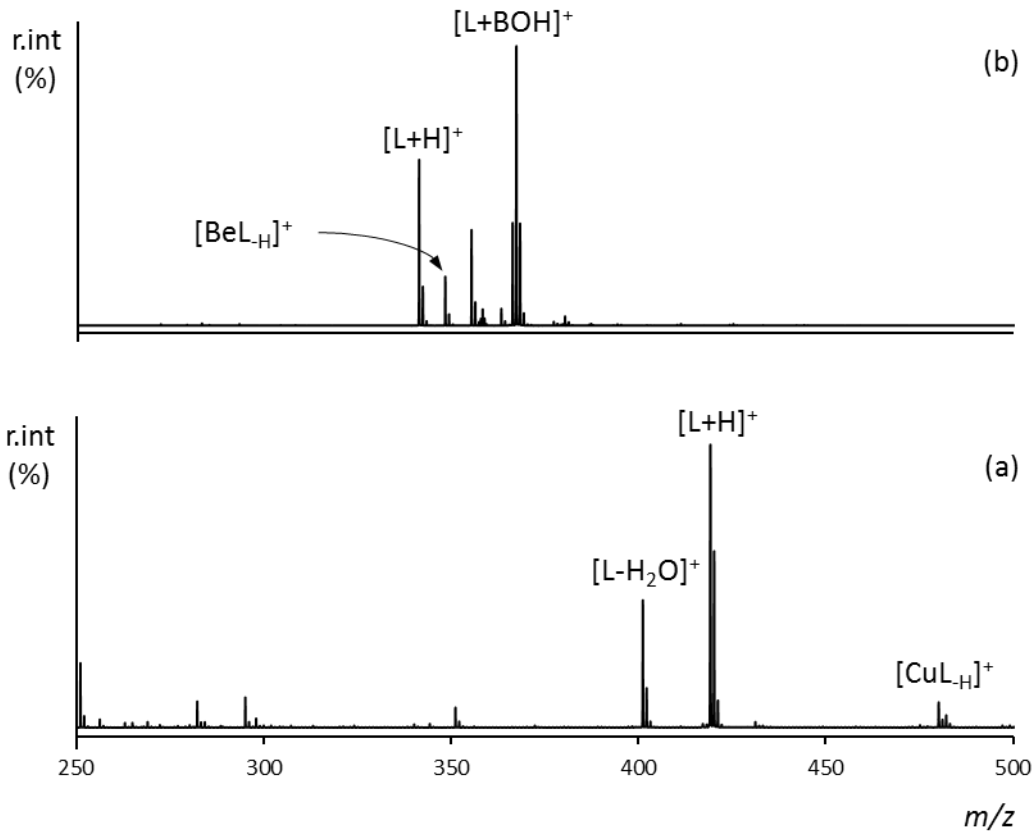

Figure 5-16 Positive ion ESI mass spectrum of Be^{2+} and (a) Ligand **L6** (b) Ligand **L7** in methanol-water (1:1) solution.

5.2.8 Macroscale syntheses and characterisation of beryllium complexes

Studies with mass spectrometry are effectively microscopic syntheses and are aimed at identifying target reaction systems where a particularly stable beryllium-ligand combination occurs. ESI-MS is also useful in identifying where an unusual or unanticipated product species is formed. However, like every other characterisation technique, mass spectrometry has its own limitations so that the most complete picture of the chemistry of a beryllium system with any ligands can only be obtained through a combination of techniques. Therefore, attempts were made to further characterise the possible beryllium complexes formed with ligands **L1**-**L8** by NMR spectroscopy and single-crystal X-ray crystallography.

Although beryllium is a quadrupolar nucleus (S=3/2), ^{9}Be NMR can be a useful technique in the characterisation of beryllium complexes and is able to provide complementary information on the coordination environment of the beryllium centre. Other properties of the ^{9}Be nucleus are that it has 100% natural

abundance but with only a relative sensitivity of 0.0139 compared to the ^{1}H proton which has a relative sensitivity of 1.00. NMR studies in solution are being increasingly explored in recent studies as a result of safety concerns surrounding beryllium. Generally, except for sample preparation of beryllium compounds, which require handling minimal amounts of beryllium solids, ^{9}Be NMR data can be acquired without major difficulties.

5.2.9 ^{9}Be NMR characterisation of the product of ligand L9 and beryllium chloride

The ^{9}Be NMR spectra of beryllium complexes with ligands **L1**-**L5** have been examined previously using beryllium sulfate.[17] However, since the first attempts to crystallise beryllium complexes of ligands **L1**-**L8** were set up in NMR tubes (see Chapter 7), the NMR spectra of **L1**-**L9** were also acquired. Moreover, this present investigation employed non-aqueous medium and beryllium chloride salt. Table 5-3 records identified ^{9}Be NMR chemical shifts for the ligands **L1**-**L9**. Unfortunately the beryllium complexes formed in the polar solvents utilized resulted in the poor solubility of the compounds and no signal in most of the beryllium-ligand mixtures as shown in Table 5-3.

Table 5-3 ^{9}Be NMR chemical shift of beryllium chloride and ligands **L1**-**L9**

Reaction mixture	Solvent	^{9}Be NMR chemical shift (ppm)
$BeCl_2$ + **L1**	CD_2Cl_2	-
$BeCl_2$ + **L2**	CD_2Cl_2	2.5, 1.15
$BeCl_2$ + **L3**	CD_2Cl_2	5.25
$BeCl_2$ + **L4**	CD_2Cl_2	-
$BeCl_2$ + **L5**	C_6D_6	-
$BeCl_2$ + **L7**	C_6D_6	-
$BeCl_2$ + **L9**	CD_2Cl_2	5.89

However, the beryllium complex of ligand **L9** in dichloromethane shown in Figure 5-17 revealed a fairly narrow single peak at δ 5.89 suggesting the beryllium ion was in a tetracoordinate environment.[35] Comparison to other heteroleptic complexes of the type LBeCl, pointed out that this value is closely related to the

^{9}Be NMR shift of δ 5.42 for the similarly tetradentate beryllium centre with L=1-tris(pyrazolyl)borate,[36] but is further downfield from the chemical shift observed for tricoordinate beryllium centre with L=diketiminates.[37] This is quite contrary to the ESI-MS speciation in aqueous and methanolic solution in which no signal was attributable to a beryllium complex suggesting that the ligand **L9** is unstable in aqueous solution.

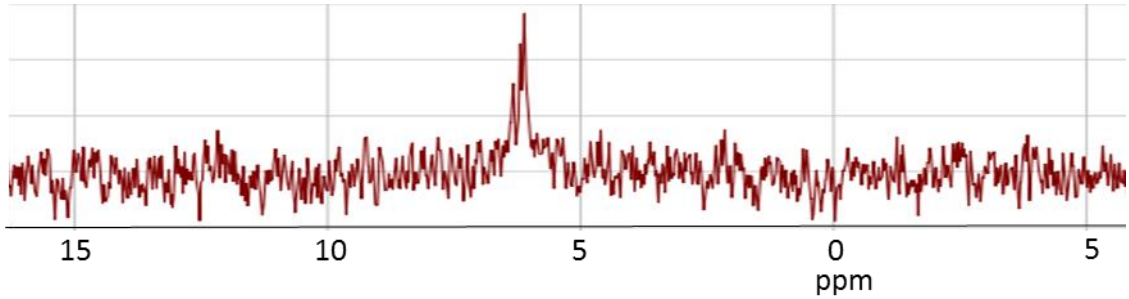

Figure 5-17 ^{9}Be NMR spectrum of ligand **L9** and $BeCl_2$

5.2.10 X-ray crystal structure of beryllium complex with ligand L9

Despite multiple attempts to crystallise beryllium complexes of ligands **L1**-**L5** directly in an NMR tube by reacting beryllium chloride and the ligands in various solvents, no crystals could be obtained. However, upon repeating the experimental procedure in THF, some of the crystallisation mixtures formed crystals suitable for X-ray study, but a preliminary scan of the cell parameters indicated the crystal to be a known beryllium complex. Due to time constraints and safety concerns with handling Be-containing solids, no attempt was made to firstly isolate the beryllium complex in order to attempt other crystallisation methods. However, upon reacting ligand **L9** and anhydrous $BeCl_2$ in acetonitrile heated up to 95^{o}C in a Schlenk flask as shown in Scheme 5-1, white needle-like crystals suitable for X-ray study were formed *in situ* in high yield but no attempt was made to accurately determine the exact yield due to a risk averse approach in manipulating beryllium solids for safety reasons.

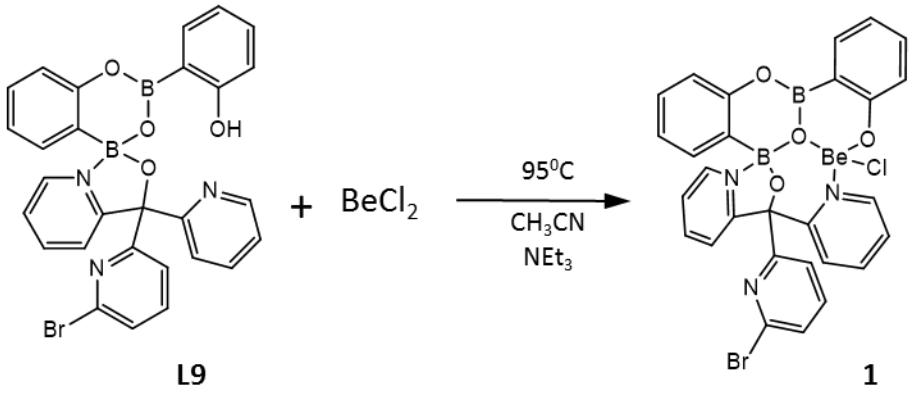

L9 1

Scheme 5-1 Reaction of ligand **L9** and anhydrous beryllium chloride in a Schlenk flask.

The crystal structure of beryllium complex **1** (Scheme 5-1) consists of a discrete molecular unit of LBeCl and an acetonitrile molecule as shown in Figure 5-18. The selected bond distances and angles for this complex are reported in Table 5-4

Table 5-4 Selected bond length and bond angles for beryllium complex **1**.

Bond lengths (Å)			
Be(1)-Cl(1)	2.005	B(1)-C(6)	1.541
Be(1)-O(1)	1.560	B(2)-O(2)	1.520
Be(1)-O(2)	1.696	B(2)-O(4)	1.450
Be(1)-N(1)	1.844	B(2)-N(3)	1.579
B(1)-O(2)	1.387	B(2)-C(16)	1.583
B(1)-O(3)	1.371		
Bond angles (°)			
Cl(1)-Be(1)-O(1)	111.64	O(3)-B(1)-C(6)	117.04
Cl(1)-Be(1)-N(1)	103.50	N(3)-B(2)-C(16)	113.97
Cl(1)-Be(1)-O(2)	113.21	O(4)-B(2)-N(3)	100.36
N(1)-Be(1)-O(1)	107.87	O(2)-B(2)-C(16)	111.27
N(1)-Be(1)-O(2)	112.29	O(2)-B(2)-N(3)	106.24
O(1)-Be(1)-O(2)	108.21	O(4)-B(2)-C(16)	115.23
O(2)-B(1)-C(6)	121.20	O(4)-B(2)-O(2)	108.92
O(2)-B(1)-O(3)	121.74		

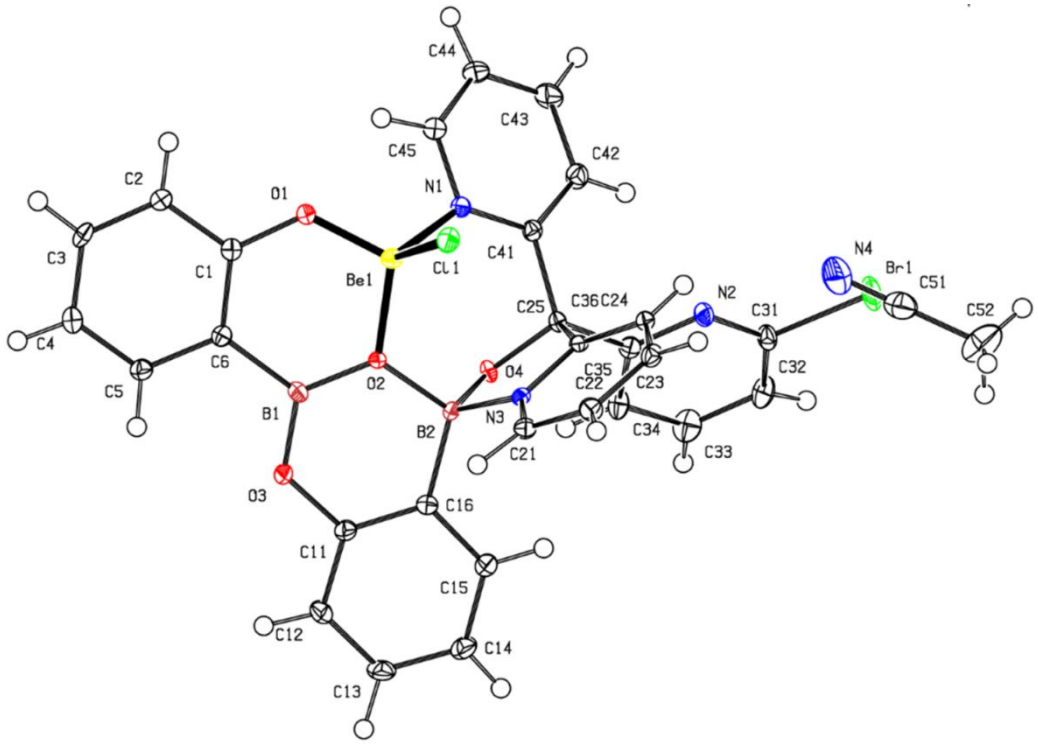

Figure 5-18 Molecular structure of beryllium complex **1**

In this complex, the beryllium centre is in a slightly distorted but rigid coordination environment as a result of the coordination from two oxygen and one nitrogen atoms while the chloride ion completes the tetrahedral geometry. Perhaps the rigidity of this complex could be the reason for its quick crystallisation. Upon complexation to beryllium, one of the pyridine ring moieties of the ligand assumes an orientation perpendicular to the plane of the rest of the ligand and sits parallel to the Be-Cl bond, revealing what appears to be a π-interaction of the chloride and the π-system of the pyridine ring.

The Be1-O1 bond distance (1.560 Å) correlates well with similar beryllium phenolate bond distances in other complexes but the B-O-Be bond linkage is rare in beryllium compounds.[38-40] In contrast, the Be-N distance is elongated in comparison to the Be-N distance observed in similar beryllium *N*-donor ligand complexes.[41] However the tetrahedral angle about the beryllium centre is only slightly deviated from the ideal tetrahedron and are all observed within the range of 107.87-113.21°. Therefore this arrangement of the *N/O*-donor atoms in the ligand provides a reasonably suitable tridentate binding pocket for the beryllium ion. Secondly, worthy of note are the two boron atoms which occupy a tetrahedral and trigonal planar coordination environment. The B-O bond distance for the boron in

the trigonal coordination environment is shortened approximately by 0.1 Å while the O-B-O angle of 121° is substantially larger than the O-B-O in a tetrahedral range of 100-111°.

The solid state packing of the compound consists of independent units of the BeLCl species and solvent molecule arranged in inverted fashion such that the apical Be-Cl bonds point away from each other while the equatorial component of the molecules appear stacked as shown in Figure 5-19.

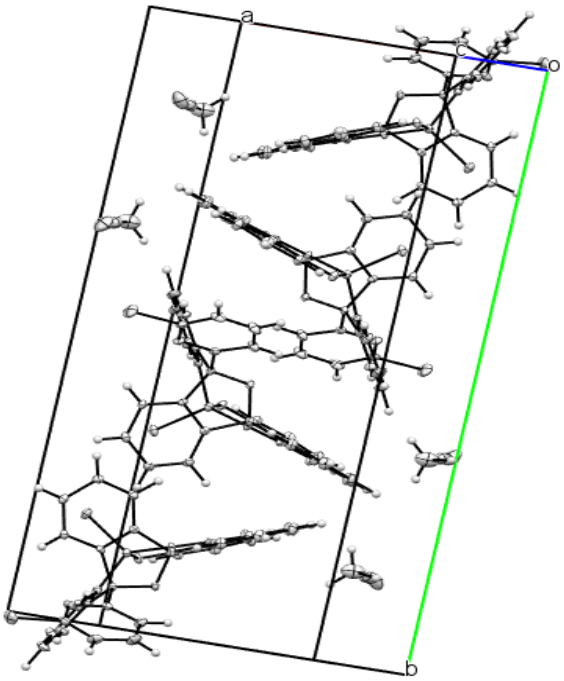

Figure 5-19 Arrangement of the molecules of the beryllium complex **1** in the unit cell.

5.2.11 Rationalizing the synthetic detour from targeted ligand L8 into ligand L9

Having successfully confirmed the structure of the beryllium complex with the ligand **L9**, it became clear that the synthesis toward the ligand **L8** by our collaborator at Massey University (see Figure 5-14) must have progressed through another path. Therefore the synthetic route was analysed in retrospect in order to highlight the point of detour and to possibly rationalize steps towards the synthesis of **L8**. The originally unsuccessful synthetic route to the ligand **L8** is outlined in Figure 5-20 while the detour to the eventual ligand is followed up in Figure 5-21. As observed in Figure 5-20, the originally proposed synthetic route failed at the Suzuki-Miyaura reaction of step 3a. The expected C-C coupling reaction appears to

be interfered with by the alcohol group at the central carbon atom such that boron-oxygen and boron-nitrogen bonds are formed instead and this product then goes on to further react with excess boronic acid to yield the ligand **L9** (see Figure 5-20).

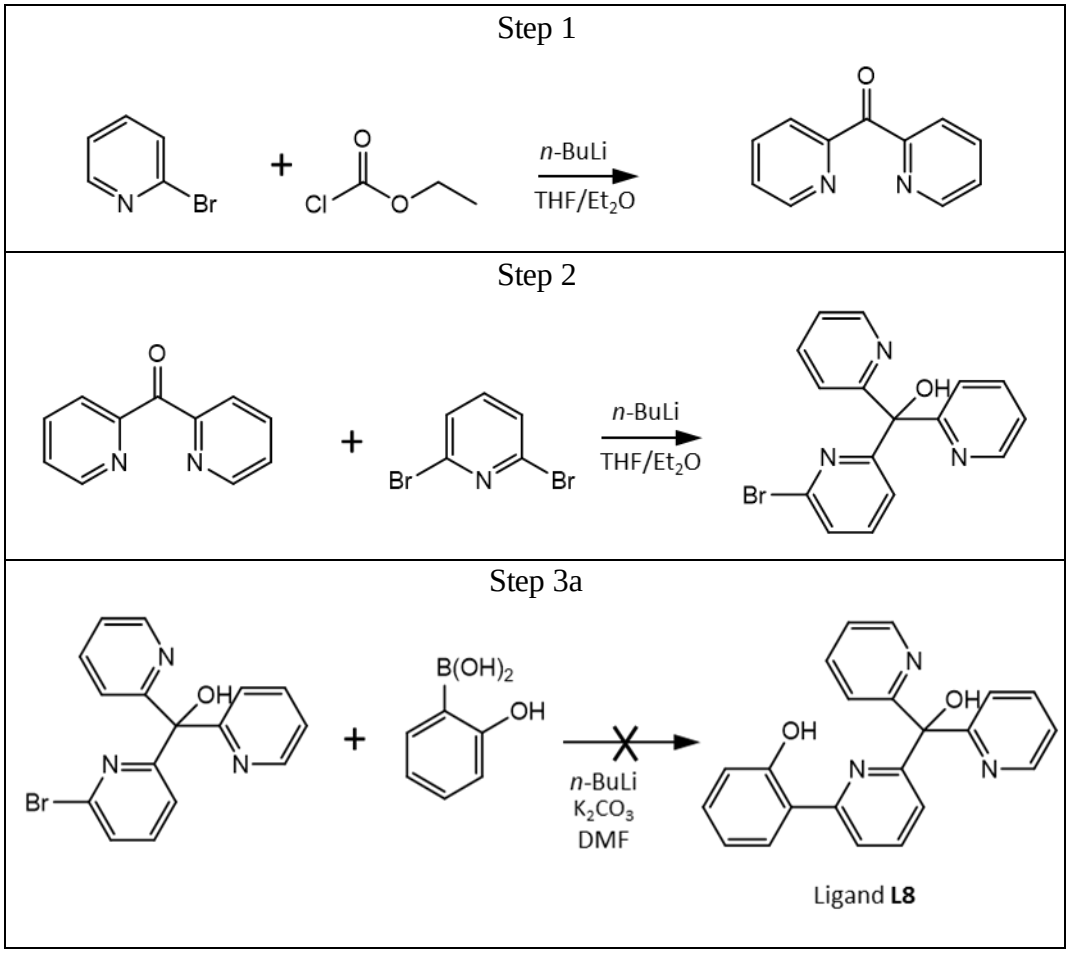

Figure 5-20 Unsuccessful synthetic route to the ligand **L8**.

Finally, it makes sense in hindsight to understand why no beryllium complexation was observed with the ligand **L9** in methanol-water solution employed during ESI-MS experiments. Apparently, the ion signal observed at *m/z* 342 (and discussed earlier in Section 5.2.7) is due to the hydrolysis of the ligand in aqueous environment which cleaves the B-O and B-N bonds to yield the starting compound as shown in Figure 5-21. This is further confirmed by the distinctive isotope pattern due to the bromide.

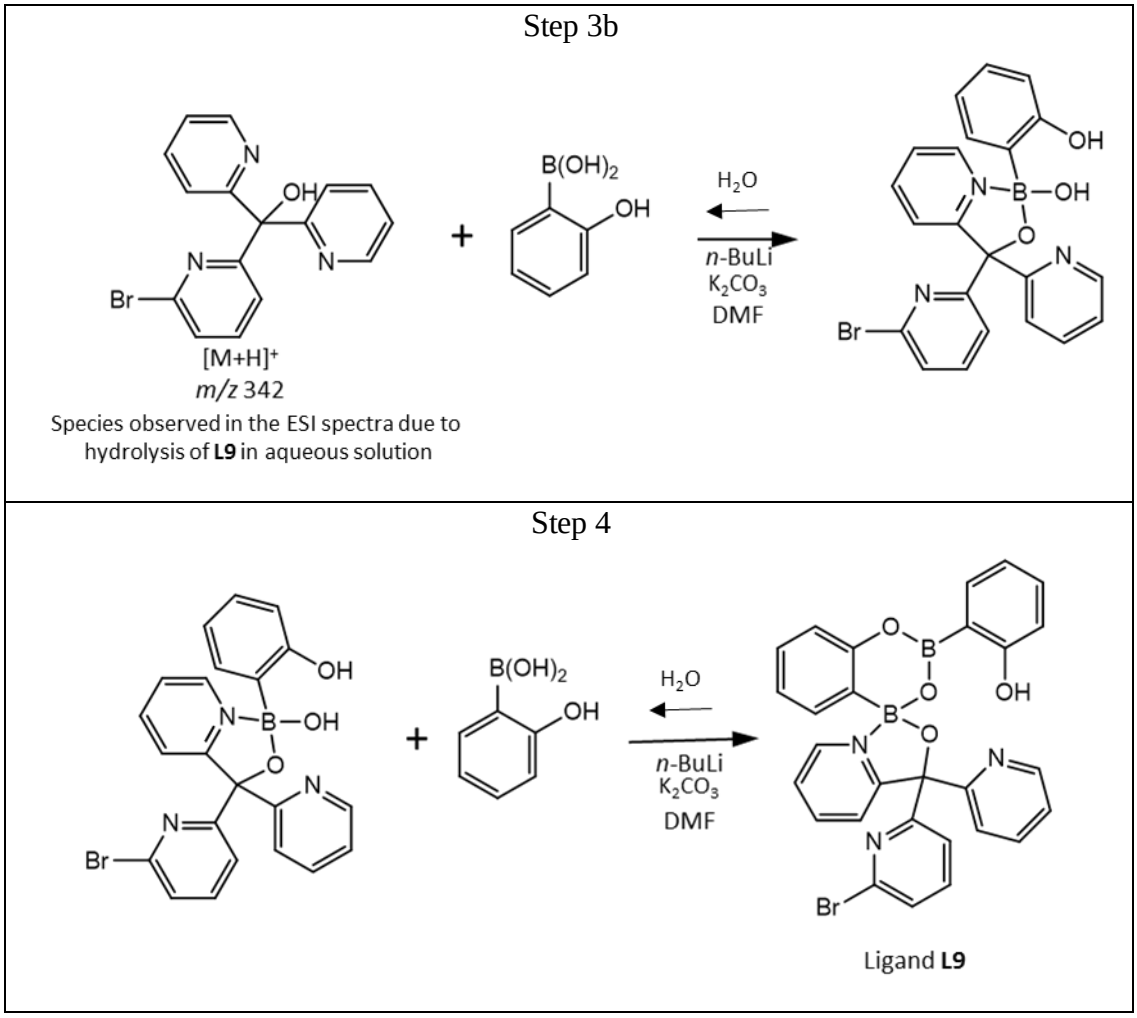

Figure 5-21 Synthetic detour to ligand **L9** and hydrolysis in water-methanol solution to yield the ESI-MS ion at *m/z* 342.

5.3 Conclusion

This chapter has employed the ESI-MS technique to examine the complexation of beryllium by polyaminocarboxylic acids including iminodiacetic acid (H_3IDA), nitrilotriacetic acid (H_3NTA), nitrilotripropionic acid (H_3NTP) and diethylenetriaminepentaacetic acid (H_5DTPA). Additionally, other multidentate *N/O*-donor ligands **L1**-**L9** designed toward tetradentate coordination to the Be^{2+} cation have also been examined. Of particular interest in these ESI-MS analyses was the binding affinity trends, selectivity and full encapsulation of the Be^{2+} cation by the ligands since such a coordination mode alongside a high specificity for the beryllium ion will invariably deactivate the toxic effect of beryllium in biological systems. The results from this Chapter have proved that ESI-MS is a potentially useful tool for probing the coordination chemistry behaviour of these beryllium-

ligand combination even when tiny amounts of materials are used in analyte solutions.

Furthermore, other Chapters in this thesis which have presented both qualitative and quantitative data from the ESI-MS screening of beryllium complexes in solution formed from a huge variety of ligands highlight the capability of the ESI-MS to handle different classes of compounds. Lastly, the role of providing an encompassing description of beryllium complexes by utilising additional and complementary techniques where possible has been portrayed.

5.4 References

1. C. H. Stephan, M. Fournier, P. Brousseau and S. Sauvé, *Chemistry Central Journal*, 2008, **2**, 1-9.

2. C. H. Stephan, S. Sauvé, M. Fournier and P. Brousseau, *Journal of Applied Toxicology*, 2009, **29**, 27-35.

3. J. R. Balmes, J. L. Abraham, R. A. Dweik, E. Fireman, A. P. Fontenot, L. A. Maier, J. Muller-Quernheim, G. Ostiguy, L. D. Pepper and C. Saltini, *American Journal of Respiratory and Critical Care Medicine*, 2014, **190**, e34-e59.

4. J. Borak, *Journal of Occupational and Environmental Medicine*, 2016, **58**, e355-e361.

5. K. Kreiss, *Occupational and Environmental Medicine*, 2011, **68**, 787-788.

6. S. J. Flora and V. Pachauri, *International Journal of Environmental Research and Public Health*, 2010, **7**, 2745-2788.

7. O. Andersen, *Chemical Reviews*, 1999, **99**, 2683-2710.

8. G. Anderegg, F. Arnaud-Neu, R. Delgado, J. Felcman and K. Popov, *Pure and Applied Chemistry*, 2005, **77**, 1445-1495.

9. A. E. Martell and R. D. Hancock, *Metal Complexes in Aqueous Solutions*, Springer Science & Business Media, New York, 1996.

10. E. Chinea, S. Dominguez, A. Mederos, F. Brito, J. M. Arrieta, A. Sanchez and G. Germain, *Inorganic Chemistry*, 1995, **34**, 1579-1587.

11. A. Mederos, J. Felipe, M. Hernández-Padilla, F. Brito, E. Chinea and K. Bazdikian, *Journal of Coordination Chemistry*, 1986, **14**, 277-284.

12. A. Mederos, S. Dominguez, E. Chinea and F. Brito, *Quimica Analitica-Bellaterra*, 1996, **15**, S21-S29.

13. J. McKinney and W. Chairman, *Toxicological & Environmental Chemistry*, 1993, **38**, 1-71.

14. J. Votava and M. Bartusek, *Collection of Czechoslovak Chemical Communications*, 1975, **40**, 2050-2058.

15. A. Mederos, S. Domínguez, A. Medina, F. Brito, E. Chinea and K. Bazdikian, *Polyhedron*, 1987, **6**, 1365-1373.

16. K. J. Shaffer, PhD Thesis, Massey Universtiy, 2010.

17. K. J. Shaffer, R. J. Davidson, A. K. Burrell, T. M. McCleskey and P. G. Plieger, *Inorganic Chemistry*, 2013, **52**, 3969-3975.

18. S. Dubey, A. Singh and D. Puri, *Journal of Inorganic and Nuclear Chemistry*, 1981, **43**, 407-409.

19. U. Jain, V. Kumari, R. Sharma and G. Chaturvedi, *Journal de Chimie Physique et de Physico-Chimie Biologique*, 1977, **74**, 1038-1041.

20. W. W. Rudolph, *Journal of Solution Chemistry*, 2010, **39**, 1039-1059.

21. W. W. Rudolph, D. Fischer, G. Irmer and C. C. Pye, *Dalton Transactions*, 2009, 6513-6527.

22. A. Mederos, S. Dominguez, M. Morales, F. Brito and E. Chinea, *Polyhedron*, 1987, **6**, 303-308.

23. O. Raymond, W. Henderson, P. J. Brothers and P. G. Plieger, *European Journal of Inorganic Chemistry*, 2017, **2017**, 2691-2699.

24. L. Alderighi, P. Gans, M. Stefeno and A. Vacca, in *Advance in Inorganic Chemistry*, eds. A. G. Sykes and A. Cowley, H, Academic Press, Califorornia, 2000, vol. 50, pp. 109-197.

25. H. Wang and G. R. Agnes, *Analytical Chemistry*, 1999, **71**, 4166-4172.

26. A. Wortmann, A. Kistler-Momotova, R. Zenobi, M. C. Heine, O. Wilhelm and S. E. Pratsinis, *Journal of the American Society for Mass Spectrometry*, 2007, **18**, 385-393.

27. E. C. Kempen and J. S. Brodbelt, *Analytical Chemistry*, 2000, **72**, 5411-5416.

28. C. Y. Wong and J. Woollins, *Coordination Chemistry Reviews*, 1994, **130**, 243-273.

29. H. Hotta, T. Mori, A. Takahashi, Y. Kogure, K. Johno, T. Umemura and K.-i. Tsunoda, *Analytical Chemistry*, 2009, **81**, 6357-6363.

30. S. L. Shirran and P. E. Barran, *Journal of the American Society for Mass Spectrometry*, 2009, **20**, 1159-1171.

31. M. Sravani, V. Nagaveni, S. Prabhakar and M. Vairamani, *Rapid Communications in Mass Spectrometry*, 2011, **25**, 2095-2098.

32. P. Stoessel, D. Joosten and E. Breuning, *US Patents*, 2010, **US20120286254 A1**.

33. R. S. Forgan, B. D. Roach, P. A. Wood, F. J. White, J. Campbell, D. K. Henderson, E. Kamenetzky, F. E. McAllister, S. Parsons and E. Pidcock, *Inorganic Chemistry*, 2011, **50**, 4515-4522.

34. W. Henderson and J. S. McIndoe, *Mass Spectrometry of Inorganic, Coordination and Organometallic Compounds: Tools, Techniques, Tips*, Wiley, Chichester, 2005.

35. P. G. Plieger, K. D. John, T. S. Keizer, T. M. McCleskey, A. K. Burrell and R. L. Martin, *Journal of the American Chemical Society*, 2004, **126**, 14651-14658.

36. D. Naglav, D. Bläser, C. Wölper and S. Schulz, *Inorganic Chemistry*, 2014, **53**, 1241-1249.

37. M. Arrowsmith, M. S. Hill, G. Kociok-Köhn, D. J. MacDougall, M. F. Mahon and I. Mallov, *Inorganic Chemistry*, 2012, **51**, 13408-13418.

38. F. Cecconi, E. Chinea, C. A. Ghilardi, S. Midollini and A. Orlandini, *Inorganica Chimica Acta*, 1997, **260**, 77-82.

39. Y. Li, Y. Liu, W. Bu, D. Lu, Y. Wu and Y. Wang, *Chemistry of Materials*, 2000, **12**, 2672-2675.

40. Y.-P. Tong, S.-L. Zheng and X.-M. Chen, *Inorganic Chemistry*, 2005, **44**, 4270-4275.

41. M. P. Dressel, S. Nogai, R. J. Berger and H. Schmidbaur, *Zeitschrift für Naturforschung B*, 2003, **58**, 173-182.

Chapter 6

General conclusion

Beryllium is a silver-grey metal possessing a unique combination of extreme stiffness, low density and tolerance to wide temperature ranges which make it vital for a variety of applications in the automotive, aviation, space, nuclear and consumer industries. Unfortunately, beryllium is also toxic and its increasing usage is of environmental, occupational and public health concern leading to rejuvenation of the bio-inorganic and coordination chemistry of this element. Given that the exploration of beryllium coordination chemistry in comparison to neighbouring periodic table elements has been hampered by its toxicity, it is imperative to devise safe methods to build a greater understanding of the fundamental coordination chemistry of Be^{2+} and its interaction with ligands. This is also significant considering the toxicology route of this element and its interaction with biological ligands culpable in the strange and uncontrollable immuno-sensitisation is yet unknown. Therefore, this investigation sought to assess the potential of ESI-MS to be developed as a quick, sensitive and safe screening technique to observe beryllium speciation with ligands of interest at low concentrations. This has been systematically pursued in this work by recording numerous ESI mass spectra of beryllium complexes involving a wide range of ligands in solution under a variety of conditions.

Firstly, the ESI-MS investigation of solutions of beryllium salts was considered, and this represents the speciation of the Be^{2+} cation in the presence of simple ligands such as water, hydroxide and salt anions (Chapter 2). Using a qualitative and semi-quantitative approach, the ability of the ESI to transfer beryllium hydroxide species from solution into the mass spectrometer was shown thereby obtaining an approximate but quick screening of the hydrolytic tendencies in acidic solution of beryllium sulfate in agreement with present understanding of the beryllium species existing in solution (see Figure 6-1). These results thereby proved that the ESI MS could provide an alternative, safe and sensitive solution-based technique for the investigation of beryllium speciation with other ligands of interest.

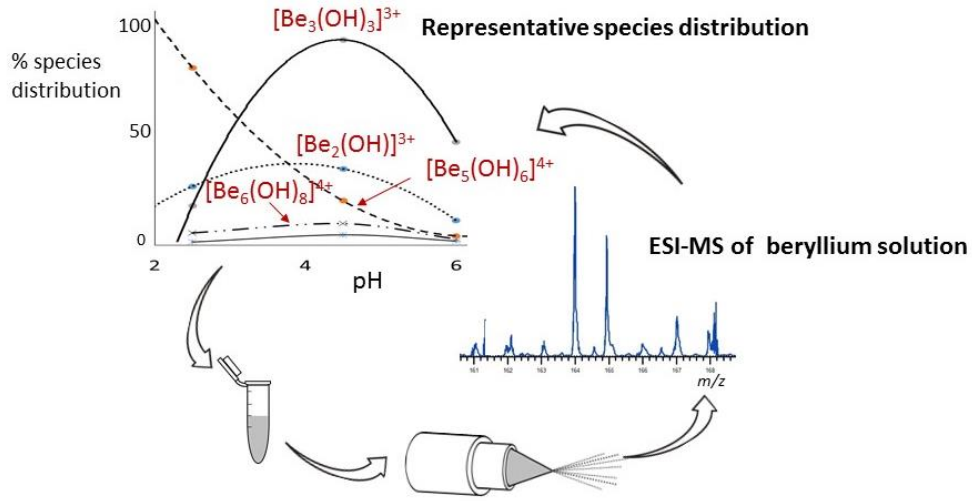

Figure 6-1 Schematic diagram showing the use of ESI-MS as an approximate but quick screening of the hydrolytic tendencies in beryllium salt solution

Given the successful application of the ESI-MS technique representing beryllium hydrolysis species, beryllium complexes with several important classes of ligands were synthesised *in situ* and subjected to detailed characterisation by the ESI-MS technique (Chapter 4). These ligands, which possessed functional groups or architecture of interest, include diketones, hydroxyl keto, dicarboxylic acid, dihydroxyl ligands, citric acid and the macrocylic ligands. The extensive investigation of a wide range of beryllium complexes alongside the in-depth description of their ESI MS behaviour provided in this study would serve as reference data both for other chemically-interesting interactions unique to this metal or other inorganic systems of interest. Most importantly however, is that the well-established sensitivity of mass spectrometry employed in providing stoichiometric data have been emphasised as the foremost and perhaps safest characterisation technique for beryllium species in solution prior to further studies. The application of the ESI-MS in identifying where an unusual or unanticipated product species is formed was also exemplified with the beryllium-citrate system.

Furthermore, the ESI-MS methodology was put to a more practical concern of biomedical and environmental interest in the search for a suitable ligand for applications as beryllium chelating agents which is the aim of the overall project to which this PhD was a part of. The development of strong, selective agents for beryllium encapsulation will require an improved understanding of the fundamental

requirements for coordination of polydentate ligands to beryllium, while at the same time meeting the challenges of working with this toxic element. Therefore the most important contribution of this thesis is the ESI-MS approach towards the coordination chemistry of beryllium and the search for beryllium chelating ligands. As illustrated in Figure 6-2 the use of stoichiometric information from the ESI-MS technique to identify full encapsulation of the Be^{2+} cation by multidentate *N*/*O*-donor ligands was explored extensively. Also, the ESI-MS was found to be amenable towards the screening of ligand selectivity and binding affinity trends in solution to the extent that newly synthesised chelating ligands for beryllium binding can be examined on a microscale. Several aminopolycarboxylate related ligands showed potentials for beryllium encapsulation and decent selectivity for the beryllium cation but a clear challenge still remains in identifying ligands which will distinguish beryllium from aluminium. Unfortunately, only a handful of the newly targeted ligands based around a substituted di-pyridyl scaffold were available for ESI-MS screening at the time of concluding this thesis. Meanwhile, experimental and computational research is ongoing in the aspect of optimising the ligand binding cavity using related cations especially aluminium (see Figure 6-2).

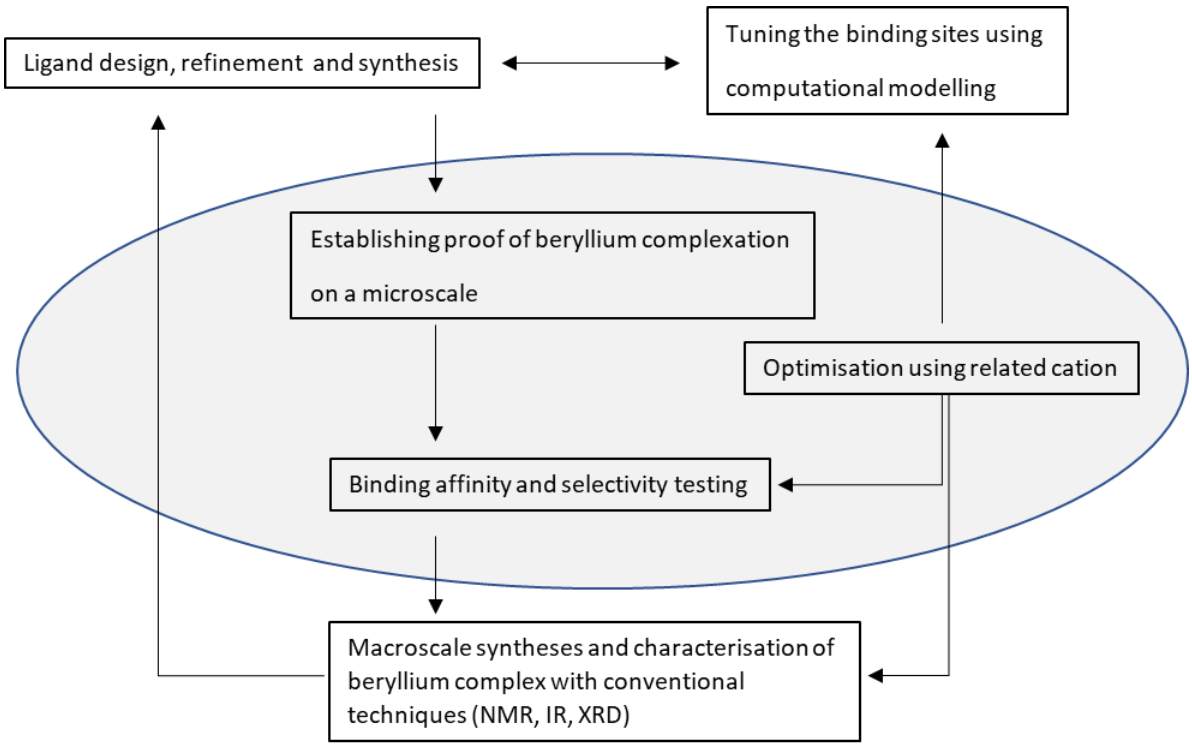

Figure 6-2 Schematic diagram showing the pivotal role of ESI-MS (encircled above) in the search for suitable chelating ligands for beryllium as employed in this thesis.

This work also considered other techniques such as NMR spectroscopy and single-crystal X-ray crystallography in the characterisation of beryllium complexes. However, it is worth pointing out that these techniques either require a larger amount of material or the successful isolation of pure compounds prior to any analysis. This is a huge deterrence in the exploration of beryllium chemistry as the exposure and inhalation hazard involved in handling solid compounds of beryllium increases. Preferentially, such a hazard could effectively be controlled by employing the ESI-MS methodology as a very sensitive solution-based technique to eliminate handling huge quantities of toxic beryllium compounds. Nevertheless, computational techniques (although not a substitute for beryllium experimentation) can be fruitfully engaged in modelling the interaction of beryllium with ligands and a particularly useful technique illustrated in this thesis is the Car Parrinello molecular dynamics simulation (Chapter 3). The laudable experimental and calculated agreement of the results described involving the ligand exchange processes on the beryllium cation can be helpful in deciphering the interaction of the metal with ligand binding sites in an aqueous environment. It is evident from this research that the coordination chemistry of beryllium has come a long way and although dwarfed in comparison to its periodic table neighbours, suitable characterisation techniques such as electrospray mass spectrometry has the potential for detailed preliminary evaluation to direct the synthesis of new beryllium metal complexes.

In closing, the current state of affairs in the coordination chemistry of beryllium is still a ripe and fruitful research area. Despite the infamous reputation of beryllium, a robust protocol and containment lab wares (eg glove box, air tight flask etc) for handling beryllium solid compounds is all that is needed to conduct beryllium experimentation just like any other hazardous chemical in the laboratory. An example is the strategy employed by the beryllium laboratory at Philipps-Universität Marburg which involves the treatment of beryllium compounds as air/moisture sensitive compounds thereby completely preventing the escape of beryllium to air. Considering the enormous amount of resources and experience acquired during this project at the University of Waikato, University of Auckland and Massey University, it would be pleasing to see another researcher take up some areas of interest which could not be pursued during the period of this thesis especially in conjunction with already established collaborators in Germany. One

possible area, is the use of beryllium chloride as a source of the Be^{2+} cation in investigating its interaction with amino acids, phosphate and simple sugars.

This thesis has shown that beryllium research can effectively be achieved by employing the ESI-MS technique and this methodology can further be extended to any other solution-based technique except that proper consideration of the larger sample requirement should be made. There is clearly a lot more work to be done on beryllium chelation but this work shows a useful approach to screening that can reasonably hope to bear fruit in a combinatorial context.

Chapter 7

Experimental and computational details

7.1.1 Health and safety

As a result of the toxicity of beryllium compounds, strict attention was paid to health and safety throughout the course of this research. Experimental work on beryllium compounds was divided into two components which were carried out on two sites. ESI-MS microscale screening of beryllium complexes was conducted at the University of Waikato while the characterisation of beryllium complexes using NMR spectroscopy and single-crystal X-ray crystallography were conducted at Philipps-Universität Marburg, Germany.

The first six months during this PhD research was spent on ESI-MS training and designing standard procedures for handling beryllium solutions at the University of Waikato. All beryllium chemistry used stringent safe handling procedures that were tested and established using aluminium complexes and brightly coloured dyes to identify potential leakages, spillages and operation with potential risks. Furthermore, preparative work for ESI-MS of beryllium solutions was carried out in a beryllium-dedicated fume cupboard while employing a containment tray. Where minor spillages of beryllium solution occurred in the containment tray during solution transfers, washing was undertaken while items potentially contaminated with beryllium were double-bagged and stored in well labelled containers. Regular personal protection equipment (PPE) such as gloves and laboratory coats, safety googles were employed to protect the experimenter from any risk of exposure. At the end of this project, all beryllium-contaminated waste was contained and disposal carried out by an authorised agency while the beryllium-dedicated fumehood was well cleaned and decontaminated to allow it to be used for other non-beryllium activities in the laboratory.

Additional training was also acquired from the beryllium laboratory at Philipps-Universität Marburg, Germany. This laboratory is one of the few academic laboratories that still conduct fundamental beryllium research so that their safety procedures are well-established.[1]

7.2 Preparative work

A 100 mL aqueous stock solution of beryllium sulfate tetrahydrate ($BeSO_4.4H_2O$) for ESI MS analysis was prepared by dissolving 2.3 mg of $BeSO_4 \cdot 4H_2O$ (BDH) in high purity distilled and deionised water to obtain a 2.2 x 10^{-3} mol L^{-1} stock solution. The pH of this unadjusted solution (measured using an ISFET S2K712 pH meter, calibration was made with the pH 4 and 7 standard buffer solution from the supplier) was 4.5. The beryllium sulfate stock solution was further diluted to obtain a dilution series ranging from 2.2 x 10^{-4} mol L^{-1} to 2.2 x 10^{-5} mol L^{-1} and portions of the solution adjusted to obtain a solution pH (pH_{feed}) of 2.5 and 6.0 using 0.1 mol L^{-1} sulfuric acid and 0.01 mol L^{-1} sodium hydroxide solution respectively. Mass spectra of beryllium sulfate in H_2O/DMSO and H_2O/MeOH mixed solvent system were obtained by mixing the aqueous solution of the beryllium sulfate with an equivalent proportion of the second solvent ion a 1:1 ratio. The total volume of the mixtures prepared for each ESI-MS experiment varied depending on the aim of the experiment.

In order to reduce the manipulation of beryllium salt, stock solutions of the ligands were prepared to correspond to the concentration of the beryllium sulfate employed in ESI-MS competition studies. Stock solutions of other metal cation were also prepared to corresponding 2.2 x 10^{-3} mol L^{-1} as shown in Table 7-1. These include the sulfate salts of aluminium, zinc, magnesium, cobalt and copper (purchased from BDH).

A 10 mL aqueous stock solution of beryllium chloride for ESI MS analysis were prepared by dissolving a 1.7 mg of beryllium metal chip in 2 mol L^{-1} HCl solution (1 mL) and the solution was made up to 100 mL with high purity distilled and deionised water to obtain a stock solution of concentration 1.9 x 10^{-3} mol L^{-1}. The pH of this solution was 4.7.

Table 7-1 Preparation of aqueous stock solutions of metal cations utilised in ESI-MS competition studies

Compound	Molar concentration (mol L^{-1})	Mass weight (g)	Volume prepared (L)
Zinc sulfate heptahydrate ($ZnSO_4 .7H_2O$)	0.0022	0.0063	0.01
Aluminum sulfate octadecahydrate ($Al_2(SO_4)_3 .7H2O$)	0.0022	0.0073	0.01
Magnesium sulfate monohydrate ($MgSO_4 .H_2O$)	0.0022	0.0030	0.01
Cobalt sulfate ($CoSO_4 .7H_2O$)	0.0022	0.0061	0.01
Anhydrous Copper sulfate	0.0022	0.0035	0.01

Aqueous solutions of the ligands for ESI MS analysis were prepared by dissolving the required amount in water or methanol solution. Stock solutions of the ligand were prepared in 10 mL or 100 mL volumetric flasks depending on the availability of the ligands and the solvent used. Also the stock solution of the ligands were prepared to correspond to the concentration of the beryllium salt solution to be employed as detailed in

Table 7-2 Preparation of stock solution of ligands for ESI-MS studies

Compound	Molar concentration (mol L^{-1})	Mass weight (g)	Solvent	Volume prepared (L)
Acetic acid	0.0022	0.00132	Water	0.01
Acetyl acetone	0.0022	0.00220	Methanol	0.01
Dibenzoylmethane	0.0022	0.00493	Methanol	0.01
Thenoyl trifluoroacetyl acetone	0.0022	0.00488	Methanol	0.01
Trifluoroacetyl acetone	0.0022	0.00338	Methanol	0.01
Hexafluoroacetyl acetone	0.0022	0.00457	Methanol	0.01
Benzil	0.0022	0.00462	Methanol	0.01
Diacetyl	0.0022	0.00189	Methanol	0.01
Phenathrenequinone	0.0022	0.00458	Methanol	0.01
Tropolone	0.0022	0.00268	Methanol	0.01
Maltol	0.0022	0.00277	Methanol	0.01
Malonic acid	0.0022	0.02289	Methanol	0.1
Chromotropic acid	0.0022	0.00704	Methanol	0.01
Picolinic acid	0.0022	0.00270	Methanol	0.01
Salicylamide	0.0022	0.00301	Methanol	0.01
8-Hydroxyquinoline	0.0022	0.00319	Methanol	0.01
Citric acid	0.0022	0.04226	Water	0.1
12-crown-4	0.0019	0.00334	Methanol	0.01
15-crown-5	0.0019	0.00418	Methanol	0.01
18-crown-6	0.0019	0.00501	Methanol	0.01
Cryptand[2.2.2]	0.0019	0.00715	Methanol	0.01
Nitrilotripropionic acid	0.0022	0.05130	Water	0.1
Nitrilotriacetic acid	0.0022	0.04205	Water	0.1
Diethylenetriaminepentaacetic acid	0.0022	0.08653	Methanol	0.1
Iminodiacetic acid	0.0022	0.02928	Water	0.1
L1	0.0022	0.00761	Methanol	0.01
L2	0.0022	0.00754	Methanol	0.01
L3	0.0022	0.00805	Methanol	0.01
L4	0.0022	0.00803	Methanol	0.01
L5	0.0022	0.00833	Methanol	0.01
L6	0.0022	0.00919	Methanol	0.01
L7	0.0022	0.00748	Methanol	0.01
L8	0.0022	0.00781	Methanol	0.01

All the ligands utilised in this thesis were purchased commercially and used as obtained except the ligands **L1-L9** which were synthesised. Ligands **L1-L5** were synthesised in conjunction with collaborator Assoc. Prof Paul Plieger according to the literature procedure previously reported.[2] As at the time of writing this thesis, the synthesis of the ligands **L6-L9** were still undergoing modification at Massey University. Stock solutions of **L1-L9** were prepared by dissolving in a tiny amount (ca. 100 µL) of dichloromethane and made up to the required volume with methanol. **L2** was particularly insoluble in many solvent and so was initially dissolved in 100 µL of DMSO and diluted with methanol. The stock solutions were shaken to effect complete dissolution and stored in the dark when not in use as the ligands were found to be light sensitive.

In order to investigate the speciation of Be^{2+} cation with these ligands in a systematic manner, aliquots of the above stock solutions were combined in a range of metal: ligand ratios and pH as noted for each reaction mixture in the Result and Discussion sections. The pH (measured using an ISFET S2K712 pH meter, calibration was made with the pH 4 and 7 standard solution from the supplier) was adjusted when required using 0.01 mol L^{-1} sodium hydroxide solution. For ligand/metal exchange experiments, appropriate portions of solution of either the metal or ligand components were thoroughly mixed before analysis. All analyses were firstly performed immediately after preparation, after 24 hours later and finally between 3-21 days after intial mixing to ensure that complete equilibrium had been attained. The concentration of the complexes in solution as revealed by their corresponding peak abundance in the mass spectra did not change significantly over this period and precipitation was not an issue in these systems due to the very low concentrations employed of the sample solutions.

7.3 ESI-MS methodology

An ESI-TOF-MS and ESI-ion trap-MS were used for project. Spectra were obtained in positive and negative mode using a Bruker Daltonics MicrOTOF high resolution mass spectrometer while tandem MS^n was carried out on a Bruker Amazon-X ion-trap mass spectrometer all fitted with an ESI interface. The instruments were calibrated using sodium formate solution and samples delivered directly into the ESI source via a syringe and micro-tubing (0.0127 cm internal diameter, 23 cm length) with the syringe pump (Cole-Parmer Instruments, Vernon

Hills, IL, USA) set at a flow rate of 180 μL h^{-1}. The source temperature was maintained at 180 °C while nitrogen was employed as the drying and nebulizing gas (0.4 L min^{-1} and 0.4 bar respectively). The spectra were acquired for a period of 10 sec between the *m/z* ranges of 100 – 1400 as this was sufficient to observe 1:1 and 1:2 metal ligand complexes. The capillary exit voltage was varied between 60 V to 180 V to obtain optimal spectra relevant to the aim of the ESI-MS experiment.

The instrument control was performed using micrOTOFcontrol software (version 2.2, Bruker Daltonics) while data analysis was performed with Data Analysis software (version 3.4, Bruker Daltonics), and mMass version 5.5 (an open source mass spectrometry tool).[3] mMass was especially relevant in data sharing and processing and presentation of spectra. Confirmation of all ESI-MS assignments in this study was aided by the comparison of observed and predicted isotope distribution patterns. Relative abundance using in semi quantitative analysis of the spectra were calculated using mMass software by setting the most abundant peak to 100%.

7.4 Macroscale beryllium experiment

Mass spectrometric studies are effectively microscopic syntheses and aim to identify target reaction systems where a particularly stable Be-ligand combination may occur or where an unusual or unanticipated product species is formed. In the final stage of this project, selected Be-ligand combination were synthesised on a small macroscopic scale in order to isolate the product in quantities sufficient to enable structural characterisation. However, the laboratories at the University of Waikato are not equipped to handle these larger amounts of beryllium compounds. For this reason, a 3 month research visit to the Nachwuchsgruppe Berylliumchemie at Philipps-Universität Marburg, Germany was undertaken in order to perform these experiments. The beryllium laboratory at Philipps-Universität Marburg, Germany has experience in handling toxic compounds (including beryllium) through a variety of containment techniques which involve the use of Schlenk-lines, gloveboxes, fume hoods and special preparative techniques. These techniques relevant to these project essentially involves the standard precautions required to exclude air/moisture from any air sensitive compounds or reaction.

7.4.1 Be NMR of beryllium chloride with L1-L9 and attempts to crystallise a beryllium complex

Anhydrous beryllium chloride (0.05 mmol, 4 mg) or (1 mmol, 8 mg) was weighed into a J. Young's NMR-tube containing **L1** (0.05 mmol,17.31 mg), **L2** (1 mmol, 34.38 mg), **L3** (0.05 mmol, 18.32 mg), **L4** (0.05 mmol, 18.26 mg), **L5** (0.05 mmol, 18.99 mg), **L7** (1 mmol, 34.03 mg) **L9** (0.05 mmol, 17.77 mg) to give a 1:1 mole ratio (depending on the quantity of the ligand). Deuterated benzene was initially distilled into the tubes containing **L5** and **L7** while the CD_2Cl_2 was distilled into the tubes with **L1**-**L4** and **L9**. The tubes were heated in an oil bath at 50°C for 48 hours (taking care to carry out the experiment under each solvent's vapour pressure to prevent the escape of particles from the solution). The tubes were cooled to room temperature and ^{9}Be NMR chemical shifts were recorded. Only the $BeCl_2$ and **L9** reaction mixture revealed a prominent signal at δ5.89 ppm due to the low solubility of these compounds. The reaction of $BeCl_2$ with these ligands at 50°C led to a large amount of insoluble material consisting of the beryllium complex product, free ligand and undissolved $BeCl_2$ at room temperature. Therefore, the procedure was repeated by distilling out the solvent and redistilling in chloroform and THF respectively. Except for ligands **L7** and **L9**, moderate dissolution was achieved for the $BeCl_2$ and ligand mixture in chloroform or THF. The reaction mixture was then filtered and set up for crystallisation by slow cooling over 48 hours and vapour diffusion of pentane. Most of the set up revealed microcrystals or oily products. A large crystal suitable for X-ray diffraction that was obtained from the $BeCl_2$ and **L4** reaction mixture was submitted for single-crystal X-ray diffraction. However, the cell parameters obtained from a preliminary scan of the crystal of the compound reported the compound as an already known beryllium complex therefore this was suspected to be the beryllium THF adduct. The low solubility of these compounds and the limited period of the research visit to Germany prevented further attempts to obtain crystals of beryllium complexes.

Meanwhile, as a result of the promising ^{9}Be NMR chemical shifts data from the $BeCl_2$ and **L9** reaction mixture, this reaction was repeated a Schlenk flask this time utilising acetonitrile as the solvent. Triethylamine (0.1 mmol, 0.01 mL) was added to acetonitrile solution (3 mL) of anhydrous beryllium chloride (0.05 mmol, 4 mg) and ligand **L9** (0.05 mmol, 17.77 mg) in a Schlenk flask and heated up to

95°C and then cooled afforded needle-like crystals which was submitted to the X-ray department.

7.4.2 X-ray crystallography of beryllium complex 1

X-ray crystal data and collection details for the complex **1** are given in Table 7-3. A Bruker D8 Quest diffractometer using graphite monochromatic Mo Kα radiation was used for X-ray measurements and were integrated with Bruker SAINT software while the structure was solved with direct methods using SHELX package.[4]

Table 7-3 Crystallographic details of beryllium complex **1**

formula	$C_{20}H_{20}BBeBrClN_3O_3$
Formula weight g/mol	485.57
Temperature (K)	110(2)
Wavelength (Å)	0.71073
Diffraction radiation type	MoK\α
Crystal system	monoclinic
Space group	'P 21/c'
Volume (Å^3)	2846.0(3)
Unit cell dimensions *a* (Å) *b* (Å) *c* (Å)	 10.4093(6) 23.9150(13) 11.4333(7)
$\alpha = \gamma$ (°) β (°)	90 90.656
D (calc.) (g cm^{-3})	1.700
Absorption coefficient (mm^{-1})	2.337
Theta range (°)	2.465-30.705
Limiting indices *h* *k* *l*	 -14,14 -33,34 -16,16
Z	6
F(000)	1476
Reflections collected	99671
Reflections unique	477
Data/parameter	8763/477
Goodness to fit	0.942
R indices[I>2σ(I)] R1	0.0471
R indices (all data) wR2	0.0812
Largest diff. peak and hole (e Å^{-3})	0.525 and -0.829

7.5 Computational details

7.5.1 Static calculations

Static calculations on the beryllium complexes in this thesis were performed using a Gaussian 09 program[5] on the University of Waikato high performance computing cluster. Non-periodic geometry optimizations using density functional theory (DFT) were performed in the gas phase and aqueous phase employing the PCM implementation of Tomasi and co-workers[6] (utilising the united-atom UFF radii and the parameters of water). The main DFT functional employed for the calculation of the exchange-correlation energy were the BLYP and the hybrid B3LYP functional. These were chosen in order to assess a close comparison with results from *ab initio* molecular dynamics simulations. The minimum or the transition state character of each geometry was verified by computation of the harmonic vibrational frequencies. Thereafter, using the optimised geometries from the respective medium, single point energies were calculated both in gas phase and the PCM with 6-311++G(d,p) and aug- cc-pQTZ basis sets. Gibbs free energy difference were obtained by subtracting reactant from the free energies of the products. In addition, the effect of empirical dispersion corrections of Grimme and the basis-set superposition error (BSSE) (evaluated using the counterpoise method) on individual bonds were computed.[7]

7.5.2 *Ab initio* molecular dynamics

Ab initio molecular dynamics were performed using the Car-Parrinello scheme[8] as implemented in the CPMD program[9] (version 3.7) on the University of St. Andrews high performance commuting facilities (Knox and Obelix). CPMD simulations were performed using the BLYP functional as this functional has been noted to display impressive performance in describing the properties of liquid water[10, 11] and could be easier compared to static calculation to verify the versatility of other variables employed in the CPMD methodology such as the pseudopotentials. Norm conserving pseudopotentials utilised in this study were generated according to the procedure by Troullier and Martins[12] and transformed into the nonlocal form using the scheme proposed by Kleinman-Bylander.[13] A new pseudopotential was generated for beryllium (discussed in Chapter 5) while the pseudopotential employed for all other elements had been previously generated and validated.[14]

Geometric parameters labelled as CP-opt involved optimisation implemented in the CPMD program until the maximum gradient was less than $5x10^{-4}$ a.u.

The electronic wave functions were described using the Kohn-Sham orbitals expanded in plane waves up to a kinetic energy cut-off of 80 Ry. The simulation were performed in periodically repeating cubic box with lattice constant varying depending on the size of the system. While a cell edge of 12.8 Å was employed for simulation of the beryllium species in the gas phase or in a box of 67 water molecules, 14 Å was employed for the simulations in 90 water molecules. Starting structures involving 67 water molecules were generated from a pre-equilibrated system from previous CPMD simulations[14] (by manually placing in the appropriate atoms with the Be complex) while the water molecules in the bigger box were generated from pre-equilibrated classical MD snapshots.

The CPMD simulations were performed with a fictitious electronic mass of 600 a.u, and a time step of 0.0121 fs, in a NVT ensemble using a single Nosé-Hoover thermostat set to 300 K (instantaneous heat-up, frequency 1800 cm^{-1}), except when otherwise stated (in order to increase the mobility of the solvent). Hydrogen was substituted with deuterium in order to increase the time step and long-range electrostatic interactions treated with the Ewald method, electrostatic decoupling between the cell was exempted since the error introduced in a related system have been reported to be insignificant.

Unconstrained CPMD were generally performed over 6-18 ps and the first 3 ps were taken for equilibration. Furthermore, constrained CPMD simulation in the gas phase and aqueous solution were conducted along well-defined reaction coordinates the complexes in the reactant and product side. Thereafter, pointwise thermodynamic integration (PTI)[15] of the mean constraint force along the chosen coordinates were evaluated to obtain the changes in the Helmholtz free energy according to the equation

$$\Delta A_{a\to b} = -\int_a^b \langle f(\Delta r)\rangle d(\Delta r) \qquad (5\text{-}1)$$

and at each point, the simulation was performed until the mean constraint force was converged.

7.6 References

1. D. Naglav, M. R. Buchner, G. Bendt, F. Kraus and S. Schulz, *Angewandte Chemie International Edition*, 2016, **55**, 10562-10576.

2. K. J. Shaffer, R. J. Davidson, A. K. Burrell, T. M. McCleskey and P. G. Plieger, *Inorganic Chemistry*, 2013, **52**, 3969-3975.

3. M. Strohalm, M. Hassman, B. Košata and M. Kodíček, *Rapid Communications in Mass Spectrometry*, 2008, **22**, 905-908.

4. G. M. Sheldrick, *Acta Crystallographica Section C: Structural Chemistry*, 2015, **71**, 3-8.

5. M. Frisch, G. Trucks, H. B. Schlegel, G. Scuseria, M. Robb, J. Cheeseman, G. Scalmani, V. Barone, B. Mennucci and G. Petersson, 2009, Gaussian 09, Revision D. 01, Gaussian Inc., Wallingford, CT.

6. J. Tomasi, B. Mennucci and R. Cammi, *Chemical Reviews*, 2005, **105**, 2999-3094.

7. S. Grimme, *Wiley Interdisciplinary Reviews: Computational Molecular Science*, 2011, **1**, 211-228.

8. R. Car and M. Parrinello, *Physical Review Letters*, 1985, **55**, 2471.

9. J. Hutter, A. Alavi, T. Deutsch, M. Bernasconi, S. Goedecker, D. Marx, M. Tuckerman and M. Parrinello, CPMD Program, MPI für Festkörperforschung and IBM Zurich Research Laboratory.

10. J. C. Grossman, E. Schwegler, E. W. Draeger, F. Gygi and G. Galli, *The Journal of Chemical Physics*, 2004, **120**, 300-311.

11. M. Sprik, J. Hutter and M. Parrinello, *The Journal of Chemical Physics*, 1996, **105**, 1142-1152.

12. N. Troullier and J. L. Martins, *Physical Review B*, 1991, **43**, 1993.

13. L. Kleinman and D. Bylander, *Physical Review Letters*, 1982, **48**, 1425.

14. M. Bühl, N. Sieffert and G. Wipff, *Chemical Physics Letters*, 2009, **467**, 287-293.

15. M. Sprik and G. Ciccotti, *The Journal of Chemical Physics*, 1998, **109**, 7737-7744.